NASA CR-24

NASA CR-24

$167p$

(NASA CR-24)

N64-18456 *

CODE-1

ELECTROMAGNETIC ATTITUDE CONTROL SYSTEM STUDY

ELECTROMAGNETIC ATTITUDE CONTROL SYSTEM STUDY

This report is reproduced photographically
from copy supplied by the contractor.

Prepared under Contract No. NAS-5-1728 by
WESTINGHOUSE ELECTRIC CORPORATION
Baltimore, Maryland

NATIONAL AERONAUTICS AND SPACE ADMINISTRATION

ABSTRACT

/8456

A а C

Actuating torques for attitude control systems in earth satel-
lites can be produced by manipulating the currents in three
vehicle-fixed coils which react with the earth's magnetic
field. Such electromagnetic actuation has been found to be
feasible and to have practical application to satellite con-
trol. The technique can take the form of direct control of the
vehicle momentum or of indirect control by removing mo-
mentum stored in reaction wheels. The study of electro-
magnetic attitude control has encompassed the analysis of
both direct and indirect systems, the optimization of actuator
designs, an examination of the reliability, weight, size, and
power requirements of a typical system in a specific appli-
cation, and the measurement of actuator effects on the de-
tection of the earth's magnetic field. Electromagnetic actu-
ation is seen to be a reliable and lightweight contribution to
the body of attitude control techniques.

AUTHOR

TABLE OF CONTENTS

1. INTRODUCTION

2. METHODS OF ELECTROMAGNETIC ACTUATION

3. SCOPE OF THE STUDY PROGRAM

4. GENERALIZED CONCLUSIONS

5. TASK I - INDIRECT MAGNETIC ACTUATION

6. TASK II - AUTOMATIC GAIN CHANGING

7. TASK III - DIRECT MAGNETIC ACTUATION

8. ELECTROMAGNETIC ACTUATOR DESIGN

9. TASK V - MAGNETOMETER INTERFERENCE

10. TASK VI - SAMPLE SYSTEM DESIGN

LIST OF APPENDIXES

LIST OF ILLUSTRATIONS

viii

LIST OF TABLES

1. INTRODUCTION

This final report presents the detailed results of a study on electromagnetic actuation for satellite attitude control conducted for the National Aeronautics, and Space Administration by the Westinghouse Electric Corporation (NASA contract NAS-5-1728).

In the course of investigating attitude control system actuation methods for use with OAO, techniques of utilizing the earth's magnetic field for the generation of useful control torques were uncovered. These techniques required neither moving parts to be exposed to the space environment nor the expulsion of mass and seemed to offer reliability and weight savings. However, many questions which arose in design reviews remained unanswered; for example, iron core actuators to react with the earth's field had not been built, and it follows that there are no actuator design equations in the texts and references despite the large general effort which had been expended on magnetic circuits. Also, even though the basic actuation techniques had been proven on the digital computer, no effort had been expended in optimizing these basic techniques or the mechanization of these techniques. As an illustration, it was not known whether the actuator field would interfere with the measurement of the earth's field.

To answer these questions and to assess the usefulness of the electromagnetic actuation techniques, as described in Section 2, in a specific application, a program of study as outlined in Section 3 has been carried out. The general conclusions of the completed study are contained in Section 4 with certain recommendations for further study in promising areas. The detailed description of each task, its manner of accomplishment, and the detailed results associated with each task are presented in Sections 5 through 10.

The objectives of this study were accomplished, and it may be stated with a reasonable degree of certainty that electromagnetic actuation systems will find their way into future unmanned earth orbiting vehicles, especially where the life of the vehicle is greater than 1 month.

2. METHODS OF ELECTROMAGNETIC ACTUATION

There are many methods by which torques can be generated through the interaction of the satellite with the earth's magnetic field and any one of these methods might appropriately be called electromagnetic actuation. The generation of eddy currents in the vehicle skin to reduce angular rates, the reduction of angular rate through the hysteresis losses in ferrous materials, and the generation of torques with current-carrying conductors are all examples of electromagnetic actuation. However, only the current-carrying coil techniques seem to exhibit both torque levels which are adequately high and have the capability of changing the direction of the torque which is required in attitude control systems. Consequently, in this study, three mutually perpendicular current-carrying coils are employed to produce control torques.

Two basic electromagnetic actuation techniques were simulated and optimized in the course of the study. One of these techniques is referred to as the "wheels and coils" technique (or indirect magnetic actuation) because the actuation system employed three inertial wheel controls as well as three coils. The second technique, referred to as the "coils only" technique (direct magnetic actuation), employs only three mutually perpendicular coils to generate control torques. The direct technique is intended for vehicles which have very low disturbance torques and when there is no requirement for slewing the vehicle. The indirect technique is used when either the disturbance torques are quite high or there is a requirement for slewing the vehicle.

2.1 INDIRECT ELECTROMAGNETIC ACTUATION SYSTEM

The basic block diagram of the wheels and coils electromagnetic actuation system is shown in figure 2-1. The attitude position errors ϕ, θ,

and ψ are fed via a lead-lag network to the three inertia wheel controls, closing the position loops.

The wheel velocities ω_x, ω_y, and ω_z are fed back into the motor control amplifiers to provide damping. The tachometer generators, which measure the wheel speeds, furnish a measurement of the unwanted momentum aboard the vehicle, this momentum being proportional to the vector sum of ω_x ω_y, and ω_z.

The unwanted momentum stored in the inertia wheels is transferred to tne earth by the interaction of the current-carrying coils with the earth's magnetic field as shown in figure 2-2. The magnitudes of the coil currents are determined by the magnitude of the earth's field components and the magnitude of the components of unwanted momentum. The equations defining the coil currents are given as follows:

$$I_{cx} = M_y B_z - M_z B_y \qquad (2-1)$$

$$I_{cy} = M_z B_x - M_x B_z \qquad (2-2)$$

$$I_{cz} = M_x B_y - M_y B_x \qquad (2-3)$$

In the system shown in figure 2-1, the components of the earth's field are measured with a three-element magnetometer and the components of unwanted momentum are measured with tachometer generators. The coil current computation includes the multiplication and summing of these components in accordance with equations 2-1 through 2-3.

The operation of the momentum transfer system may be more clearly seen by referring to figure 2-2. In Case I, the earth's field is represented by $\vec{B}$ and the vector sum of the wheel speeds is represented by $\vec{M_1}$. The coil current vector which is defined by equations 2-1 through 2-3 will be constrained to be along the negative Z axis as well as the flux vector which the coil currents produce. The interaction of the coil flux vector with the earth's field vector $\vec{B}$ will generate the torque T on the vehicle. The direction of T is directly opposite to the direction of the $M_1 \sin \theta$ component of the unwanted momentum vector.

The torque T produced by the coils will remain until the $M_1 \sin \theta$ component of the unwanted momentum vector is reduced to zero. The remaining

2-2

Figure 2-1. Indirect Electromagnetic Actuation System

Y

B

M_1

M_2

θ

M_1 SIN θ

T

X

Z

CASE I

$M_2 = M_1 \cos \theta$

Y

B

M_2

M_3

ψ

M_2 SINψ

X

T

Z

CASE II

$M_3 = M_2 \cos \psi$

95258AY-IB-VA2
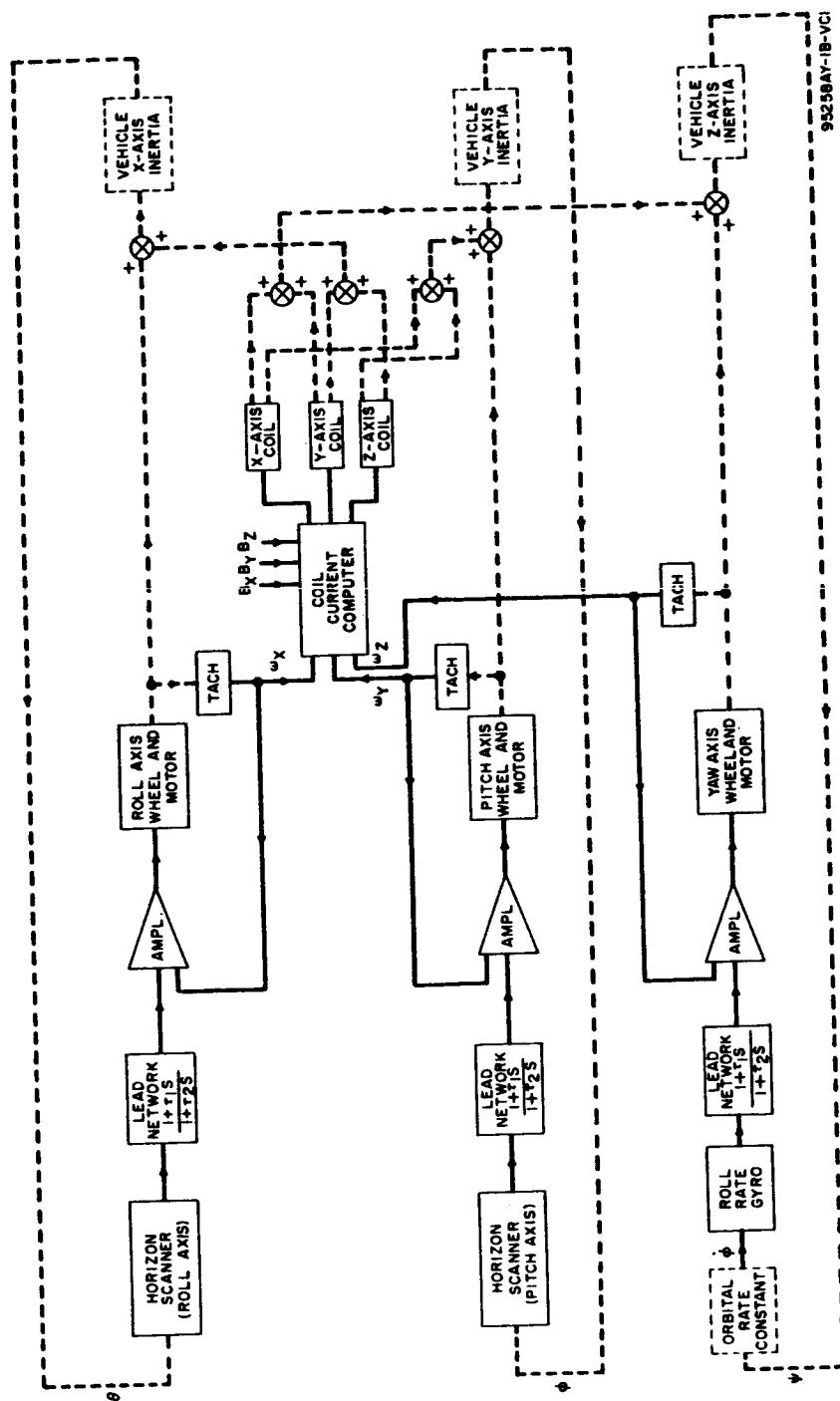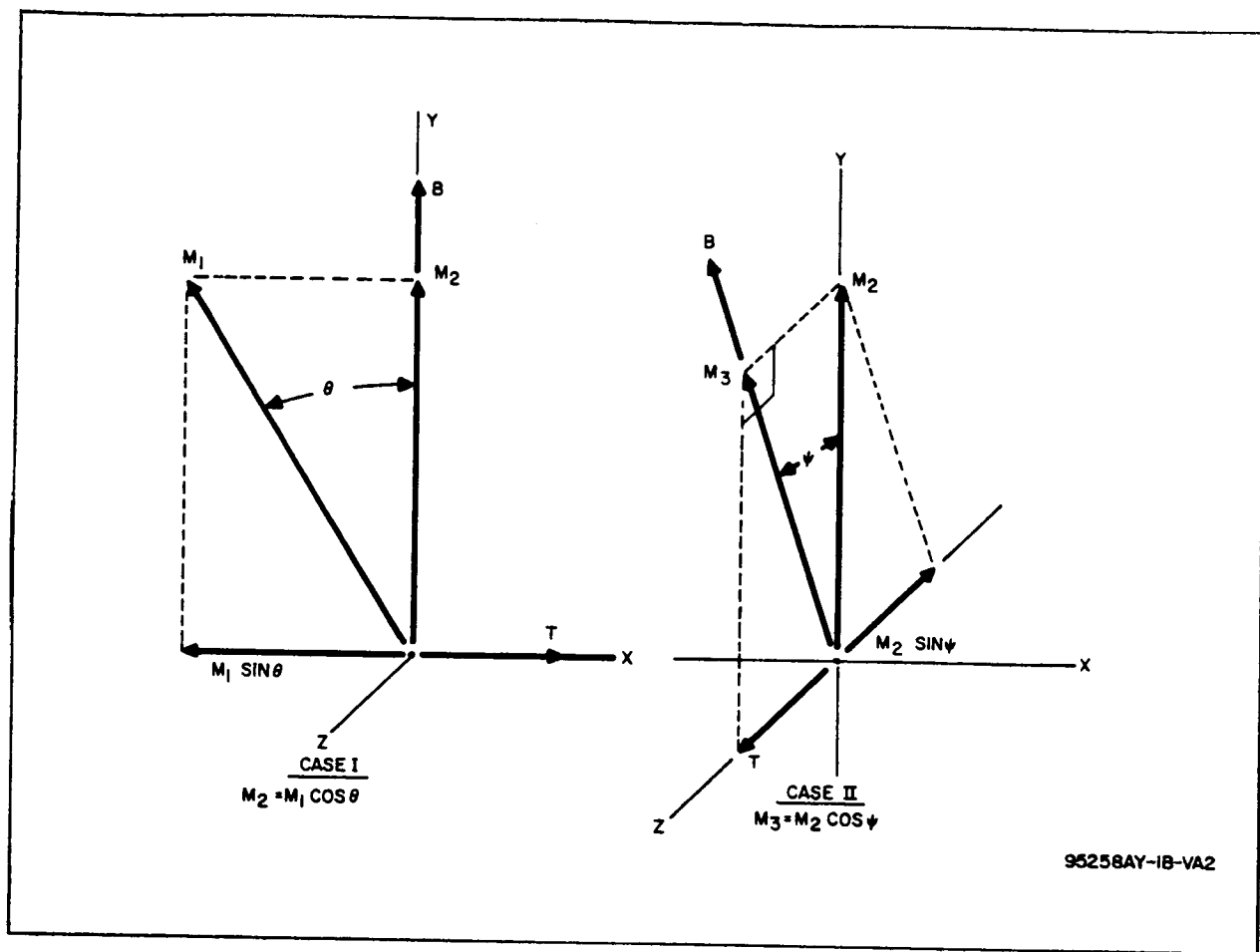
Figure 2-2. Operation of Momentum Dumping

unwanted momentum $M_1 \cos \theta$ (M_2) cannot be removed or reduced until the direction of B and M has changed again. As is depicted vectorially in Case II of figure 2-2, when the B vector has changed direction with respect to the vector M_2, the $M_2 \sin \psi$ component of the unwanted momentum can be removed. The reduction of unwanted momentum continues acting at this level.

In the mechanization of this type of electromagnetic momentum transfer system for application to a given system, the following fundamental characteristics of this system must be observed. It is necessary that the direction of the earth's field vector be variable with respect to a set of inertial axes in the vehicle. The only case in which this condition is not fulfilled is that of a synchronous equatorial orbit. However, in the case of a synchronous equatorial orbit, a direct form of electromagnetic actuation may be used in

2-4

two axes. The torque available from a given electromagnetic actuator decreases with orbital altitude due to the decrease in the strength of earth's magnetic field. While each vehicle application must be examined when the disturbance torques and slewing requirements are known, an altitude of approximately 30,000 to 40,000 statute miles is presently suggested as the limit of applicability of electromagnetic actuation.

The consideration of optimization and mechanization of the indirect electromagnetic actuation system are presented in Sections 5 and 10, respectively.

2.2 DIRECT ELECTROMAGNETIC ACTUATION SYSTEM

The basic block diagram of the direct electromagnetic actuation system is shown in figure 2-3. The attitude position errors ϕ, θ, and ψ are fed directly into the coil current computation system. Also, the vehicle angular rate signals as determined by onboard rate gyros or by ground computation from magnetometer signals are fed into the coil current computation system along with the earth's field component signals as determined by an onboard magnetometer. The expressions for the coil currents are given as follows:

$$I_{cx} = (M_y + \theta) B_z + (M_z + \psi) B_y \tag{2-4}$$

$$I_{cy} = (M_z + \psi) B_x + (M_x + \phi) B_z \tag{2-5}$$

$$I_{cz} = (M_x + \phi) B_y + (M_y + \theta) B_x \tag{2-6}$$

The operation of the direct electromagnetic actuation can be seen by referring to figure 2-4 which represents a typical kinematic condition that may exist on a given vehicle. The unwanted momentum aboard the vehicle is represented by M_1 which is proportional to the vector sum of the angular rates of the vehicle. Again, as in the case of the indirect system, the torque T_m is generated to remove the $M_1 \sin \theta$ component of the unwanted momentum vector. The vector sum of the position errors is represented by the vector E_1. The torque T_E is generated by the cross-product computation to remove the $E_1 \sin \alpha$ component of the position error vector. The vehicle ultimately responds to the sum of the coil torques $(T_M + T_E)$.

Figure 2-3. Direct Electromagnetic Actuation System
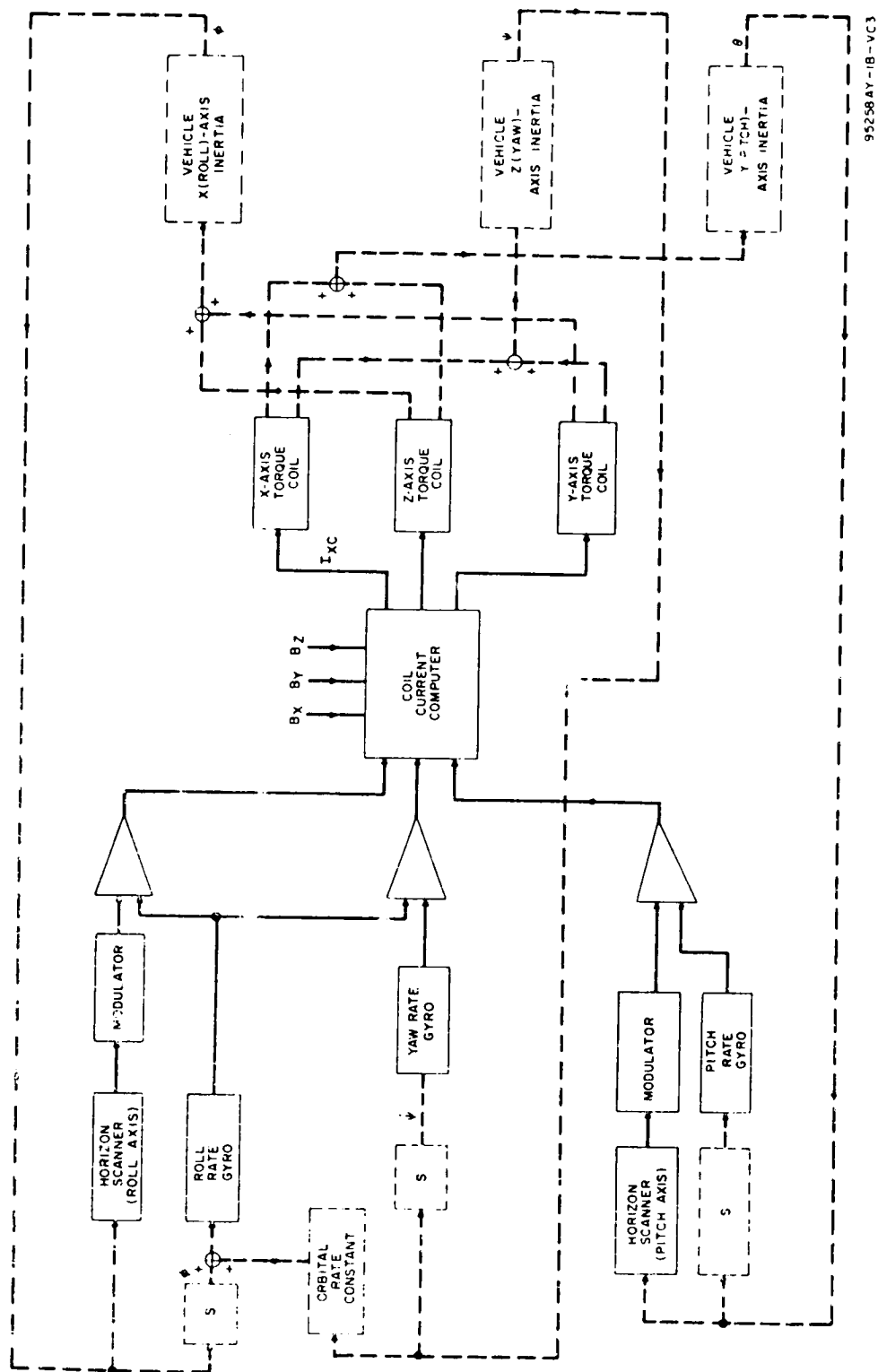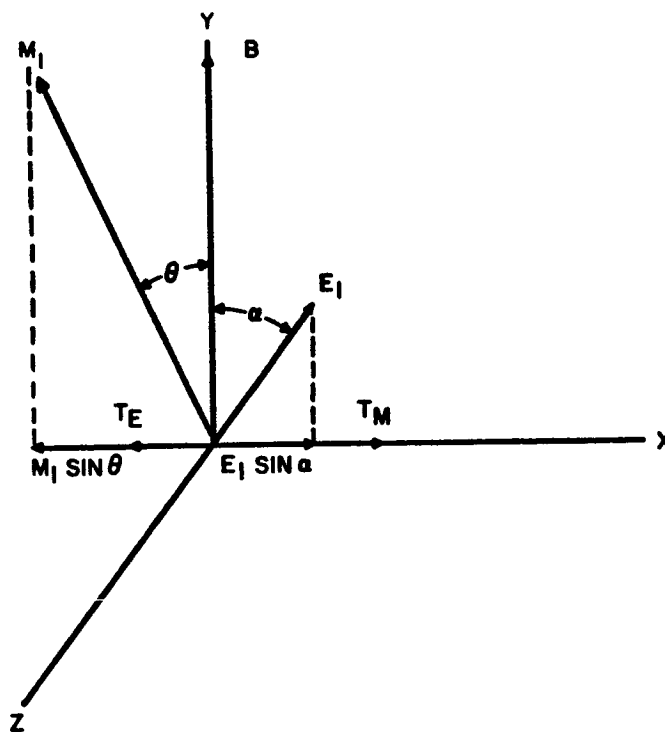
Figure 2-4. Principles of Direct Electromagnetic Actuation

With this controller configuration, it can be seen that in the absence of disturbance torques, a vehicle with initial angular rates will have essentially zero angular rate with zero position error after an extended period. In reality, because of the presence of disturbance torques, this condition is never reached. The objective of the study presented in Section 7 is to establish what the position and rate errors are as a function of disturbance torque when the loop gains are optimized.

In the mechanization of this method of electromagnetic actuation, the same considerations with regard to usage apply as with the indirect system. In addition, the level of the disturbance torques which can be sucessfully coped with using this technique is considerably lower.

3. SCOPE OF THE STUDY PROGRAM

The purpose of the study program was to establish more precisely than heretofore the form taken by electromagnetic actuation for satellite attitude control and to find where and how such a control system can be optimized. One typical orbit was chosen for the study.

The first areas of interest were the relationship between the torque coils and stored momentum for the indirect (wheels and coils) system and the relationship between the torque coils and satellite attitude error for the direct (coils only) system. The investigation here took the form of analog computer simulations, where the vehicle disturbance level was a parameter. A subsidiary study dealt with the possible benefits to be derived from changing the torque coil gains as a function of resultant momentum.

Another area of interest was the design of the iron-cored torque coils, answering questions which included the following:

a. What are the design equations for torque coils, using desired torque rating and length as independent variables?

b. What are the effects of actuator length, core-length-to-coil-length ratio, and rated power in achieving an optimum design?

c. Are iron-cored coils superior to air-cored coils and, if so, to what degree?

d. What levels of residual torque due to the remanence of the core are obtained?

Analyses made to answer these questions were supported and adjusted by gathering data on a number of experimental units.

A more restricted area of the study was concerned with the degree to which typical satellite torque coils interfere with the detection of the earth's

field by magnetometers. Here the general idealized method of calculation was evaluated by testing a specific set of iron-cored actuators in a three-axis configuration.

Finally, a typical attitude control system employing electromagnetic actuation was designed so that the performance, reliability, weight, size, and power requirement characteristics could be defined with reasonable confidence.

The scope of the study program can be summarized in the following listing of six tasks:

I. Optimum reaction wheel-torque coil relationship as a function of disturbance level.

II. The feasibility of automatic gain change in an electromagnetic momentum dumping system.

III. The feasibility of a system using torquing coils for direct control (no reaction wheels).

IV. Methods of torque coil design, substantiated by prototype tests.

V. Possible interference of torque coils on the sensing of the earth's field of magnetometers.

VI. The preliminary design of a system using reaction wheels as primary actuators, removing wheel momentums by means of electromagnetic actuators.

4. GENERALIZED CONCLUSIONS

The most significant of the conclusions reached in Sections 5 through 10 are summarized below.

4.1 OPTIMIZATION OF WHEEL - COIL RELATIONSHIP

In an attitude control system employing reaction wheels as primary actuators and torque coils as indirect actuators, there will be a specific coil gain (expressed in $\frac{\text{dyne-cm/gauss}}{\text{gauss-lb-ft-sec}}$) which yields a minimum combined weight for the wheel and coil. This optimum coil gain will increase with the level of satellite disturbance torque. The optimum coil gain also implies optimum wheel momentum and coil torque ratings as equipment design figures. In the general case, as coil gain is increased, the peak coil torque will trend upward, the required wheel momentum storage capability will approach a minimum, and the combined weight will reach a minimum and then rise again.

In the study reported here, for a typical satellite in a 6-hour, 32-degree inclined orbit with disturbances ranging from 50 to 500 dyne-cm, the parameters were such that the peak coil torque was constant in the range of gains near that which produced minimum wheel momentum or minimum combined weight.

In the application studied, the optimum peak coil torque rose linearly with disturbance level. The optimum wheel momentum rating for the range of disturbance levels studied was always below that of the wheel with minimum practical weight (2 pounds). The optimum combined three-axis wheel and coil weight in pounds was approximately

$$W = 6 + 0.03 \, T_d,$$

where T_d is the disturbance torque in dyne-cm, and the number 6 represents the practical minimum weight of three reaction wheel controls.

4.2 FEASIBILITY OF AUTOMATIC GAIN CHANGING

At the outset of the study program, it seemed that a method of changing coil gain continuously as a function of the magnitude of the wheel momentum vector (explained in Section 6) would produce a more responsive momentum dumping system, and hence a smaller wheel and coil weight. Better response was achieved, but weight was not improved; furthermore, the mechanization is complex.

A simplified version of the gain changing idea is to change the gain in a few steps as an inverse function of the sum of the absolute values of vehicle momentum components. This approach, when applied to the special case of detumbling a satellite by means of magnetic actuation, significantly shortened the time required for detumbling. However, complexity is still added to the coil system, and the coil sizes must be increased to many times that required for routine momentum dumping. Since detumbling is a one-shot operation requiring little total impulse it is sometimes better accomplished by means of some mass-expulsion system.

4.3 DIRECT COIL MOMENTUM CONTROL

When the reaction wheels are eliminated, leaving the torque coils as the only actuators, a workable system is still obtained, but the range of application is greatly reduced. This system was analyzed under the same vehicle and orbit conditions as for the indirect system. It was found, for a given disturbance torque level, that there is a specific combination of coil rate and position gains which produces the lowest peak position excursion from the nominal. For the case studied (6-hour orbit) at a 2 dyne-cm disturbance level, the peak pitch error was 7 degrees, and the peak roll and yaw errors were each 4 degrees. These position errors would decrease with the square of the orbital period, be directly proportional to the disturbance torque level, and be inversely proportional to vehicle moments of inertia.

While the direct magnetic actuation system holds much promise for simplicity, care must be taken to design the satellite for very low disturbances.

4.4 CHARACTERISTICS OF IRON-CORED MAGNETIC ACTUATORS

The study program has resulted in an improvement of the completeness and accuracy of the optimum magnetic actuator design equations, such that it is now possible to design a unit quickly with torque accuracy of better than 15 percent in most cases.

It was found that minimum actuator weight is obtained when the core length and coil length are equal. It was known at the outset of the study that weight decreases as actuator length increases. The study showed that the use of iron-cored actuators resulted in one-half to one-fifth of the total mass (including power supply) required by the air-cored coils.

In most cases, the residual torque was found to be less than 1/2 percent of the maximum rated torque, although a more exhaustive study of core materials might further improve this figure.

4.5 MAGNETOMETER INTERFERENCE

By testing a typical set of magnetic actuators, the parameters to substitute in the theoretical expression for determining the degree of interference were inferred. There is no all-inclusive answer as to the adequacy of avoiding excessive interference by merely separating the torque coils and magnetometer. The goal would be to obtain sufficient separation within the greatest dimension of a satellite in order to avoid extending the magnetometer on a boom. The data in Section 9 show that this will be possible in some cases, impossible in others. Using the system design of Section 6 as an example, the coils and magnetometer must be 4 feet apart, which is reasonable.

In cases where mere separation is not practical, it was found that the interference can be adequately attenuated by centering the magnetometer in a set of controllable Helmholtz coils. Cancellation of the unwanted field can be achieved even more precisely by using a coil in the shape of a truncated cone.

4.6 MAGNETIC ACTUATION IN A TYPICAL CONTROL SYSTEM

The magnetic actuation subsystem, including actuators, magnetometer, multipliers, and supporting electronics was found to have a probability of successful operation for 1 year of 91 percent, a weight of 9 pounds, and an average power drain of 7.5 watts. The application considered was relatively pessimistic with regard to actuator weight and power, since the orbital period was 6 hours with an attendant weak earth's field. The weight and power consumption of the subsystem are relatively insensitive to satellite disturbance level.

When magnetic actuation is compared to a stored gas system for dumping reaction wheel momentums, the latter will be lighter is some cases, but the magnetic technique will have a superior reliability.

5. TASK I - INDIRECT MAGNETIC ACTUATION

5.1 PROBLEM STATEMENT

In certain satellite applications where the disturbance torque to satellite inertia ratio is relatively high, it becomes necessary to store momentum aboard the vehicle if electromagnetic actuation is employed and a specific pointing direction is to be maintained. Momentum storage normally takes the form of an inertia wheel control in each of three mutually perpendicular axes of the satellite. The electromagnetic actuation system includes three mutually perpendicular coils, a magnetometer, and electronic elements to derive the coil currents as functions of the earth's field and the stored momentum.

Previous studies of this type of electromagnetic actuation system revealed that, as the disturbance torque level was increased at a given coil torque level, the amount of momentum which must be stored aboard the vehicle is also increased. The questions which remained to be answered were:

a. In a given satellite for which the disturbance torque levels can be defined, what is the optimum relation between the wheels and coils? Or, in a given application, what size should the inertia wheel and coil be to realize a system with minimum overall weight when due consideration has been given to the weight of the power supply for the inertia wheel controls and the coils?

b. As the disturbance torque level is varied, reflecting variation in the satellite design, how is the optimum relation between the wheels and coils affected?

c. In a given satellite, is there any benefit to be derived through the use of automatic gain control?

To answer these questions, consideration was given to a 500-pound satellite in a 6-hour orbit inclined at 32 degrees. The moments of inertia of the vehicle were considered to be equal as would be the case with either a sphere or a cylindrical vehicle with an L/D ratio of 2. The optimum relation between the wheels and coils was established for a range of disturbance torques between 50 and 500 dyne-cm as is shown in figure 5-1. Also it was established that, while improved response results from the use of automatic gain control, the use of it is not recommended because improved response is not necessary for adequate system performance. Also, the added hardware to achieve automatic gain control reduces the reliability of the system.
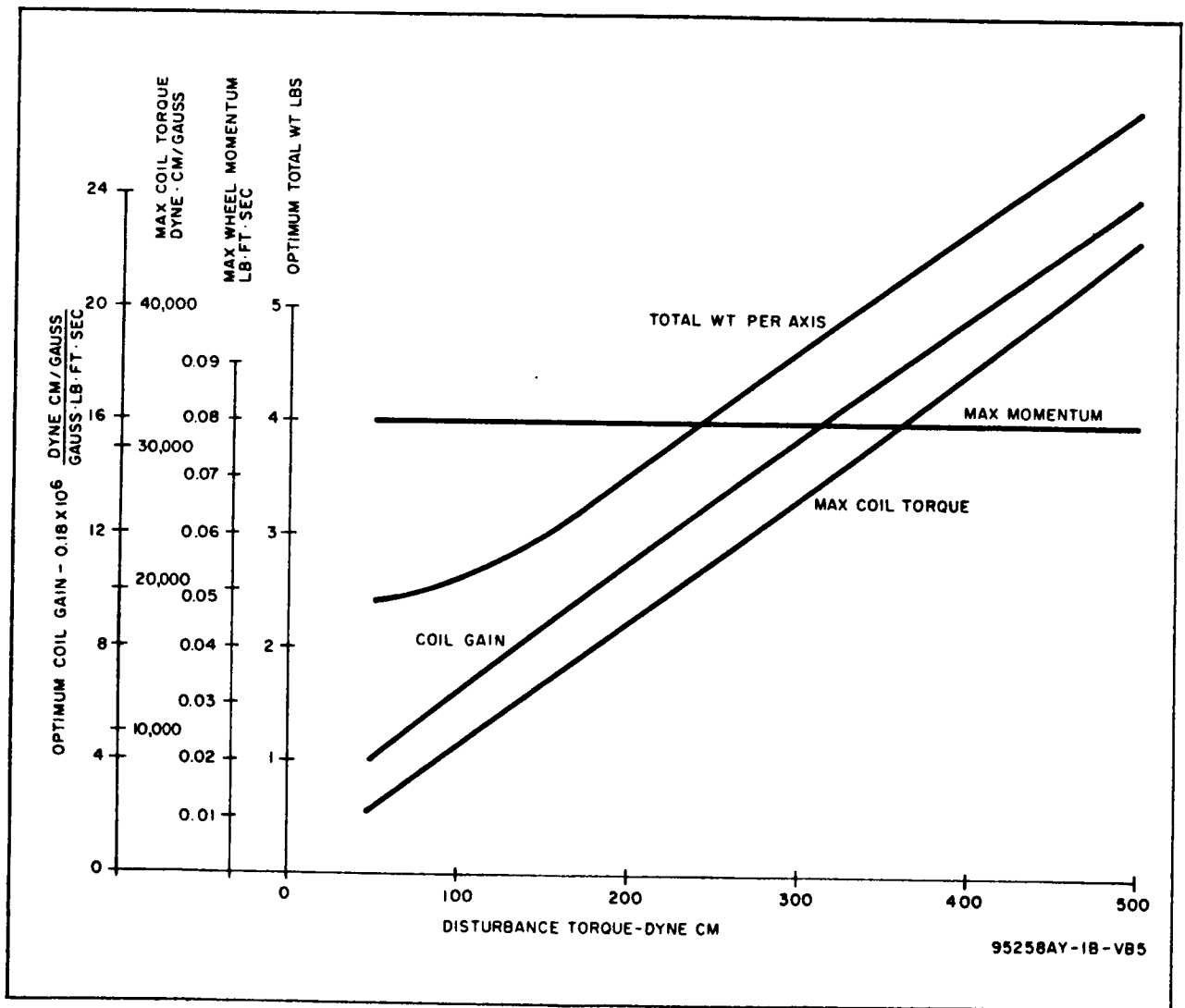
Figure 5-1. System Parameters vs Disturbance Torque Level

The analog simulations of the wheels and coils systems and the detailed results of the wheels and coils optimization and gain change studies are presented in the following paragraphs.

5.2 SIMULATION METHOD

The three-axis simulation of the wheels and coils system is shown in figure 5-2. The axes of the vehicle were constrained to point along the local vertical, perpendicular to the orbit plane, and in the orbit plane perpendicular to the other two axes. This assumption of vehicle orientation is valid when inertia wheel controls are used for position control. The earth's field components as measured with respect to the vehicle axes in the 300-km circular orbit inclined at 32 degrees are shown in figure 5-3. The components for the 6-hour orbit were derived by multiplying these curves by the appropriate attenuation factor of 0.0715 which reflects the cube of ratio of radii. The time compression used in the simulation was 2160/1, with a typical orbit being completed in 10 seconds. Hence the field components were generated with the oscillator as shown in figure 5-2 with the period set at 10 seconds.

The coil current equations which are mechanized with the servos are given as follows:

$$I_{cx} = (M_y B_z - M_z B_y) K_1 \qquad (5-1)$$

$$I_{cy} = (M_z B_x - M_x B_z) K_2 \qquad (5-2)$$

$$I_{cz} = (M_x B_y - M_y B_x) K_3 \qquad (5-3)$$

where:

I_{cx}, I_{cy}, I_{cz} = coil currents

M_x, M_y, M_z = wheel rates

K_1, K_2, K_3 = gain constants

B_x, B_y, B_z = earth's field components
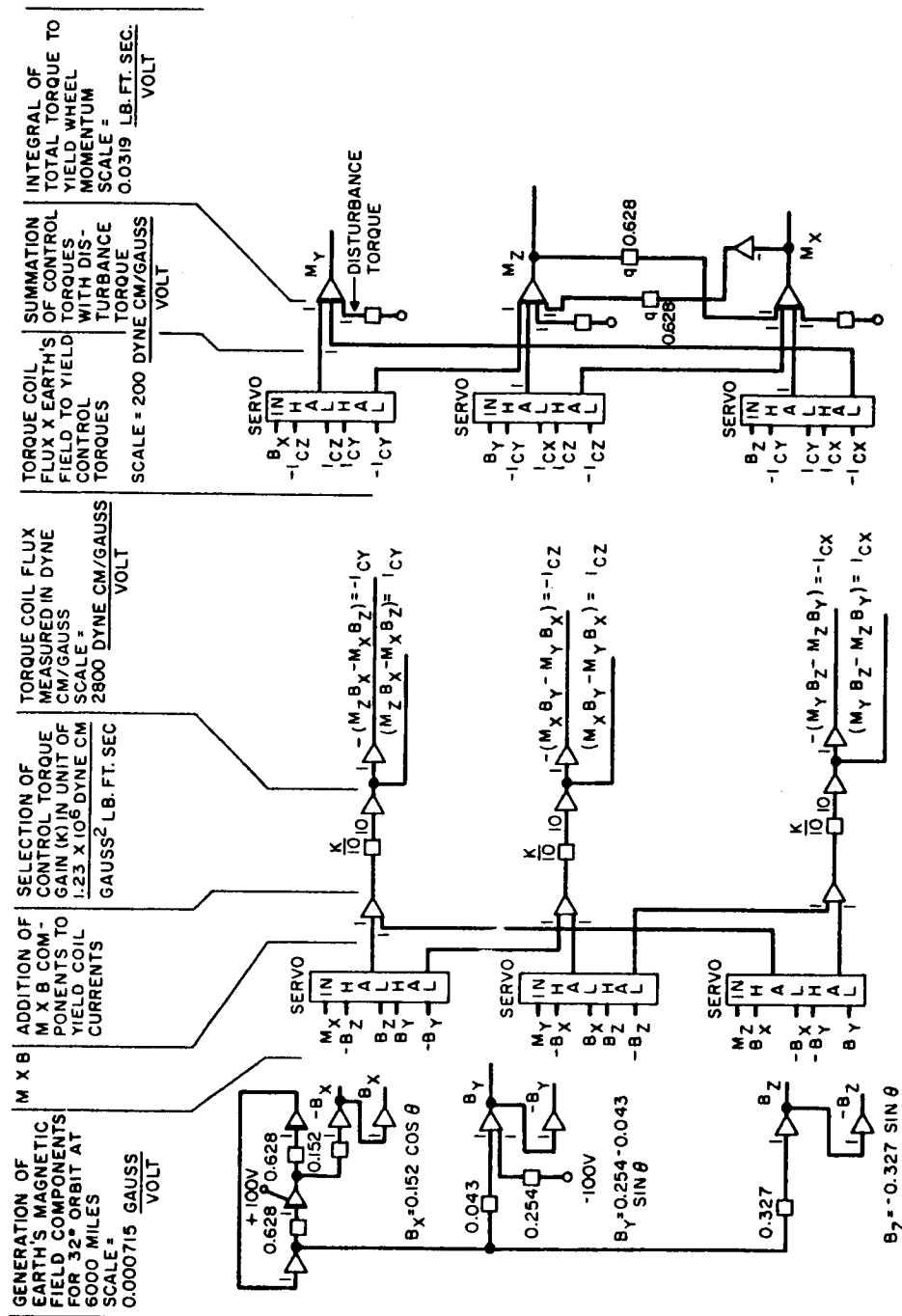
Figure 5-2. Simulation Diagram, Indirect System

95258AY-1B-VB6
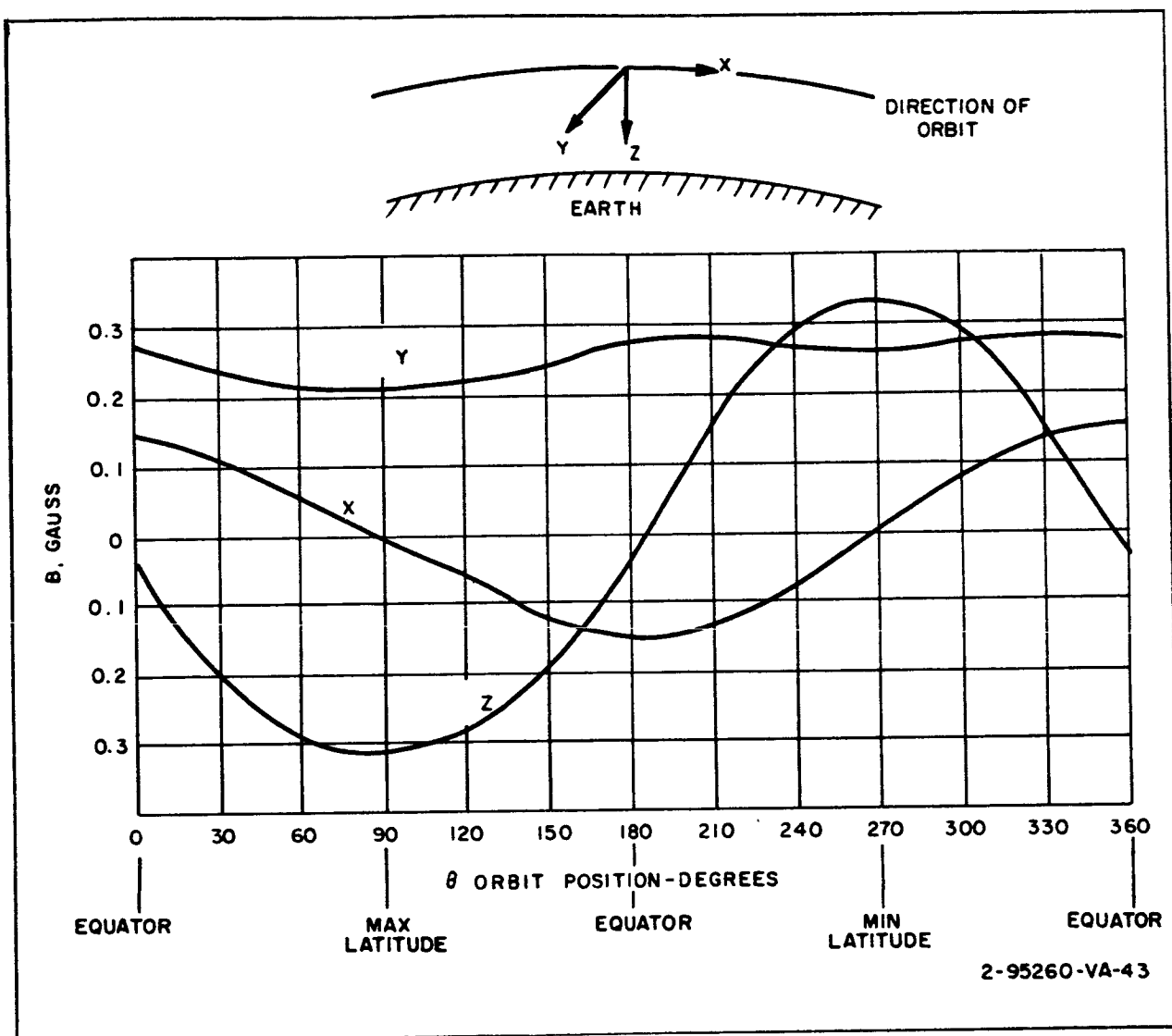
Figure 5-3. Field Strength Distribution

The wheel-vehicle equations which were simulated are given as follows:

$$I_x \dot{\omega}_x = A \dot{p} + I_y (\omega_y + q) r - I_z (\omega_z + r) q + Bqr - Crq \tag{5-4}$$

$$I_y \dot{\omega}_y = B \dot{q} + I_z (\omega_z + r) p - I_x (\omega_x + p) r + Crp - Apr \tag{5-5}$$

$$I_z \dot{\omega}_z = C \dot{r} + I_x (\omega_x + p) q - I_y (\omega_y + q) p + Apq - Bqp \tag{5-6}$$

where:

I_x, I_y, I_z = wheel moments of inertia

A, B, C   = vehicle moments of inertia

p, q, r   = vehicle angular rates

ω_x, ω_y, ω_z = wheel rates

Since A $\cong$ B $\cong$ C, and p = r = 0, the simulation was reduced to:

$$I_x \dot\omega_x = A\dot{p} - I_z (\omega_z) q \tag{5-7}$$

$$I_y \dot\omega_y = B\dot{q} \tag{5-8}$$

$$I_z \dot\omega_z = C\dot{r} + I_x (\omega_x) q \tag{5-9}$$

The cross coupling terms were simulated by setting the period of cross-coupling oscillation equal to the orbit period.

The torques on the vehicle are summed in integrators to generate vehicle rates. The vehicle rates are then converted to wheel rates directly and fed back to the coil current computation servos.

5.3 TEST RESULTS

The procedure of system test was to apply various levels of disturbance torque to each of the three axes, measuring the wheel rates and coil currents. Recordings were made at various values of loop gain until the optimum system configuration was obtained.

With the aid of inertia wheel control suppliers, a curve of angular momentum storage versus inertia wheel control weight was prepared as shown in figure 5-4. The total reaction wheel weight will be relatively constant in a given design as the momentum rating is decreased below a specific level.

A curve of coil weight versus coil torque was also prepared, as shown in figure 5-5, from data derived in Task IV of the study program. The coil weight also reflects the weight of the power supply for the coil. These curves were used to find the wheel and coil weight required for the peak signals on recordings such as figures 5-6 and 5-7. The wheel and coil weight versus coil, gain curves are shown in figures 5-8 through 5-11.

At any given value of loop gain, the gains in each of the three axes being held equal, the momentum storage required in the Y-axis was largest. Also the peak torque required in the Z-axis was largest. This result is as one
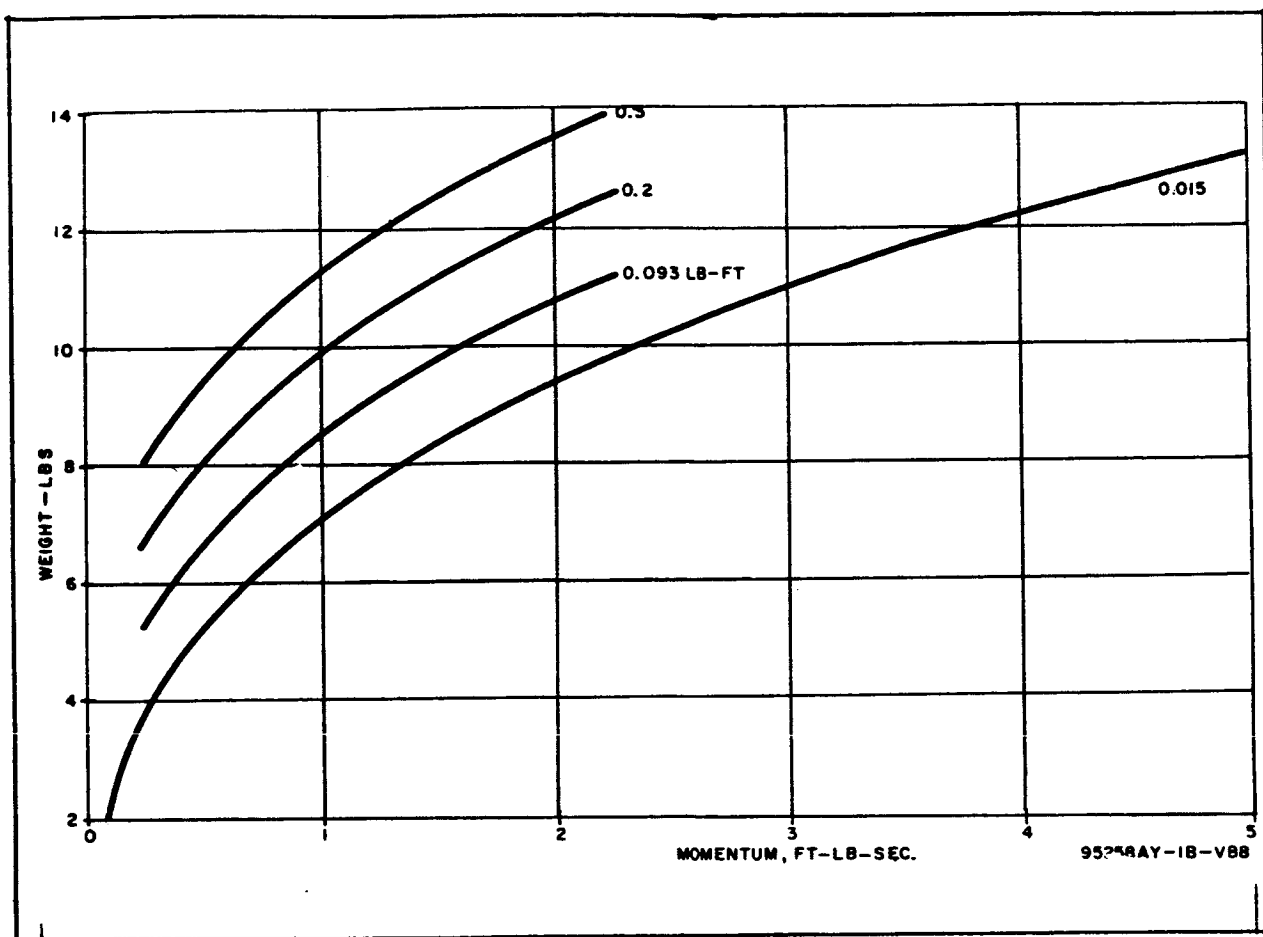
Figure 5-4.   Wheel Storage vs Total Wheel Plus Motor Weight

would expect, because $B_{y, avg} > B_{z, avg} > B_{x, avg}$.   In other words, the momentum storage in the Y-axis is largest because the weaker two components of field are used to dump the Y-axis.   The Z-axis coil must generate the largest torque because it is reacting with the weakest field component.

In the case shown in figure 5-8, if the loop gain is raised to 4, the overall system weight is minimized.   In figure 5-8 the peak coil torque required is independent of loop gain.   It may also be observed that if the gain of the loop is reduced sufficiently (2) then the momentum storage requirement is increased due to the reduced response of the momentum transfer system.

Similar curves were prepared for disturbance torque levels of 100, 200, and 500 dyne-cm as shown in figures 5-9 through 5-11.   Comparing figures
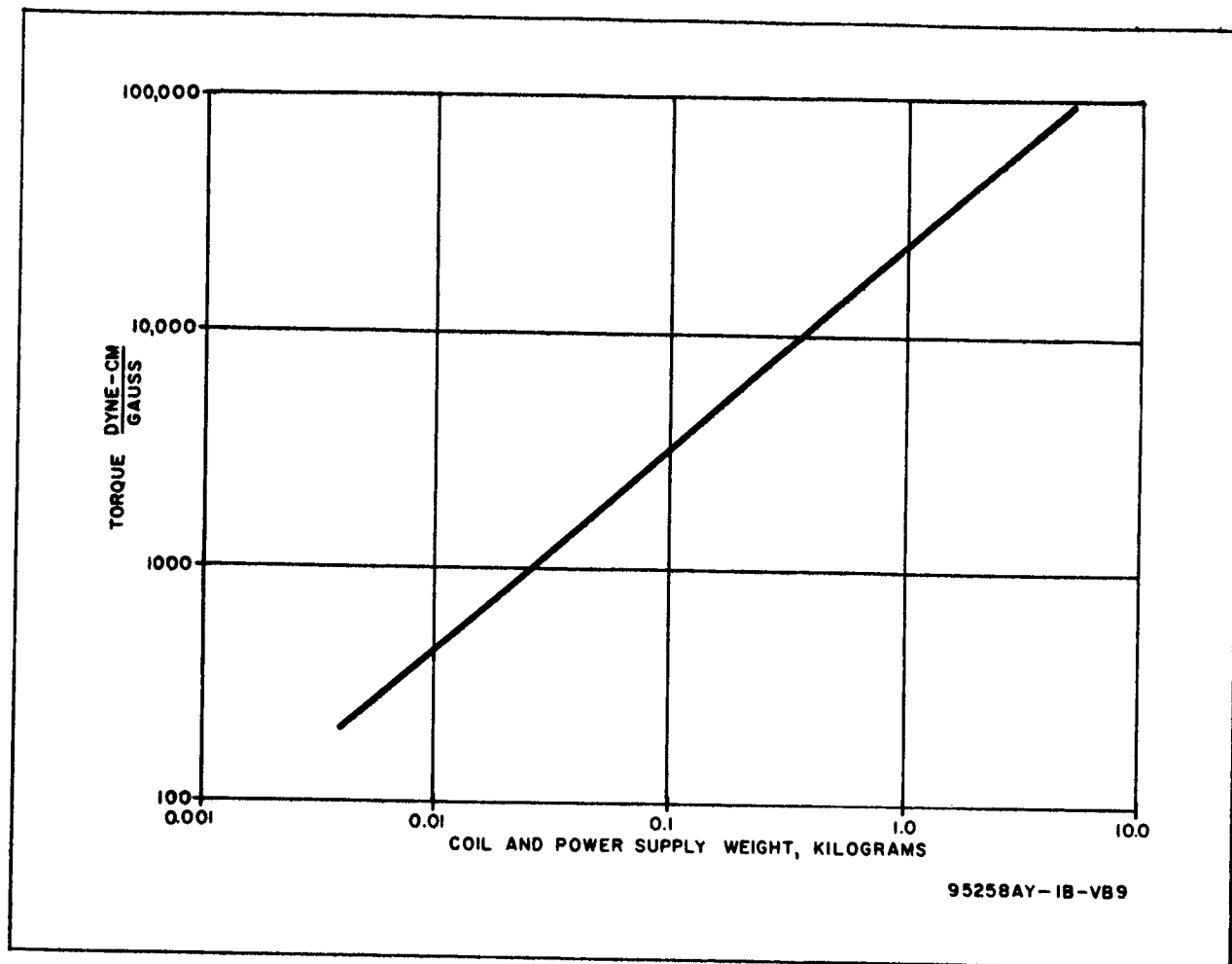
Figure 5-5. Torque vs Weight for Iron-Core Coils

5-8 and 5-9, it is evident that the same general shape of the weight vs gain exists. The peak coil torque required is increased as the disturbance torque level is increased. Also, the gain required to achieve a minimum overall weight system is increased. At any disturbance torque level, it was possible to raise the gain sufficiently high that a minimum weight of the wheel control was achieved.

From figures 5-8 through 5-11, the variations of optimum total weight, coil gain, coil weight, and momentum storage requirement vs disturbance torque level were plotted as shown in figure 5-1. It may be observed that the maximum coil torque would vary linearly with the disturbance torque level. Also, the optimum loop gain varies linearly with disturbance torque
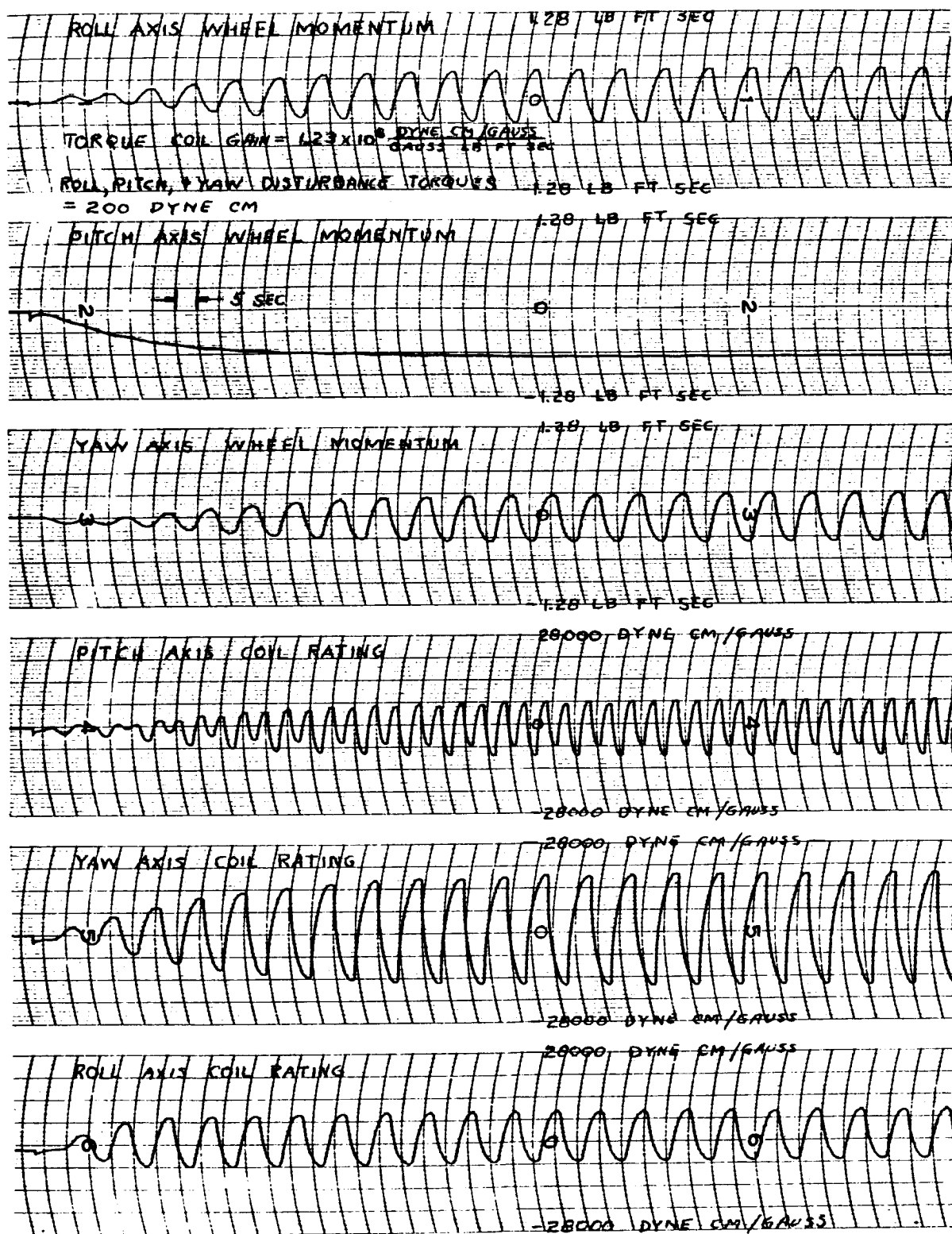
Figure 5-6. Typical Results of Wheels and Coils Simulation,
T_D = 200 Dyne Cm
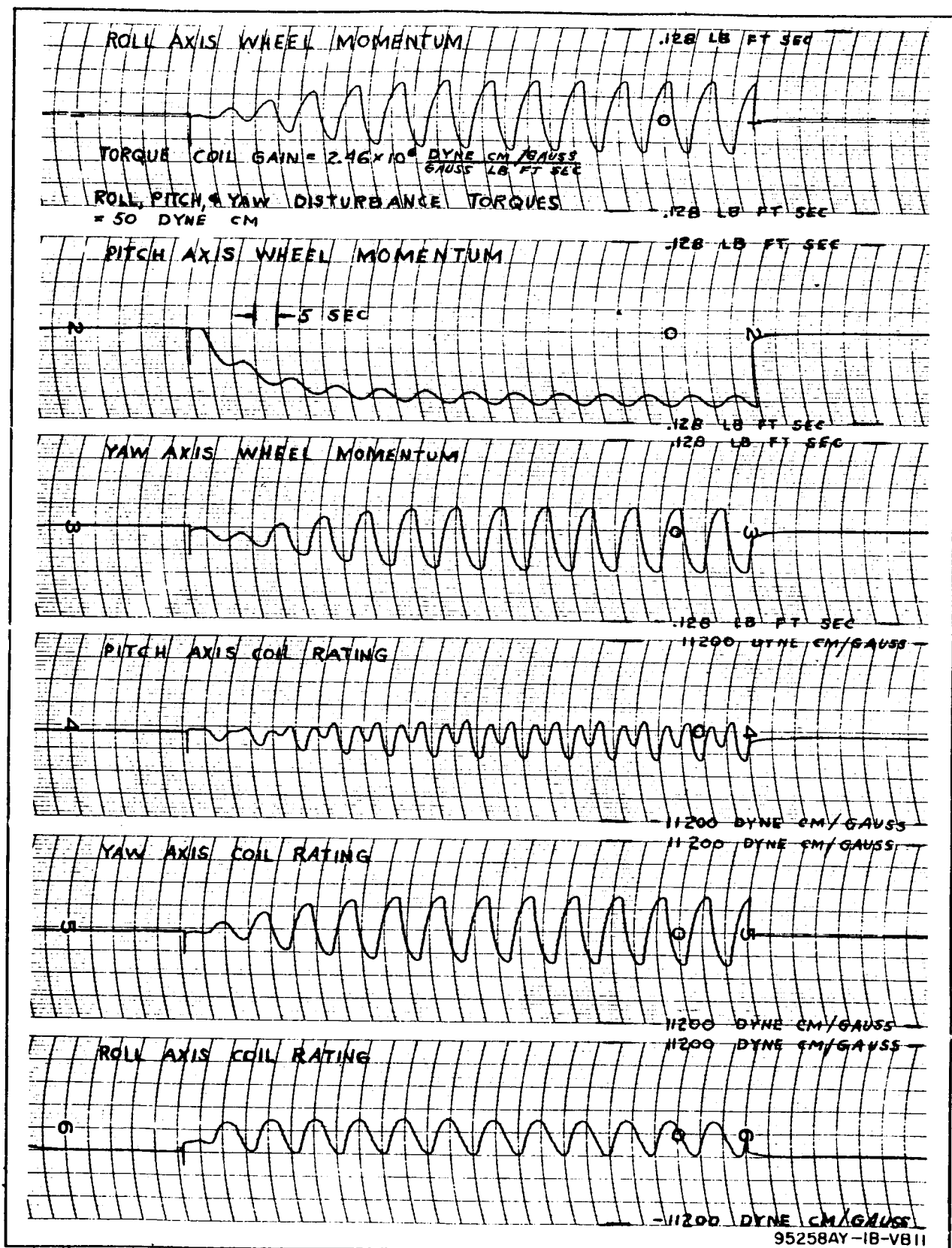
Figure 5-7. Typical Results of Wheels and Coils Simulation,
T_D = 50 Dyne Cm
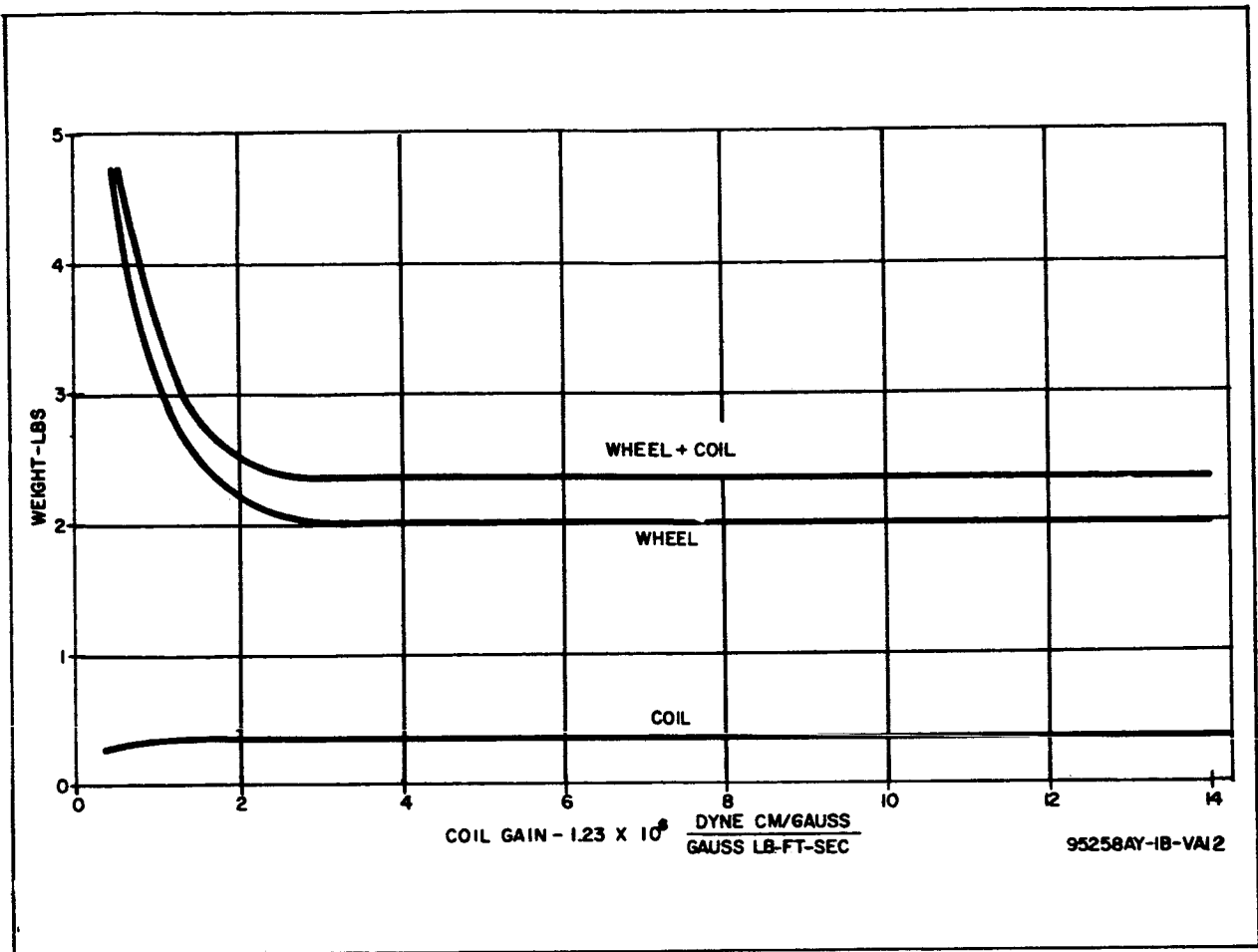
Figure 5-8. Actuation Weight vs Coil Gain, Disturbance Torque
= 50 Dyne-Cm (Pitch Axis Wheel and Yaw Axis Coil)

level. The momentum storage requirement remains essentially constant
over the range of disturbance level examined, and the increase in total weight
reflects the added coil weight as the disturbance torque level is increased.

However, in figure 5-11, (for the largest disturbance level tested), it is
seen that peak coil torque (or coil weight) has begun to rise with coil gain.
If the simulations had been extended to even larger disturbance levels, the
optimum weight point would have required a wheel larger than the 2-pound
unit. In terms of figure 5-1, this means that the maximum wheel momentum
plot, shown constant at 0.08 lb-ft-sec, would begin to rise at some disturb-
ance level exceeding 500 dyne cm. Thus, while the combined weight vs coil
gain has approached an asymptote in all of the curves presented here, an
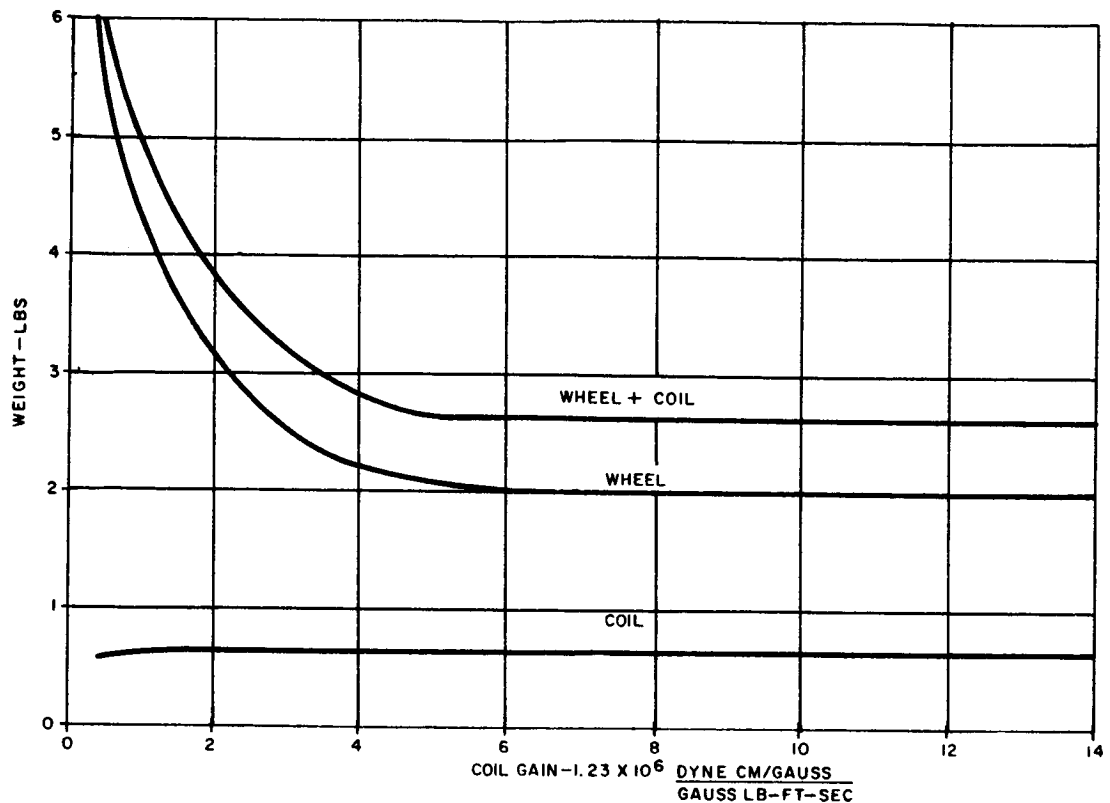
Figure 5-9. Actuation Weight vs Coil Gain, Disturbance Torque
= 100 Dyne-Cm (Pitch Axis Wheel and Yaw Axis Coil)

actual minimum would be reached in the general case for larger disturbance levels.

The foregoing curves reflect the momentum storage in the Y-axis and the coil weight in the Z-axis. It should be pointed out that the coil sizes in the X and Y axes must equal the coil size in the Z-axis in order that a true cross product operation be performed. Also, the momentum storage requirements in the X and Z axes are always less than in the Y axis as is shown in figure 5-12. Further, since most satellites are provided with a random orientation capability, the magnitude of the momentum storage provided in each axis should be equal. Thus the total optimum actuation
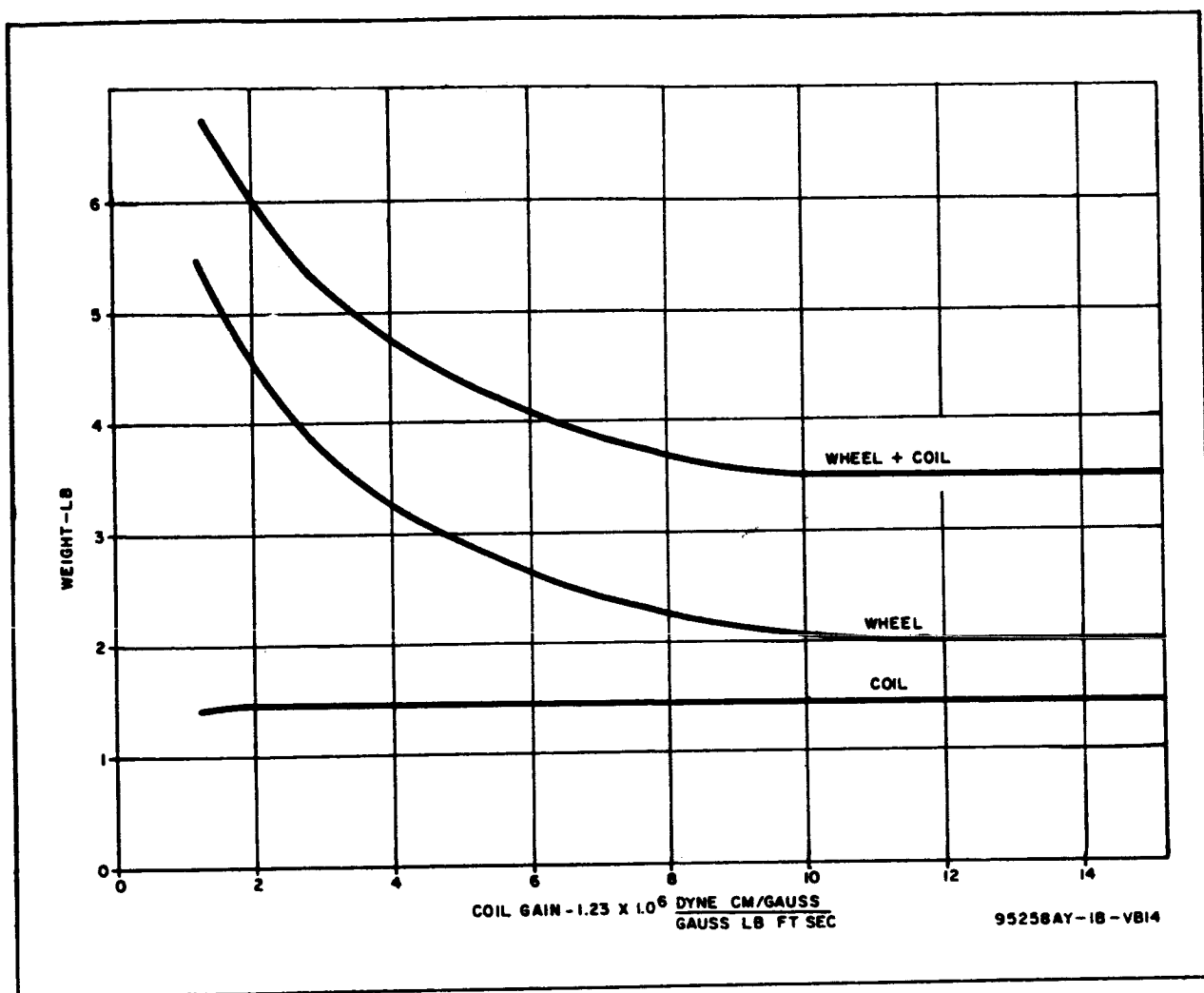
Figure 5-10. Actuation Weight vs Coil Gain. Disturbance Torque
= 200 Dyne-Cm (Pitch Axis Wheel and Yaw Axis Coil)

system weight is given by the following expression which holds true for the
disturbance range and orbit considered herein:

W = 3 (Wwy + KTd)

For the foregoing study, the wheel weight Wwy = 2 pounds, and K = 0.01
lb/dyne cm. Also for the range of the foregoing study, the optimum loop
gain is given by:

$$G_L = K_1 + K_2 T_D$$
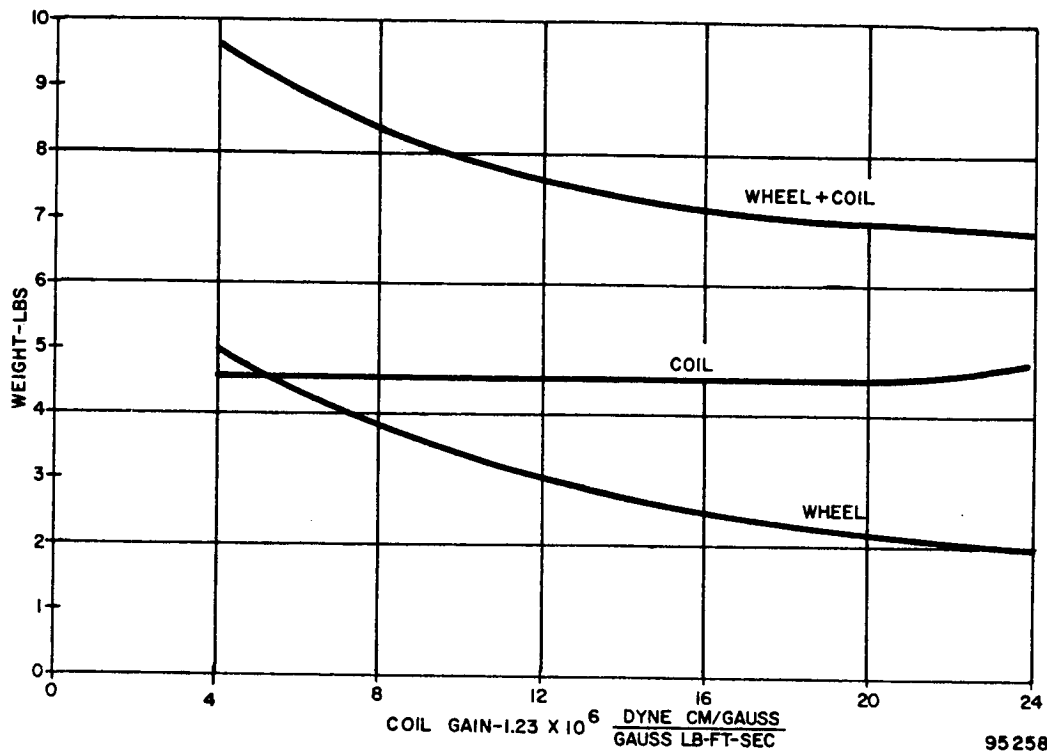
Figure 5-11. Actuation Weight vs Coil Gain, Disturbance Torque
= 500 Dyne-Cm (Pitch Axis Wheel to Yaw Axis Coil)
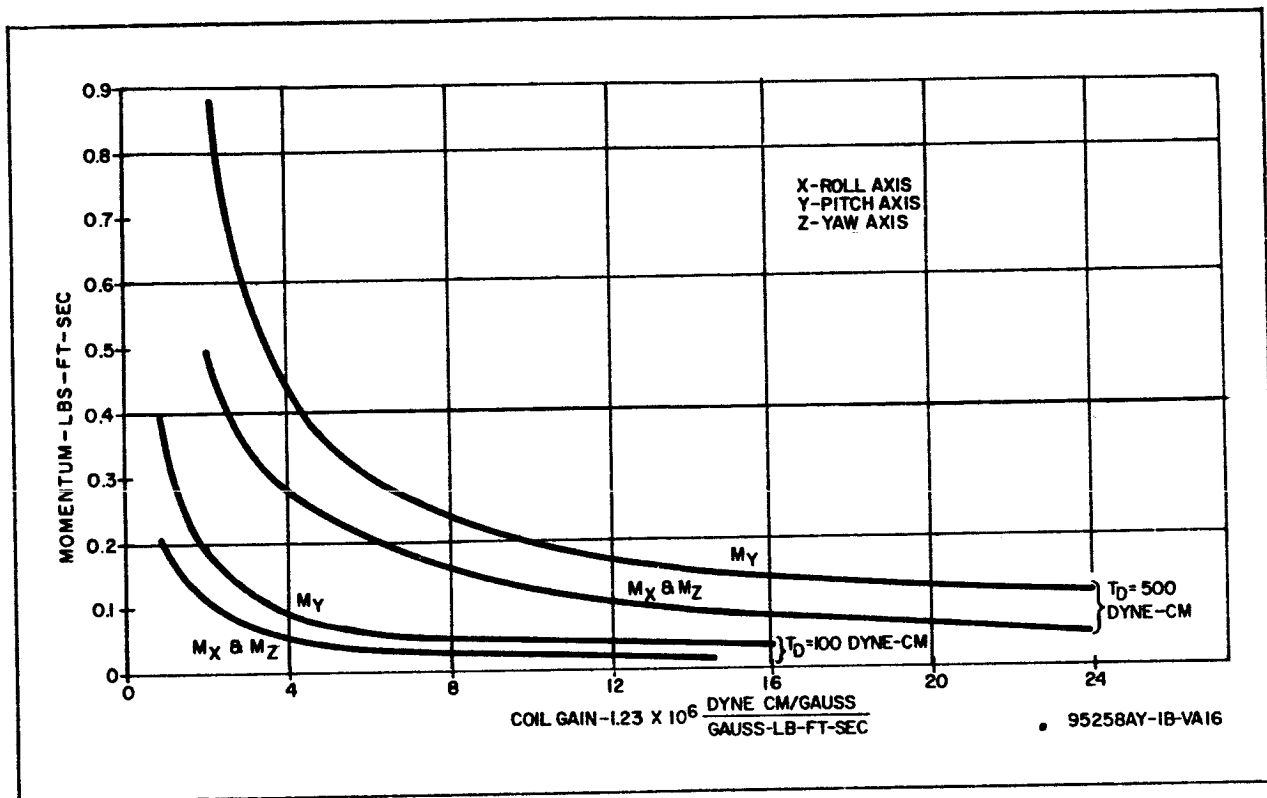
Figure 5-12. Three-Axis Momentum Storage vs Coil
Gain at Two Disturbance Levels (T_D)

6. TASK II - AUTOMATIC GAIN CHANGING

The computation of coil currents in the indirect electromagnetic actuation system is in accordance with the following expression:

$$\vec{I}_c = \vec{M} \times \vec{B}$$

The function performed by the electromagnetic actuation system is to reduce M to zero or to cause it to remain as close to zero as possible when disturbance torques are applied. With this mechanization, it may be seen that the current is dependent upon the magnitudes of $\vec{M}$ and $\vec{B}$ and hence as M is reduced in magnitude, so are the coil currents and the resulting corrective torques. Thus, it would appear that the time required to reduce M to zero would be infinite. In reality, the wheel rates never get below values which are determined primarily by the disturbance torque level and the loop gain. It would seem then in mechanizing the coil current computation equation that it would be desirable to make the coil current vector a unit vector. The mechanization of the coil current computation would then be:

$$\vec{I}_c = \frac{\vec{M} \times \vec{B}}{|M| \, |B^2|}$$

In so doing, the magnitude of the corrective torque would be independent of M and B which should bring about a considerably improved response and a greater momentum transfer capability for a given size actuation system.

The system was simulated as is shown in figure 6-1 and is the same as the wheels and coils simulation as shown in figure 5-2, except that the mechanization of the denominator term $|M|$ was added. The $|B^2|$ term was not mechanized because its variation is relatively insignificant (3/1) compared to the (100/1) variation of the $\vec{M}$ vector. Again recordings of the coil currents and wheel rates were made as a function of orbit position. Typical recordings are shown in figure 6-2. From these recordings, the peak coil

Figure 6-1. Simulation Diagram, Indirect System With AGC
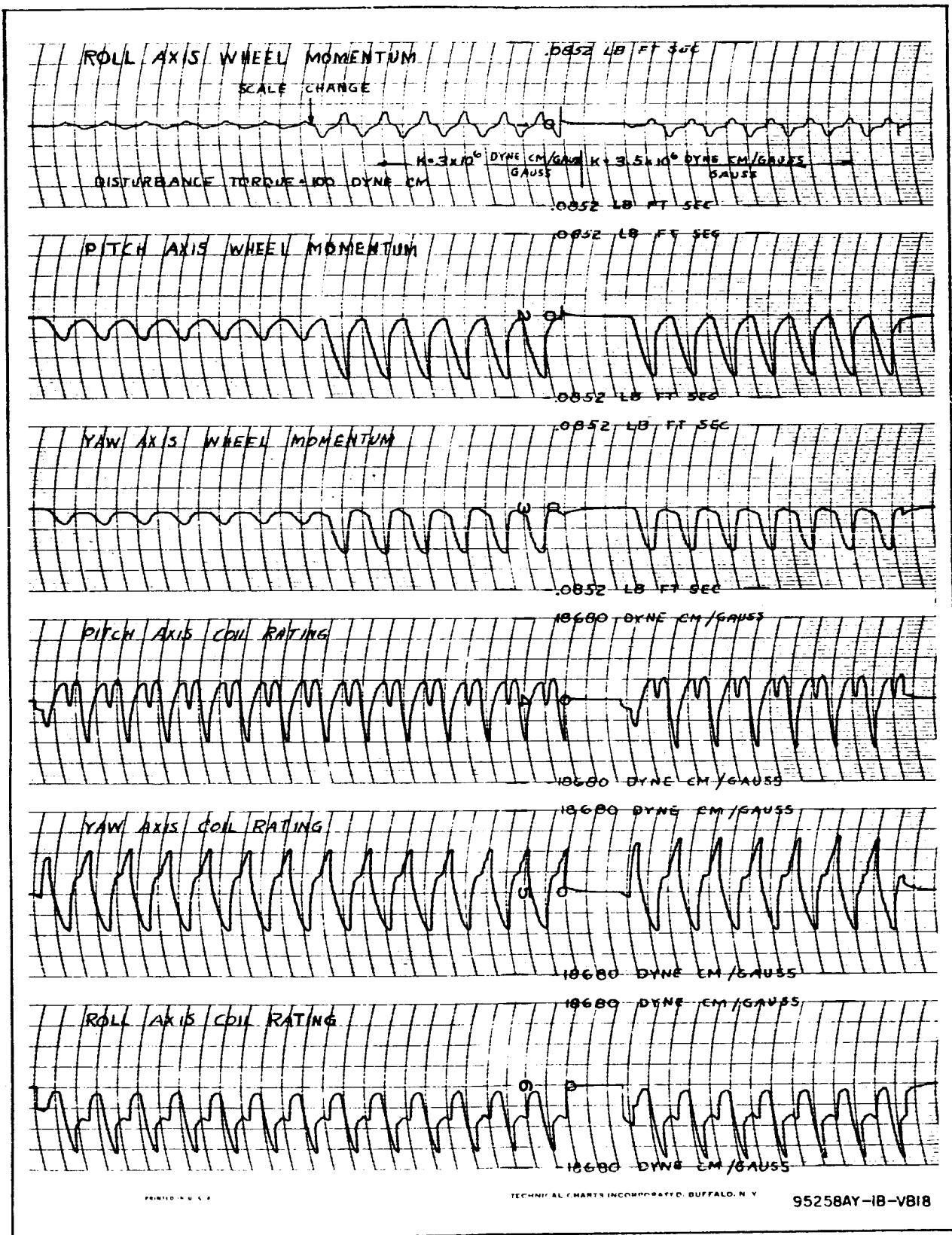
Figure 6-2. Results of Indirect Electromagnetic Actuation
Simulation With AGC

torque and the peak momentum storage requirement were determined and the optimum wheel plus coil weight versus gain curves were prepared for the usual spectrum of disturbance torque from 50 to 500 dyne-cm. Smaller coil gains are omitted because the system becomes unstable for coil gains below those shown. These curves are shown in figure 6-3. Reviewing these curves and comparing them to figures 5-8 through 5-11 which show the optimum weight for comparable disturbance levels without automatic gain control, it is obvious that no weight saving results from the use of AGC. Further, the analog circuitry required to square the ω_x, ω_y, and ω_z then sum ω_x^2, ω_y^2, and ω_z^2 then take the square root of the sum, and finally divide each component of coil current by the resultant $\sqrt{\omega_x^2 + \omega_y^2 + \omega_z^2}$ is extensive and complex. It is therefore recommended that AGC not be employed for removing inertia wheel momentums.
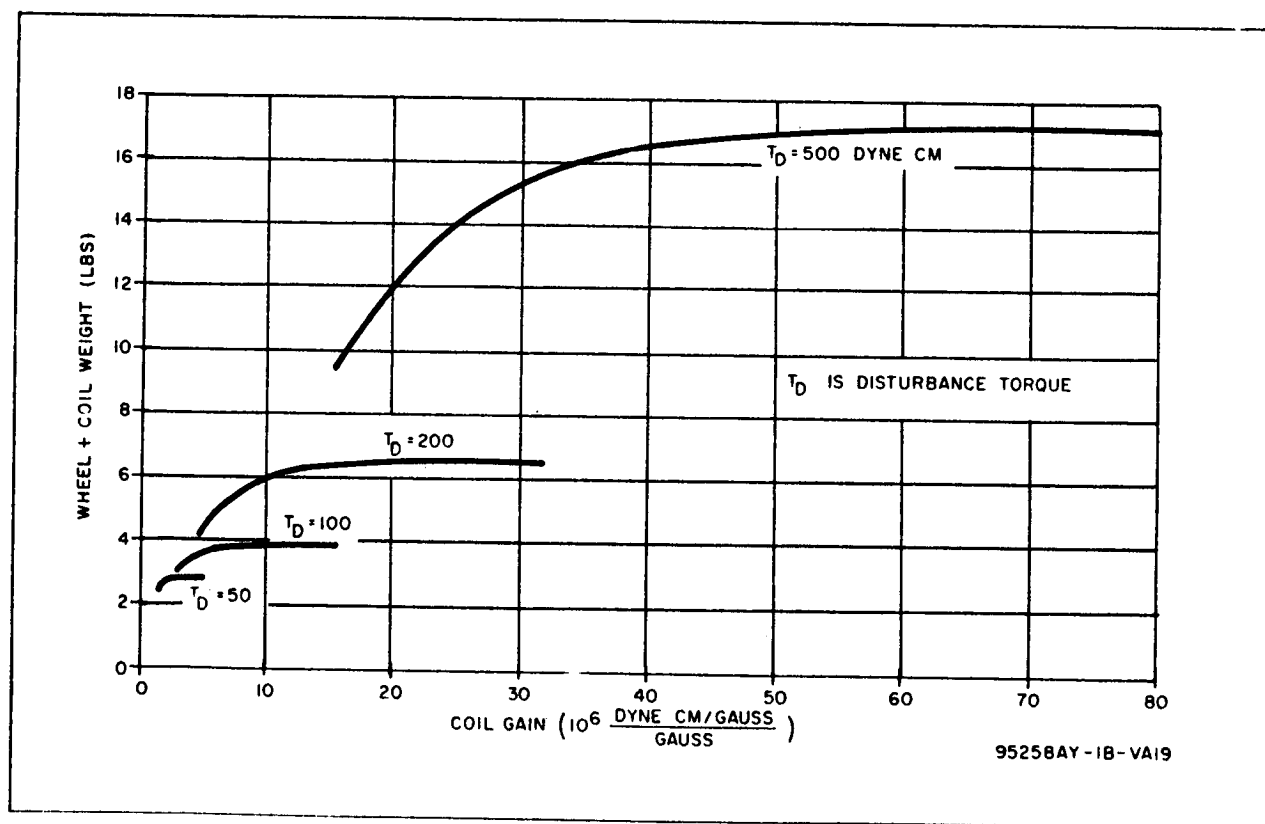
Figure 6-3. Actuation Weight Versus Coil Gain With AGC

The only form of AGC evolved which demonstrated usefulness is a form of step gain control. When removing the initial angular momentum from a satellite immediately after orbital injection, the time to remove the initial rates has been reduced significantly by the use of step AGC. In one particular mechanization, the angular rates of the vehicle were summed and the signal proportional to the sum was used to switch the loop gain in steps, as follows:

when

$$(|\omega_x| + |\omega_y| + |\omega_z|) > 1.0 \text{ deg/sec}, \quad G = 0.5$$

$$1.0 \text{ deg/sec} > (|\omega_x| + |\omega_y| + |\omega_z|) > 0.5 \text{ deg/sec}, \quad G = 1.0$$

$$0.5 \text{ deg/sec} > (|\omega_x| + |\omega_y| + |\omega_z|) > 0.25 \text{ deg/sec}, \quad G = 2.0$$

$$0.25 \text{ deg/sec} > (|\omega_x| + |\omega_y| + |\omega_z|) > 0.125 \text{ deg/sec}, \quad G = 4.0$$

The time required to reduce the initial rate of the vehicle from 1 deg/sec in each axis to a total vehicle rate of 50 deg/hour was reduced from 50 to 5 orbits with the step AGC. Thus, it is seen that improved response results with step AGC, and this form of AGC may prove useful in some applications.

7. TASK III - DIRECT MAGNETIC ACTUATION

7.1 PROBLEM STATEMENT

If the ratio of disturbance torque to vehicle inertia is sufficiently low, then it is not necessary to provide angular momentum storage aboard the vehicle. However, when the inertia wheel controls are eliminated from the vehicle, the wheel speed signals are no longer available to define the unwanted momentum stored aboard the vehicle and an alternate means must be provided. Essentially, the angular rates of the vehicle must be measured and this can be accomplished either with onboard rate gyros or by deriving the rate of change of position signals. The inclusion of rate gyros is not considered a desirable solution because of their low reliability and hence the rate of change of position signals is considered as the means of deriving angular rates of the vehicle. Tentatively, it is intended that the magnetometer and solar sensors be utilized to provide the position information from which the rates are derived. The purposes of the simulation study are to establish the band width of these position and rate signals and also to determine the relation between position error and disturbance torque level. In addition, the loop gain and coil sizes will be established.

7.2 SIMULATION METHOD AND TEST RESULTS

The simulation diagram of the "coils-only" system is shown in figure 7-1 and is similar to the indirect system simulation as shown in figure 5-2, except that the three integrators have been included to generate angular errors, and these position signals are summed with the rate signals. The coil current computation then becomes:

$$I_{cx} = (K_1 M_y + K_2 \theta) B_z + (K_1 M_z + K_2 \psi) B_y$$

$$I_{cy} = (K_1 M_z + K_2 \psi) B_x + (K_1 M_x + K_2 \phi) B_z$$

$$I_{cz} = (K_1 M_x + K_2 \phi) B_y + (K_1 M_y + K_2 \theta) B_x$$
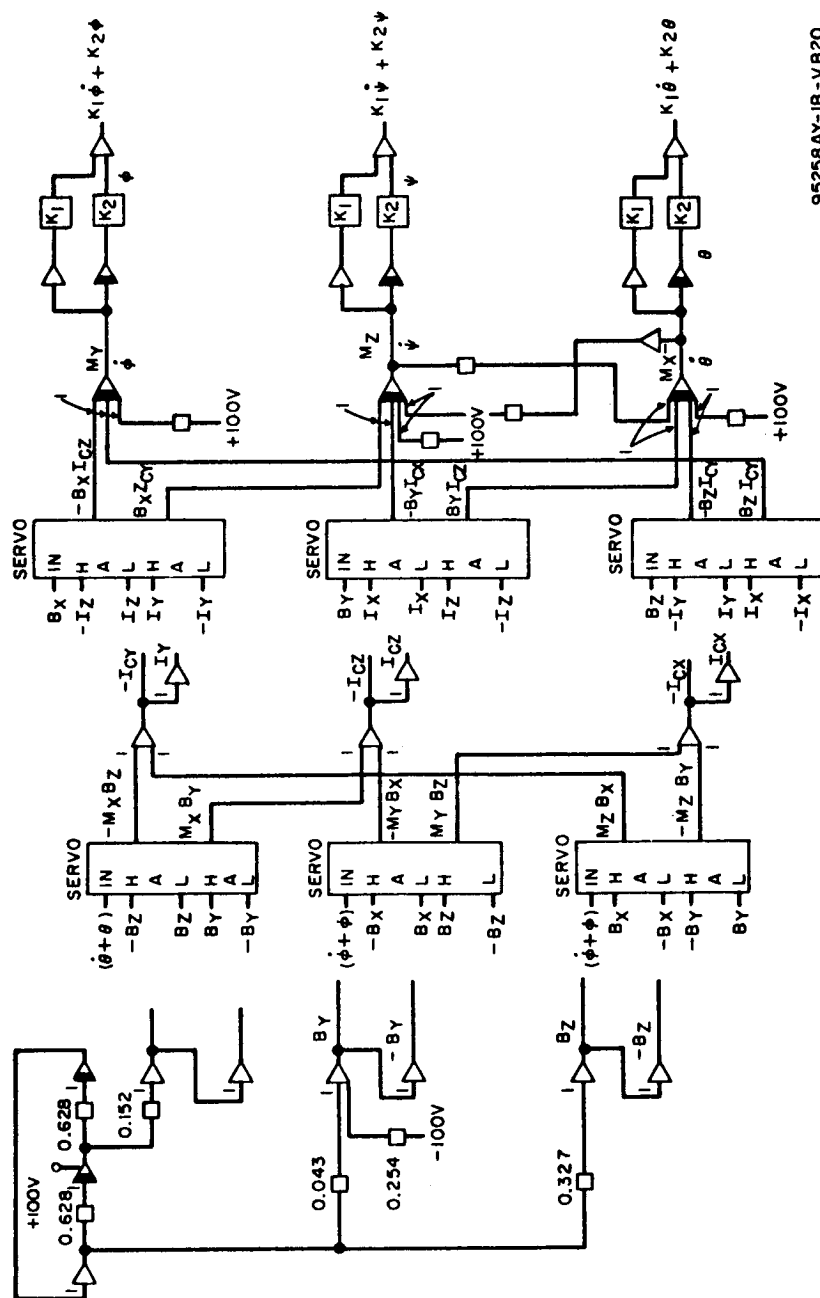
Figure 7-1. Simulation Diagram – Direct Electromagnetic Actuation System

95258AY-IB-VB20

As seen from the current equations, the same rate gains and position gains have been assumed for all three axes. The three rate and position gains were varied independently but no combination was found which significantly reduced the vehicle displacements.

As for the other systems, the earth's field components generated for the "coils only" simulation apply to an earth-oriented vehicle, which is valid for small displacements.

The voltage scaling for the simulation is described in Appendix A, paragraph A.2.

Figures 7-2 and 7-3 are oscillograph recordings of the vehicle rates and angles for two combinations of rate and position gain. The curves of figures 7-4 through 7-6 are the peak steady state values of the angles from several such recordings. Results from a 90-minute orbit and a 6-hour orbit are included to show that for the same disturbance torque, and the same absolute control torque (dyne-cm) in each orbit, the vehicle displacements increase with orbit time. This occurs because control torques cannot be generated about the earth's total field vector, which changes direction more slowly as the orbit time increases.

The same absolute control torques are produced in each orbit by making the coil gain and coil size larger for the higher altitude orbit, where the earth's field is weaker.

As seen in figures 7-4 through 7-6, the optimum combination of rate and position gains for the 6-hour orbit is:

$$K_1 = 8 \times 297 \ \frac{\text{dyne-cm/gauss}}{\text{gauss-deg/hour}}$$

$$K_2 \cong 4.2 \times 497 \ \frac{\text{dyne-cm/gauss}}{\text{gauss-deg}}$$

in all three axes. The vehicle displacement with these gains represent the smallest peak steady state displacements obtainable in a 6-hour orbit with constant 2 dyne-cm disturbance torques in each axis.
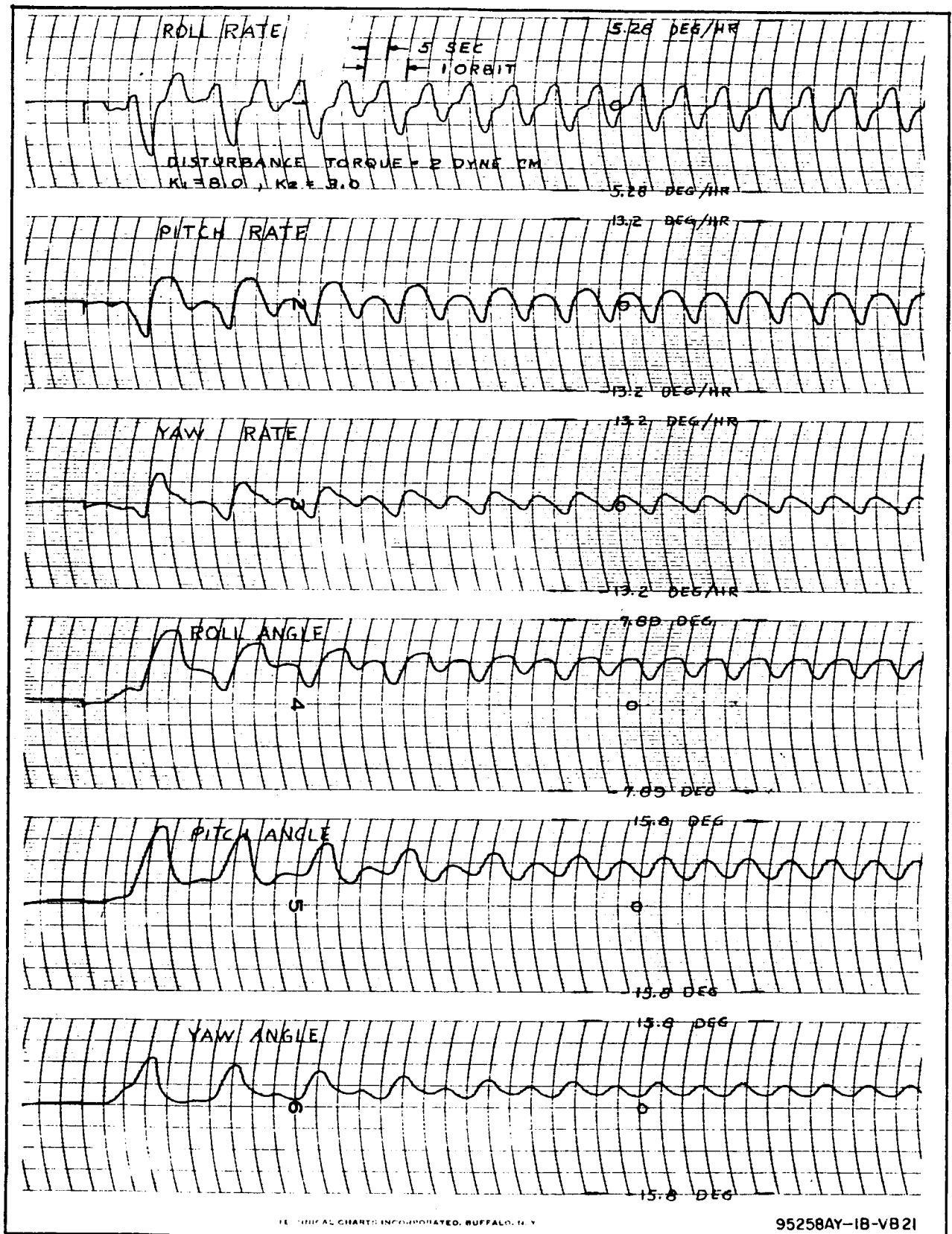
Figure 7-2. Results From Direct Electromagnetic
Actuation Simulation
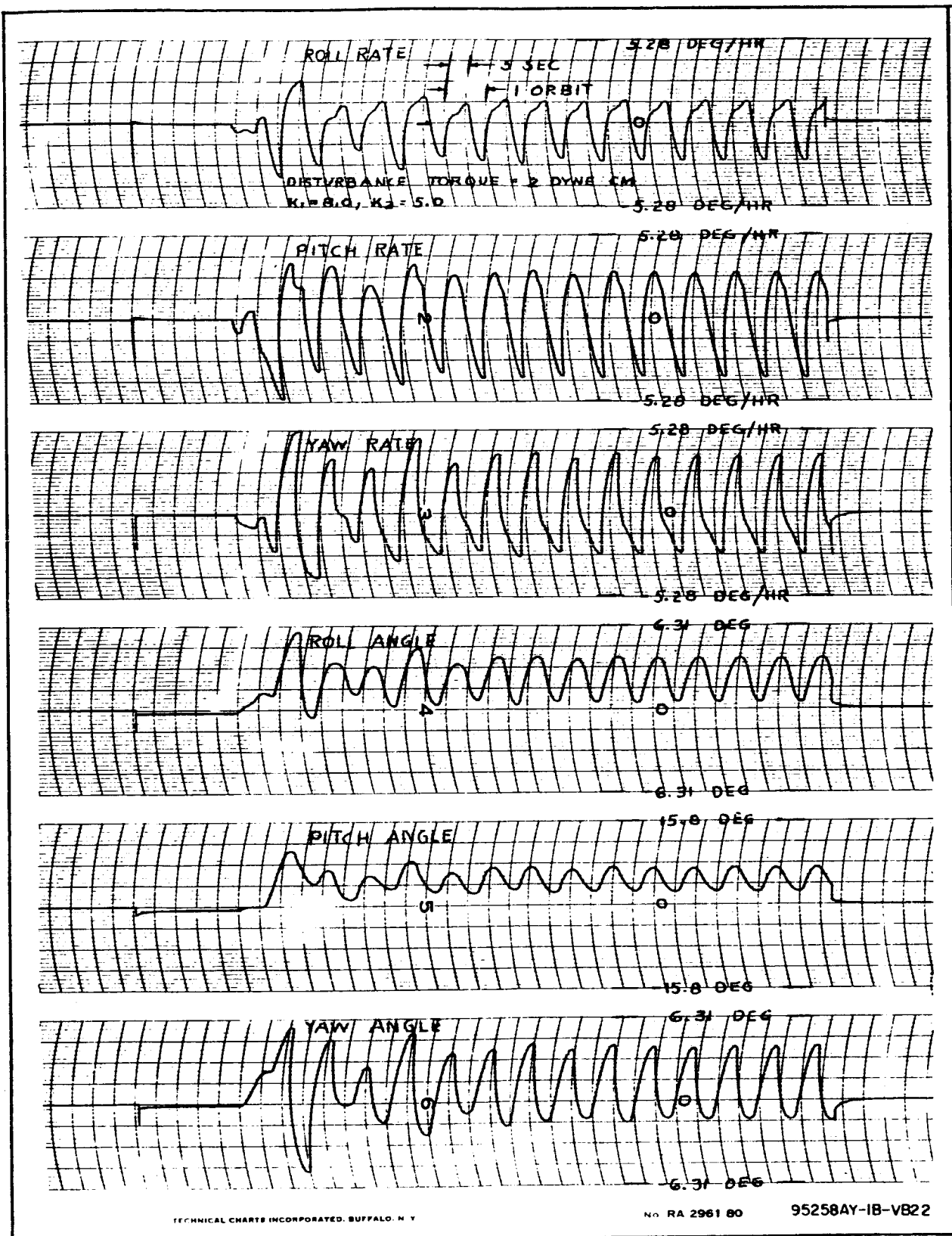
Figure 7-3.   Results From Direct Electromagnetic
Actuation Simulation
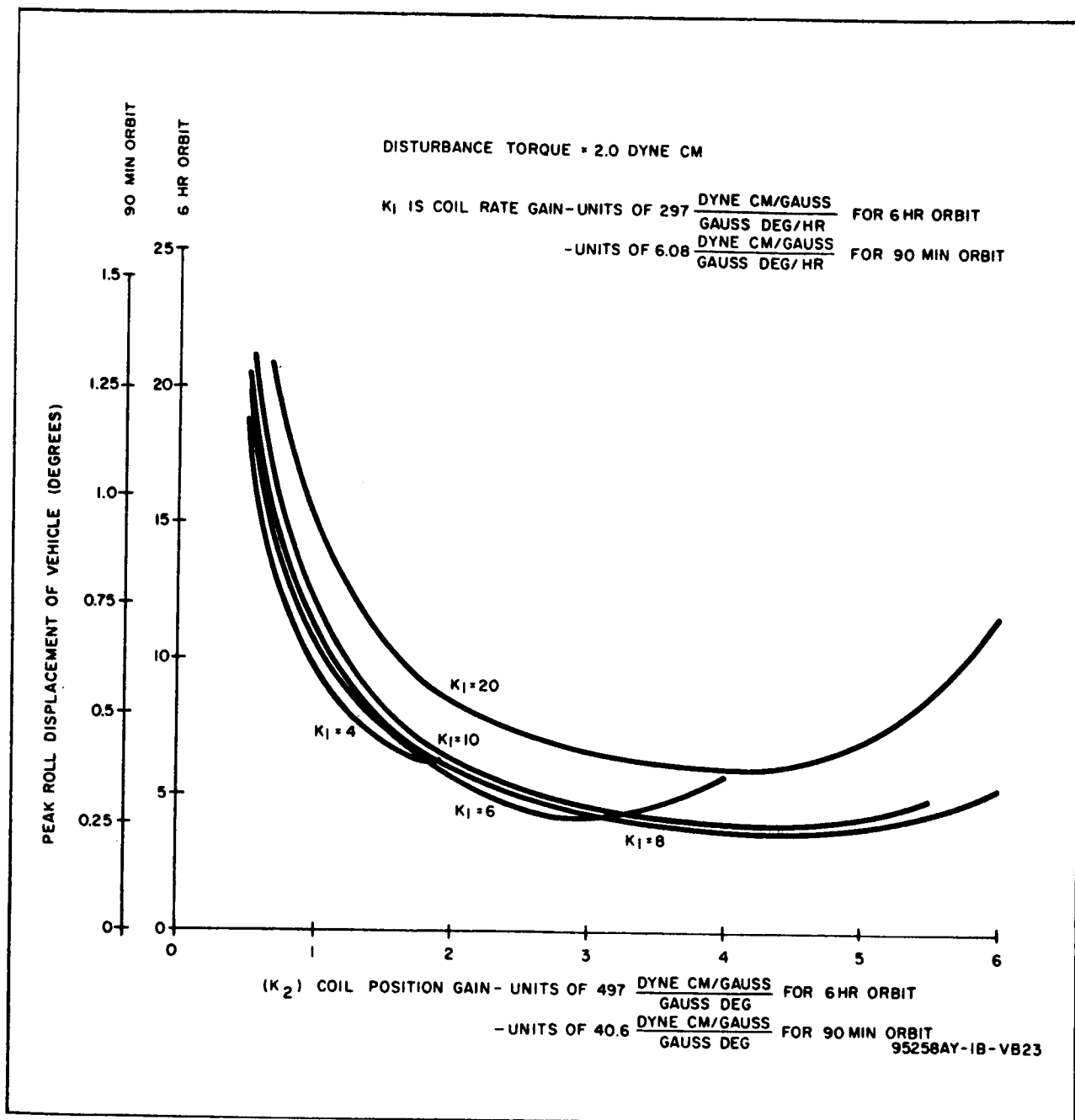
Figure 7-4. Peak Roll Displacement Versus Coil
Rate and Position Gains

Figure 7-7 shows the optimum peak vehicle displacement as a function of
orbit time. The curves were analytically derived from the 6-hour orbit data.
Since the earth's fields generated in the simulation are for an earth oriented
vehicle, the curves lose validity as the orbit time increases. The curves

DISTURBANCE TORQUE = 2.0 DYNE CM

K_1 IS COIL RATE GAIN—UNITS OF 297 $\frac{\text{DYNE CM/GAUSS}}{\text{GAUSS DEG/ H R}}$ FOR 6HR ORBIT

UNITS OF 6.08 $\frac{\text{DYNE CM/GAUSS}}{\text{GAUSS DEG/HR}}$ FOR 90 MIN ORBIT

90 MIN ORBIT

6 HR ORBIT

PEAK PITCH DISPLACEMENT OF VEHICLE (DEGREES)

3.125 — 50

2.5 — 40

1.875 — 30

1.25 — 20

0.625 — 10

0 — 0

$K_1 = 20$

10

4

6

8

0   0   1   2   3   4   5   6

(K2) COIL POSITION GAIN—UNITS OF 497 $\frac{\text{DYNE CM/GAUSS}}{\text{GAUSS DEG}}$ FOR 6HR ORBIT

UNITS OF 40.6 $\frac{\text{DYNE CM/GAUSS}}{\text{GAUSS DEG}}$ FOR 90 MIN ORBIT

95258AY-1B-VA24

Figure 7-5. Peak Pitch Displacement Versus Coil
Rate and Position Gains

are sufficiently accurate to approximately a 6-hour orbit, but beyond this
they merely indicate the trend of increasing displacements due to the earth's
total field vector changing direction more slowly.
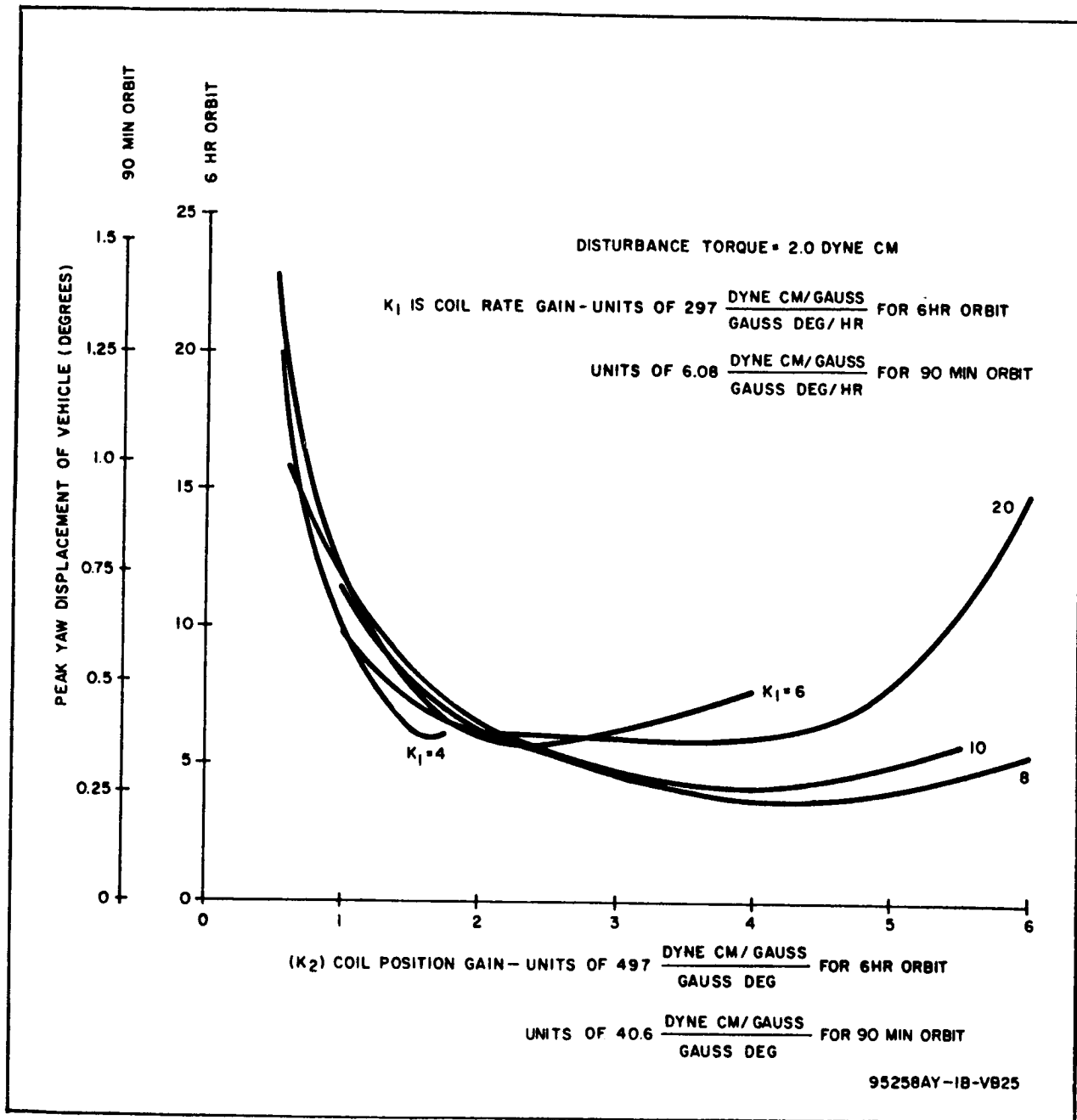
Figure 7-6. Peak Yaw Displacement Versus Coil
Rate and Position Gains
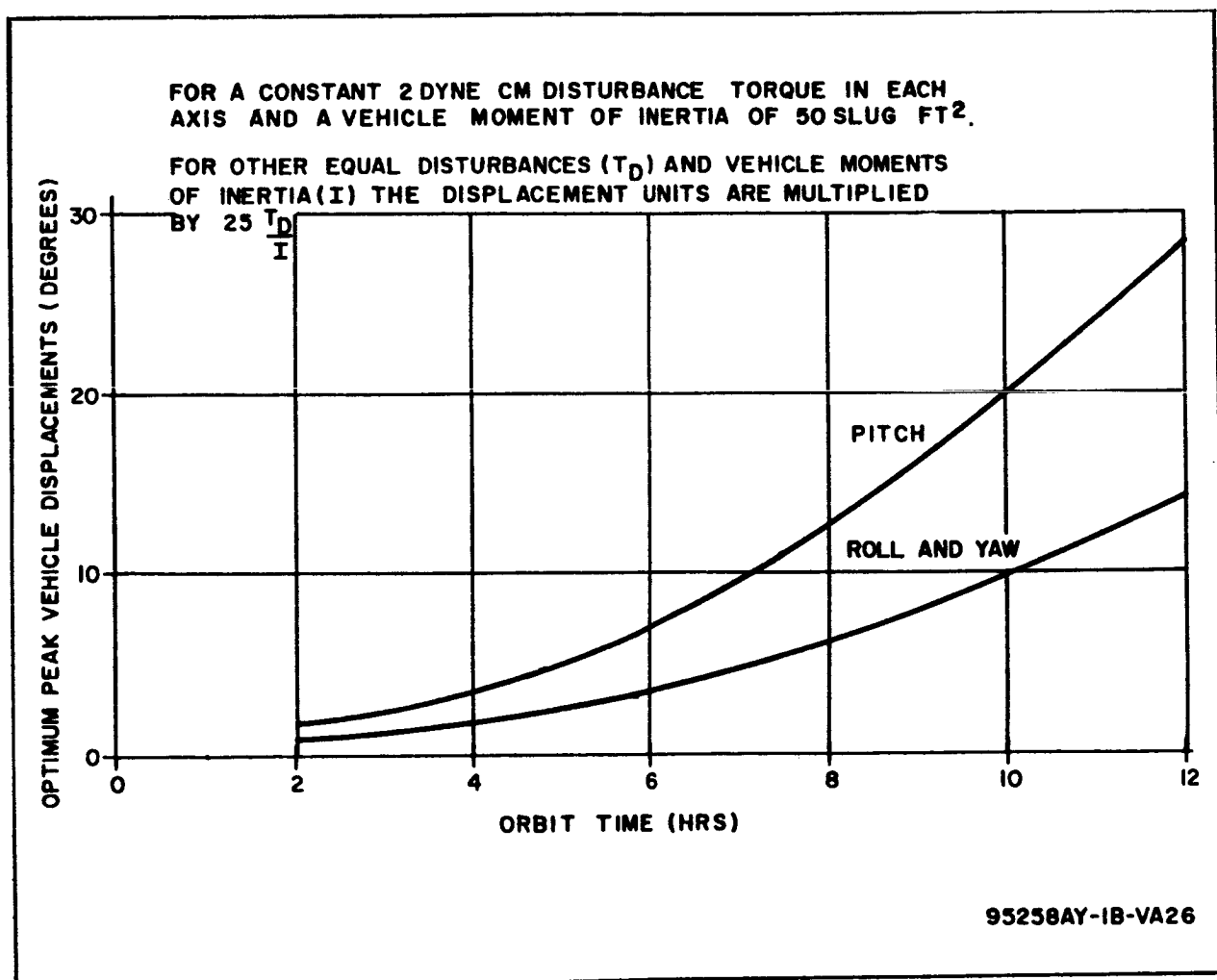
Figure 7-7. Optimum Peak Vehicle Displacement
Versus Orbit Time

8. ELECTROMAGNETIC ACTUATOR DESIGN

8.1 SCOPE OF STUDY

A reasonable body of literature exists concerning control of satellite attitude through generation, within the satellite, of a magnetic field which reacts with the terrestrial field to produce the torque required for proper attitude orientation. In the literature, an air-cored coil has been assumed as the device for field generation. The present task was performed to see if an iron-cored solenoid might be more efficient than air-cored coils and, if so, to arrive at useful design equations and techniques.

In judging efficiencies, some parameter must be chosen which will be a meaningful measure of diverse properties for comparative purposes. For a long-lived satellite application the parameter chosen was minimum total mass placed in orbit. Total mass is defined here as the mass of the actuator plus the mass of the solar cell power supply required to provide continuously the maximum power for which the actuator is designed. The design of actuators for this contract assumed an oriented solar cell array capable of delivering 1 watt for every 388 grams of power supply.

8.2 CRITERIA FOR AIR-CORED COIL OPTIMIZATION

To provide an objective criterion with which the performance of iron-cored solenoids can be compared, the design of air-cored coils was optimized with respect to minimum total mass. In this derivation it is assumed that the shape of the satellite is approximately spherical, that the coil can be wound about the outer periphery of the satellite, and that the coil will have a square cross section, the dimensions of which are very small compared to the diameter. The last assumption introduces second order errors which, for diameters greater than 1 meter and torques less than 5×10^{-4} newton-meter, should not exceed 10 percent of the calculated power and mass.

The following symbols are defined for use in this derivation:

T = torque

N = number of turns

A = area included by coil

B_t = terrestrial field

I = coil current

D = coil diameter

P = power to coil

ρ = resistivity of wire material

a = cross section area of conductor

k = mass-to-power ratio of power supply

M_w = mass of the wire

M_{ps} = mass of power supply

M_t = total mass of system

R = d-c resistance of coil

g_w = density of wire material

(mks units are used throughout)

Assuming that the terrestrial field is directed orthogonally to the normal to the plane of the coil, the resulting torque can be expressed as:

$$T = NIAB_t \qquad (8-1)$$

Since the coil area may be expressed (with regard to the assumptions) as $\pi \dfrac{D^2}{4}$, equation 8-1 may be written:

$$T = \pi NI \, B_t \frac{D^2}{4} \qquad (8-2)$$

The resistance of the coil may be approximated by:

$$R = \pi ND \frac{\rho}{a}$$

and the power then is:

$$P = \pi ND \rho \frac{I^2}{a}$$

Hence the mass of the power supply is:

$$M_{ps} = k \pi ND \rho \frac{I^2}{a}$$

The mass of the wire in the coil is nearly:

$$M_w = \pi \, ND \, a \, g_w$$

and the total system mass $(M_{ps} + M_w)$:

$$M_t = \frac{k \, \pi \, ND \, \rho \, I^2}{a} + \pi \, ND \, a \, g_w \tag{8-3}$$

By rearranging equation 8-2, an expression for N may be obtained:

$$N = \frac{4T}{\pi} \, I \, B_t \, D^2 \tag{8-4}$$

Substituting equation 8-4 into equation 8-3:

$$M_t = \frac{4T}{D \, B_t} \left(\frac{k \, I \, \rho}{a} + \frac{a \, g_w}{I} \right) \tag{8-5}$$

To minimize the total mass with respect to current, equation 8-5 can be differentiated with respect to I, the result set equal to zero, the value of I for minimum mass obtained, and this value substituted into equation 8-5 to obtain minimum total mass. When these operations are performed:

$$M_t = \frac{8 \, T}{D \, B_t} \, (k \, \rho \, g_w)^{\frac{1}{2}} \tag{8-6}$$

Other useful expressions can be derived such as current density in the conductor:

$$\frac{I}{a} = \left(\frac{g_w}{k\rho} \right)^{\frac{1}{2}} \tag{8-7}$$

power consumption:

$$P = \frac{4T}{B_t \, D} \left(\frac{g_w \, \rho}{k} \right)^{\frac{1}{2}} \tag{8-8}$$

power consumption per unit torque:

$$\frac{P}{T} = \frac{4}{B_t \, D} \left(\frac{g_w \, \rho}{k} \right)^{\frac{1}{2}} \tag{8-9}$$

and total mass per unit torque:

$$\frac{M_t}{T} = \frac{8}{D B_t} (k \rho g_w)^{\frac{1}{2}} \tag{8-10}$$

While the approximations given in equations 8-2 through 8-10 will introduce errors, they were derived only to serve as a basis of comparison for the iron-cored solenoids. A more rigorous, complicated approach would give answers which would tend to be more favorable to the iron-cored solenoids. The equations given above, then are worst-case conditions for the iron-cored actuators which are the primary concern of this task.

8.3 OPTIMIZED DESIGN OF IRON-CORED ACTUATORS

In addition to symbols defined previously, the following symbols will be used:

M = magnetization per unit volume

V_i = volume of iron

B = induction or flux density

T_b = torque produced by iron

T_i = maximum torque

T_c = torque produced by windings

H = effective magnetic field intensity

H_a = applied magnetic field intensity

μ_o = permeability of freespace

μ_i = intrinsic permeability

μ_r = relative permeability

A_c = mean area of coil

8.3.1 Derivation of Somewhat Idealized Equations

The torque produced by the iron bar can be expressed vectorially as:

$$T_b = V_i (M \times B_t) \tag{8-11}$$

As with the air-cored coils of the preceding section, it will be assumed that the terrestrial field is directed orthogonally to the magnetization vector and the maximum torque can then be written:

$$T_i = MV_i \, B_t \qquad (8-12)$$

Since the magnetization of a core is a difficult parameter with which to deal, a more familiar parameter B will be introduced which is related to M by:

$$M = \frac{B}{\mu_o} - H$$

Substituting this in equation 8-12:

$$T_i = (\frac{B}{\mu_o} - H) \, V_i \, B_t \qquad (8-13)$$

Recognizing that $B = \mu_i H$ and $\mu_i = \mu_o \mu_r$, equation 8-13 can be written:

$$T_i = (\mu_r - 1) \, H \, V_i \, B_t \qquad (8-14)$$

Because of the demagnetizing effects associated with the geometry of the cylindrical cores to be used, the field H_a generated by the solenoidal winding is not equal to the field H which determines the induction state of the material. As a result of the demagnetizing effects, the effective field is related to the applied field by the expression:

$$H = H_a - \frac{L}{4\pi} (\frac{B}{\mu_o} - H) \qquad (8-15)$$

where $\frac{L}{4\pi}$ is the demagnetizing factor.

Upon appropriate substitution ($B = \mu_i H$) and after further manipulation, equation 8-15 can be written:

$$H = \frac{H_a}{1 + (\mu_r - 1) \frac{L}{4\pi}} \qquad (8-16)$$

Since $B_m = \mu_o \mu_r H$ when H is at some maximum, equation 8-16 can be written (recognizing that $\mu_r \gg 1$):

$$H_a = \frac{B_m}{\mu_o} (\frac{1}{\mu_r} + \frac{L}{4\pi}) \qquad (8-17)$$

Combining equations 8-14, 8-16, and 8-17:

$$T_i = \frac{H_a V_i B_t}{(\frac{1}{\mu_r} + \frac{L}{4\pi})}$$ (8-18)

or

$$T_i = \frac{B_m B_t V_i}{\mu_o}$$ (8-18a)

For some design calculations equation 8-18a is written in terms of the bar dimensions

$$m = 2 \left(\frac{\mu \mu_o T_i}{\pi \ell B_m B_t}\right)^{\frac{1}{2}}$$ (8-18b)

where the dimensions are defined in figure 8-1.

95258AY-IB-VA27
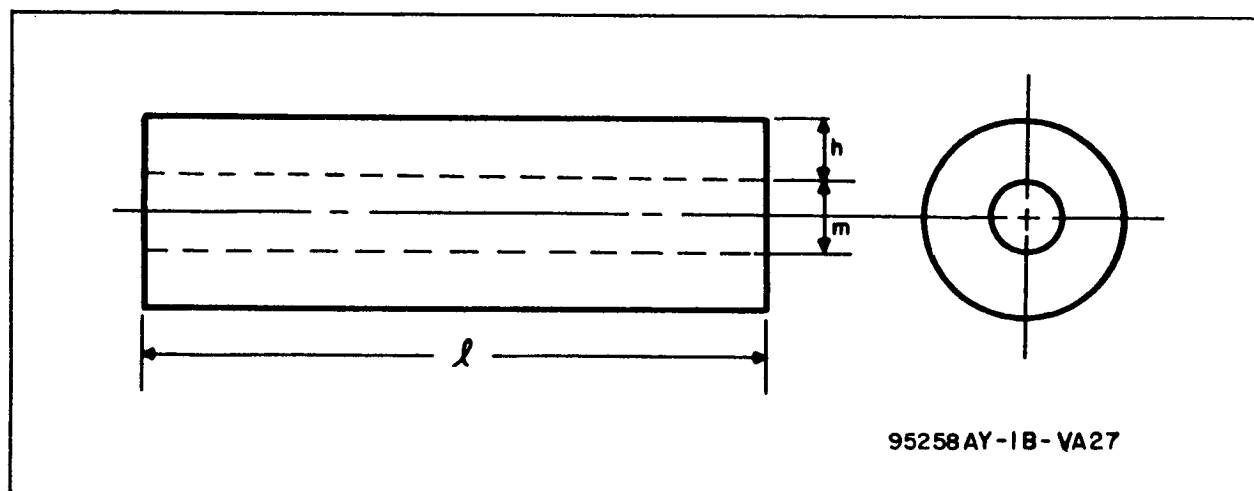
Figure 8-1. Dimensions of Core-Coil Combination

In addition to the torque produced by the iron, there is a torque produced independently by the current flowing in the solenoidal winding. This torque T_c can be expressed as

$$T_c = NI A_c B_t$$ (8-19)

Because the magnetic field intensity applied to the iron core is produced by the current in the windings, and is related to it by $H_a \ell = NI$, equation 8-19 can be written in terms of H_a:

8-6

$$T_c = H_a \ell A_c B_t \qquad (8\text{-}20)$$

The total torque T_t produced by the system is the sum of T_c and T_i and is written

$$T_t = H_a B_t \left[\frac{V_i}{\left(\dfrac{1}{\mu_r} + \dfrac{L}{4\pi}\right)} + \ell A_c \right] \qquad (8\text{-}21)$$

It is more convenient, for design calculations, to write equation 8-21 in terms of physical dimensions of the actuator and magnetic properties of the core used. The meaning of the dimensional symbols is given in figure 8-1. In rewriting equation 8-21 it is assumed that:

    a. The length of the winding is equal to the length of the core.

    b. The mean winding area effective in producing the torque due to the coil is expressed as $A_c = \pi (m^2 + 2\,mh + 2h^2)/4$

    c. The core volume is expressed as $V_i = \pi m^2 \ell /4$

Substituting equation 8-17 and the dimensional relationships into equation 8-21 the expression for total torque becomes:

$$T_t = \frac{\pi B_m B_t \ell}{4 \mu_o} \left\{ m^2 + \left[m^2 + 2h\,(m + h) \right] \left(\frac{1}{\mu_r} + \frac{L}{4\pi} \right) \right\} \qquad (8\text{-}22)$$

As a convenience in further mathematical manipulations, a new variable will be defined as the ratio of the volume of the winding to the volume of the iron:

$$\psi = \frac{4h\,(m + h)}{m^2} \qquad (8\text{-}23)$$

Equation 8-23 is needed, for design purposes, in the form:

$$h = \frac{m}{2} \left[(\psi + 1)^{\frac{1}{2}} - 1 \right] \qquad (8\text{-}23a)$$

Expressing equation 8-22 in terms of the new variable

$$T_t = \frac{\pi B_m B_t m^2 \ell}{4 \mu_o} \left[1 + \left(1 + \frac{\psi}{2}\right) \left(\frac{1}{\mu_r} + \frac{L}{4\pi} \right) \right] \qquad (8\text{-}24)$$

Expressions for power and mass will now be derived. Additional quantities will be defined as:

P = power

$M_{(x)}$ = mass of x

d = diameter of insulated wire

d_1 = diameter of bare wire

s = area space factor of winding

ρ = resistivity of wire material

g_i = density of core material

g_w = density of bare wire

It was originally assumed that the mass of the wire insulation would be negligible with respect to the mass of the conductor material and g_w was defined accordingly. Subsequently, it was found that the error introduced by this simplifying assumption is a function of wire size and a more accurate expression can be obtained if the value used for g_w is increased to the density of the insulated wire. Since handbook values of the density of insulated wires are not obtainable, it was decided to accept a nominal error and derive the expressions in terms of values which are available to a designer. An additional assumption made in these derivations is that no interlayer insulation is used in constructing the windings.

A cross section of turns wound to achieve a maximum space factor for round wire is illustrated in figure 8-2. It can be shown that the number of turns which can be wound in this manner is:

$$N = (s^{\frac{1}{2}} \frac{\ell}{d}) (s^{\frac{1}{2}} \frac{h}{d \sin \frac{\pi}{3}})$$

$$= 1.15 \, \ell \, h \, s/d^2 \tag{8-25}$$

The current can be expressed as a function of the magnetic field intensity it produces, $I = H_a \ell / N$ and by substituting equations 8-21 and 8-25 into this expression:

$$I = \frac{0.866 \, d^2 \, B_m}{\mu_o \, h \, s} (\frac{1}{\mu_r} + \frac{L}{4\pi}) \tag{8-26}$$
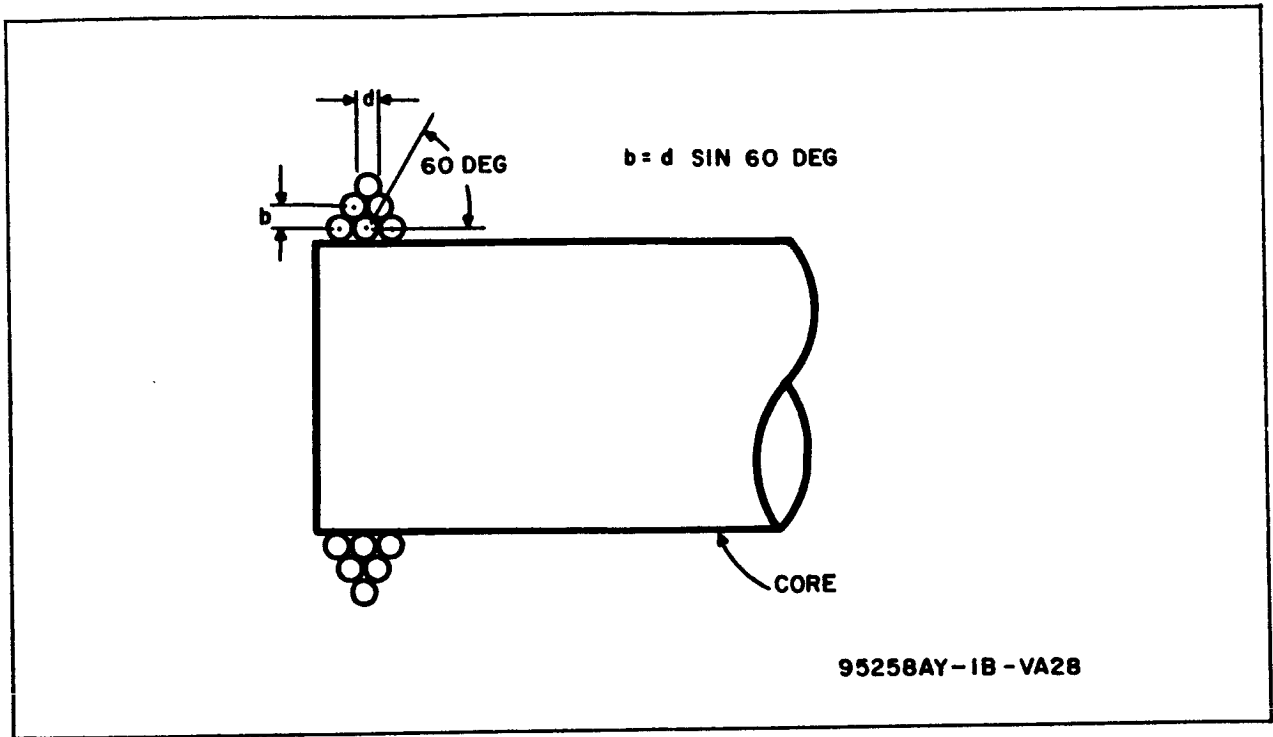
Figure 8-2. Cross Section of Winding

The resistance of the coil can be expressed in terms of the wire parameters. The wire length ℓ_w can be found from the mean length of turn, $\pi (m + h)$, and the number of turns, equation 8-25:

$$\ell_w = \frac{1.15 \, \pi \ell s \, h \, (m + h)}{d^2} \tag{8-27}$$

The conductor area is given by $\pi \, d_1^2/4$ and the resistance can be found from the expression:

$$R = \rho \ell_w / A_w$$

$$= 4.60 \, \rho \ell s \, h \, (m + h)/(d_1 \, d)^2 \tag{8-28}$$

The voltage V appearing across the actuator terminals when nominal current I is flowing can be expressed as the product of equations 8-26 and 8-28:

$$V = \frac{4 \, \rho \ell (m + h) \, B_m}{\mu_o \, d_1^2} \left(\frac{1}{\mu_r} + \frac{L}{4\pi} \right) \tag{8-29}$$

8-9

The power dissipated is the product of equations 8-26 and 8-29:

$$P = \frac{3.464 \, \rho \, \ell \, (m + h) \, B_m^{\,2}}{\mu_o^{\,2} \, h \, s} \left(\frac{d}{d_1}\right)^2 \left(\frac{1}{\mu_r} + \frac{L}{4\pi}\right)^2 \qquad (8\text{-}30)$$

Or, expressing P in terms of the variable ψ, equation 8-30 becomes:

$$P = \frac{3.464 \, \rho \, \ell \, B_m^{\,2}}{\mu_o^{\,2} \, s} \left(\frac{d}{d_1}\right)^2 \left(\frac{1}{\mu_r} + \frac{L}{4\pi}\right)^2 \frac{\left[1 + (1 + \psi)^{\frac{1}{2}}\right]^2}{\psi} \qquad (8\text{-}31)$$

The mass of the actuator M_a can be expressed as the sum of the products of the volume and density of each material used. The wire volume is $A_w w$ and the volume of the iron is $\pi \, m^2 \ell / 4$. Multiplying by the densities and summing

$$M_a = 1.15 \, g_w \, \pi^2 \ell \, sh \, (m + h) \left(\frac{d_1}{d}\right)^2 / 4 + \pi \, m^2 \ell \, g_i / 4 \qquad (8\text{-}32)$$

Introducing the variable ψ again and using a modified form of equation 8-17, equation 8-32 can be written:

$$M_a = \frac{T_i \, \mu_o}{B_m \, B_t} \left[g_i + 0.288\pi \, g_w \, s \left(\frac{d_1}{d}\right)^2 \psi \right] \qquad (8\text{-}33)$$

It has been stated earlier that the proper criterion to be used in comparing actuators is the total mass of the system which includes the power supply. If it is assumed that the power supply can be characterized by a mass to power ratio expressed as a constant k, in kilograms per watt, then the total system mass is the sum of the actuator mass and the product of k and the maximum power required by the actuator:

$$M_t = M_a + k \, P \qquad (8\text{-}34)$$

Making the appropriate substitutions, equation 8-34 can be written

$$M_t = \frac{T_i \, \mu_o}{B_m \, B_t} \left[g_i + 0.288\pi g_w \, s \left(\frac{d_1}{d}\right)^2 \psi \right] + \frac{3.464k \, \rho \, \ell \, B_m^{\,2}}{\mu_o^{\,2} \, s} \left(\frac{d}{d_1}\right)^2 \left(\frac{1}{\mu_r} + \frac{L}{4\pi}\right)^2 \frac{\left[1 + (1 + \psi)^{\frac{1}{2}}\right]^2}{\psi} \qquad (8\text{-}35)$$

It is seen that equation 8-35 expresses the total mass as a function of the torque due to the iron alone. As will be discussed later, this form of the total mass expression is the easiest to use for design purposes but for completeness, the total mass in terms of total torque will be given.

$$M_t = \frac{T_t \mu_o}{B_m B_t} \frac{\left[g_i + 0.288\,\pi g_w s\left(\frac{d_1}{d}\right)^2 \psi\right]}{\left[1 + (1+\psi/2)\left(\frac{1}{\mu_r} + \frac{L}{4\pi}\right)\right]} + \frac{3.464 k\rho \ell B_m^2}{\mu_o^2\, s}\left(\frac{d}{d_1}\right)^2\left(\frac{1}{\mu_r} + \frac{L}{4\pi}\right)\frac{\left[1+(1+\psi)^{\frac{1}{2}}\right]^2}{\psi}$$

(8-36)

Since it can be shown that, to a first approximation, the power required to produce a given magnetic field intensity is independent of wire size, it will be recognized that the variable which determines the mass of the power supply as well as the mass of the coil is the coil volume. As coil volume is increased (for a fixed magnetic field intensity), the power supply mass decreases and the coil mass, hence the actuator mass, increases. A coil volume must exist, then, which will optimize the actuator design with respect to minimum total mass of the system. Because, for a given magnetic material, the mass of the core is proportional to core volume and since, in almost all cases, the total torque is almost independent of coil volume and is dependent only on core volume, the ratio ψ will, for a given torque, vary directly with coil volume. Therefore, if equation 8-35 is differentiated with respect to ψ to obtain a minimum total mass, only second-order errors are introduced compared to the more rigorous but much more complicated procedure of differentiating equation 8-36 with respect to coil volume. Differentiating equation 8-35 with respect to ψ, equating the result to zero, and solving for ψ yields:

$$\frac{\left[1+(1+\psi)^{\frac{1}{2}}\right]^2}{\psi^2(1+\psi)^{\frac{1}{2}}} = \frac{0.0832\,\pi \mu_o^3 g_w s^2}{k\rho B_t B_m^3 \ell\left(\frac{1}{\mu_r}+\frac{L}{4\pi}\right)^2}\left(\frac{d_1}{d}\right)^4 T_i$$

(8-37)

The expression on the left-hand side of equation 8-37 is defined as $f(\psi)$ and cannot be solved explicitly for ψ. However, it yields readily to numerical analysis and a curve of ψ as a function of $f(\psi)$ over the range of interest is

given in figure 8-3.   The value of ψ obtained can be substituted into equation 8-36 and the minimum total mass capable of producing the desired torque in the desired length is obtained.

$$F(\psi) = \left[\frac{1 + (1+\psi)^{1/2}}{\psi^2(1+\psi)^{1/2}}\right]^2$$

95258AY-1B-V829
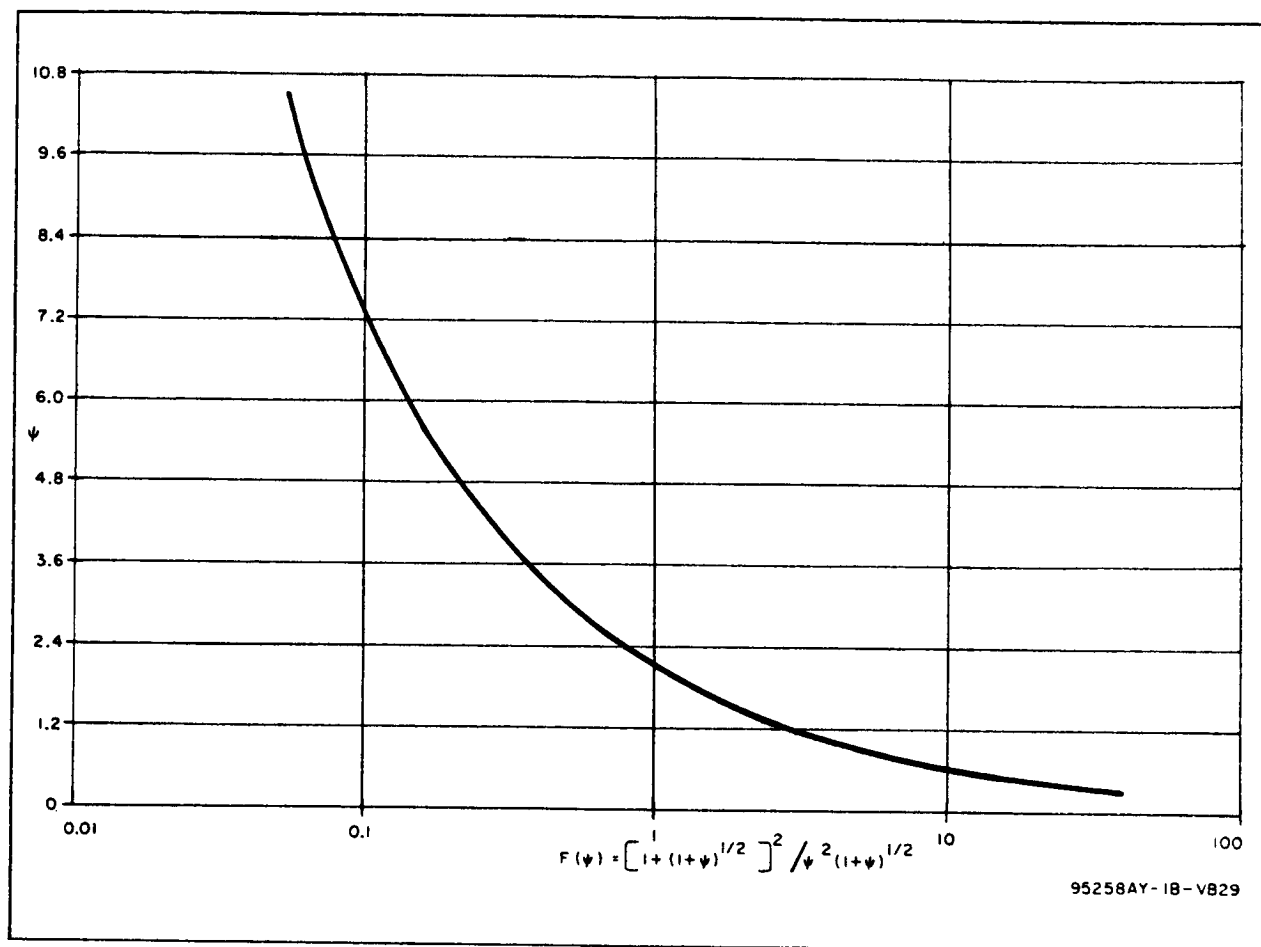
Figure 8-3. ψ Versus $f(\psi)$

8.3.2   Empirical Corrections to Idealized Conditions

In deriving many of the expressions in paragraph 8.3.1, it was assumed that the flux density within the iron was uniform along the length of the bar. The actual distribution is indicated in figure 8-4.   In this figure the ratio e_o/e_m is plotted as a function of distance along the bar for a typical core. The maximum voltage e_m induced in a single-turn sense coil wrapped close to the windings is equal to $(\pi\, m^2/4)\, db_m/dt$ and is observed at the midpoint of the bar.   As the sense coil is moved toward an end of the bar, the voltage

8-12
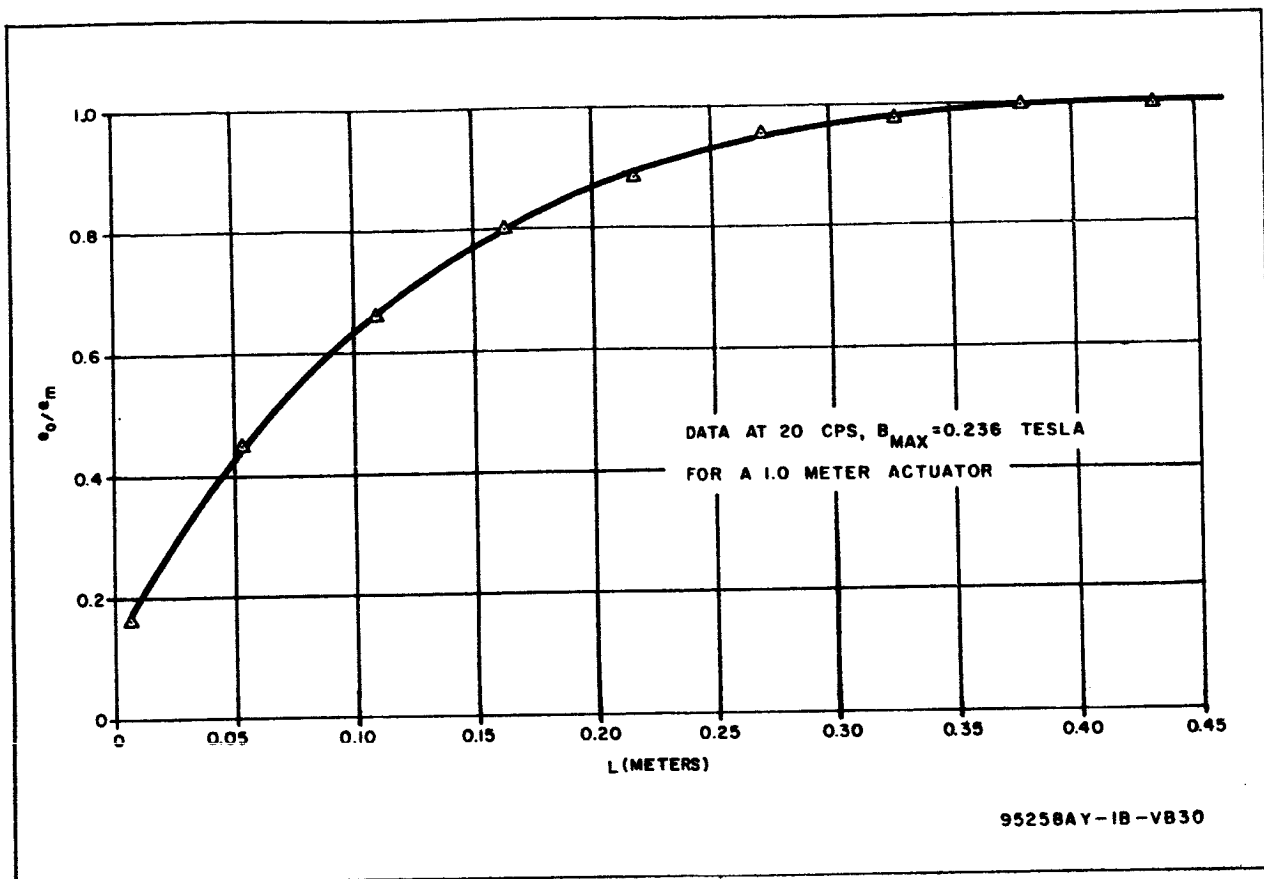
Figure 8-4. Flux Distribution in Bar as a Function of Distance From End

observed decreases as shown in figure 8-4. Since the other parameters included in the expression for e_o, $(\pi m^2/4)$ dB/dt, remain relatively constant, the decrease in e_o must be attributed to a decrease in B as the sense coil is moved farther from the midpoint of the bar. The voltage is observed by applying a low frequency current to the actuator windings and observing the voltage in a one-turn sense coil.

While the distribution shown in figure 8-4 is typical of all bars, the exact shape of the curve is a function of ℓ/m ratio. The change of the average flux density in the bar as ℓ/m changes is shown in figure 8-5. Because bars with a small ℓ/m have a greater buildup than bars with a greater ℓ/m for the same nominal torque, the results shown in figure 8-5 are not to be accepted blindly. All of the factors affecting flux distribution along the length of the bar should be investigated more fully before an accurate correction can be made for this phenomenon.
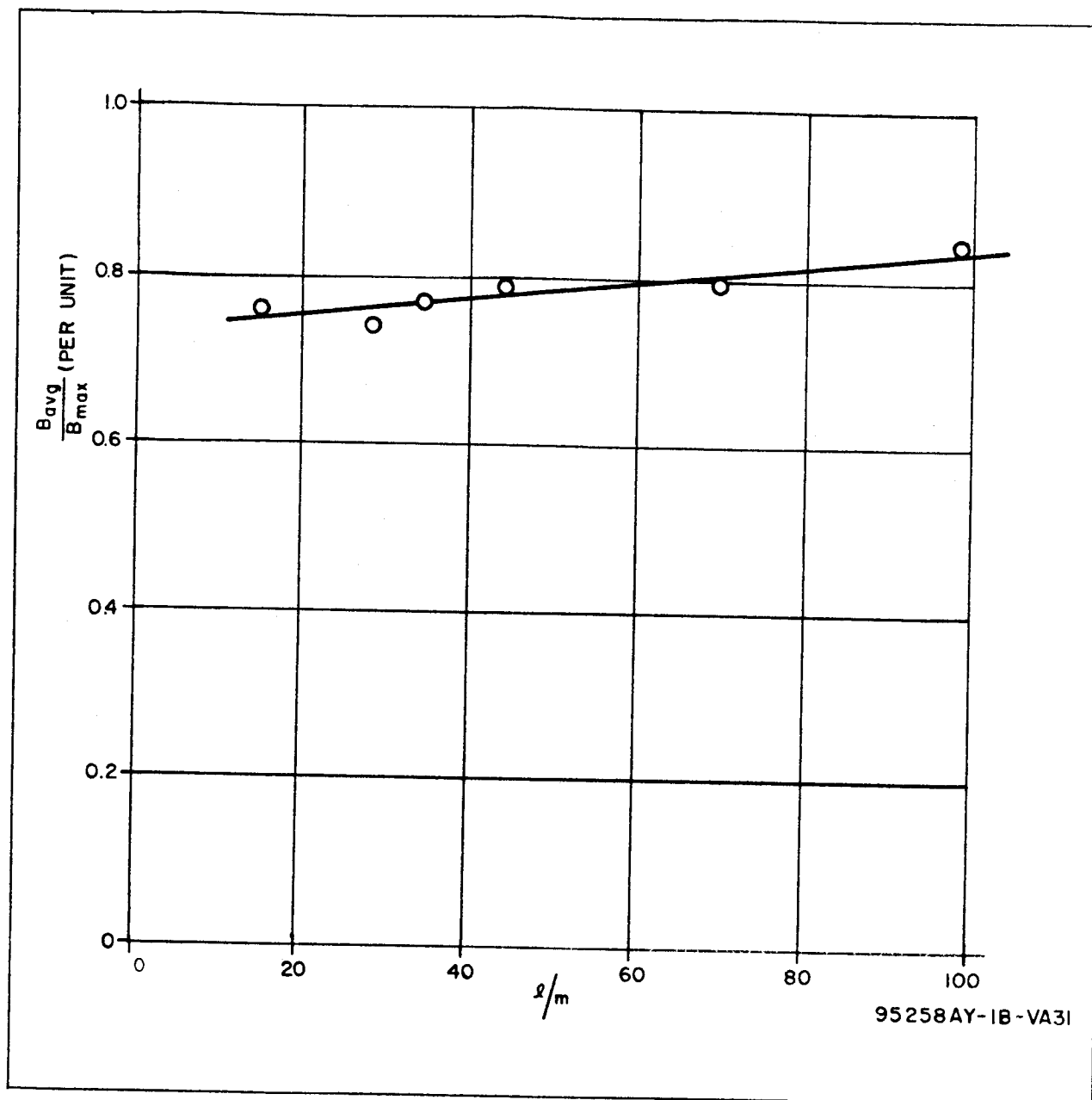
Figure 8-5.   Average Flux Density in Bar Versus Core Length -
Diameter Ratio

The correction now applied consists of a numerical integration of the area under the curve (of which figure 8-5 is a typical example) and then obtaining an average flux density.   The ratio of average flux density to idealized flux density is designated as α.   The desired torque is divided by this figure and the actuator optimized with respect to the larger, fictitious torque.   Equation 8-24 becomes:

8-14

$$T_t = \frac{\pi B_m B_t m^2 \ell}{4\mu_o} \left[\alpha + (1 + \psi/2) \left(\frac{1}{\mu_r} + \frac{L}{4\pi} \right) \right] \qquad (8\text{-}38)$$

and equation 8-36 becomes:

$$M_t = \frac{\mu_o T_t}{B_m B_t} \frac{\left[g_i + 0.288 \pi g_w s \left(\frac{d_1}{d} \right)^2 \psi \right]}{\left[\alpha + (1 + \psi/2) \left(\frac{1}{\mu_r} + \frac{L}{4\pi} \right) \right]} + \frac{3.464 k e \ell B_m^2}{\mu_o^2 s} \left(\frac{d}{d_1} \right)^2 \left(\frac{1}{\mu_r} + \frac{L}{4\pi} \right) \frac{\left[1 + (1+\psi)^{\frac{1}{2}} \right]^2}{\psi}$$

$$(8\text{-}39)$$

Other equations also need correction. Equation 8-18b should be:

$$m = 2 \left(\frac{\mu_o T_i}{\pi \ell \alpha B_m B_t} \right)^{\frac{1}{2}} \qquad (8\text{-}40)$$

Equation 8-18a should be:

$$T_i = \frac{\alpha B_m B_t V_i}{\mu_o} \qquad (8\text{-}41)$$

Equation 8-21 becomes:

$$T_t = H_a B_t \left[\frac{\alpha V_i}{\left(\frac{1}{\mu_r} + \frac{L}{4\pi} \right)} \right] + \ell A_c \qquad (8\text{-}42)$$

Equation 8-22 should be:

$$T_t = \frac{\pi B_m B_t \ell}{4\mu_o} \left\{ \alpha m^2 + \left[m^2 + 2h(m + h) \right] \left(\frac{1}{\mu_r} + \frac{L}{4\pi} \right) \right\} \qquad (8\text{-}43)$$

Equation 8-33 becomes:

$$M_a = \frac{T_i \mu_o}{\alpha B_m B_t} \left[g_i + 0.288 \pi g_w s \left(\frac{d_1}{d} \right)^2 \psi \right] \qquad (8\text{-}44)$$

Equation 8-35 should be:

$$M_t = \frac{T_i \mu_o}{\alpha B_m B_t} \left[g_i + 0.288 \pi g_w s \left(\frac{d_1}{d} \right)^2 \psi \right] + \frac{3.464 k \rho \ell B_m^2}{\mu_o^2 s} \left(\frac{d}{d_1} \right)^2 \left(\frac{1}{\mu_r} + \frac{L}{4\pi} \right) \frac{\left[1 + (1+\psi)^{\frac{1}{2}} \right]^2}{\psi}$$

$$(8\text{-}45)$$

Equation 8-37 becomes:

$$f(\psi) = \frac{\left[1 + (1 + \psi)^{\frac{1}{2}}\right]^2}{\psi^2 (1 + \psi)^{\frac{1}{2}}} = \frac{0.0832 \, \pi \, \mu_o^{\,3} \, g_w \, s^2}{a \, k \, \rho \, B_t \, B_m^{\,3} \, \ell \, (\frac{1}{\mu_r} + \frac{L}{4\pi})^2} \, (\frac{d_1}{d})^4 \, T_i \qquad (8\text{-}46)$$

8-16

8.4 SAMPLE ACTUATOR DESIGN

To clarify the use of the equations derived in the preceding paragraphs, typical design parameters will be assumed and an optimum actuator designed to these parameters. Let it be assumed that a maximum torque of 7.9×10^{-5} newton-meter (790 dyne-cm) is required from an actuator not to exceed one-half meter in length. This torque shall be developed in a terrestrial field of 1.56×10^{-6} tesla (0.0156 gauss). The power source is assumed to produce 1 watt for every 0.388 kilograms of mass.

The preferred core material at this time is annealed 50 percent Ni-50 percent Fe and the preferred wire material is aluminum. A reasonable wire size will be assumed as #24AWG. The following material constants are thus established.

$$\rho = 2.83 \times 10^{-8} \text{ ohm-m}$$
$$d = 5.56 \times 10^{-4} \text{ m}$$
$$d_1 = 5.11 \times 10^{-4} \text{ m}$$
$$s = 0.845$$
$$g_i = 8.2 \times 10^{3} \text{ kg/m}^3$$
$$B_m = 1 \text{ tesla}$$
$$\mu_r = 10^{4}$$
$$g_w = 2.67 \times 10^{3} \text{ kg/m}^3$$

The first step is to assume for the moment that all the torque will be produced by the iron. Making the appropriate numerical substitutions into equation 8-40

$$m = 2 \left(\frac{4\pi \times 10^{-7} \times 7.9 \times 10^{-5}}{\pi \times 0.5 \times 0.79 \times 1 \times 1.56 \times 10^{-6}} \right)^{1/2} = 0.0143 \text{ meter}$$

Using this value of m,

$$\ell/m = \frac{0.5}{0.0143} = 35$$

From figure 8-6 the demagnetizing factor $L/4\pi$ is found for this value of ℓ/m to be 2.22×10^{-3}. If the proper numerical substitutions are made in equation 8-46
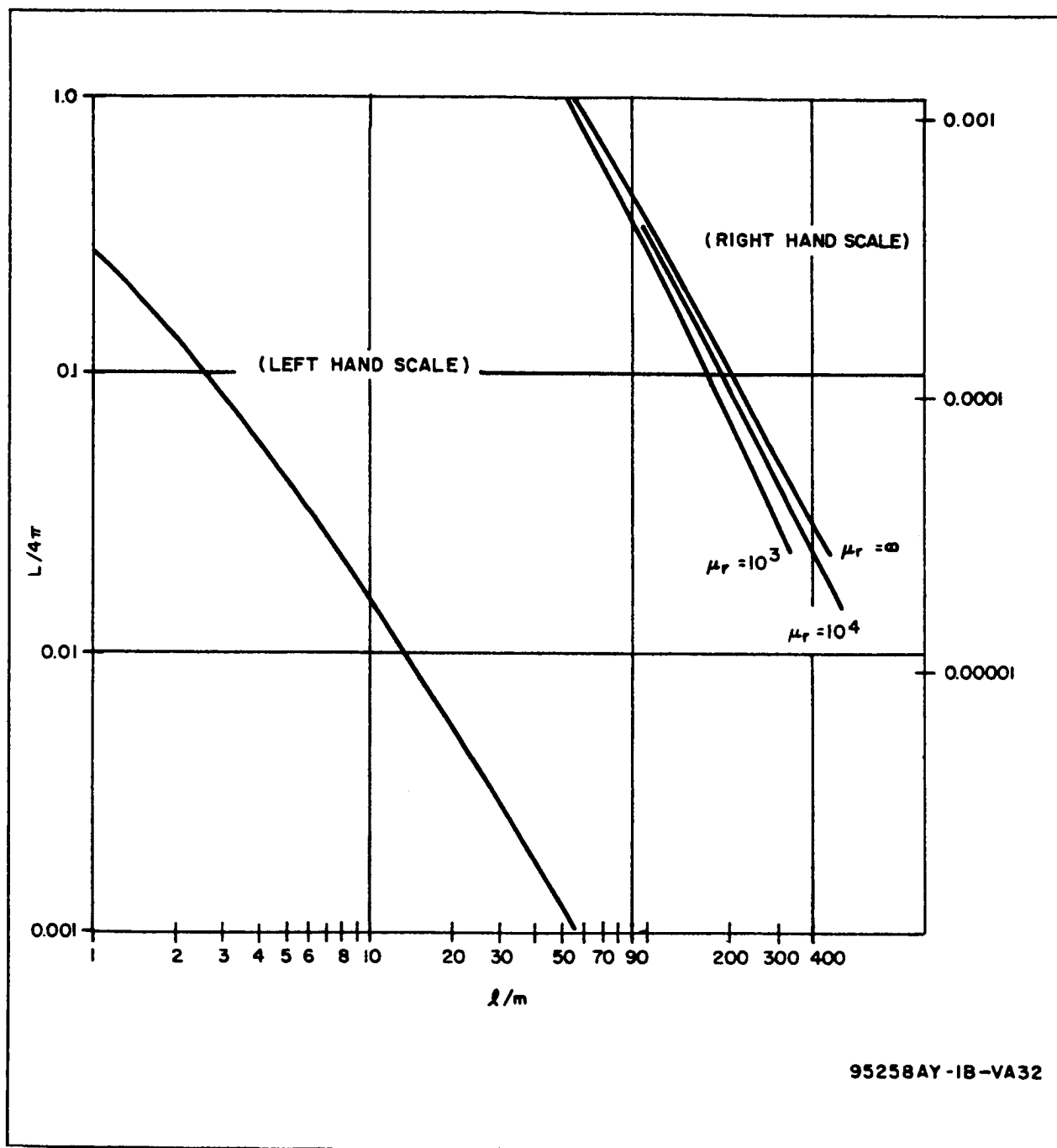
Figure 8-6. Demagnetizing Factor As a Function of ℓ/m

$$f(\psi) = \frac{0.0832\,\pi\,(4\pi \times 10^{-7})^3\;2.67 \times 10^3\,(0.845)^2\,(\frac{5.11}{5.56})^4\;7.9 \times 10^{-5}}{0.79 \times 0.388 \times 2.83 \times 10^{-8} \times 1.56 \times 10^{-6} \times 1 \times 0.5\,(\frac{1}{10^4} + 2.22 \times 10^{-3})^2}$$

$$= 1.524$$

8-18

Entering the graph of figure 8-3 at this value of $f(\psi)$, ψ is found to be 1.67.

It is now necessary to calculate the total torque from equation 8-38 to ensure that the original assumption that the torque produced by the coil is negligible. Making the required substitutions

$$T_t = \frac{\pi \times 1 \times 1.56 \times 10^{-6} (0.0143)^2 \ 0.5}{4 \times 4\pi \times 10^{-7}} \left[0.79 + (1 + 1.67/2)(\frac{1}{10^4} + 2.22 \times 10^{-3}) \right]$$

$$= 7.9 \times 10^{-5} \ \text{newton-meter}$$

Had the value of total torque been higher than the desired value, it would have shown that the torque produced by the coil was appreciable. This usually happens for low ℓ/m ratios. When this happens, it is necessary to decrease the torque assumed to be produced by the iron by an appropriate amount, solve again for m, $L/4\pi$, and ψ, and recheck. This process must be iterated until the total torque calculated agrees with the specified torque. This is a rapidly converging technique, and it has never been necessary to make more than three trials.

With the foregoing constants determined, equation 8-23a can be solved

$$h = \frac{0.0143}{2} \left[(1.67 + 1)^{1/2} - 1 \right] = 4.51 \times 10^{-3} \ \text{meter}$$

The rest of the calculations are indicated below in proper order and reference made to the appropriate equation without comment.

From equation 8-25

$$N = 1.15 \ (0.5) \ 4.51 \times 10^{-3} \times 0.845/(5.56 \times 10^{-4})^2$$

$$= 7090 \ \text{turns}$$

From equation 8-26

$$I = \frac{0.866 \ (5.56 \times 10^{-4})^2 \times 1}{4\pi \times 10^{-7} \times 4.51 \times 10^{-3} \times 0.845} (\frac{1}{10^4} + 2.22 \times 10^{-3})$$

$$= 0.130 \ \text{ampere}$$

From equation 8-28

$$R = \frac{4.60 \times 2.83 \times 10^{-8} \times 0.5 \times 0.845 \times 4.51 \times 10^{-3} (0.0143 + 4.51 \times 10^{-3})}{(5.11 \times 10^{-4} \times 5.56 \times 10^{-4})^2}$$

$$= 57.6 \ \text{ohms}$$

From $P = I^2R$

$$P = (0.130)^2 \, 57.6 = 0.975 \text{ watt}$$

From equation 8-45

$$M_t = \frac{7.9 \times 10^{-5} \times 4\pi \times 10^{-7}}{0.79 \times 1 \times 1.56 \times 10^{-6}} \left[8.2 \times 10^3 + 0.288\pi \times 2.67 \times 10^3 \times 0.845 \left(\frac{5.11}{5.56}\right)^2 1.67 \right]$$

$$+ \frac{3.464 \times 0.388 \times 2.83 \times 10^{-8} \times 0.5 \times 1}{(4\pi \times 10^{-7})^2 \, 0.845} \left(\frac{5.56}{5.11}\right)^2 \left(\frac{1}{10^4} + 2.22 \times 10^{-3}\right) \frac{\left[1 + (1 + 1.67)^{1/2} \right]^2}{1.67}$$

$$= 1.267 \text{ kilograms}$$

Thus, for the parameters specified, the total actuator system mass is
1.267 kilograms. This figure can be broken down into actuator mass and
power supply mass. These figures are

$$M_a = 0.887$$

$$M_{ps} = 0.38$$

8.5 DESCRIPTION OF MEASUREMENTS

8.5.1 Measurement Techniques

The basic mechanization for the torque measurements is illustrated in figure 8-7. The actuator was supported by a bifilar pendulum so that the axis of the actuator was perpendicular to the horizontal component of the local terrestrial field. A beam of light was split by a knife edge and projected on a mirror affixed to the pendulum. The reflected beam intercepted a scale fastened to a distant plane surface. The mirror was adjusted so that the axis of rotation of the pendulum lay in the mirror surface, and the light beam was adjusted so that the shadow of the knife edge was coincident with the intersection formed by the rotational axis and the mirror surface.

Current is conducted to the actuators through the wires used for the bifilar suspension. The torque resulting from the interaction of the terrestrial field with the field produced by the actuator causes an angular deflection of the pendulum, generating a restoring torque. By properly choosing the pendulum parameters, the angular deflection can be kept small so that errors introduced by the deflection may be neglected. As a consequence of achieving reasonable sensitivity, the damping constants of the system were low and external damping was introduced by fins attached to the pendulum. These fins were immersed in an aqueous solution of glycerol. A viscosity index of greater than 350 centipoises was maintained. It was empirically determined that the surface tension of the solution did not introduce a measurable error in the torque ranges employed. However, a correction for the displacement mass of the damping medium was necessary in computing the torques for a given deflection.

The magnitude and direction of the local field were monitored with a Schonstedt magnetometer at the start and finish of each set of measurements. No observable changes were found between these readings although long term changes were observed during the several weeks of measurement.

The restoring torque of the pendulum can be calculated from the equation

$$T_r = M_p D_u D_\ell \sin\theta / 4L$$
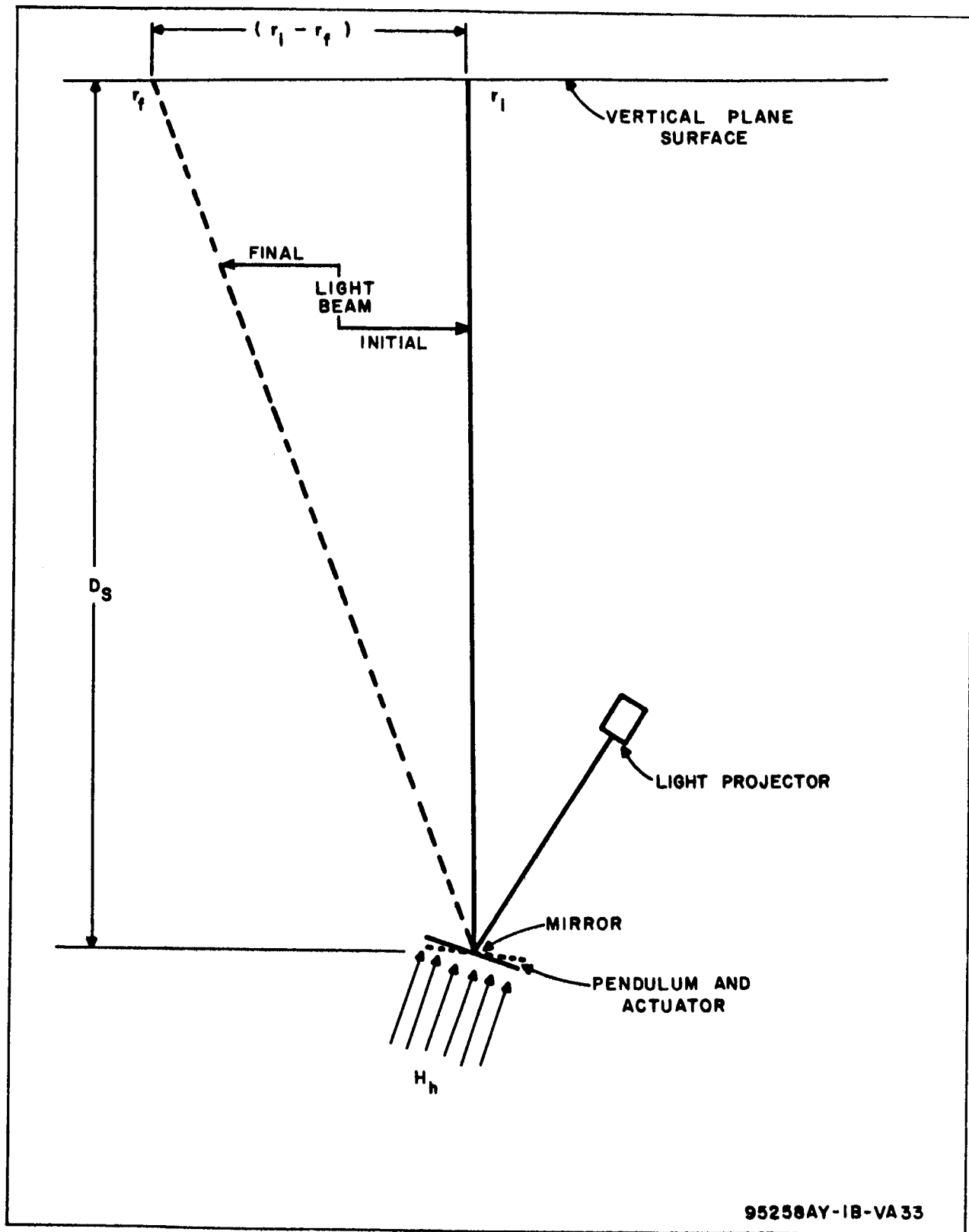
Figure 8-7. Measurement Scheme

95258AY-IB-VA33

where:

T_r = restoring torque

M_p = total mass supported

D_u = wire separation at upper end

D_ℓ = wire separation at lower end

θ = angular displacement from null

L = length of supporting wires

The angle θ is calculated from the initial and final readings on the scale to which the light beam is reflected:

$$\theta = 1/2 \tan^{-1} \frac{r_i - r_f}{D_S}$$

where:

r_i = initial reading

r_f = final reading

D_s = distance from axis of rotation of pendulum to scale. For the laboratory conditions used,

D_s = 12.475 meters

D_u = 0.149 meters

D_ℓ = 0.0381 meters

L = 1.68 meters

A photograph of the pendulum and associated equipment is shown in figure 8-8.

8.5.2 Actuators on Which Measurements Were Made

Several actuators were designed, fabricated and tested to verify the equations developed in paragraph 8.3. Other factors were also investigated empirically such as the uniformity of flux distribution, residual torque caused by remanent induction, and the effects of variation in the core length/coil length ratio. Actuators were designed using mild steel and annealed 50 percent Ni-50 percent Fe as core materials. Design torques (at orbital altitude) were 5, 2, and 1×10^{-4} newton-meters. The horizontal component of the local terrestrial field was almost exactly 10 times the expected field

95258AY-IB-PF34
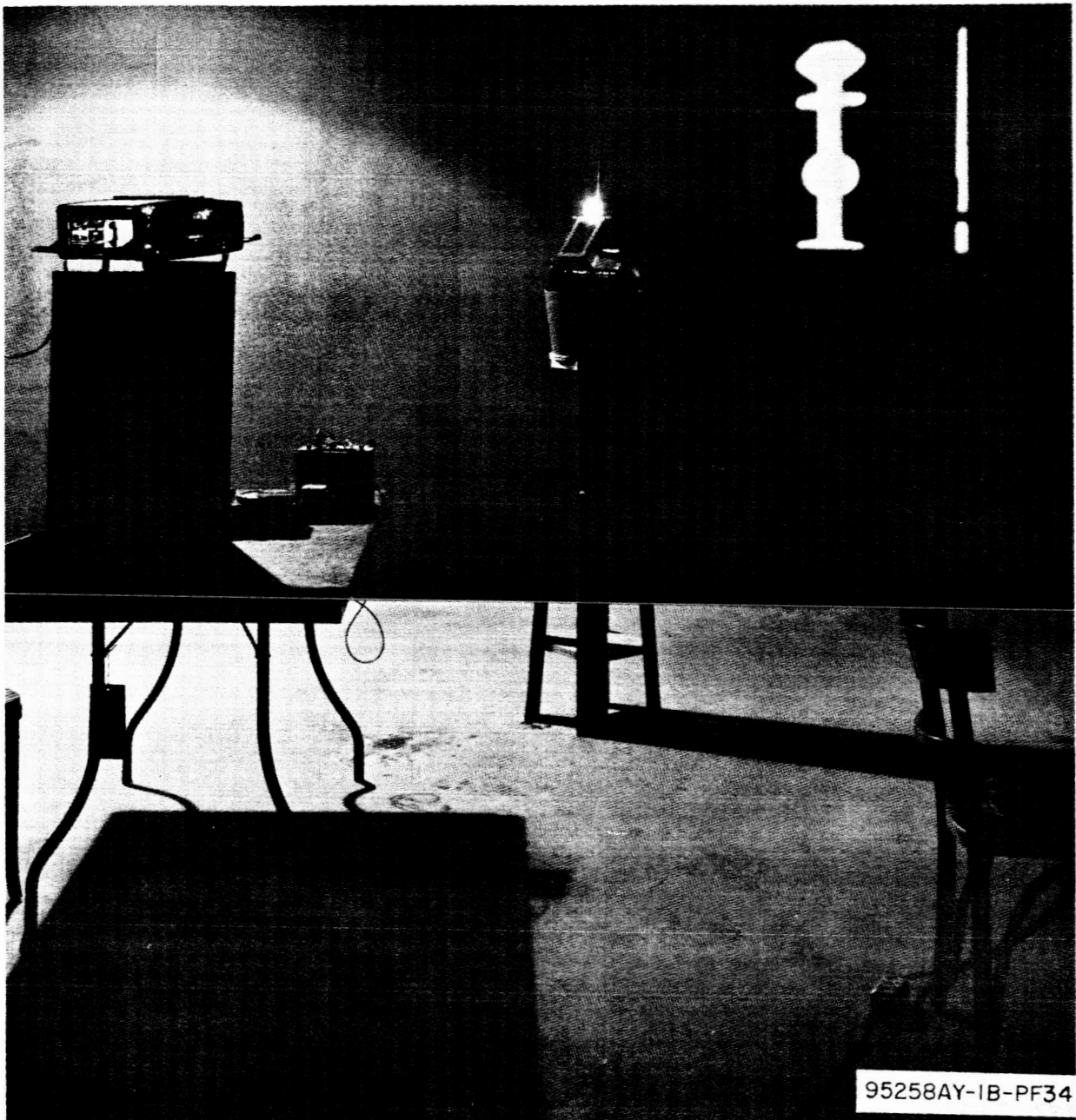
Figure 8-8.   Test Pendulum

in orbit, yielding design torques of approximately 5, 2, and 1×10^{-3} newton-meters.   The core lengths examined were 1/4, 1/2, 3/4, and 1 meter.   In addition five lengths of 50 percent Ni-50 percent iron (unannealed) were made of uniform diameter for each of two coils wound on special coil forms. These items were used to investigate the core length/coil length ratio effects.

8-24

The parameters of the designed actuators are shown in tables 8-1 and 8-2 for the 50 percent Ni-50 percent Fe and the mild steel cores, respectively, Those items marked with an asterisk were designed but not fabricated. A typical group of actuators are shown in figure 8-9. The variable length bars and the coils used with them are shown in figure 8-10.

TABLE 8-1

ACTUATOR PARAMETERS

(50 Percent Ni-50 Percent Fe Cores)

#	$T \times 10^4$	ℓ	$m \times 10^2$	ℓ/m	I	P	M_{wi}	M	Remarks
1	2.0	0.25	2.75	9.1	0.172	14.3	3.29	8.83	
2	2.0	0.50	2.02	24.8	0.134	2.53	1.92	2.90	Unannealed
3	2.0	0.75	1.65	45.4	0.120	0.969	1.61	1.99	
4	2.0	1.00	1.43	70.0	0.114	0.461	1.47	1.65	
5*	5.0	0.25	4.17	5.99	0.180	43.8	8.57	25.6	
6	5.0	0.50	3.18	15.72	0.140	9.09	5.25	8.78	
7	5.0	0.75	2.61	28.70	0.124	3.26	4.20	5.46	
8	5.0	1.00	2.26	44.2	0.118	1.74	3.83	4.50	
9	1.0	0.25	1.98	12.6	0.167	5.94	1.55	3.85	
10 a,b,c	1.0	0.50	1.43	35.0	0.130	0.982	0.905	1.29	For three-axis Prototype
11	1.0	0.75	1.17	64.1	0.118	0.379	0.778	0.93	
12	1.0	1.00	1.01	98.8	0.111	0.191	0.726	0.80	
25A	0.52	0.15	1.43	10.5	0.124	2.32	0.794	1.63	
B	0.52	0.20	1.43	14.0	0.124	2.32	0.860	1.69	
C	0.52	0.25	1.43	17.5	0.124	2.32	0.928	1.76	
D	0.52	0.30	1.43	21.0	0.124	2.32	0.991	1.82	
E	0.52	0.45	1.43	31.5	0.124	2.32	1.19	2.02	For $\dfrac{\text{Core Length}}{\text{Coil Length}}$ investigation
26A	1.5	0.45	1.43	31.5	0.095	0.510	.891	1.14	
B	1.5	0.60	1.43	42.0	0.095	0.510	1.09	1.34	

*Not Constructed

TABLE 8-1 (Continued)

#	$T \times 10^4$	ℓ	$m \times 10^2$	ℓ/m	I	P	M_{wi}	M	Remarks
26C	1.5	0.75	1.43	52.5	0.095	0.510	1.28	1.52	
D	1.5	0.90	1.43	62.9	0.095	0.510	1.47	1.72	
E	1.5	1.35	1.43	94.4	0.095	0.510	2.06	2.30	

TABLE 8-2

ACTUATOR PARAMETERS

(Mild Steel Cores)

#	$T \times 10^4$	ℓ	$m \times 10^2$	ℓ/m	I	P	M_{wi}	M	Remarks
13	1.0	0.25	1.97	12.7	0.171	6.89	1.60	4.27	
14	1.0	0.50	1.43	35.0	0.138	1.71	0.944	1.66	
15	1.0	0.75	1.17	64.1	0.130	1.04	0.871	1.28	
16	1.0	1.00	1.01	98.8	0.128	0.900	0.848	1.20	
17*	2.0	0.25	2.74	9.2	0.175	15.6	3.33	9.36	
18*	2.0	0.50	2.02	24.8	0.140	3.60	2.00	3.40	
19	2.0	0.75	1.65	45.3	0.130	2.01	1.73	2.51	
20	2.0	1.00	1.43	70.0	0.125	1.45	1.62	2.18	
21*	5.0	0.25	4.15	6.03	0.186	46.6	8.37	26.5	
22*	5.0	0.50	3.17	15.8	0.144	10.7	5.22	9.37	
23*	5.0	0.75	2.60	28.8	0.130	4.94	4.30	6.21	
24*	5.0	1.00	2.26	44.3	0.124	3.38	3.98	5.29	

*Not Constructed

8.6 DATA OBTAINED

In figure 8-11, the deflection measured is shown for the sequence of currents applied. The zero of the bifilar pendulum was first established as each actuator was to be tested. This reading is shown as point BZ. The
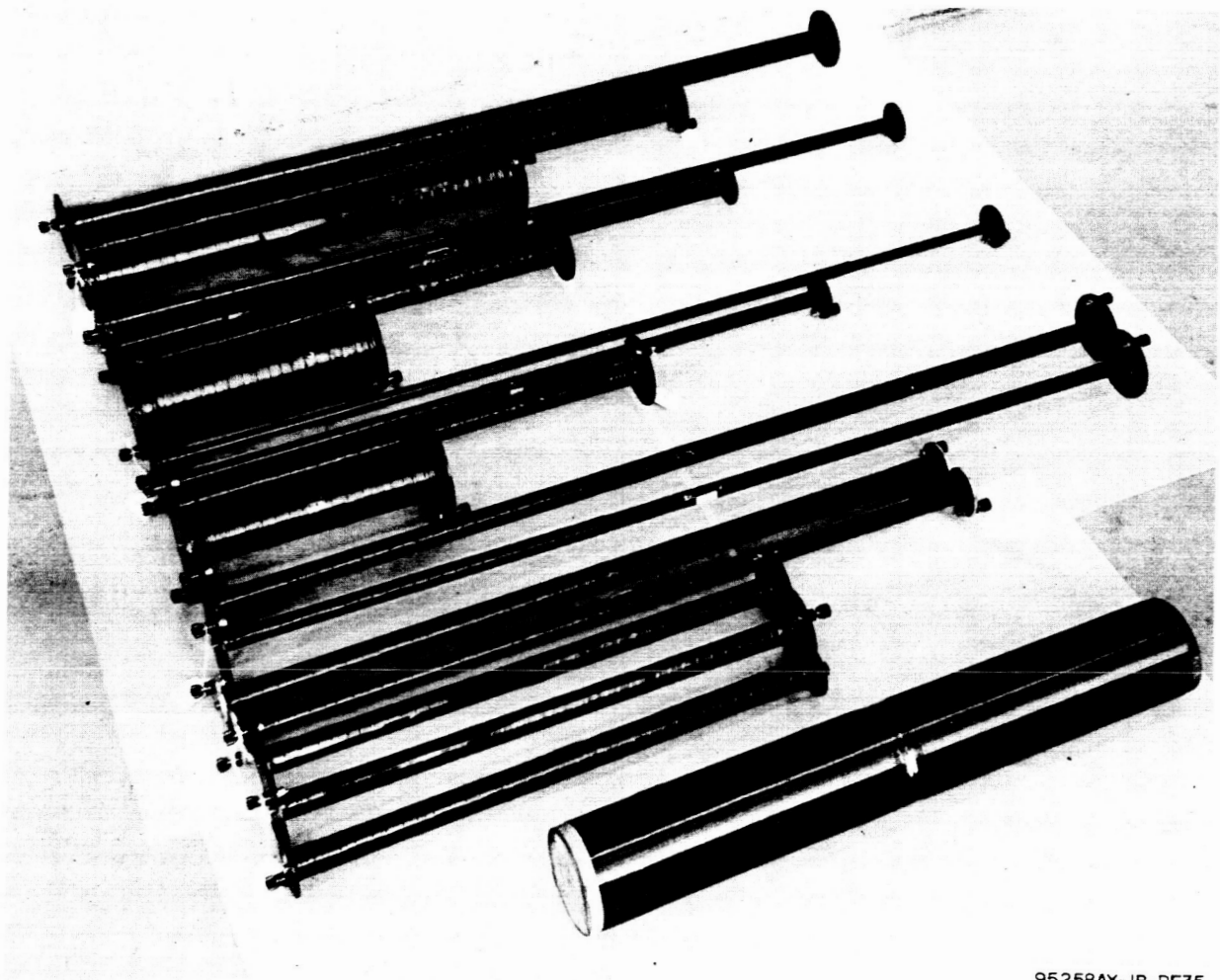
Figure 8-9.   Typical Group of Actuators

actuator was then laid in the pendulum and connected.   A reading was taken,
indicated in figure 8-11 as zero.   Current equal to 175 percent of rated
current (current calculated to produce rated torque) was applied in an
arbitrarily assigned positive direction and a reading taken.   This same
value of current was applied in the negative direction and a reading taken.
Current was then reduced to zero and a reading taken.   This last reading
(shown as -R) is indicative of the residual torque level possible in the system.
A small (10 percent of rated) current was then applied in the positive dir-
ection and a reading taken.   Current was again reduced to zero and another
residual indication read (shown as +R).   Current was then applied alternately

95258AY-IB-PF36
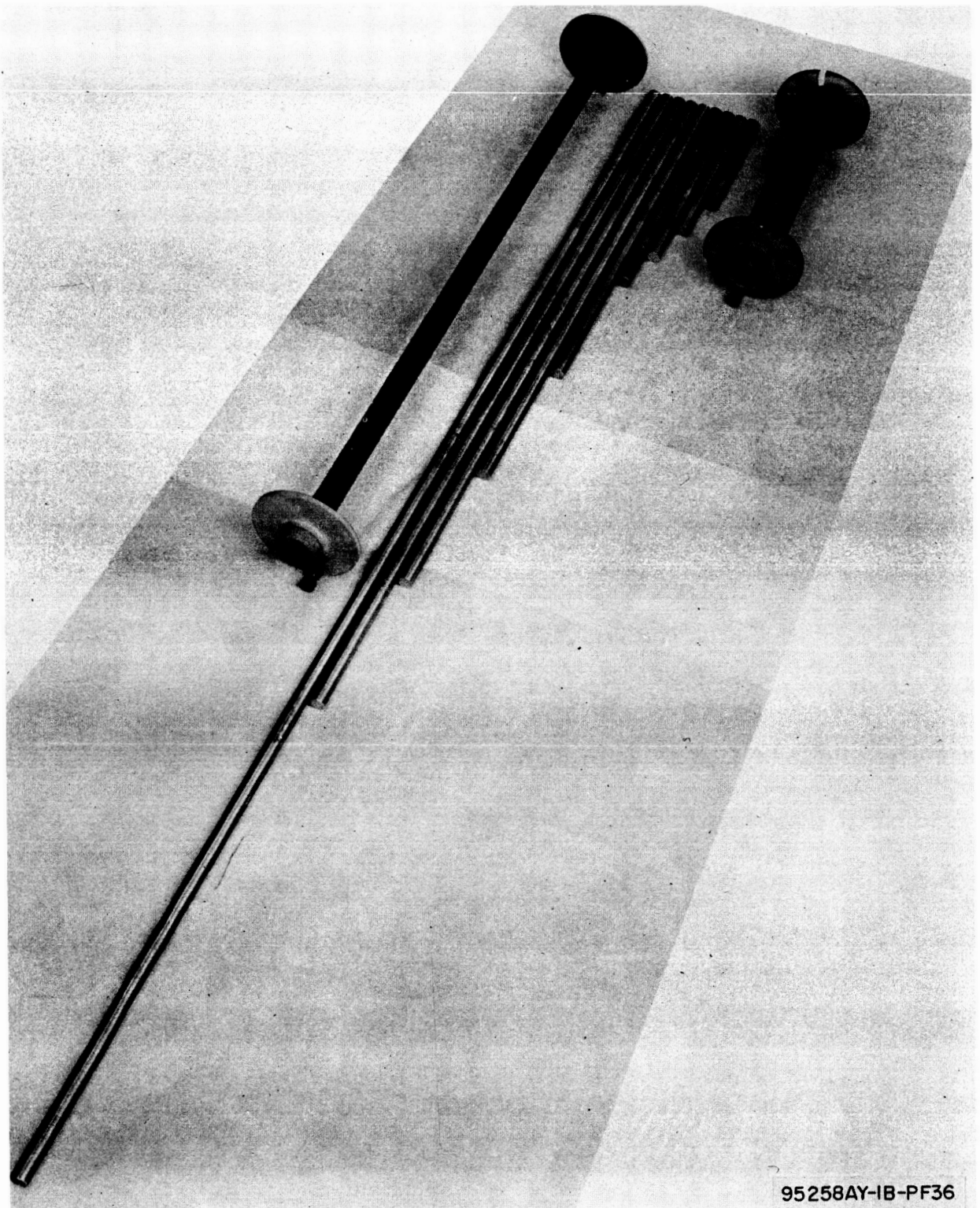
Figure 8-10. Core Length/Coil Length Test Units
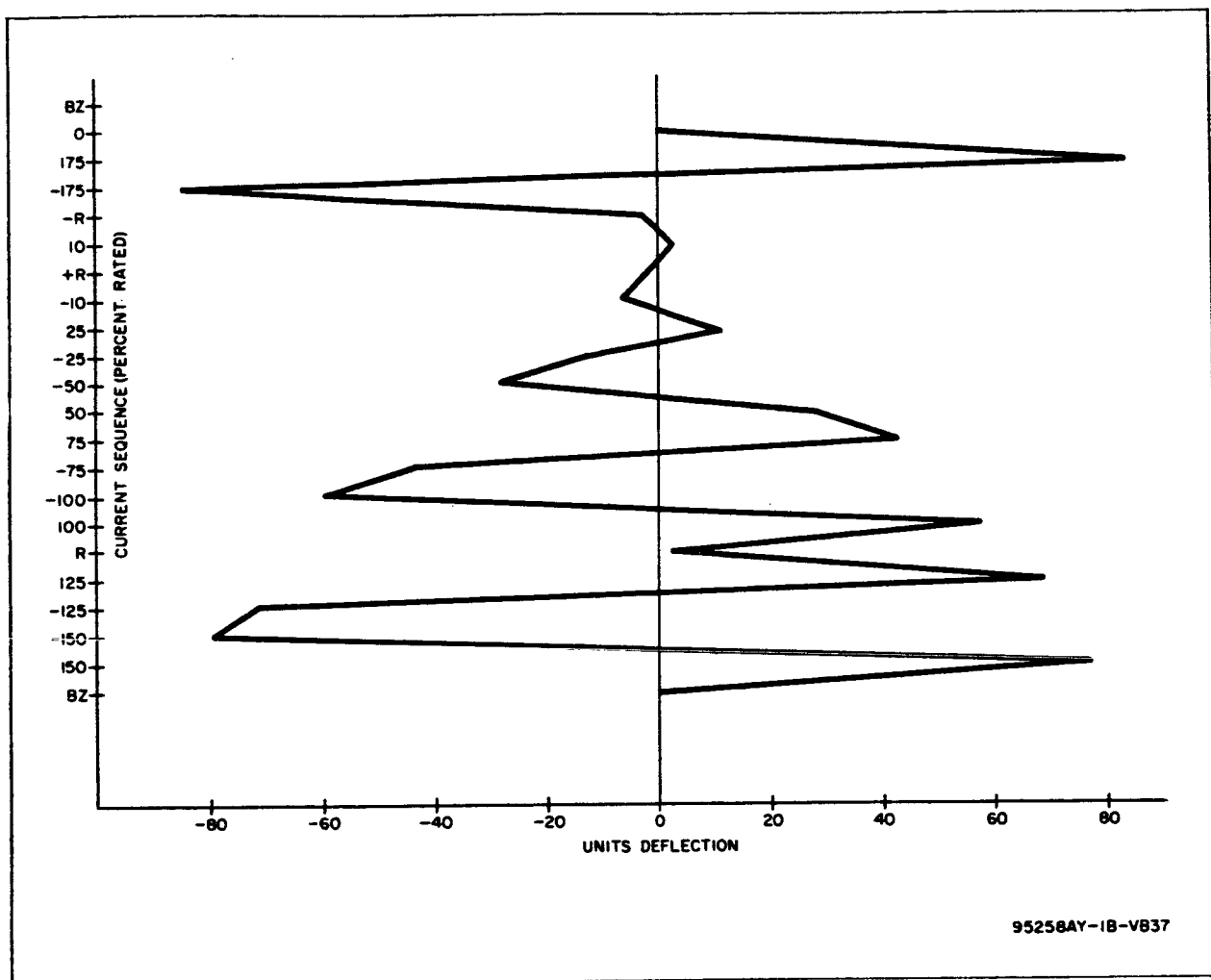
Figure 8-11. Typical Actuater Test Record

negative and positive in increasing steps until +100 percent was reached. Current was then reduced to zero again and a reading taken. This reading (shown as R) is indicative of the maximum residual torque level which could be expected under normal conditions of operation. Current was again increased in alternate steps and readings taken to fill out the curve between 100 percent and 175 percent of rated current. At the end of these readings the actuator was removed from the pendulum and another reading of BZ made. No difference in BZ readings was ever found which exceeded the sensitivity of the system. Torque was calculated from one-half the sum of the deflections for plus and minus readings to plot a curve of torque as a

function of current as shown in figure 8-12. In this figure per unit values of torque and current are used to allow comparison between different parameters.

The percent of calculated torque obtained experimentally at one per unit current is shown in figure 8-13 as a function of the ℓ/m ratio for the 50 percent Ni-50 percent Fe material. These data have already been corrected for nonuniform flux distribution as described in paragraph 8.3.2. If the two un-annealed specimens are accepted as exceptions, the points are seen to be in good agreement with the straight line shown. The largest deviation is about 7 percent. One suspects, therefore, that a relationship exists between observed torque and ℓ/m that has yet to be thought of. Because of the scatter observed at lower ℓ/m ratios, one might assume first that the effect is more important at the higher ℓ/m ratios. Further investigation of this effect should wait upon more data including work on other core materials.

A similar plot is shown in figure 8-14 for cores of a mild steel material. The points are widely scattered with respect to any straight line which might be drawn. The reason for this is not entirely clear but it has been hypothesized that, because a very common material was used, no effort was made by the manufacturer or manufacturers to control the magnetic properties between batches. It is entirely probable that a different material batch might have been sampled for each bar made. The permeability, particularly, could be expected to vary over wide limits.

In figures 8-15 and 8-16, the plots of residual torque as a function of length and ℓ/m ratio respectively are given for the 50 percent Ni-50 percent Fe material and in figures 8-17 and 8-18 for the mild steel material. Even after the unannealed specimens are ignored, the scatter of points is quite bad. One generalization can be made concerning the 50 percent Ni-50 percent Fe material, however. The residual torque is less than 3 percent of rated torque if the length is one-half meter or less. Also, the mild steel yields a residual torque roughly four times greater than that of 50 percent Ni-50 percent Fe.

The residual torque as a function of the core length/coil length ratio for the unannealed bars are given in figures 8-19 and 8-20 for the 1/4 meter
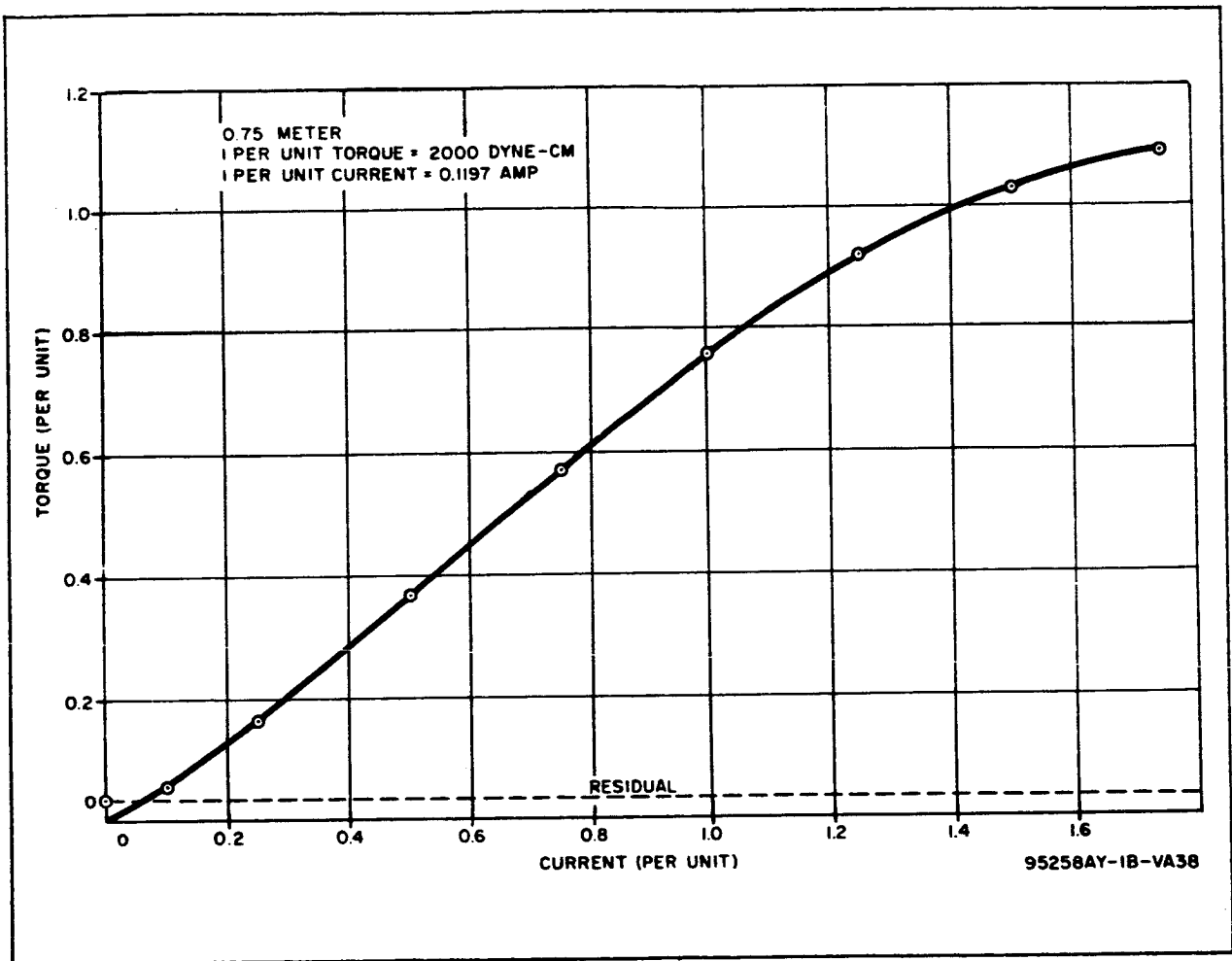
Figure 8-12.   Actuator Torque-Current Characteristic.
50 Percent Ni - 50 Percent Fe

and 3/4 meter coils, respectively. The curves are relatively smooth and, as would be expected from the discussion in the preceding paragraph, the residual torques for the 3/4 meter coil are more than three times the residual torques for the 1/4 meter coil.

In figure 8-21, the per unit torque is plotted as a function of the core length/coil length ratio. It can be seen that the incremental increase in torque per incremental increase in length is greatest in the neighborhood of a length ratio of unity. In figure 8-22 the torque per unit mass is plotted as a function of the length ratio. It was anticipated that this function would exhibit a maximum near unity. It is obvious that this expectation was not
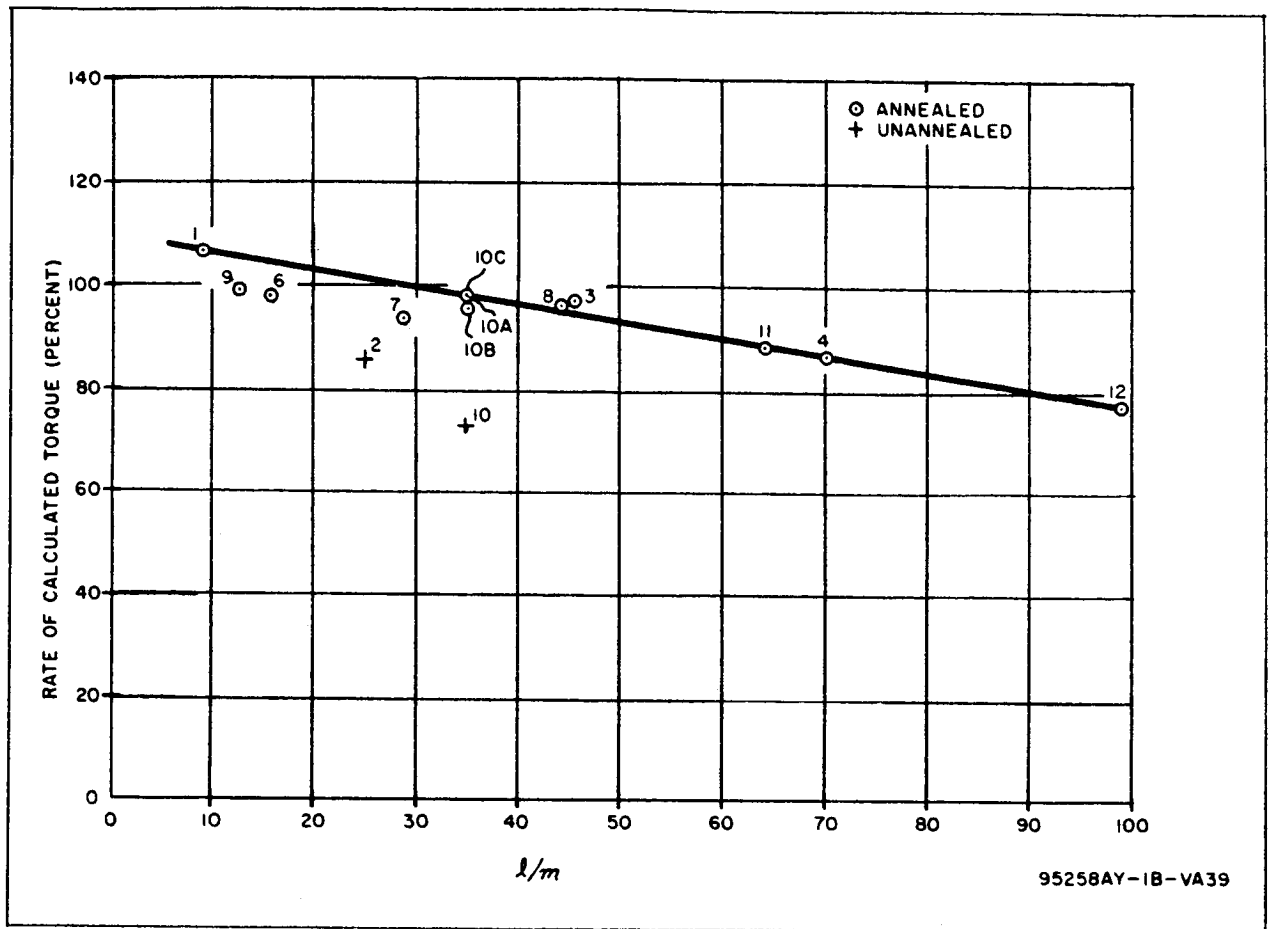
Figure 8-13. Experimental Torque Versus Length-Diameter Ratio
50 Percent Ni-50 Percent Fe

realized in practice. Because the data of figure 8-22 seemed to indicate that a smaller total mass could be achieved by making the core longer than the coil, an actuator was designed on this principle. There is a subtle illusion in the data of figure 8-22 that was not at first appreciated. As the experiment was designed, the coil was fixed and the core length varied. But, for comparison purposes, the maximum length should be fixed and the coil length adjusted; i.e., the comparison should be made on the basis that a certain length is available for the actuator. Assuming that the core is this long, will a minimum mass be obtained if the coil is designed to be as long as the bar or if it is designed to be somewhat shorter? To resolve this question, an optimized design for a core 30 centimeters long was calculated, assuming the coil to be as long as the core. This design was then compared
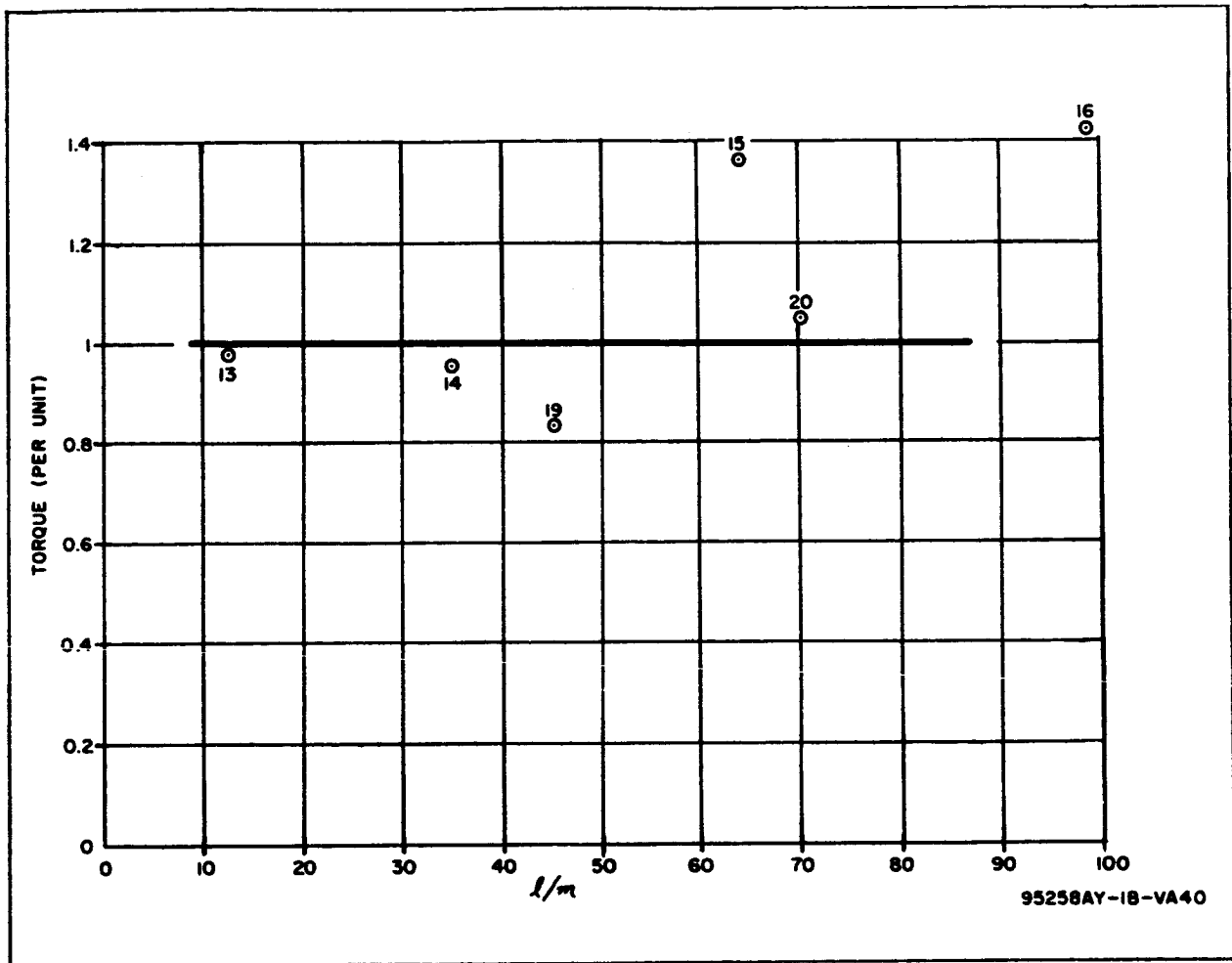
Figure 8-14. Experimental Torque Versus Length-Diameter
Ratio (Mild Steel Cores)

with the experimental results obtained with the 30-cm core and 25-cm coil.
On this basis, the total mass for a length ratio of unity was found to be
1.67 kilograms while the total mass for a length ratio of 1.2 was found to be
1.824 kilograms. The results shown in figure 8-22, therefore, are illusory
in that they really assume that the core length can be made greater than the
total allowable length.

8.7 CONCLUSIONS

8.7.1 Accuracy of Design Equations

After the correction for nonuniform flux distribution is made, the design
equations are found to yield torques within ±15 percent of the experimental
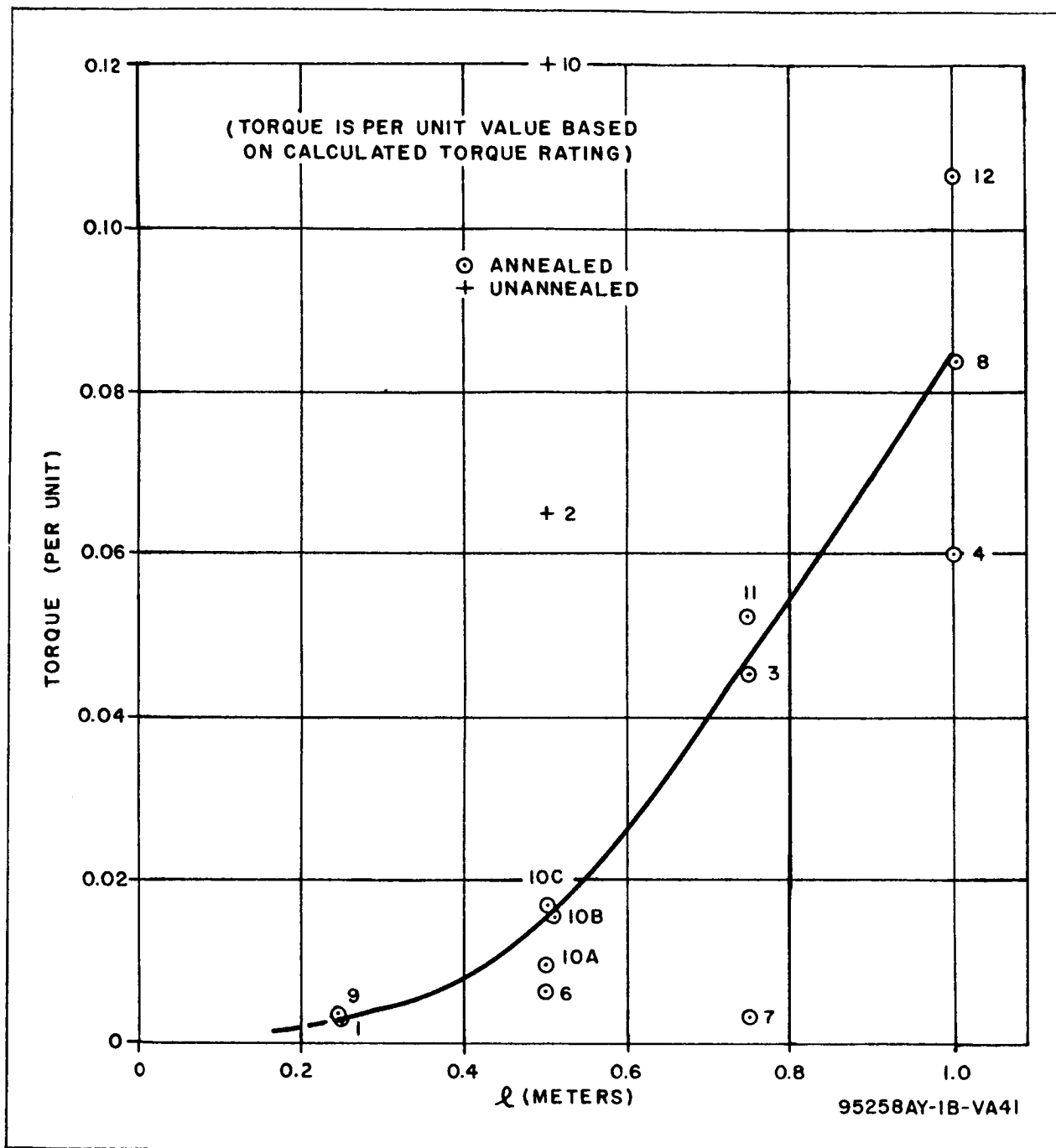
Figure 8-15.   Residual Torque Versus Length of Core
50 Percent Ni-50 Percent Fe Cores

values as shown in figure 8-13.   The calculated actuator (not total) mass
agreed with the actual actuator mass within 2 percent, except for design
No. 1 where the discrepancy approached 8 percent.   No reason for this one
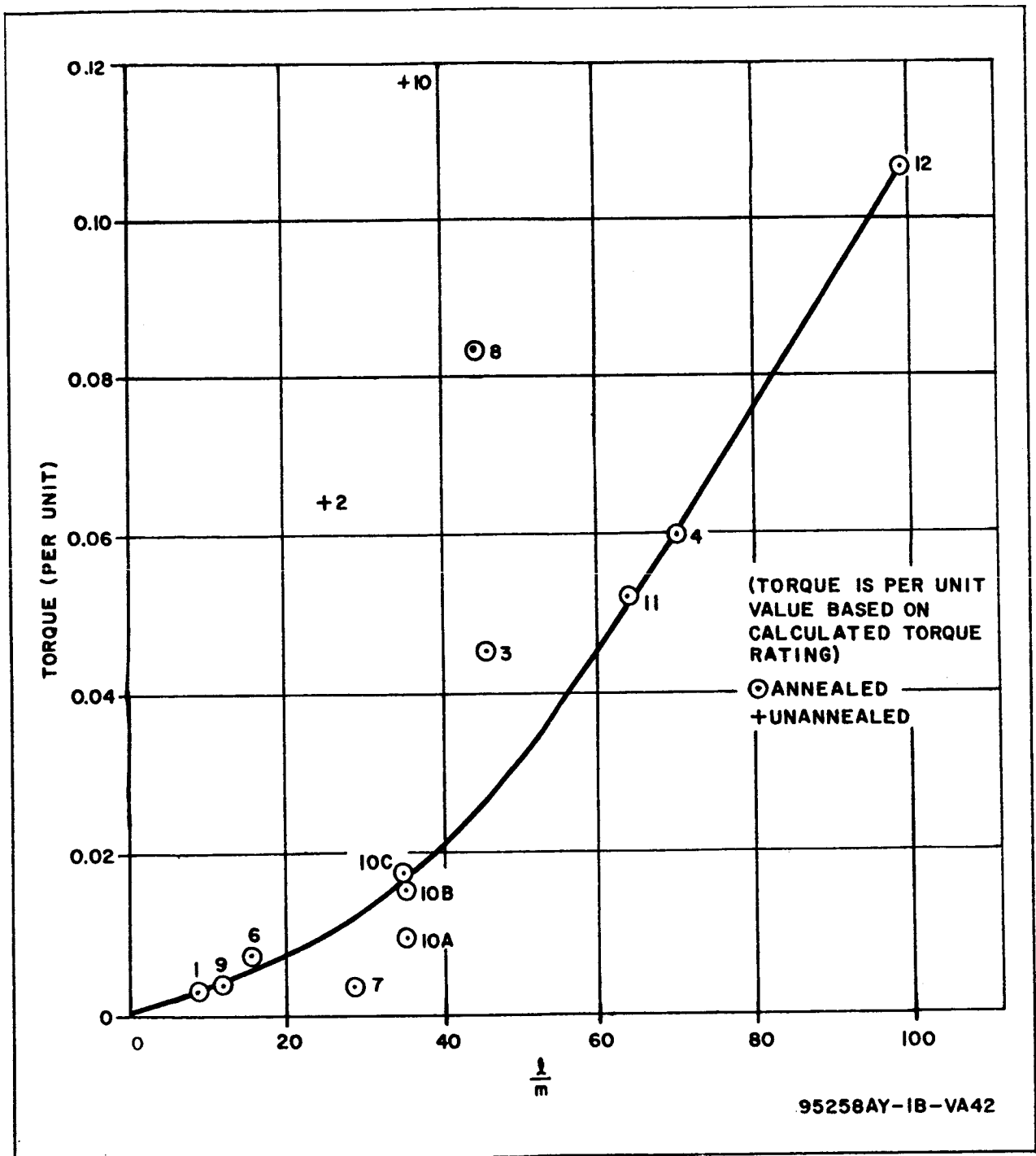
Figure 8-16. Residual Torque Versus Length-Diameter Ratio
50 Percent Ni-50 Percent Fe Cores

large discrepancy was found. The experimental resistances varied quite widely in both directions and the equation accuracy is estimated to be no worse than ±10 percent.
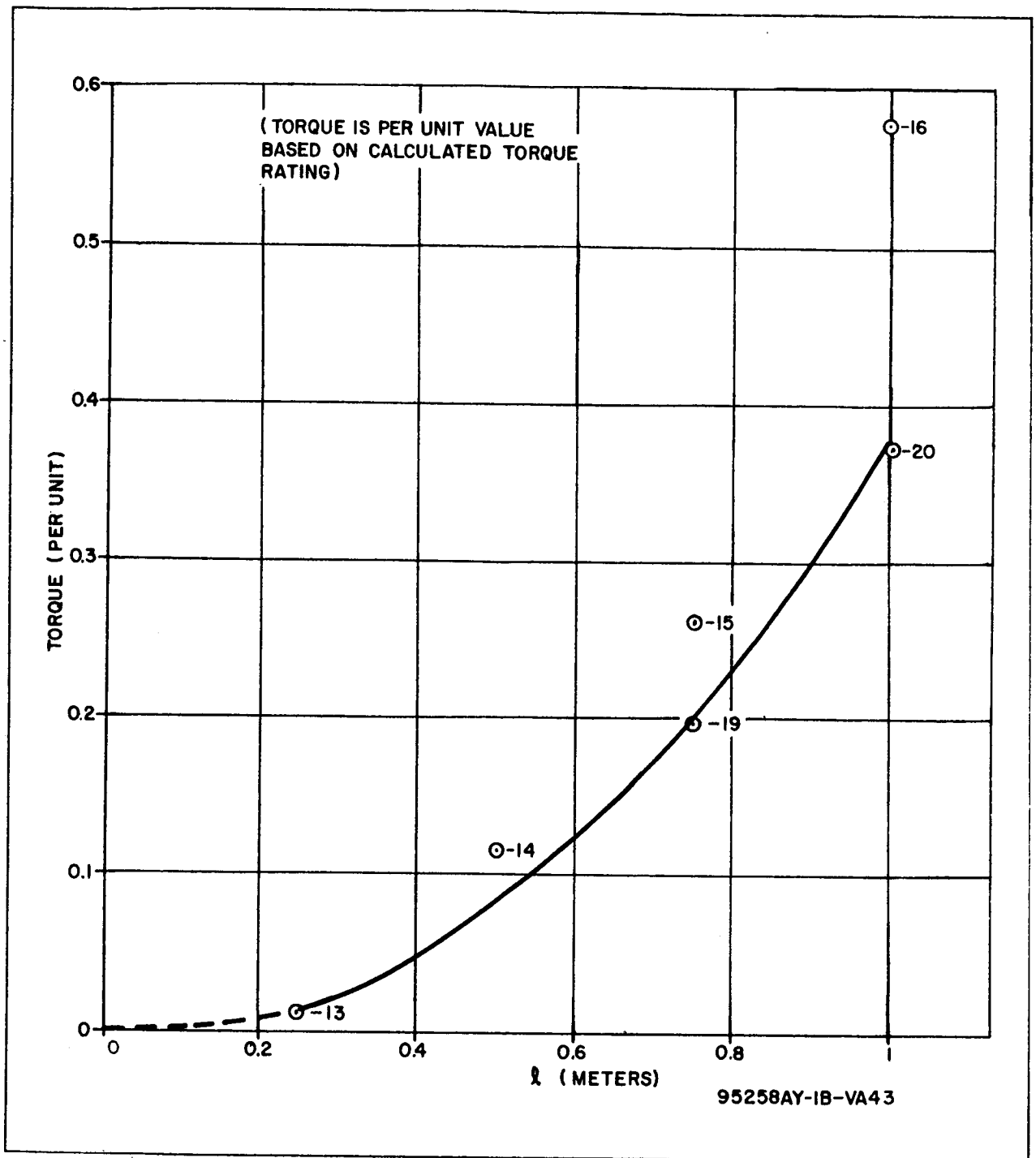
Figure 8-17. Residual Torque Versus Length of Core
(Mild Steel Cores)

8.7.2 Comparison with Air-Cored Coils

An optimum idealized air-core coil was computed for the same torque level and maximum dimension as each of the 50 percent Ni-50 percent Fe

8-36
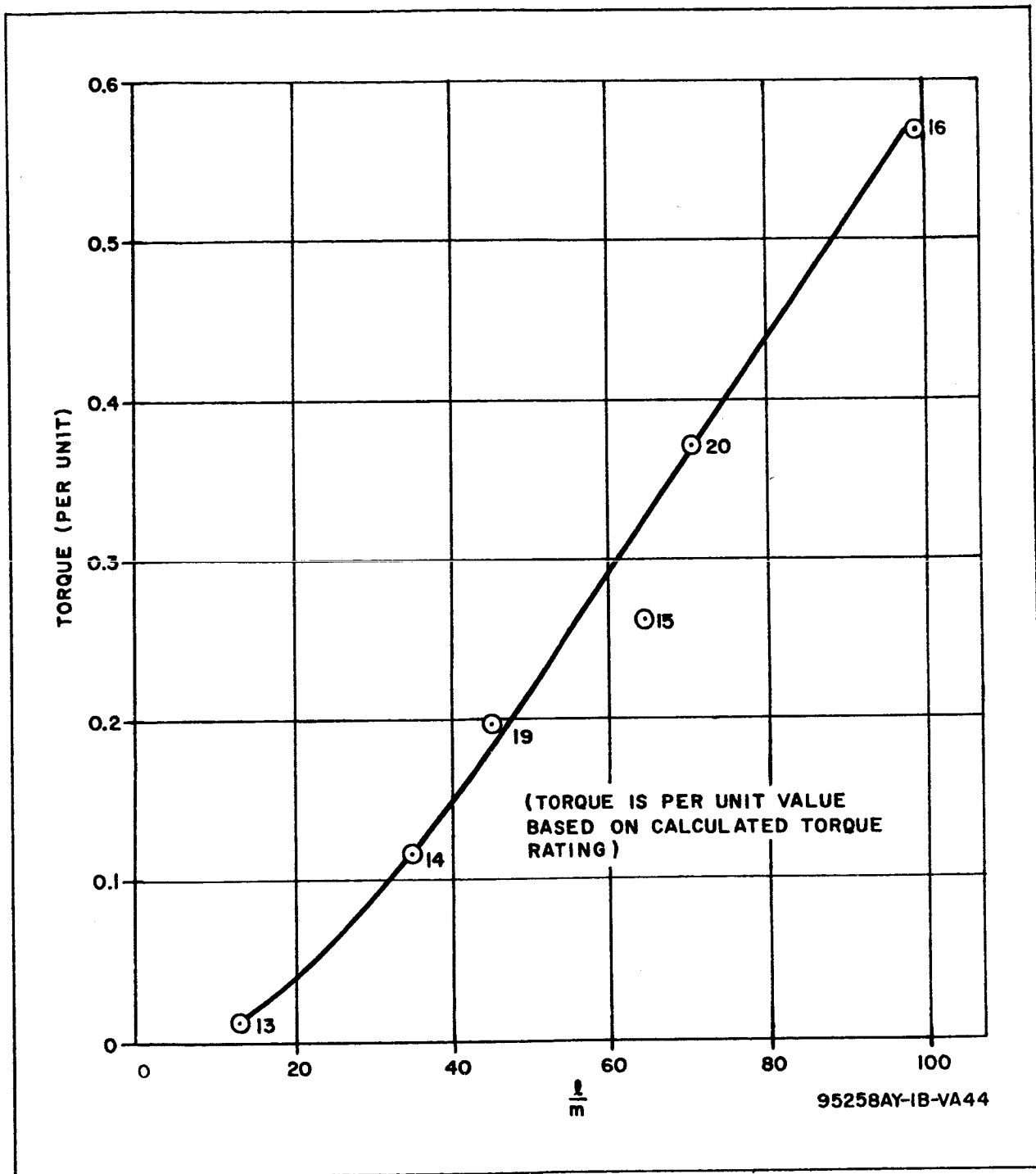
Figure 8-18. Residual Torque Versus Length-Diameter Ratio
of Core (Mild Steel Cores)

cores designed. A comparison of the total mass ratios, M_t air-core/M_t iron-core, is shown in figure 8-23. In this figure, the total mass ratio is
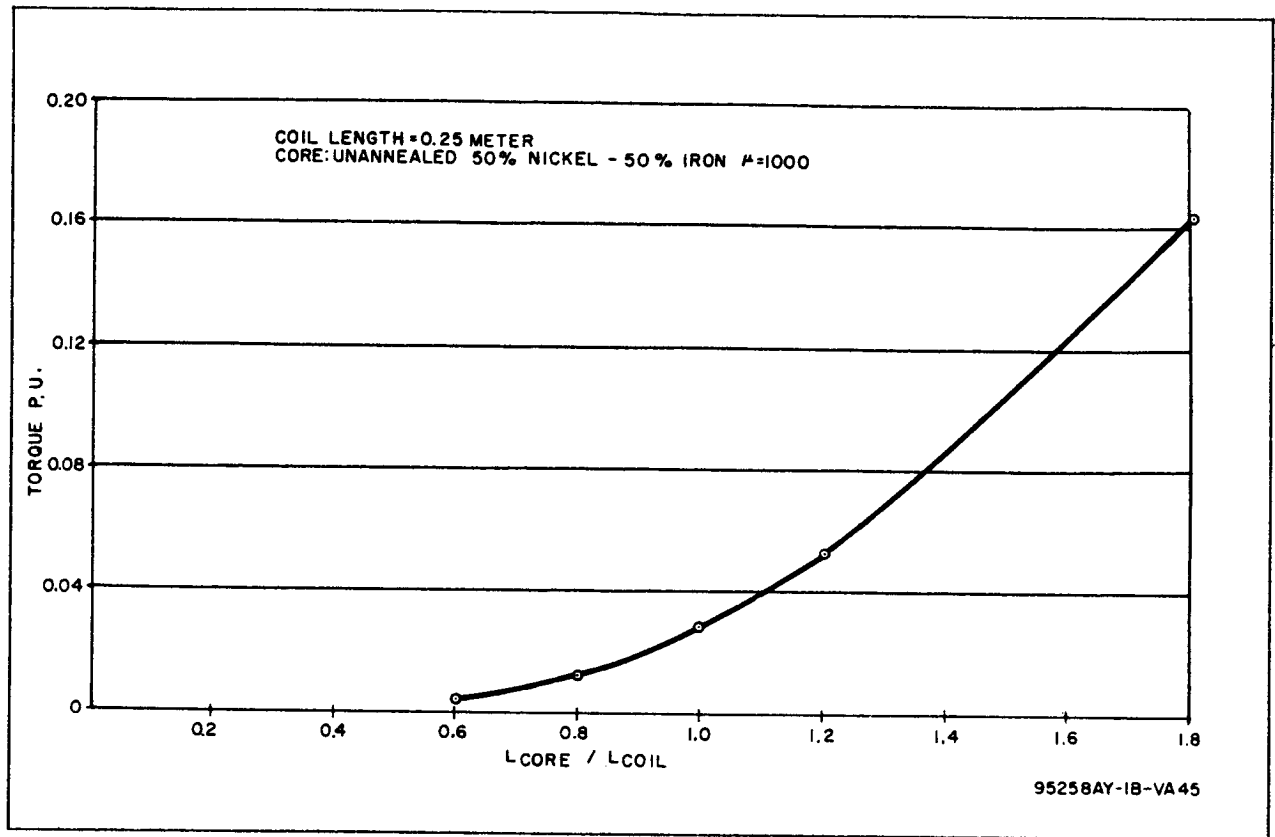
Figure 8-19. Residual Torque (Per Unit) Versus
Core Length-Coil Length Ratio

plotted against maximum dimension with torque level as a parameter. On the basis of these data, it would appear that the use of an iron core is most favorable at the lower torque levels and at moderate maximum dimensions. In no case was the total mass for the air-cored device less than twice the total mass for the iron-cored actuator.

8.7.3 Effect of Varying Core Length/Coil Length Ratio

As discussed in the section dealing with the experimental results, optimum results are obtained when the core length is equal to the coil length. The apparent advantage of making the core longer deduced from the results shown in figure 8-22 is illusory in that there is a difference between making the core longer and making the coil shorter. Once a mazimum length is specified, more total mass is required if the coil is shortened.

8-38
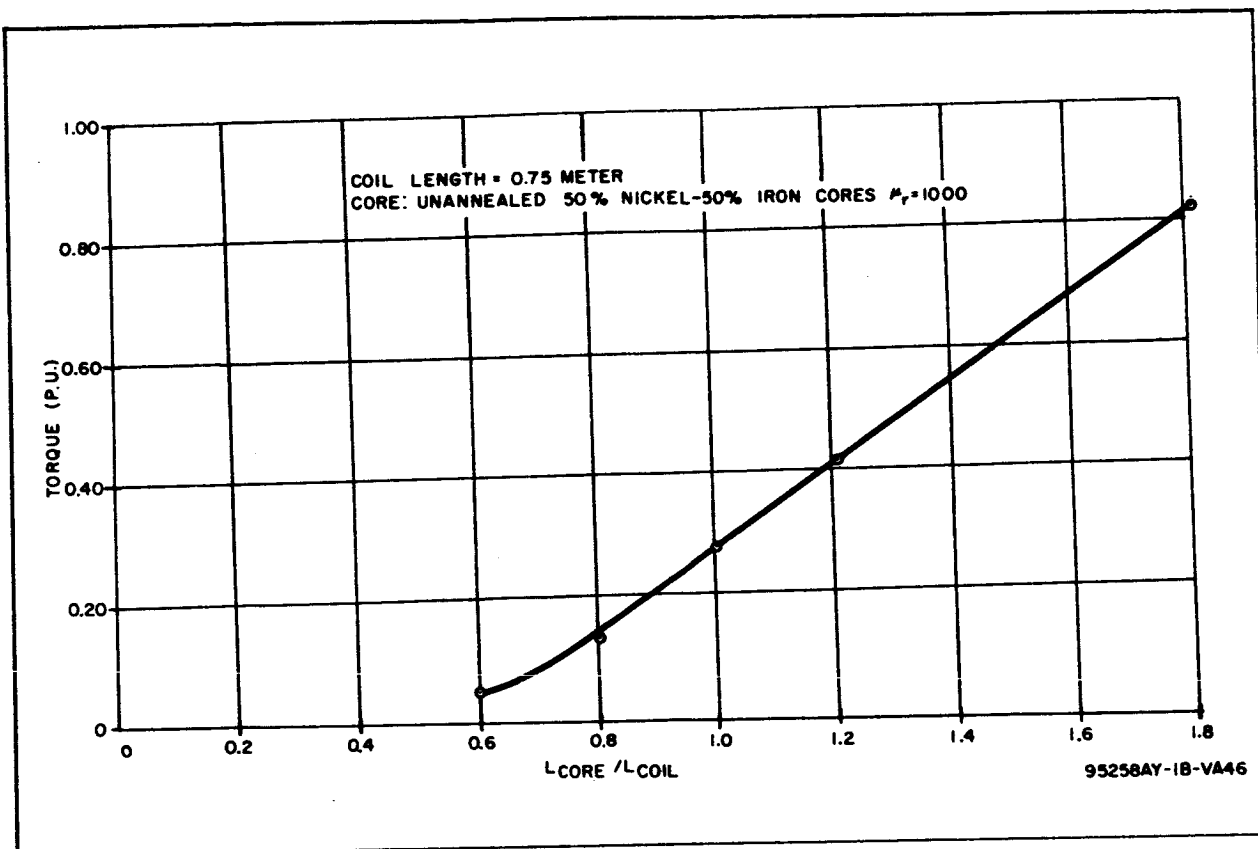
Figure 8-20.   Residual Torque Versus Core Length-Coil Length Ratio

8.7.4 Residual Torques

It has been found that the residual torques of 50 percent Ni-50 percent Fe cores can be made quite low if the core length is kept below 50 centimeters. This material, when annealed, is far superior to mild steel.   If the length is kept below 30 centimeters, it seems reasonable to expect that the residual torque can be made less than 1/2 percent of rated torque.

8.7.5 Recommendations for Future Study

It is recommended that future studies include new core materials; that, if the new materials show the same trend as 50 percent Ni-50 percent Fe, the effect of length/diameter ratio on the accuracy of the design equations be investigated (see figure 8-13).   It is also recommended that the range of torques and maximum lengths be decreased in a future study to see if the apparent trends shown in figure 8-23 continue.
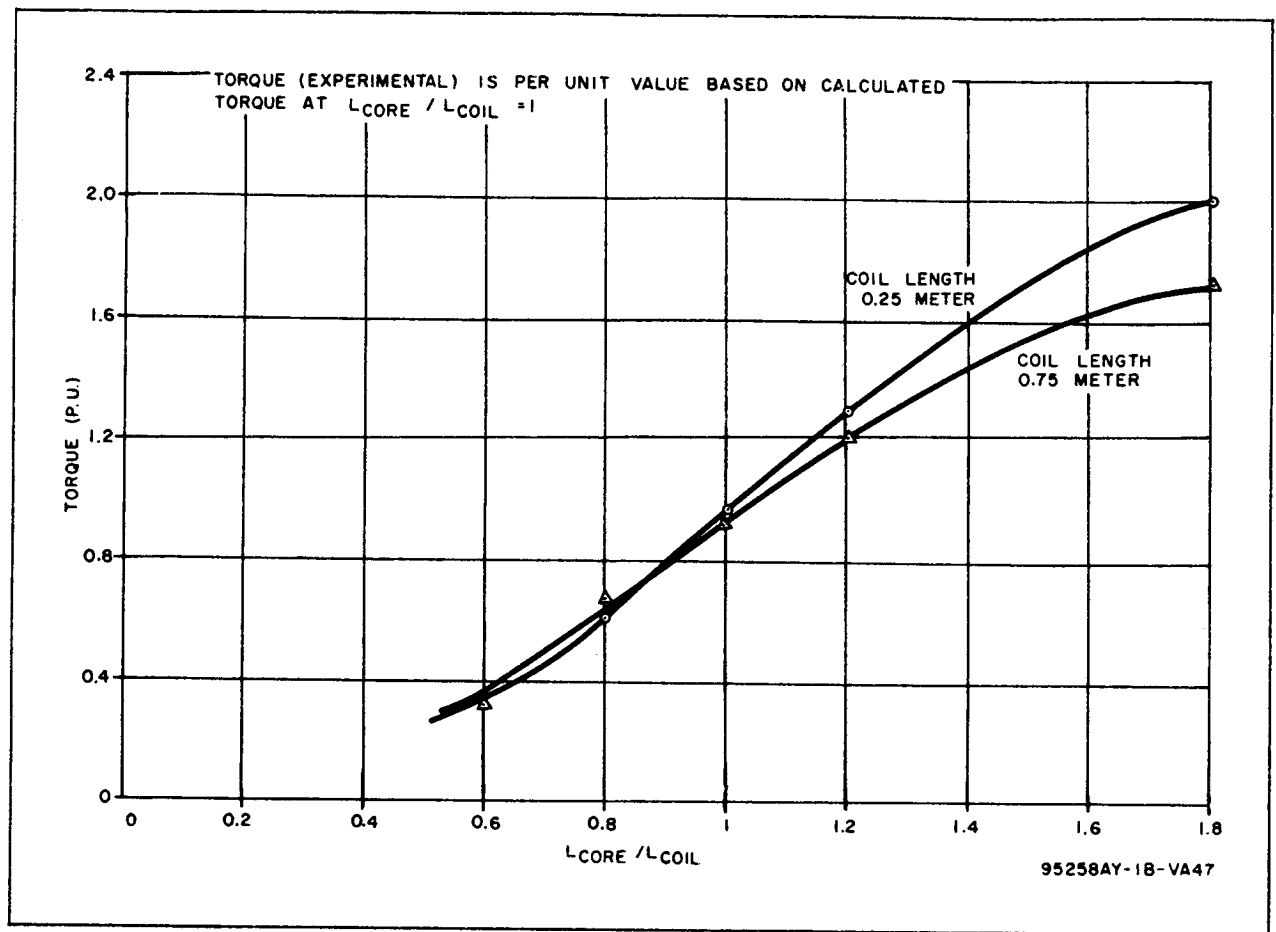
Figure 8-21. Torque Versus Core Length-Coil Length Ratio

8-40
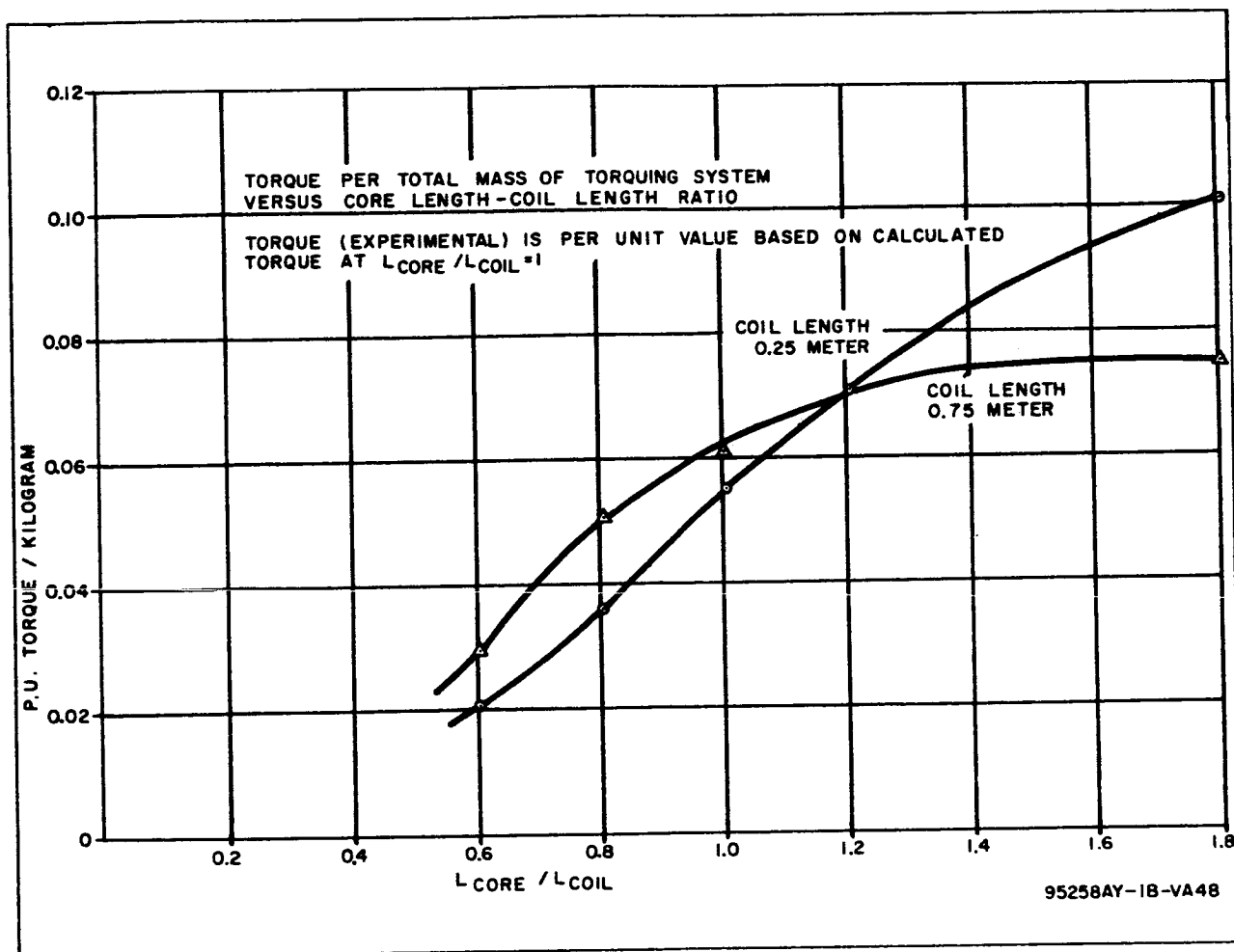
Figure 8-22.   Torque Efficiency Versus Length Ratio
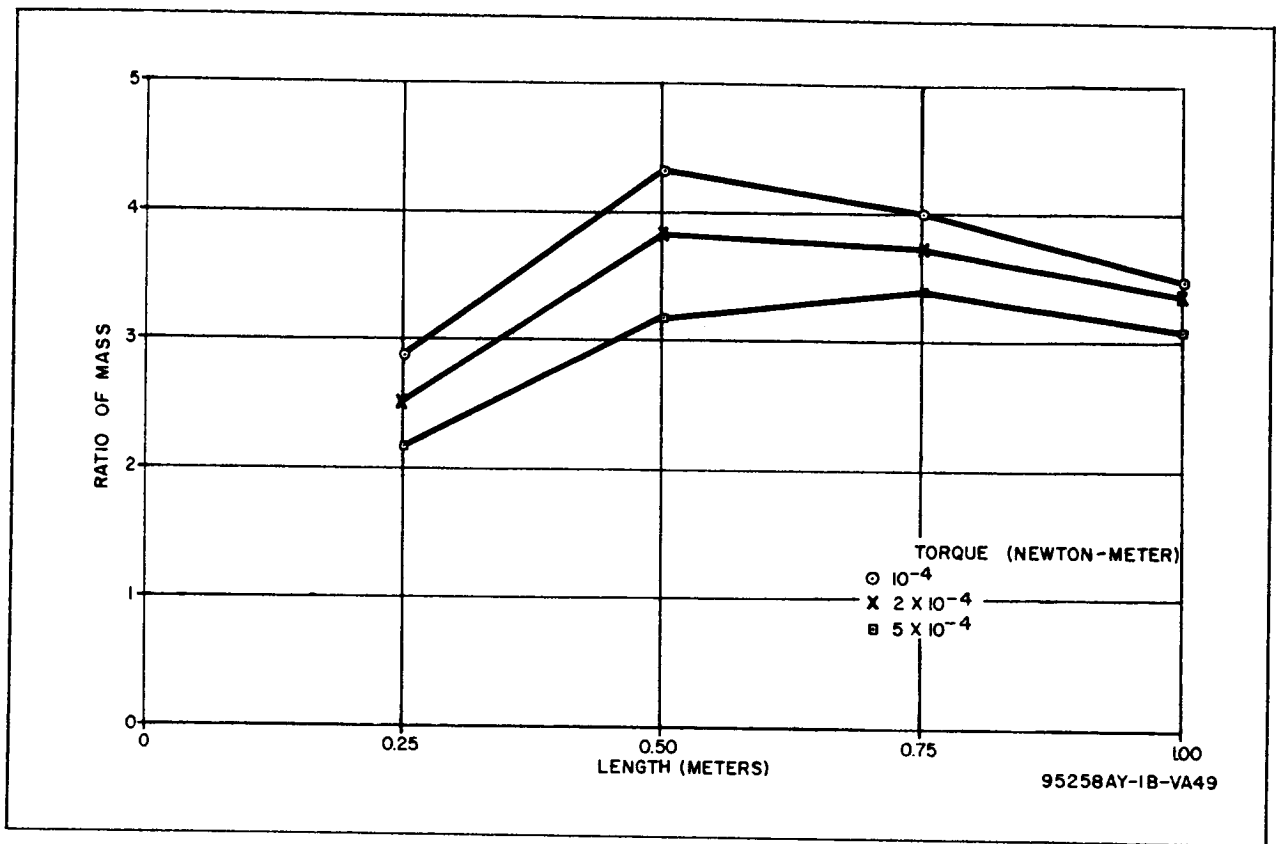
Figure 8-23.   Total Mass Ratio, Air-Cored to Iron-Cored
Actuators Versus Actuator Length

9. TASK V - MAGNETOMETER INTERFERENCE

9.1 STATEMENT OF PROBLEM

In applying an electromagnetic torquing system to a satellite, it is necessary that the earth's field magnetometers be relatively free of influence by the torque coils. There are at least three methods by which the magnetometers can be made relatively free of the influence of the magnetic field of the torque coils. (1) It is possible to time-share earth's field measurements and torquing functions, but this approach leads to complexity, both in programming and in storing the magnetometer information. (2) A compensating magnetic field can be created at each magnetometer probe to cancel out the interference magnetic field of the torque coils. This can be accomplished by supplying a fraction of the interfering torque coil current to an air-core coil that is wound on the magnetometer probe in such a manner that the compensating magnetic field is of equal and opposite polarity to that of the interfering torque coil's magnetic field. (3) The most desirable approach to the problem, from the standpoint of simplicity and reliability, is to provide sufficient coil-magnetometer separation. However, the field map of a typical set of three orthogonal, iron-cored torque coils cannot be predicted with accuracy or confidence purely by calculations, and it is necessary to gather empirical data. In Task V, such data have been measured for a typical set of coils to develop a "feel" for the problem and to make it possible to estimate the field contours of actuators other than those tested.

9.2 DESCRIPTION OF TEST

The three coils in the typical set tested are identical, and each has the following characteristics:

Nominal torque-64,000 dyne-cm per gauss (1000 dyne-cm in 6-hour orbit)

Weight-910 grams

Length - 0.50 meter

Core diameter - 1.43 centimeters

Core material - annealed hipernik

Turns - 7090

Flux density - 10,000 gauss (computed)

Current - 130 milliamperes

Resistance - 55 ohms

The test was performed outdoors, to avoid the field-warping effect of steel structure in the building. Ideally, the test would be made in a flux-free environment, but it is felt that sufficient accuracy can be achieved by first calibrating the earth's field and then subtracting this effect from the coil data.

At each test point, three mutually perpendicular components of the field (aligned with the coil axes) are measured. Test points are at incremental distances on three lines radiating out from the center of the coil set (see figure 9-1). Where 0 degree azimuth, 0 degree elevation lies on one of the coil axes, the three lines are as follows:

Azimuth (deg)	Elevation (deg)
0	0
45	0
45	45

All measurements are repeated for four conditions of coil current polarity, as indicated by the following code:

Coil A	Coil B	Coil C
N	N	N
N	N	S
N	S	N
N	S	S

The test setup is shown in figure 9-2. The coils are mounted on an all-aluminum rotatable stand, such that all magnetometer readings are actually measured along a single fixed aluminum track. Thus, the earth's field is defined only along this track.
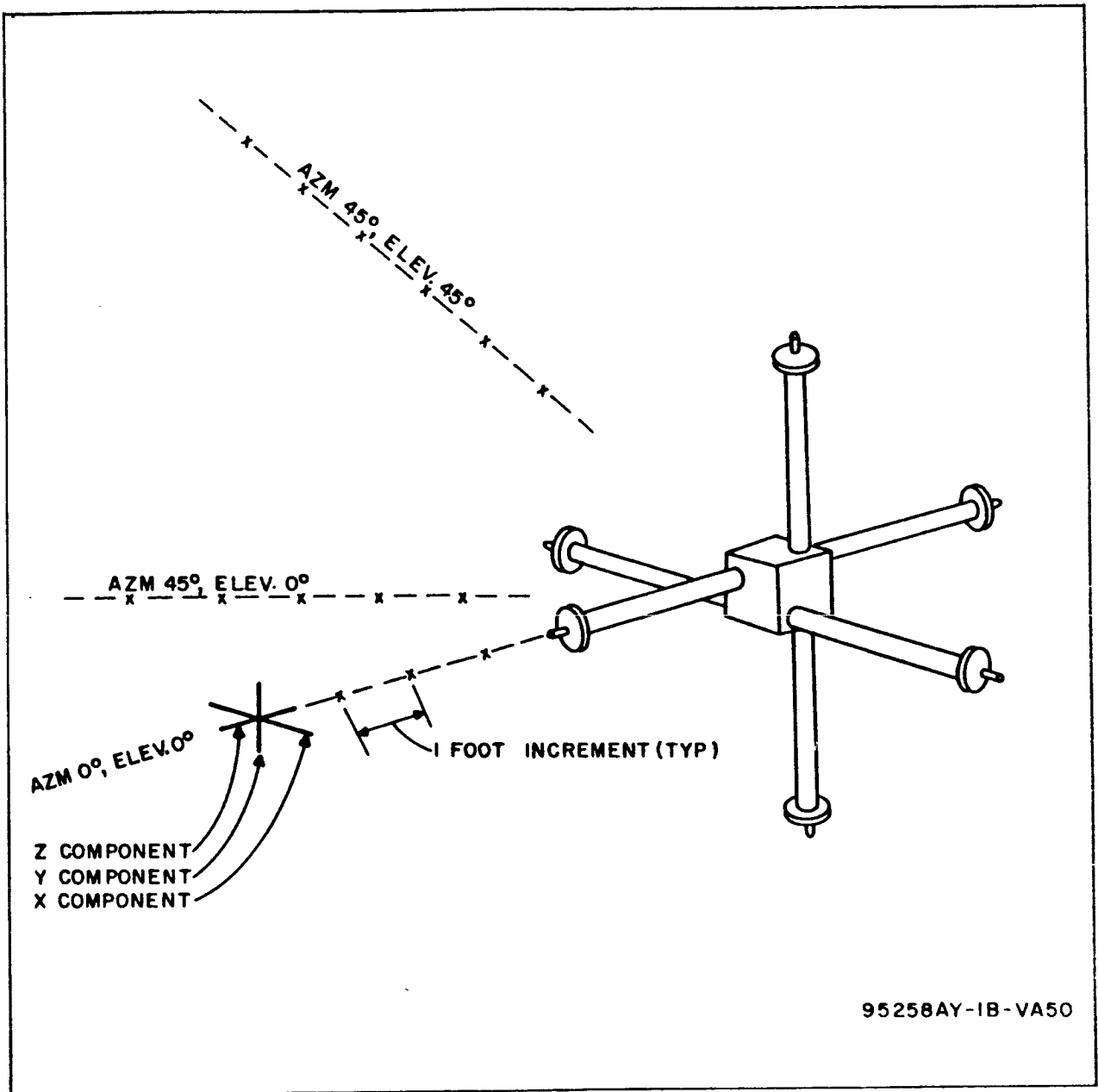
Figure 9-1. Field-Mapping Test Points

The magnetic field data were obtained using a Schoenstedt magnetometer in a sensitive bridge circuit.

9.3 TEST RESULTS

The magnetic field of the torque coils was plotted on log-log paper and is shown in figures 9-3 through 9-13. Each of the three respective magnetic components are plotted for each of the three runs. The greatest interfering

95258AY-IB-PF51
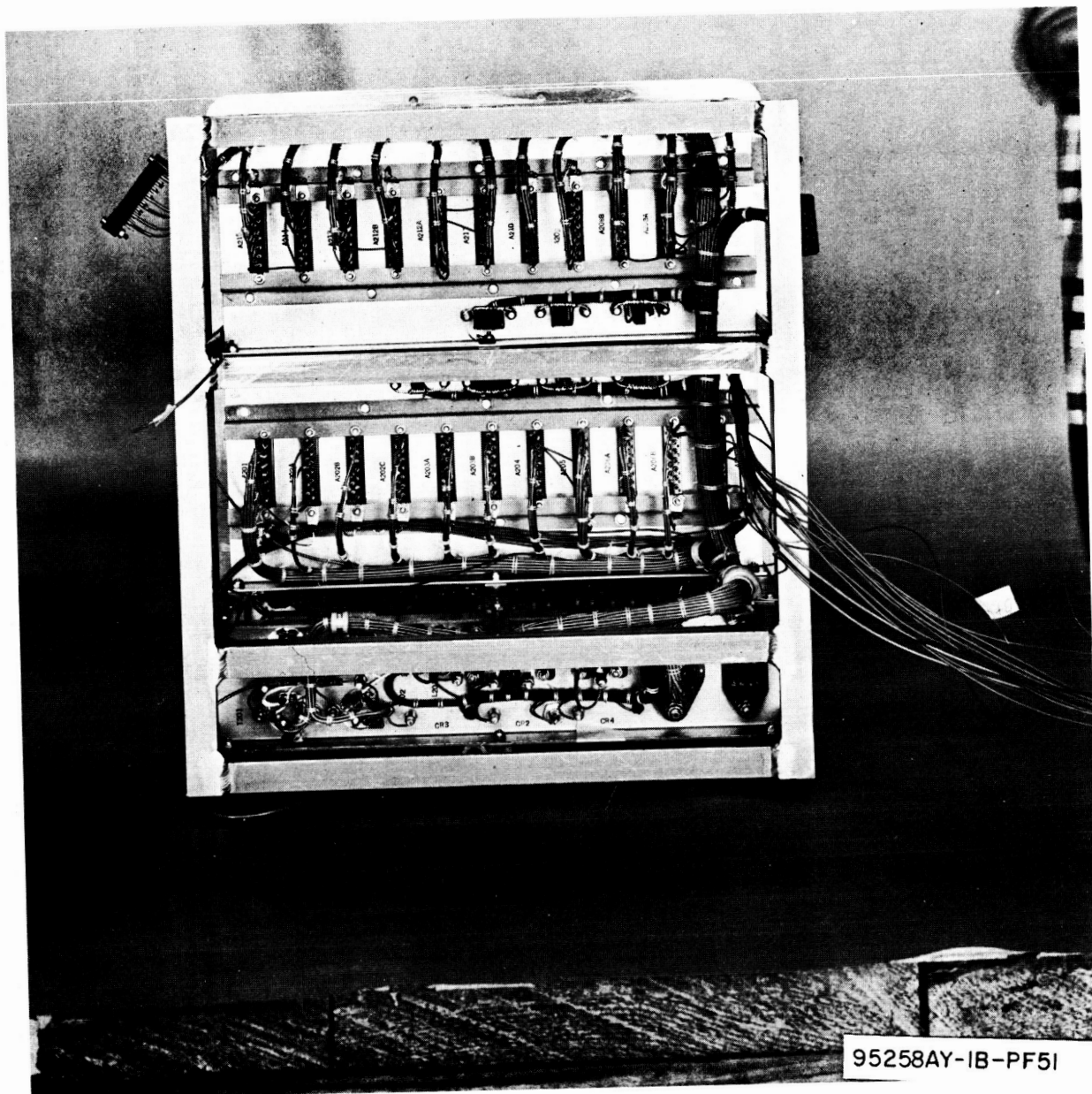
Figure 9-2.   Test Setup for Task V

magnetic field components of the three runs is shown in figure 9-3.   In this
figure the Z component, for 0 degree azimuth, 0 degree elevation, is plot-
ted from 3 to 10 feet and then extended to approximately 70 feet using dipole
theory.   The extension is shown by the dotted line.   The dipole equation
used to make this extension is:
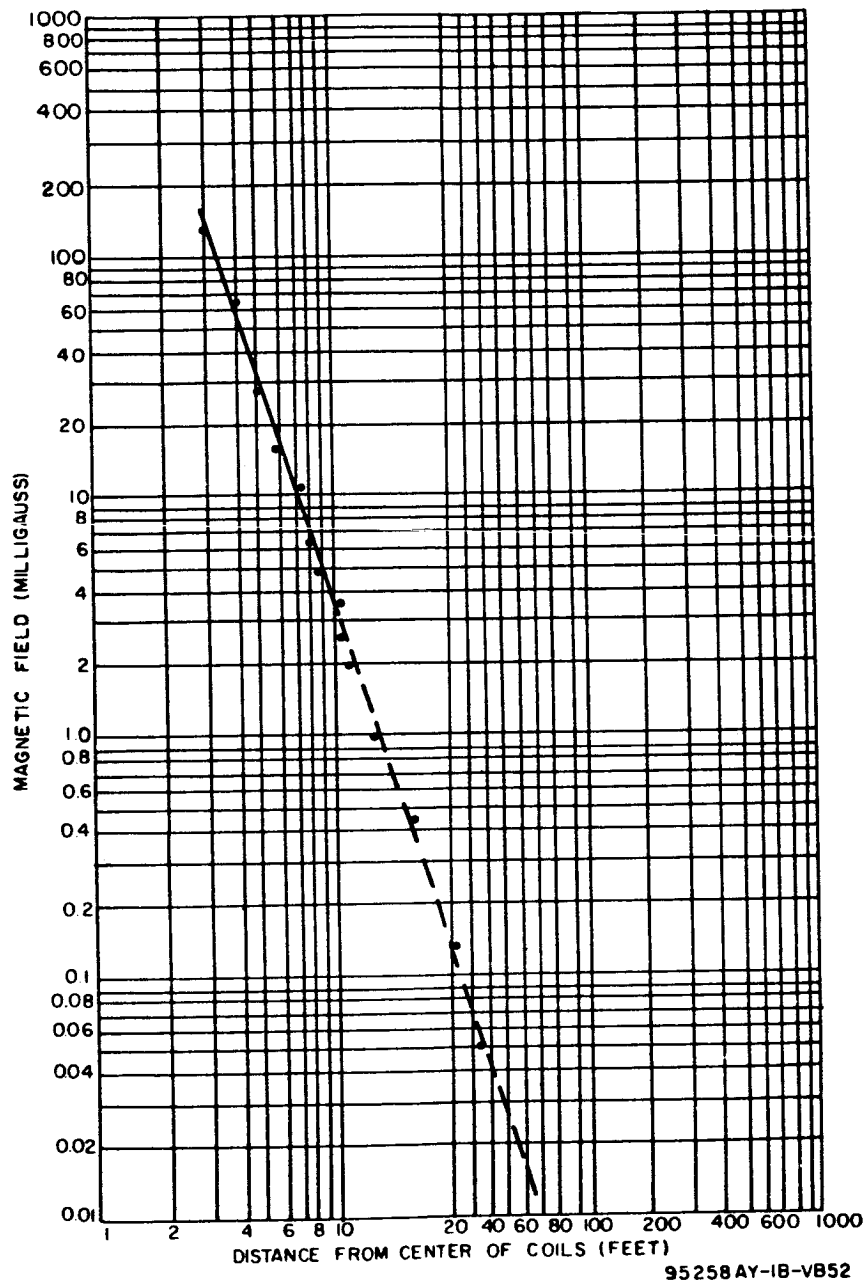
Figure 9-3. Magnetic Field Plot for Z Component,
0 Degree Azimuth, 0 Degree Elevation
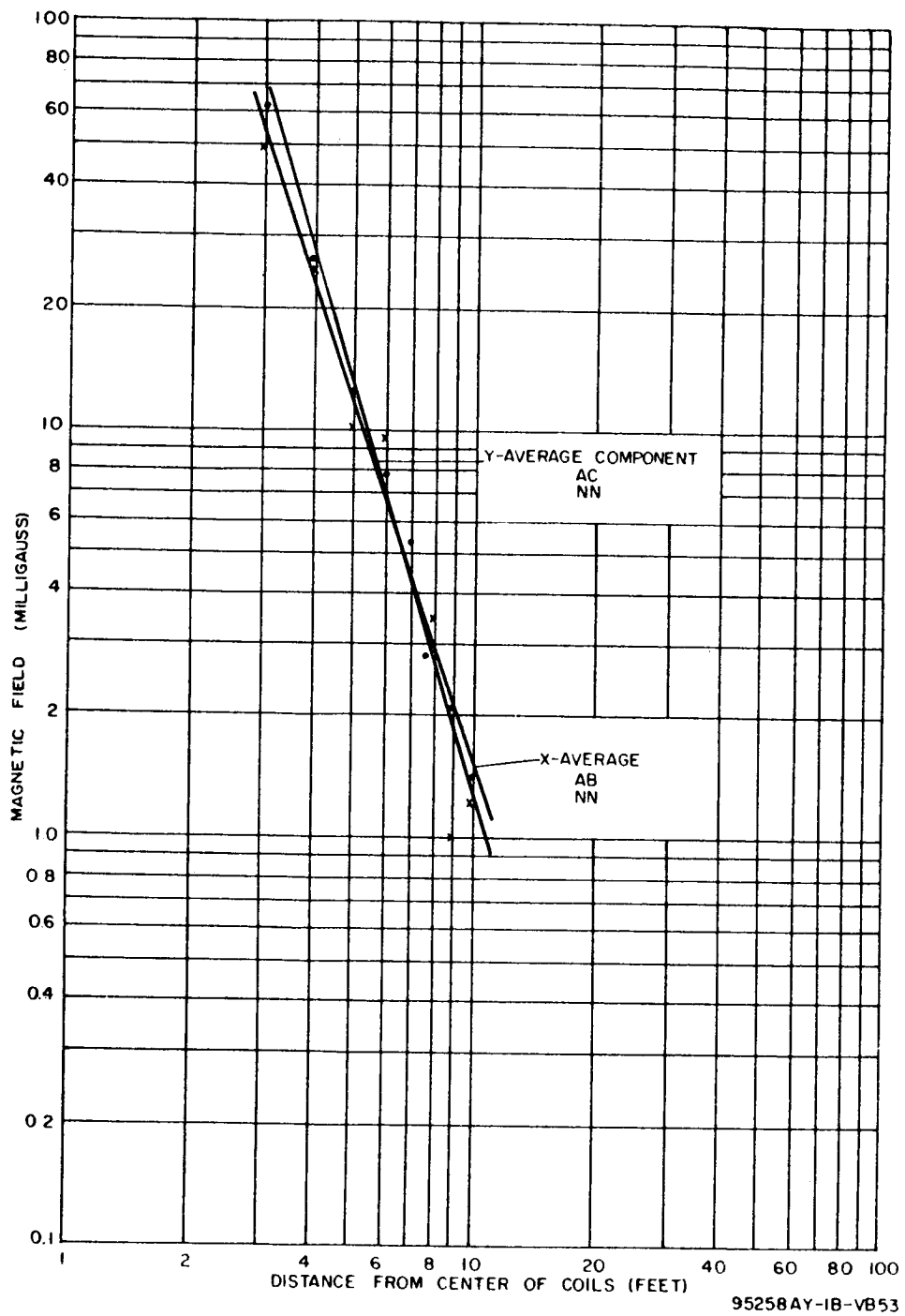
Figure 9-4. Magnetic Field Plot for X and Y Components,
0 Degree Azimuth, 0 Degree Elevation
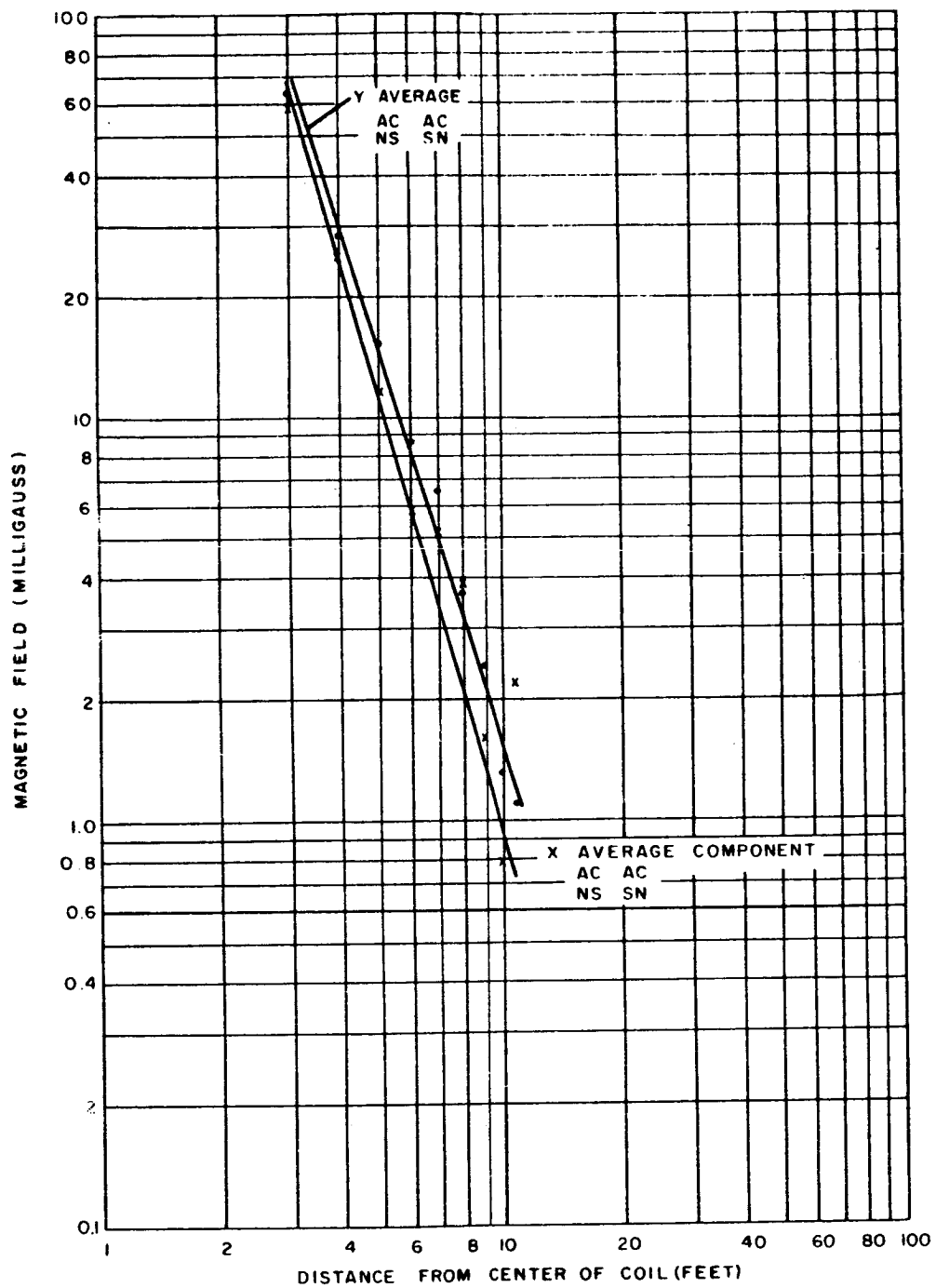
Figure 9-5. Magnetic Field Plot for X and Y Components,
0 Degree Azimuth, 0 Degree Elevation
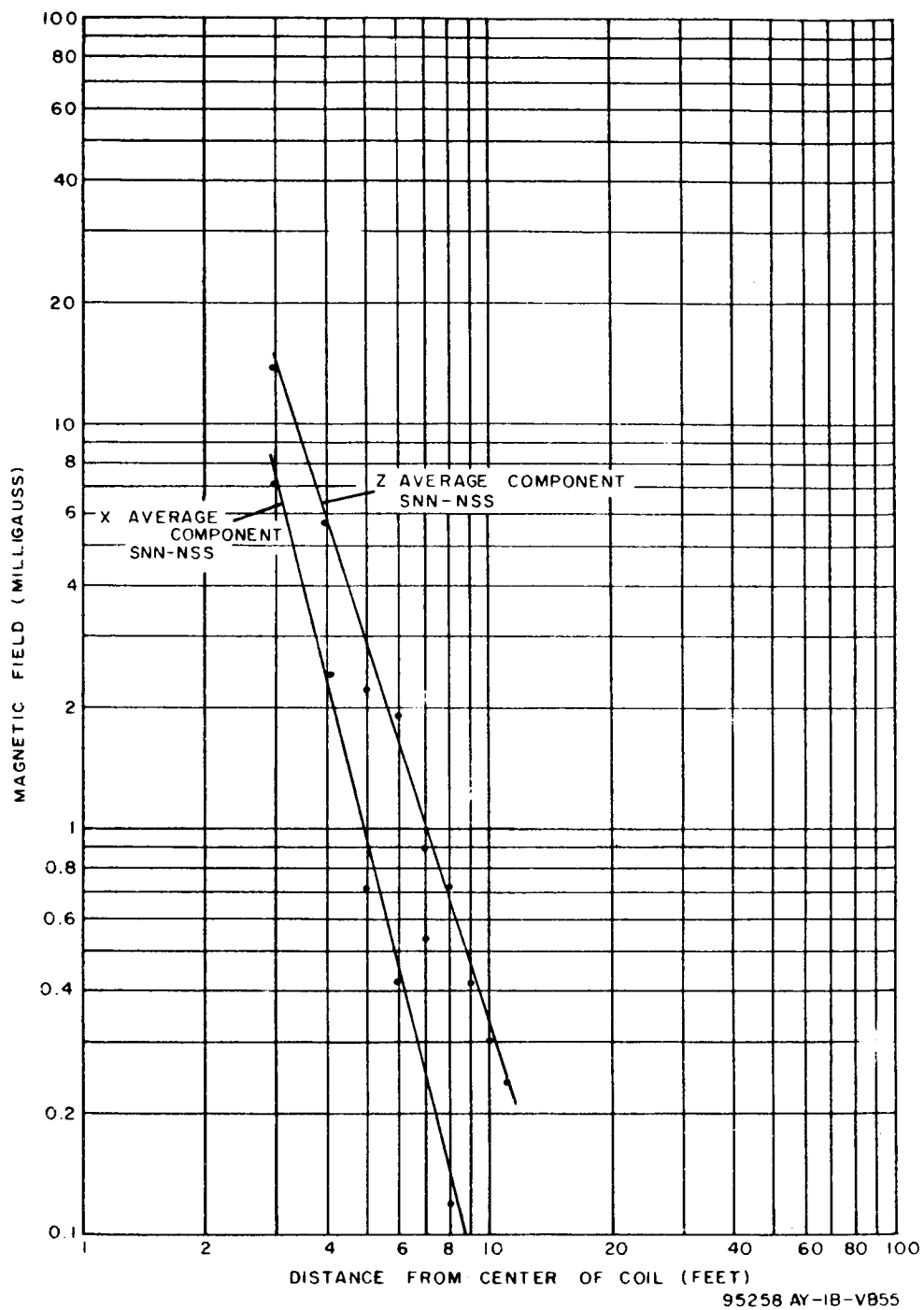
Figure 9-6. Magnetic Field Plot for X and Z Components,
45-Degree Azimuth, 45-Degree Elevation
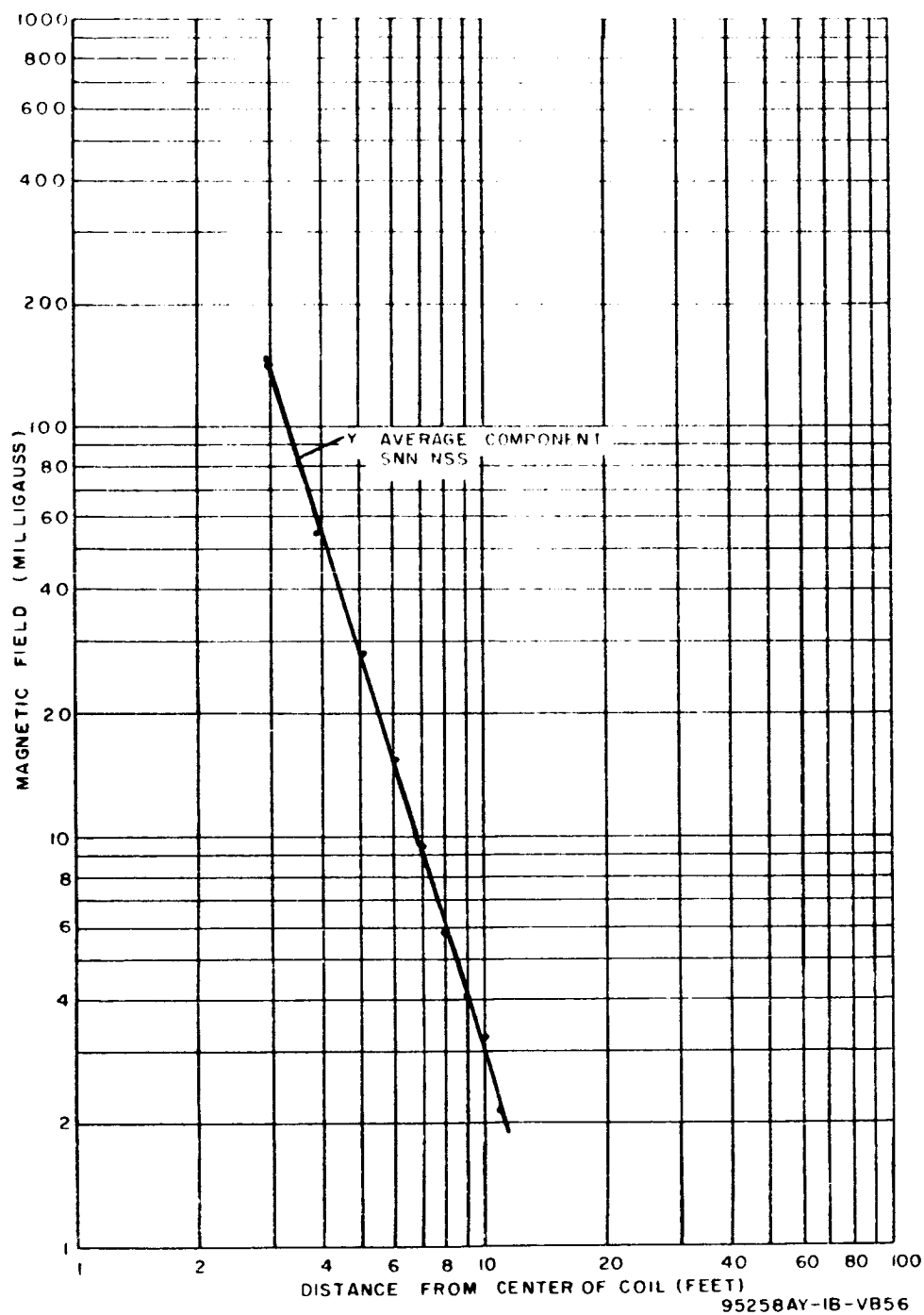
Figure 9-7. Magnetic Field Plot for Y Component,
45-Degree Azimuth, 45-Degree Elevation
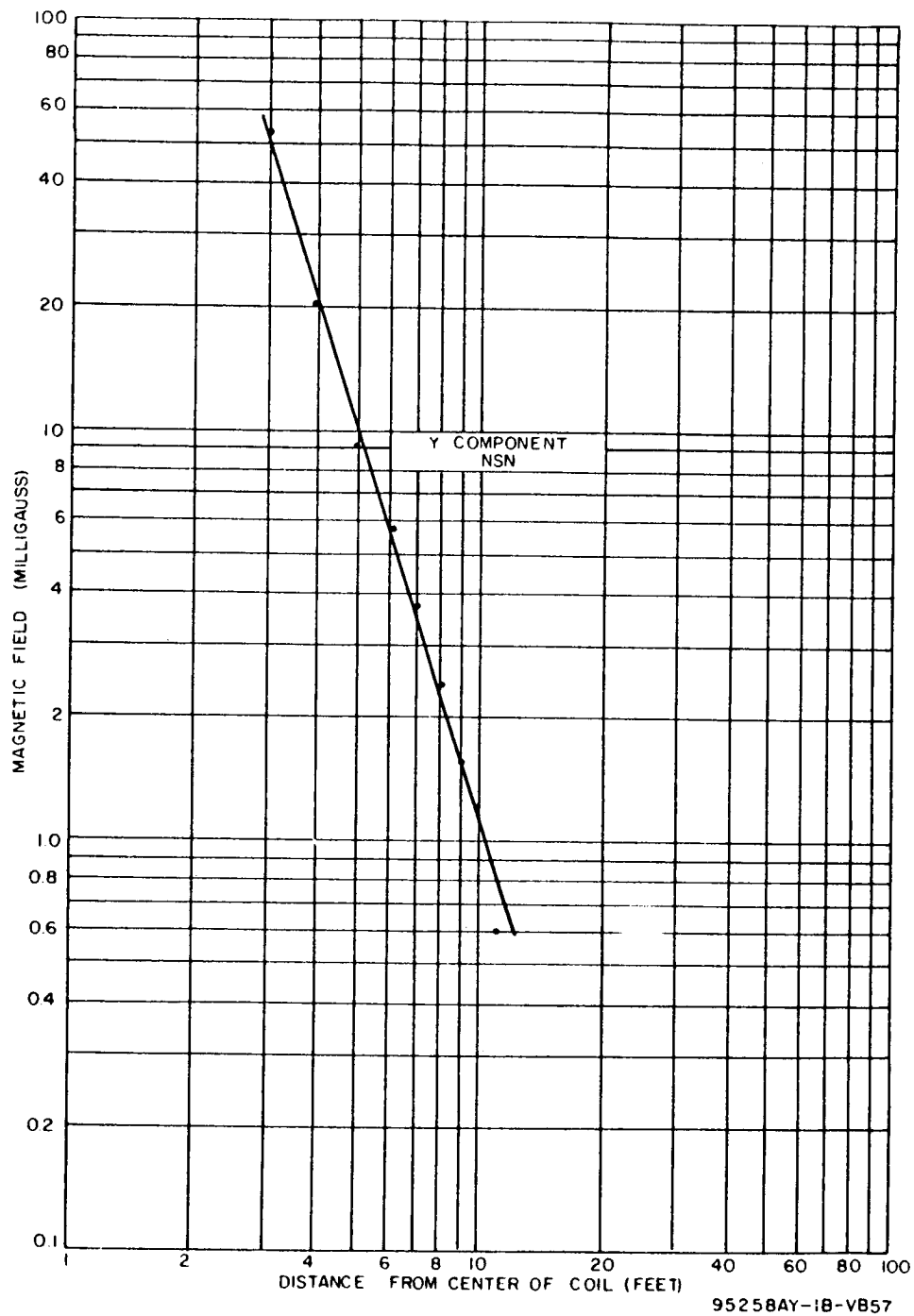
Figure 9-8.   Magnetic Field Plot for Y Component,
45-Degree Azimuth, 45-Degree Elevation
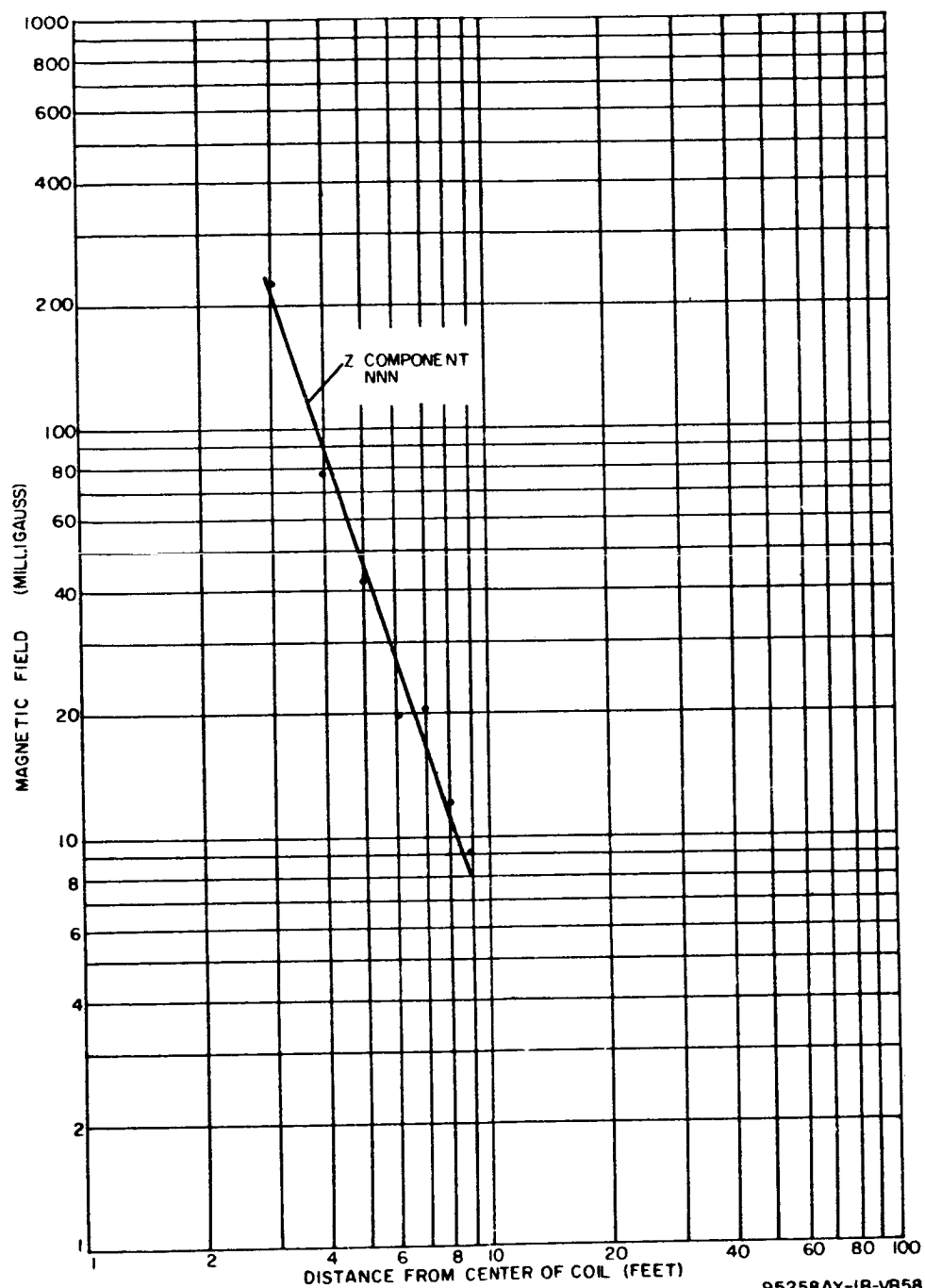
Figure 9-9. Magnetic Field Plot for Z Component,
45-Degree Azimuth, 45-Degree Elevation
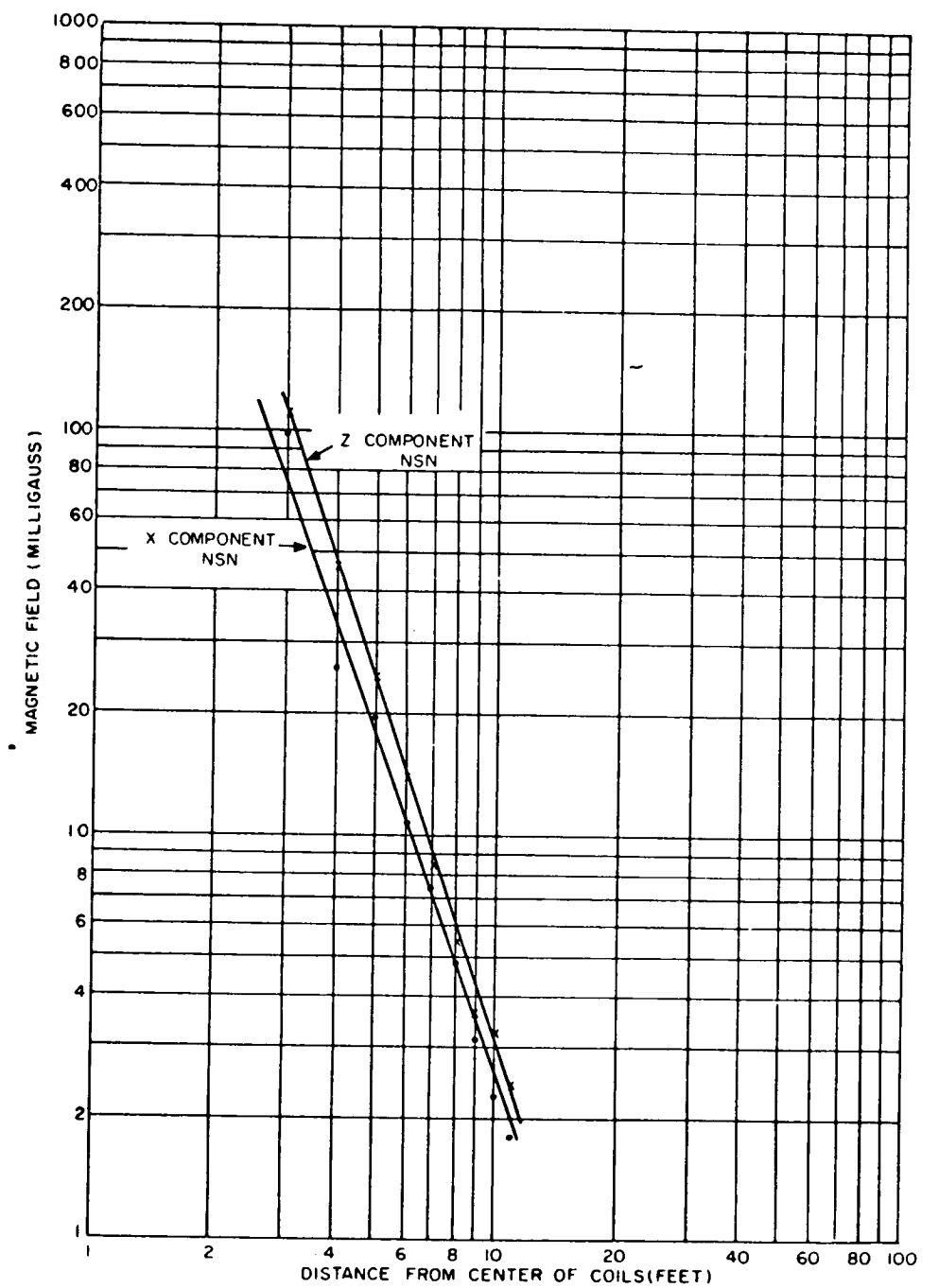
Figure 9-10. Magnetic Field Plot for X and Z Components,
45-Degree Azimuth, 45-Degree Elevation
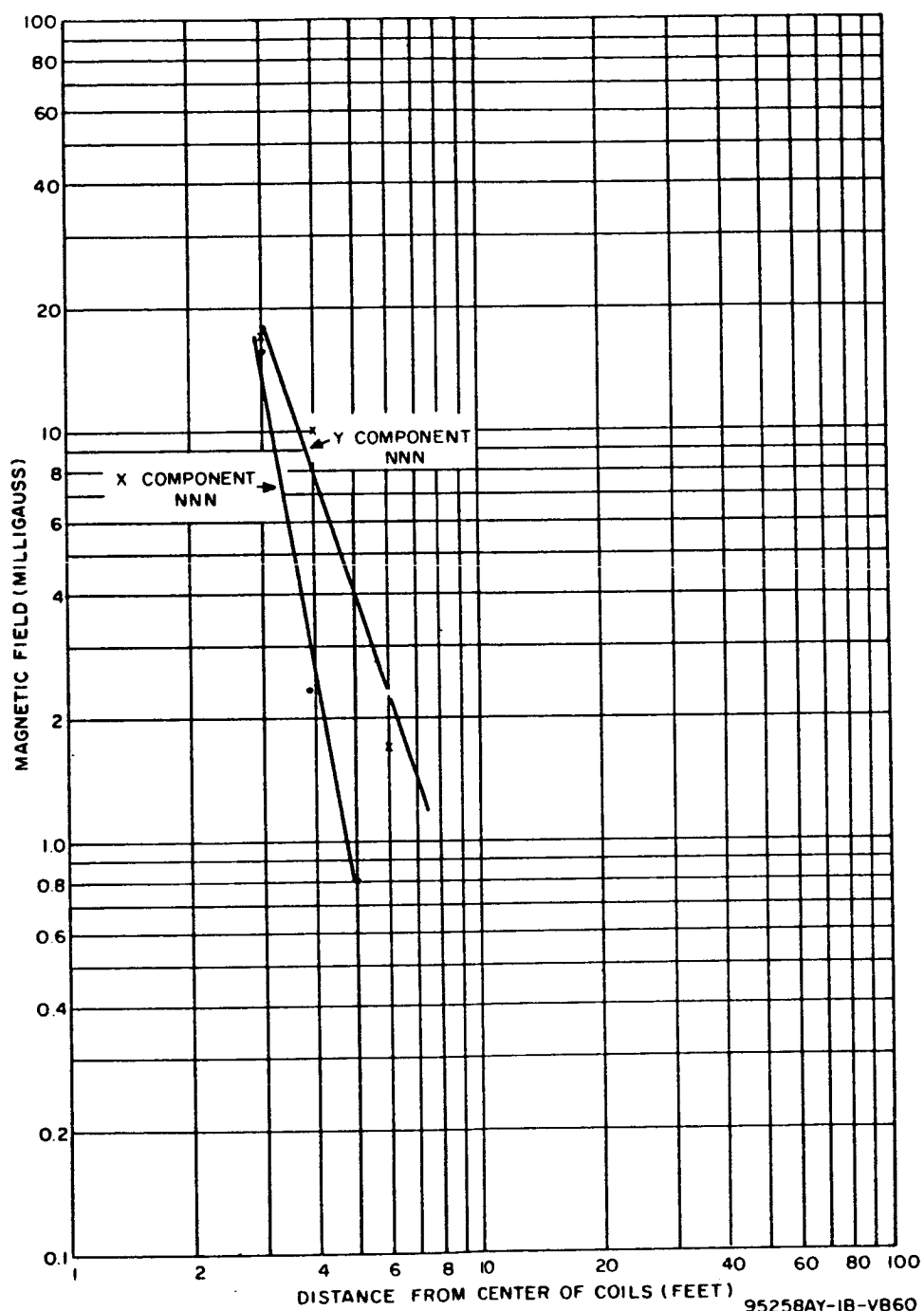
Figure 9-11. Magnetic Field Plot for X and Y Components, 45-Degree Azimuth, 45-Degree Elevation
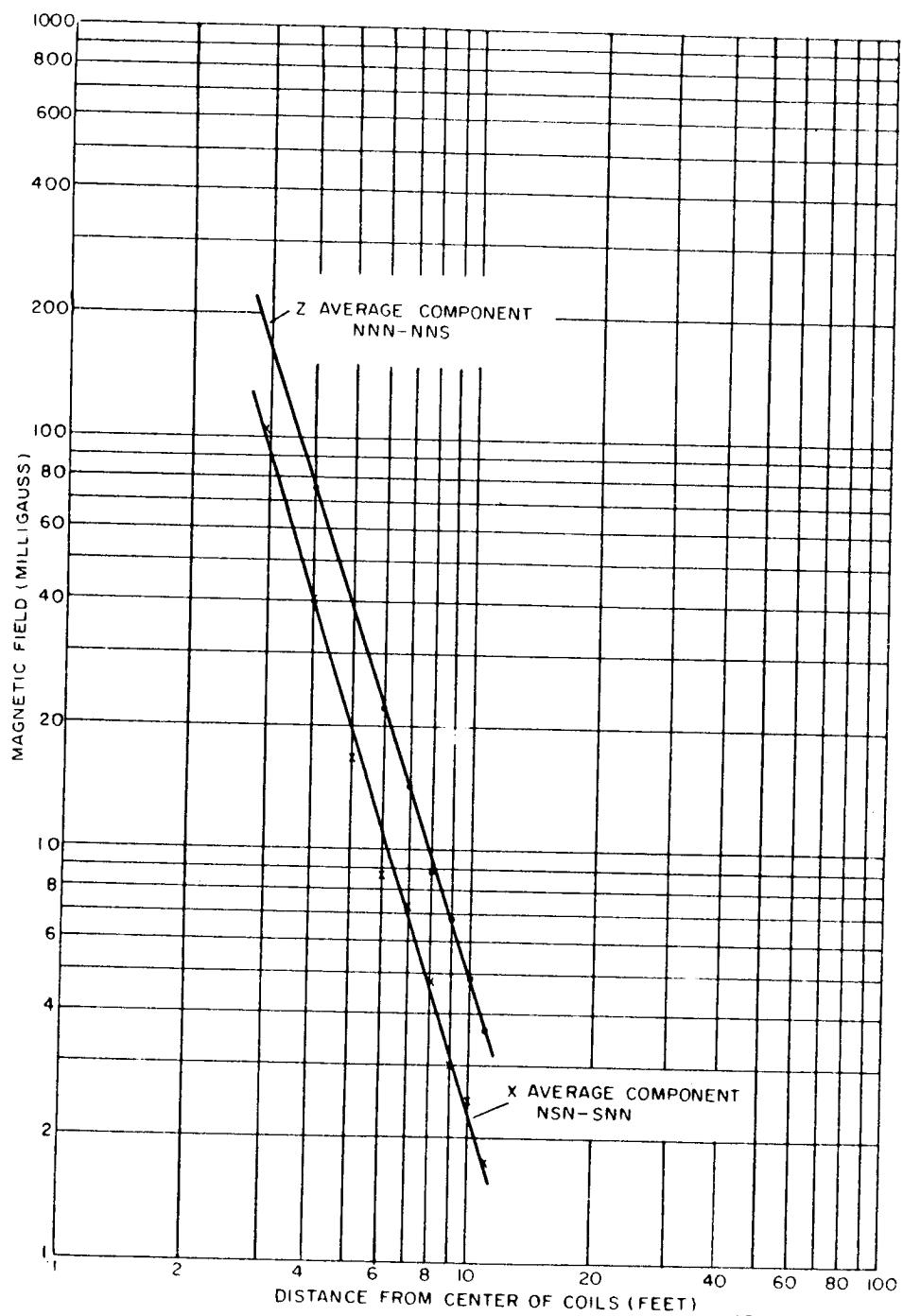
Figure 9-12.   Magnetic Field Plot for X and Z Components, 45-Degree Azimuth, 0-Degree Elevation
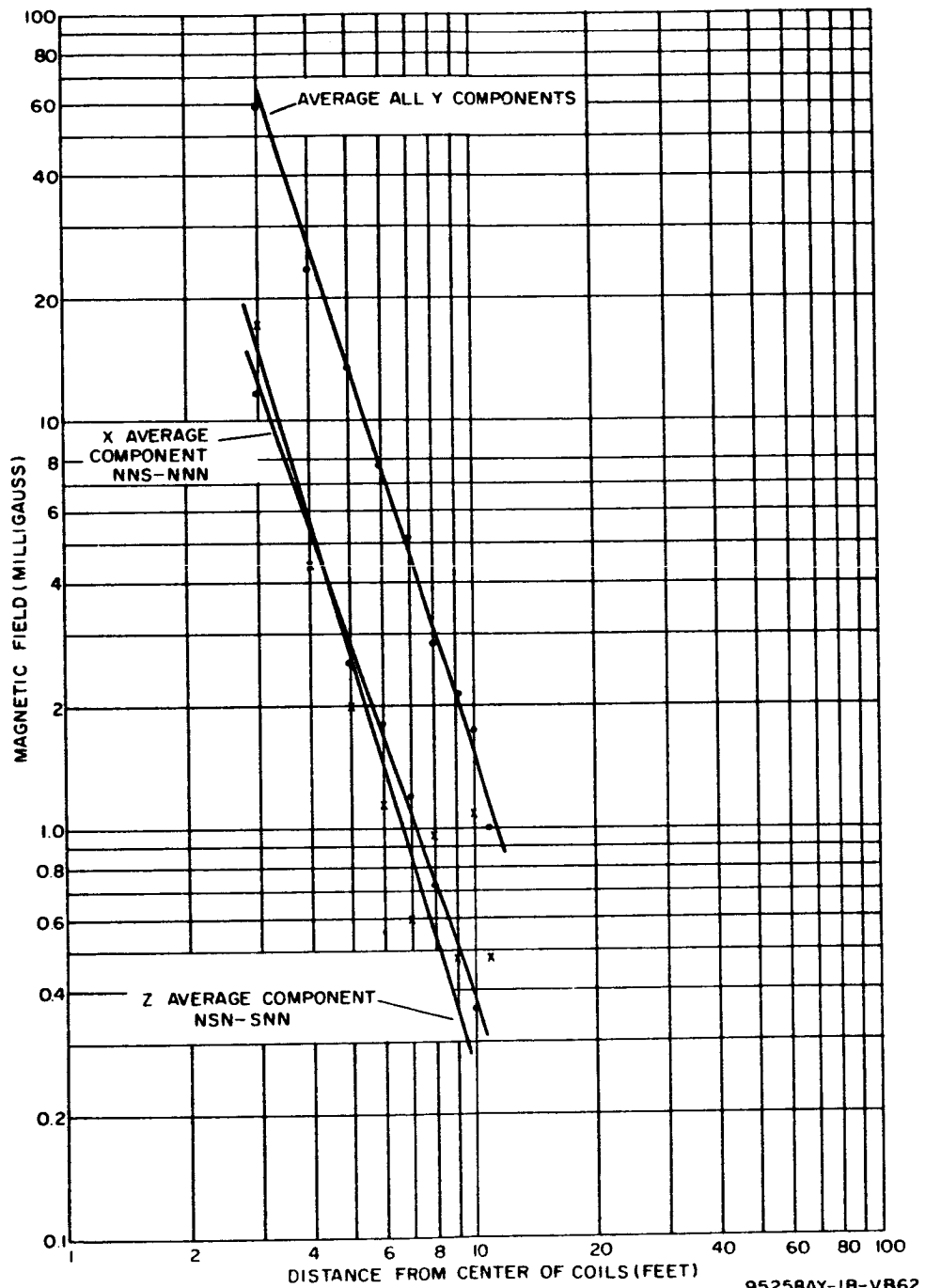
Figure 9-13. Magnetic Field Plot for X, Y, and Z Components, 45-Degree Azimuth, 0-Degree Elevation

$$H = \frac{k\, 2\, l\, m}{d^3} \quad ; \quad K = k\, 2 l m$$

where H is the magnetic field in milligauss, d is the distance from the center of the coil in feet, k is the constant of proportionality, and l is the distance in inches between the two poles of strength m. The method of least squares was used to determine a K of 3510 milligauss-feet^3 for the magnetic field plot of figure 9-3. Of the eight points obtained from the test data, to make the plot of figure 9-3, there was a maximum error of only 6 percent for the best straight line drawn on log-log paper.

Using the dipole equation and the K of 3510 milligauss-feet^3 for the tested torquer as a basis, three new magnetic field plots were made for various size torquers. Although the method used to determine these new plots for various size torquers is not a rigorous one, it is felt that it is of sufficient accuracy to warrant a generalization from the specific case. The three magnetic field plots were determined using the original test coil K from the 64,000 dyne-cm per gauss coil and the information below:

| Coil No.	Torque (dyne-cm per guass) (expressed as a fraction of the original torque)	Length (in.) (expressed as a fraction of the original length)
1	0.25 (64,000) = 16,000	0.5 (20) = 10
2	0.10 (64,000) = 6400	0.25 (20) = 5
3	0.05 (64,000) = 3200	0.15 (20) = 3

The original equation for the magnetic field of the Z component is:

$$H = \frac{3510}{d^3}$$

and since the new desired information is expressed as a fraction of the orig-inal parameters of l and m, the new K can be determined in the following manner, using coil No. 1 as an example:

$$H = \frac{(0.25)\,(0.5)\,(3510)}{d^3} = \frac{439}{d^3} = \frac{K}{d^3}$$

Coils No. 2 and No. 3 were treated similarly. Values of H were then determined by substituting in various values of d in the above and are plotted in figures 9-14 through 9-16. In performing the mathematical operations for the three new coils, it is assumed that H varies linearly with both the pole strength m and the distance, l, between them. This assumption is only approximately true, but should be adequate for initial design. An empirical determination of the field map would be a necessary later design step for satellite magnetic actuators.

From the information gained in figures 9-14, 9-15, 9-16, and 9-3, a curve was made of 5-percent magnetic interference for various torque ratings in a 6-hour orbit (5 percent of the maximum earth's field of 15.6 milligauss, or 0.78 milligauss). See figure 9-17.

9.4 COMPENSATION TECHNIQUES

In paragraph 9.1, it was stated that there are at least three methods for decreasing the interference of the torque coils on the magnetometer probes. If sufficient coil-magnetometer separation connot be provided, then the interfering field can be compensated for by creating a field of equal but opposite polarity at the location of the magnetometer probes.

There are several types of coils that can be designed and built to compensate for the interfering fields. The two coils that seem to be the most feasible from the standpoint of simple construction are the Hemholtz coil and the elliptic cone segment coil, as shown in figure 9-18. The interference field is also shown in figure 9-18 along with the created field from each of the two compensation coils. The interference field is the Z-axis field of the coils used in the interference study (see figure 9-3).

The bend in the interference field is exaggerated in figure 9-18 and is 0.1 foot long. The 0.1-foot length is approximately equal to the length of one of the magnetometer probes and is placed at a point 5.0 feet from the torque coils. If the separation between the two Helmholtz coils is made equal to their radius, then the field created between the coils will be near constant at a value depending on their radius, the number of turns, and the unidirectional current passing through the windings. As seen from the graph, the
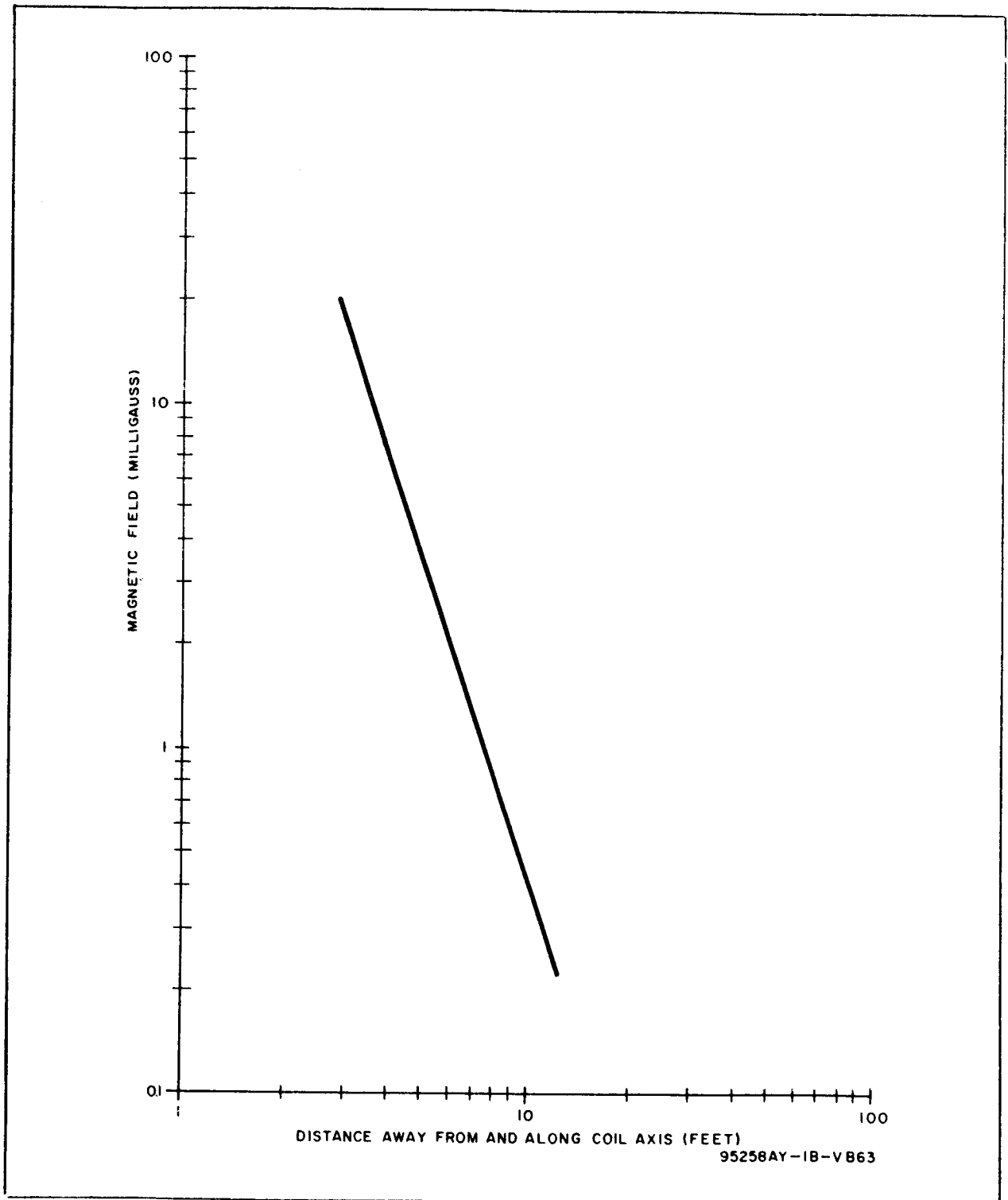
Figure 9-14. Magnetic Field Plot for a 16,000 $\frac{\text{Dyne-cm}}{\text{Gauss}}$ Torquer (Length of Coil = 10 Inches)
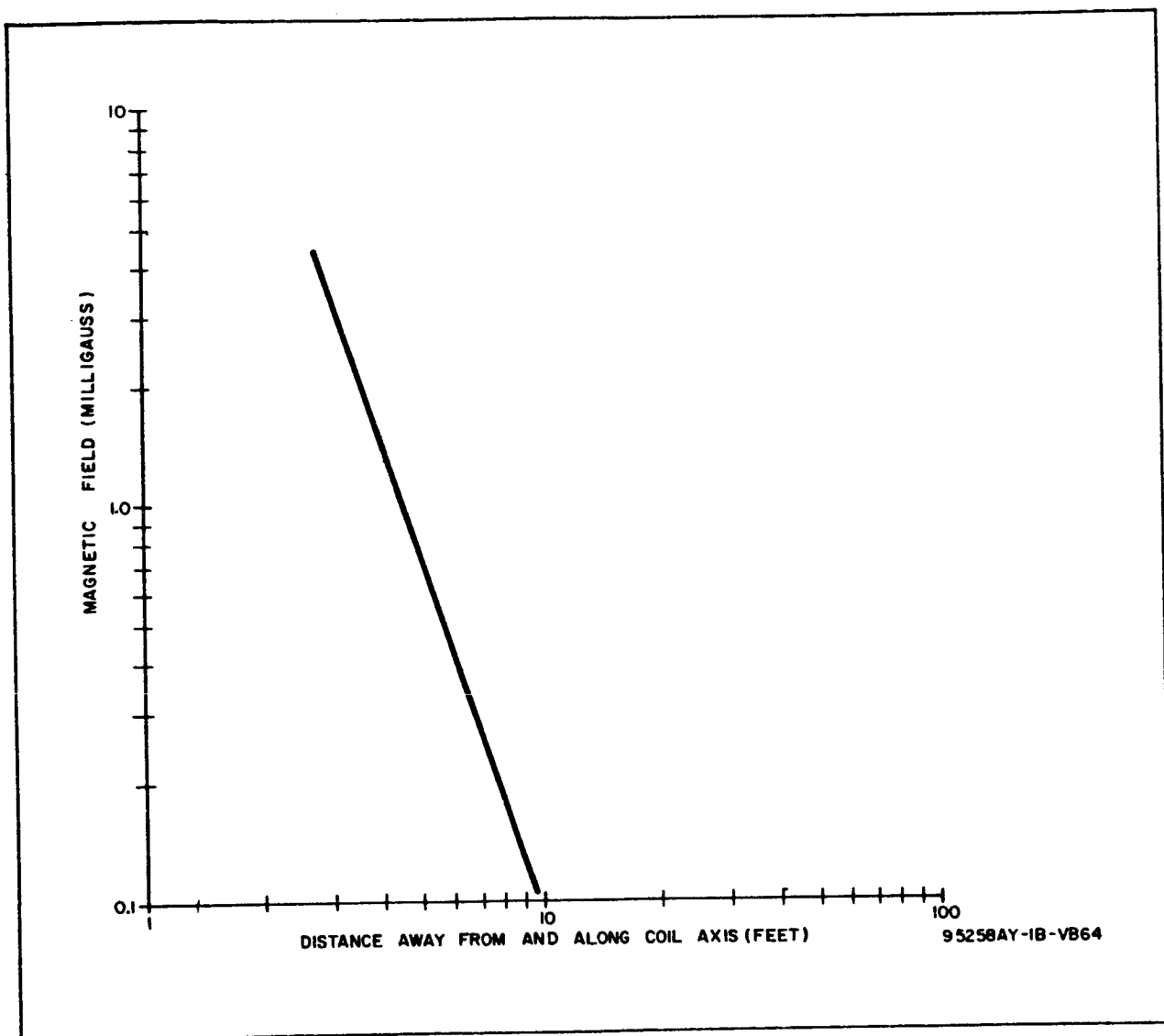
Figure 9-15. Magnetic Field Plot for a 6400 $\frac{\text{Dyne-cm}}{\text{Gauss}}$ Torquer (Length of Coil = 5 Inches)

Helmholtz coils could cancel the interference field up to 26. 5 milligauss. The percent interference that the torque coils' field will have on the magnetometer probes, assuming a 6000-mile orbit and a earth's magnetic field of 15. 6 milligauss is:

$$\frac{(28.0 - 26.5)}{15.6 \times 2} \times 100 \text{ percent} = 5.2 \text{ percent average interference}$$

However, it is possible to create a Helmholtz field midway between 26. 5 and 28. 0 milligauss, and the resultant field integrated over the sensitive axis of the magnetometer probe could almost cancel the interference field
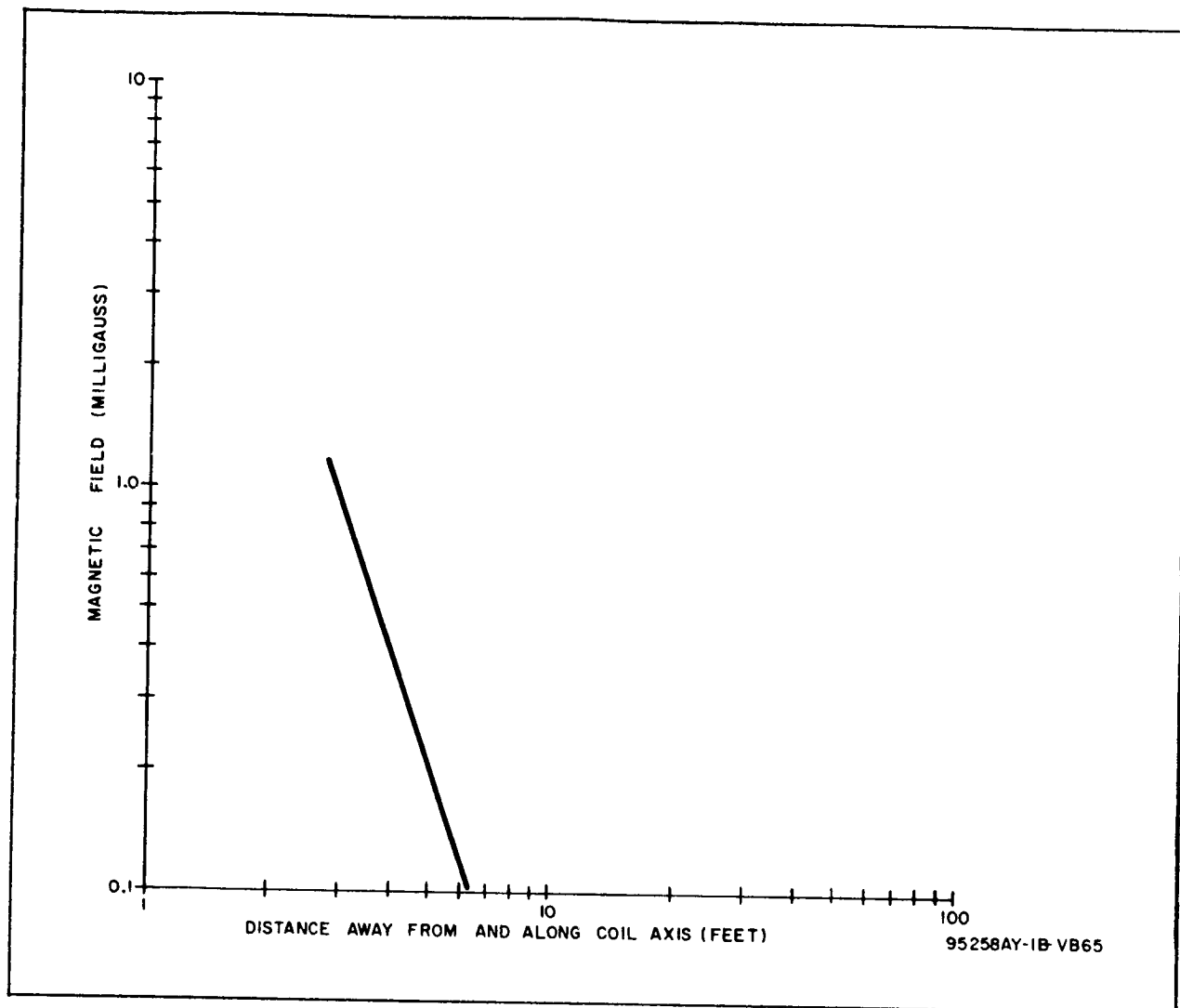
Figure 9-16.   Magnetic Field Plot for a 3200 $\dfrac{\text{Dyne-cm}}{\text{Guass}}$ Torquer (Length of Coil = 3 Inches)

completely.   However, it is not known at this time if the permeable core of the sensitive axis of the magnetometer would integrate this resultant field.

The elliptic cone coil (truncated right circular cone) could cancel the interference field to approximately 0.1 percent interference.   The interference field is a third order function but over the short distance of 0.1 foot appears to be a linear function.   To produce a linear field with the correct slope from the elliptic cone coil, it is necessary to select the correct radii, number of turns, magnitude of unidirection current, and a length somewhat longer than the length of the sensitive axis of the magnetometer probe.
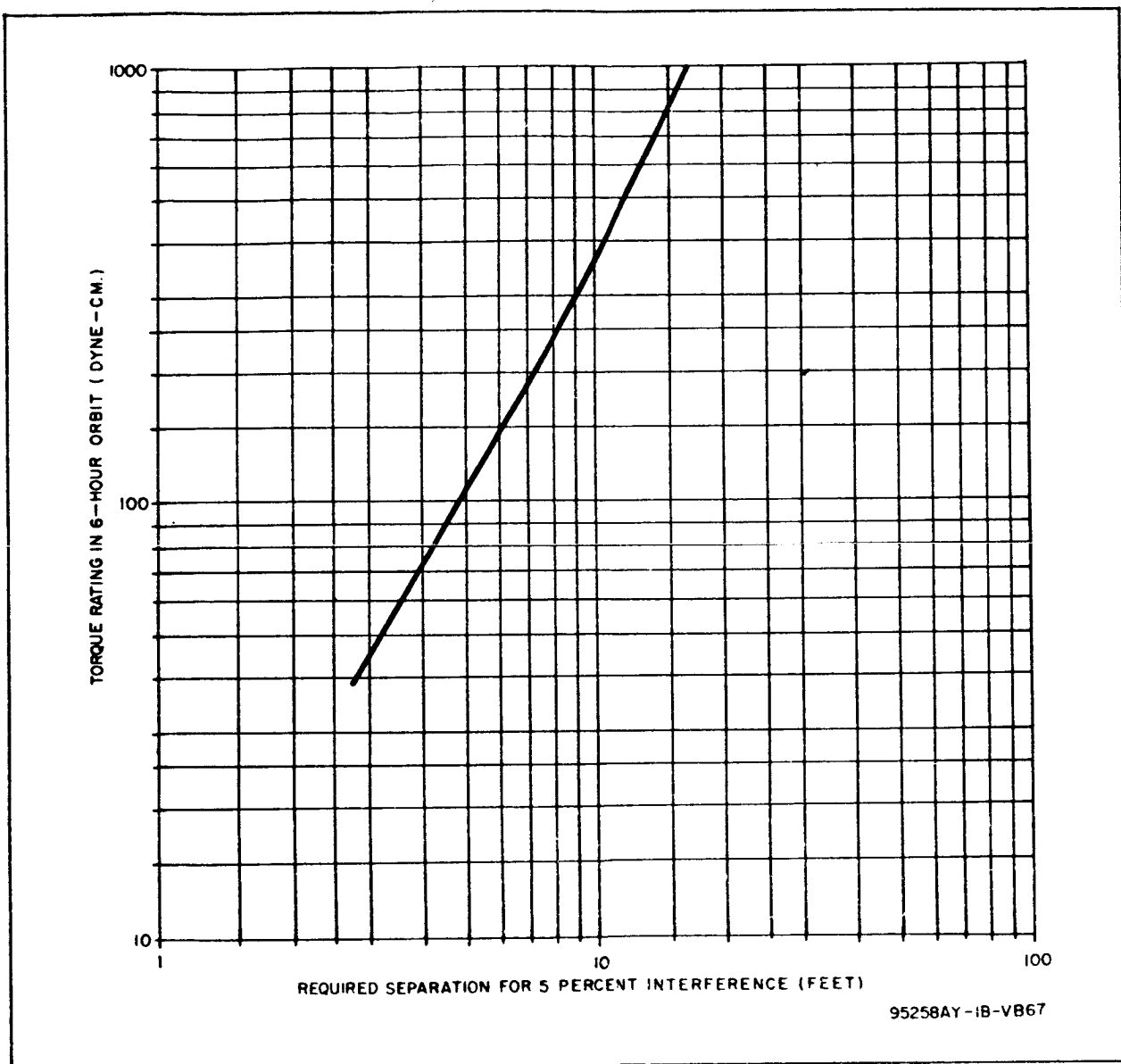
Figure 9-17. Compensation With Air-Core Coils

The figure is a log-log plot. The vertical axis is labeled "TORQUE RATING IN 6-HOUR ORBIT (DYNE-CM.)" ranging from 10 to 1000. The horizontal axis is labeled "REQUIRED SEPARATION FOR 5 PERCENT INTERFERENCE (FEET)" ranging from 1 to 100.

95258AY-iB-VB67
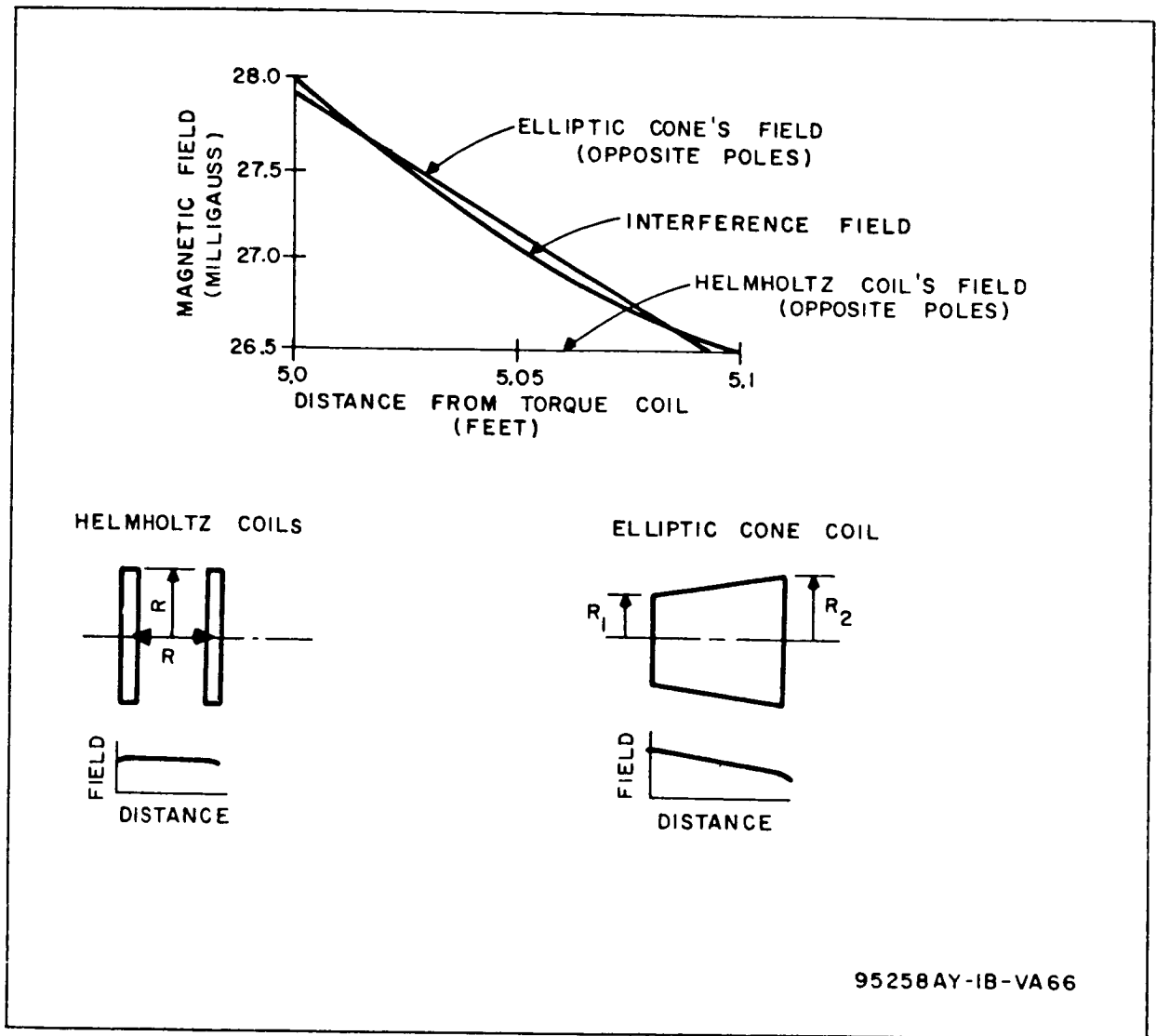
Figure 9-18. Torque Versus Separation for 5-Percent Interference

10.   TASK VI - SAMPLE SYSTEM DESIGN

10. 1   SCOPE

The goal for Task VI was to accomplish a preliminary design for an attitude control system utilizing three reaction wheels as primary torquers and three torque coils as momentum dumpers, as well as finding the following:

a.   Performance

b.   Reliability

c.   Weight and size

d.   Power requirements

In a sense, the choice of a three-wheel, three-coil system for study was arbitrary.   It was not assumed that such a system is optimum for any specific application.   Instead, the aim was to establish the parameters and potentialities of the system for use in future tradeoffs against other approaches to the attitude control problem.

The definition of this sample system involving electromagnetic actuation is not limited to actuation, but encompasses sensing, means of damping, detumbling, and erection as well, so that the complete picture of an attitude control system can be presented.   However, the electromagnetic actuation subsystem is of prime interest.   The basic steps constituting Task VI were as follows:

a.   Assumption of a vehicle, its orbit, and the required orientation.

b.   Calculation of the attitude disturbances that might reasonably be expected.

c.   Development of a system plan.

d.   Choice and definition of components.   Here the required wheel and coil ratings grew out of the knowledge gained in Task I, while the specific coil design is a byproduct of Task IV.

e. Examination of system performance.

f. Calculation of system reliability.

g. Estimate of power requirements.

h. Estimate of weight and size.

10.2 PROBLEM ASSUMPTIONS

The vehicle was assumed to be a cylindrical shape, 2-1/2 feet in diameter, and 5 feet long, with roughly equal moments of inertia, 50 slug-feet^2, and a weight of 500 pounds. The orbit was assumed to be a 6-hour, circular one, inclined at 32 degrees.

It was also assumed that the vehicle must be oriented to the local vertical and the orbital plane, such as might be required in a communications satellite where velocity control is employed. It was also assumed that power is generated by a solar array requiring orientation; however, since the magnetic actuator design work of Task IV is based on an oriented array, this method of orientation is not considered. Yaw control is dictated only by the orbital plane requirement. The long axis of the cylinder is the yaw axis (aligned with the local vertical). The roll axis is in the orbital plane, and the pitch axis is therefore perpendicular to this plane. It is assumed that the vehicle is initially tumbling at component rates not exceeding 1 degree per second.

In a sense, the criteria and plan for yaw control is unrealistic or incomplete, since the solar array orientation problem is ignored. It might be assumed that the yaw control used herein operates during periods of velocity control application and that the yaw system reverts to solar orientation at other times. In addition, an array rotatable about one axis would be needed to complete the orientation.

10.3 SYSTEM DESIGN

The purpose of the system is to maintain vehicle attitudes within predetermined limits during the lifetime of the vehicle. To achieve this end, the control system must be capable of several modes of operation, progressing from detumbling to steady state control including continuous momentum interchange with the earth's magnetic field. The block diagram of the complete system is illustrated in figure 10-1.
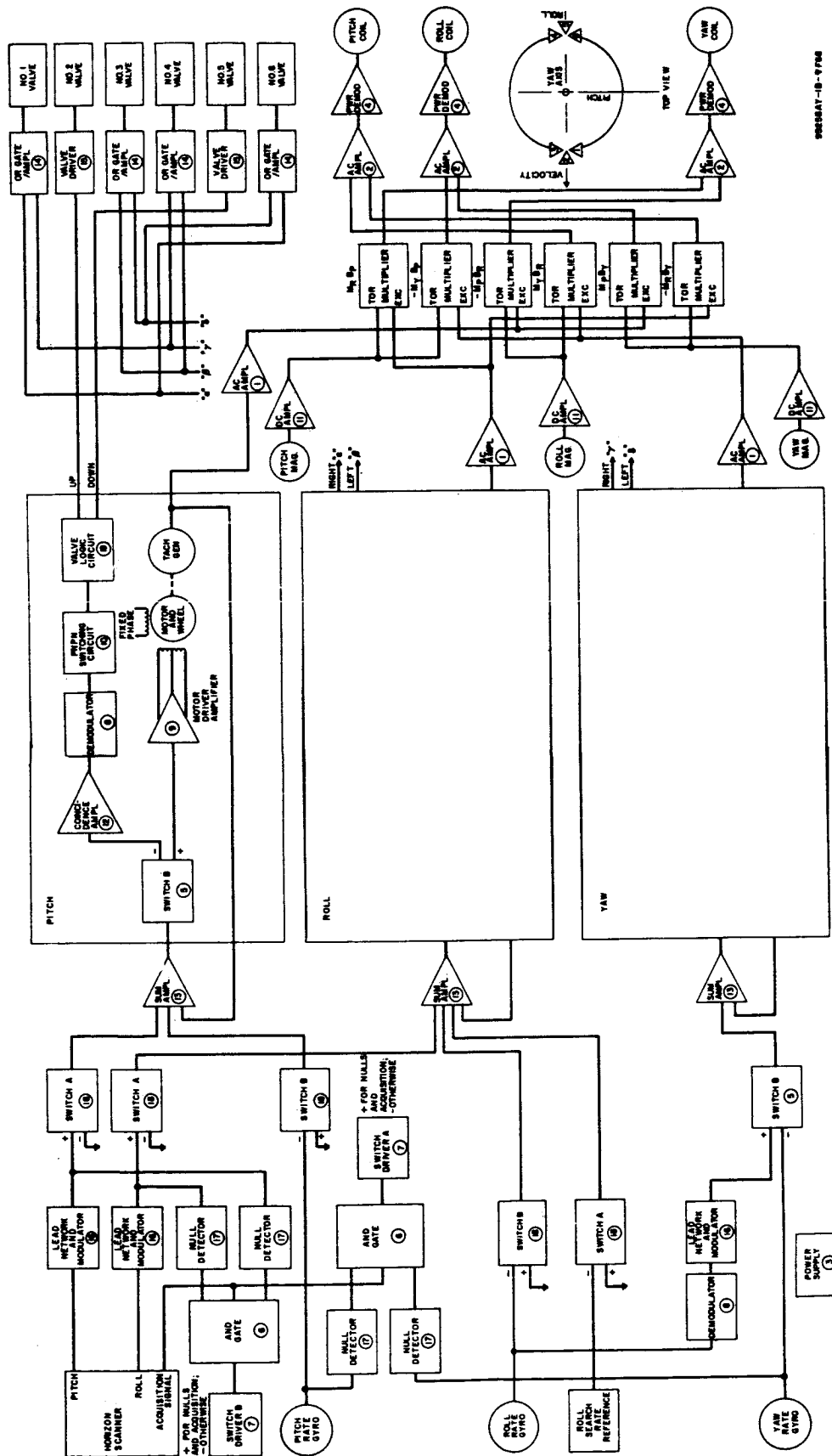
Figure 10-1. Overall Block Diagram, Task VI

10-3

10.3.1 Detumbling and Search Mode

The detumbling and roll search mode occurs first. When the vehicle is injected into orbit, the separation from the final stage will generate satellite tumbling rates, which must be reduced to zero prior to establishing the vehicle in its final attitude. The mechanization consists of generating rate signals which switch on the proper gas valve(s) to produce a decelerating torque. The portion of the system which functions during this mode is the same for the pitch and yaw axes and is illustrated in figure 10-2. Because of the hysteresis in the gyro and switching circuit, the vehicle rates in these axes will never be reduced exactly to zero, but instead will oscillate about the zero-rate point. The components of this limit cycle are illustrated on figure 10-3. The roll axis during this mode is biased to produce a 1-degree-per-second search rate for horizon acquistion as shown in figure 10-2.
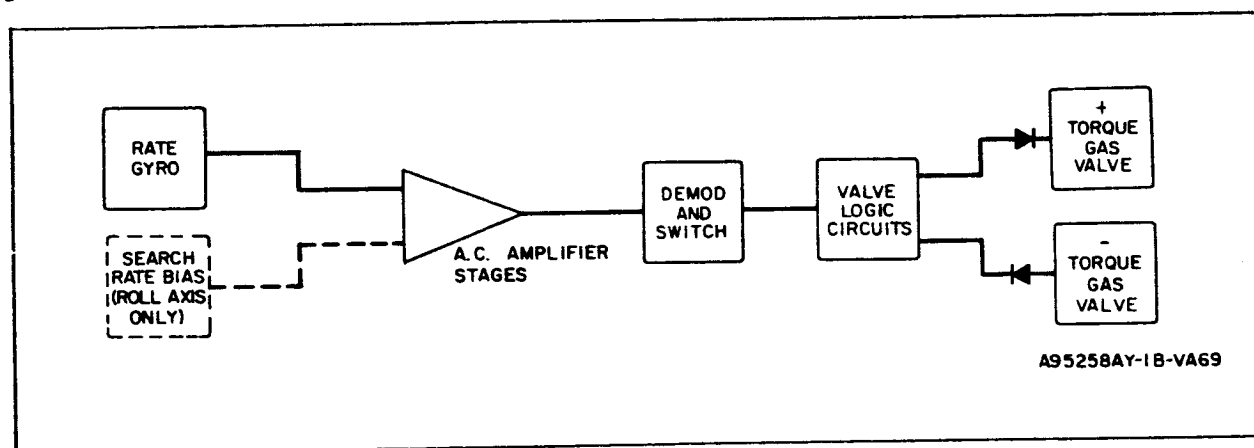
Figure 10-2. Basic Detumbling and Search Mechanization

The use of gas to detumble and erect is justified on the basis of the large angular momentum storage capability which would be required if the vehicle rates were absorbed in the wheels. Since the present wheels are designed for 0.14 lb-ft-sec storage, the detumbling requirement of 0.88 lb-ft-sec, when added to the disturbance momentum of 0.08 lb-ft-sec, would raise the required wheel inertia by a factor of 6.8, substantially increasing wheel weight.
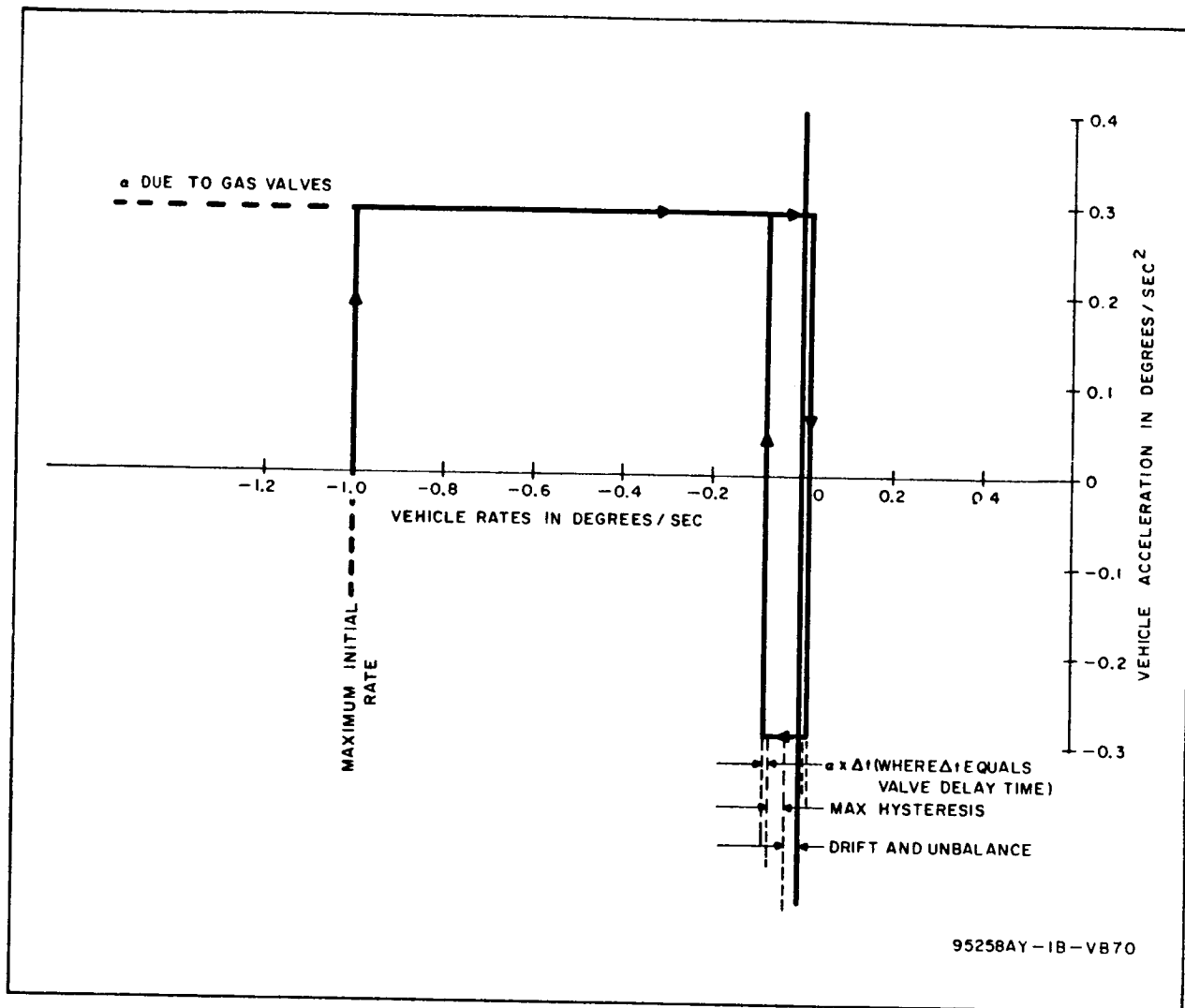
Figure 10-3.   Detumbling Limit Cycle

The mode ends when the horizon scanner detects the horizon, and the pitch and yaw rates are nulled.   The coincidence of these events triggers self-holding switch driver circuit A.

10.3.2   Erect to Vertical Mode

When the switch driver A circuit is energized, the roll bias is removed and the pitch and roll servos receive position reference signals from the horizon scanner.   These signals are limited and summed with the rate gyro signals to provide the servo input.   The vehicle then slews in both axes until

the horizon scanner signals are both nulled. At this point the switch driver B circuit is energized and the vehicle progresses to the normal pointing mode.

10.3.3 Normal Pointing Mode

During this mode the gas system is disabled and the servo input signals are switched to the motor driver amplifiers, which control the input current to the control phase of the motor. The fixed phase of each motor remains connected to the supply at all times.

At the time the switch driver B circuit is energized, the roll rate gyro and pitch rate gyro signals are switched out, and both servos then receive only position reference information from the horizon scanner and the vehicle is driven about both axes until the horizon sensor outputs are nulled. Damping is provided by a lead network and motor-tachometer feedback.

In the normal pointing mode, the yaw axis servo receives its signal from the accurate roll rate gyro, which senses the percentage of orbiting rate which is coupled to the roll axis by the yaw pointing error. The yaw axis error input is zero when the vehicle is pointing along the orbital path.

During long periods of orbiting, the disturbance torques described in paragraph 10.4 will build up large wheel velocities due to the motor torques generated to maintain the required pointing accuracy. Since these wheel-speed buildups will eventually saturate the motors and make them ineffective, a means is provided for generating vehicle torques which will decelerate the wheels. The indirect electromagnetic actuation technique described in Sections 2 and 5 will perform this function. The mechanization is illustrated on figure 10-4 and consists of the circuit elements necessary to generate the coil currents in accordance with the following equations:

$$I_R = (B_P \, \omega_Y - B_Y \, \omega_P) \, k$$

$$I_P = (B_Y \, \omega_R - B_R \, \omega_Y) \, k$$

$$I_Y = (B_R \, \omega_P - B_P \, \omega_R) \, k$$
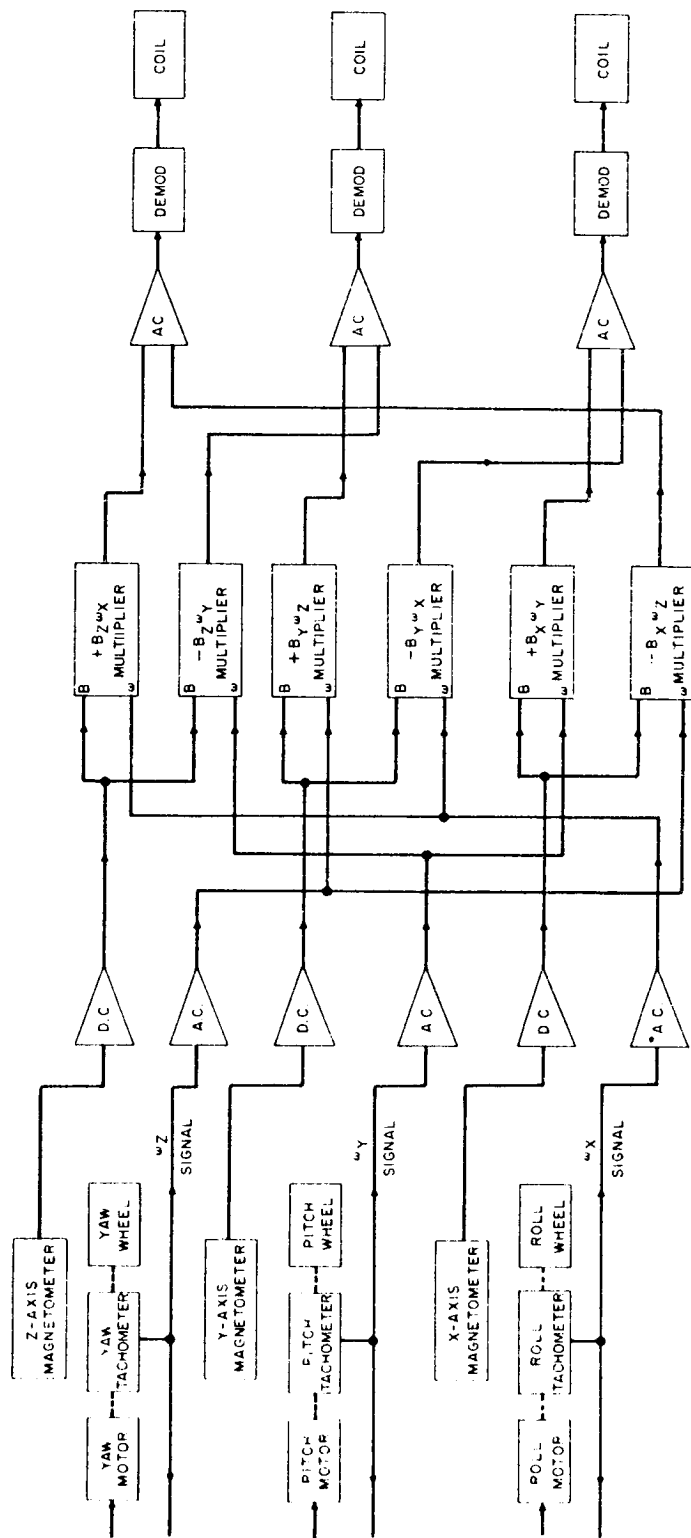
Figure 10-4. Momentum Dumping - Block Diagram of Mechanization

where

> B = field strength component along subscript axis
>
> ω = angular velocity in wheel of subscript axis
>
> I = current in coil whose axis coincides with the subscript axis
>
> P, R, Y = pitch, roll, yaw, respectively
>
> k = constant of proportionality

The heart of the mechanization is the electromechanical multiplier which forms the product of field strength component times wheel speed. The multiplier consists of a spring-restrained floating element which is displaced from zero by the torque generated in a coil. The displacement of the floating element then varies the coupling of a displacement transducer. If one signal drives the torque coil and the other signal supplies the primary excitation of the displacement transducer, the displacement transducer secondary signal is then proportional to the product of the two driving signals.

A total of six multipliers are used. The output of each wheel tachometer (400 cps) and each magnetometer element drives two multipliers, the pair connected to each driver signal being determined by the equations to be mechanized. Since the magnetometer signals, when modulated, are square wave a-c voltages, it was decided that it would be more efficient to demodulate them after amplification and use them to drive the torque coils of the multipliers. The wheel tachometer outputs, being sine waves, are amplified and drive the displacement transducer. If square wave driving were used for the displacement transducer, the secondary waveforms would be badly distorted and result in inaccuracies in the computation of coil currents.

10.4 ASSUMED DISTURBANCES

At the altitude considered, the disturbances will be very low. A short discussion of each disturbance is given below.

10.4.1 Solar Pressure Torques

The satellite is assumed to be symmetrical about the yaw axis. Along the yaw axis, it is assumed that the distance between satellite centers of pressure and gravity is 6 inches. The maximum area is 12.5 feet^2. To obtain

the most pessimistic torque, it is assumed that specular reflection from a surface of unity reflectivity is obtained. Then

$T = P_r \, Ad$, where P_r is the radiation pressure, A the area, and d the lever arm.

$$T = 1.9 \times 10^{-7} \frac{lb}{ft^2} \times 12.5 \, ft^2 \times \frac{ft}{2} = 1.19 \times 10^{-6} \, ft\text{-}lb = 16 \, dyne\text{-}cm$$

This is the maximum torque. For pitch and roll axes, the torque can be as high as:

$$T = 1.19 \times 10^{-6} \sin \omega_o t \, ft\text{-}lb,$$

where ω_o is the orbital rate. This torque exists for the case in which the yaw axis is perpendicular to the sun line. Although this condition will rarely occur, the control system must be capable of handling this torque level.

10.4.2 Aerodynamic Torques

At the altitude of 5750 nautical miles, the air density is less than 10^{-20} slug/feet^3. Since the velocity is relatively low, the aerodynamic torque value is negligibly low.

10.4.3 Gravity Gradient Torques

There will be no significant gravity gradient disturbance, since the vehicle will have nearly equal moments of inertia about the major axes and will be vertically oriented.

10.4.4 Orbit Ellipticity Disturbances

A satellite in a circular orbit obtains a constant pitch rate when oriented to the local vertical. If the orbit is actually elliptical, the direction of the local vertical varies sinusoidally because the earth's center is at one focus of the ellipse. If the orbit altitude is $R \pm \Delta R$, then the maximum angular excursion is

$$\theta_M = \tan^{-1} \left(\frac{\Delta R}{R} \right),$$

where θ_M is the angular variation of the actual local vertical from a circular local vertical, and R is the mean orbital radius. Then

$$\theta = \theta_M \sin \omega_o t$$

$$\alpha = \frac{d^2\theta}{dt^2} = -\theta_M \omega_o^2 \sin \omega_o t$$

$$T = I\alpha = -I\theta_M \omega_o^2 \sin \omega_o t$$

$$= -I \tan^{-1}\left(\frac{\Delta R}{R}\right) \omega_o^2 \sin \omega_o t$$

$$= -I \tan^{-1}\left(\frac{\Delta R}{R}\right)\left(\frac{2\pi}{\tau}\right)^2 \sin\left(\frac{2\pi t}{\tau}\right)$$

where T is the torque required, I is the vehicular moment of inertia, τ is the orbital period, and α is the acceleration.

Assuming that the ellipticity will be such that Δ R is 50 nautical miles, the disturbance torque will be $2.3 \times 10^{-8} \sin \omega_o t$ ft-lb or $0.311 \sin \omega_o t$ dyne-cm.

10.4.5 Magnetic Torques

Magnetic torques produce continuous disturbances on the satellite. The earth's magnetic field components can be approximately as follows:

$B_1 = 0.01815 + 0.00307 \sin \omega_o t$ (parallel to roll axis)

$B_2 = 0.01087 \cos \omega_o t$ (parallel to pitch axis)

$B_3 = 0.0234 \sin \omega_o t$ (parallel to yaw axis)

The value ω_o is the orbital rate. These values are approximate only, since the earth rotates with respect to the orbit plane. The values assume a 32-degree orbit inclination.

The satellite is assumed to be balanced on the ground such that the maximum torque in any axis in 100 dyne-cm in a 0.3 gauss field. This gives:

$$\frac{100}{0.3} = 333 \frac{dyne\text{-}cm}{gauss}$$

The torques due to B_1 are in the pitch and yaw axis and are:

$$333 \frac{\text{dyne-cm}}{\text{gauss}} (0.01815 + 0.00307 \sin \omega_o t) \text{ gauss}$$

$$= 6.05 + 1.02 \sin \omega_o t \text{ dyne-cm}$$

The torques due to B_2 are in the roll and yaw axes and are:

$$3.62 \cos \omega_o t \text{ dyne-cm}.$$

The torques due to B_3 are in the roll and pitch axis and are:

$$7.78 \sin \omega_o t \text{ dyne-cm}.$$

The above torques are maximum and will rarely be this high for each component. Because of the orbit inclination angle, the third axis will have a value averaging half the value given.

10.4.6 Disturbance Summary

Table 10-1 lists the various torques:

TABLE 10-1

SUMMARY OF VARIOUS TORQUES

Maximum Torques	Dyne-Cm		
	Pitch	Roll	Yaw
Solar Pressure	16	16	0
Aerodynamic	0	0	0
Gravity Gradient	0	0	0
Orbit Ellipticity	0.31	0	0
Magnetic B_1	7.1	3.5	7.1
Magnetic B_2	1.8	3.6	3.6
Magnetic B_3	7.8	7.8	3.9
Totals	23.0	30.9	14.6

Note that no mechanical disturbances have been considered.

10.4.7 Initial Detumbling

It is assumed that the maximum initial tumbling rate will be 1 degree per second. The position is random. To initially detumble the vehicle will require

$$H = (50 \text{ ft-lb-sec}^2)\left(\frac{\text{rad}}{57.3 \text{ sec}}\right) = 0.873 \text{ ft-lb-sec/axis}$$

The rate gyro dead zones are ±0.08 degree per second total. The momentum wheels must control the residual momentum of:

0.08 x 0.873 = 0.07 ft-lb-sec

10.5 COMPONENTS

The components to be used in the sample design of the automatic control system are described below.

10.5.1 Horizon Scanner

A Minneapolis-Honeywell horizon scanner is chosen for this application because it uses no moving parts. The device used is not a new, but an adaptation of an existing design. The image is focused on a bolometer array, such that angular errors cause image motion relative to the array, providing asymetrical light flux distribution which results in bolometer error signals. The image is chopped by means of a solid state chopper, in which the transmittance of a germanium filter is varied sinusoidally by means of an applied voltage. The specific design data are shown below:

Accuracy approximately ±0.3 degree

Field of view ±67 degrees

Volume 120 in.^{3}

Weight 6 pounds

Power 6 watts

The unit uses the solid state chopper as a sun shutter when the sun's image is seen directly. The shutter operates only when the sun image strikes the bolometer array and only in the axis which is affected.

10.5.2 Magnetometer

A three-axis magnetometer operating on the flux gate principle was chosen for this application. Each probe is excited at 2000 cps. The probe output contains even harmonics, the amplitudes of which are proportional to the component of magnetic field parallel to the probe axis. The probe output is amplified by an amplifier tuned to 4000 cps, the second harmonic of the excitation frequency. This signal is phase-sensitive demodulated, amplified, and used to produce a current which produces a field in the probe which cancels the earth's field, driving the probe output to null. A magnetometer of this type is available from Dalmo-Victor.

The probes are orthogonally mounted in a location relatively remote from the processing electronics; they must be located 4 feet from the torque coils to ensure less than 5 percent interference.

The three-axis magnetometer has the following physical characteristics:

Weight 2.5 pounds

Volume 97 in.^{3}

Power 2 watts

Range 0.001 to 0.3 gauss

Linearity within 1 percent

10.5.3 Rate Gyros

Rate gyros will be used in the pitch and yaw axes only to provide initial rate damping previous to erection to the earth. These spring-restrained units will be packaged together in a compact block. The probable parameters are:

Maximum linear rate -5 deg/sec

Linearity ±0.2 percent to 2 deg/sec

Zero errors 0.06 deg/sec

Damping ratio 0.5

Weight 1.5 pounds

Volume 10 in^3

Power 7 watts

The package will contain all capacitors and transformers necessary for obtaining and maintaining voltage levels and phases.

To insure the capability or stabilizing the yaw axes to within 5 degrees of the velocity vector, it is necessary to use the gyrocompassing technique for obtaining yaw position. For this job, an accurate closed-loop integrating rate gyro is used.

Where ψ is the yaw angle, $\dot{\phi}$ is the roll rate indicated by the gyro, and ω_o is the orbital pitch rate (2.91×10^{-4} rad/sec), for an error of 5 degrees,

$$\omega_o \sin \psi = \dot{\phi} = (2.91 \times 10^{-4} \frac{rad}{sec})(\frac{5}{57.3}) = 2.53 \times 10^{-5} \frac{rad}{sec}$$

This would be the maximum threshold, or zero rate uncertainty, allowed for the gyro if the gyro's error were the only cause of yaw pointing error. The gyro planned for this application has the following characteristics:

Maximum rate 2.2 deg/sec

Maximum drift rate 10^{-5} rad/sec, approximately

Linearity 0.01 percent

Power 2.5 watts, plus an occasional 10-watt heater

Volume 9 in.^{3}

Weight approximately 3.5 pounds

This unit is more than adequate for the task. Its MTBF of 15,000 hours, however, makes redundancy desirable.

10.5.4 Multipliers

It is planned to use electromechanical multipliers in place of more conventional electronic circuits for multiplying the earth's field components by the wheel speeds to obtain dumping coil torque levels. In this type of multiplier, one variable is fed into a linear variable differential transformer as an a-c voltage. The variable slug of the LVDT is connected through a pivot to a magnet which is spring-restrained inside a d-c winding. When the second variable is applied to the d-c winding, the magnet, and thus the LVDT slug, takes a position proportional to the d-c current. The output of the

LVDT is thus proportional to the product of the LVDT excitation voltage and the d-c magnetizing voltage. The unit to be used will have a volume of 2.5 in.^{3}, and will react to 0 to 5 volts, 400 cps as the first variable, and to 0 to 0.01 ampere d-c as the second variable. It will be accurate within 1 percent in its specified range. Six multipliers will have a total weight of approximately 0.5 pounds.

10.5.5 Reaction Wheels

The reaction wheels must be capable of storing the momentums produced by the disturbances, as well as the residual momentum initially left in the vehicle when the gyros reach their dead zones. This amounts to 0.14 ft-lb-sec. To obtain good operational characteristics, the wheel torque obtainable will be constant over 75 percent of its operational range and will be about 3 in-oz to ensure adequate control above the existing friction levels. The wheel momentum will be 0.14 ft-lb-sec at 1000 rpm, producing a moment of inertia of 1.34×10^{-3} slug -feet^2. The no-load speed will be 1400 rpm and the synchronous speed will be 1500 rpm to provide a momentum margin.

Each wheel will integrally contain a 400-cps tachometer generator, the output voltage of which is proportional to the wheel speed. The entire assembly for each wheel will be hermetically sealed to protect the bearings. The specific parameters are:

Operating speed 1000 rpm

No-load speed 1400 rpm

Synchronous speed 1500 rpm

Moment of inertia 1.34×10^{-3} ft-lb-sec^2

Momentum at 1000 rpm 0.14 ft-lb-sec

Size 3 inches high x 6 inches diameter

Weight 3 pounds

Power 7.5 watts, including tachometer generator

10.5.6 Torque Coils

The coils used will be cored with annealed Hypernik metal, and wound with aluminum wire to obtain minimum power and weight. The coil will be

10-16

filled with plastic to gain rigidity and resistance to environment. The plastic shell will also provide a good mounting surface. Choice of plastic will depend on its sublimation rate and its weight. The description of the coils is given below:

Maximum torque 75 dyne-cm

Residual torque 1 percent

Length 0.25 meter

Diameter 0.0129 meter

Weight 0.11 kg.

Power 0.228 watt

Current 0.1453 ampere

Voltage 1.57-volt

N = 2600 T, No. 24 Al wire

R = 10.8 ohms

The above data are calculated using the optimum weight techniques described in Section 8.

.

10.5.7 Gas System

The gas system is used to initially detumble and orient the vehicle. Six gas nozzles will be assumed to be mounted on one end of the vehicle. The yaw axis will require a couple to prevent axis crossfeed. Each nozzle will produce 0.1-pound thrust. Since the center of gravity is assumed to be in the center of the vehicle, the effective lever arm is 2.5 feet. The maximum momentum to be dumped is:

$$\frac{50 \text{ ft-lb-sec}^2}{57.3 \text{ sec}} = 0.873 \text{ ft-lb-sec per axis}$$

The gas is also used to spin the vehicle to 1 degree per second and despin it during the acquisition mode. This will also require 0.873 ft-lb-sec in each direction.

The total requirement per axis is then:

$$\frac{2.619 \text{ ft-lb-sec}}{2.5 \text{ ft} \times 68 \text{ sec}} = 0.071 \text{ pounds of gas.}$$

The gas system will consist of a tube assembly, a fill valve, a pressure vessel, the thrust valve manifold, and a pressure regulator. Assuming a capacity of 0.3 pound gas, the system total weight will be approximately 4 pounds. It is assumed that nitrogen will be used as the expelled gas.

10.5.8 Circuit Design

To make an accurate reliability estimate possible, a complete set of circuit designs have been evolved. The detailed operation of each numbered circuit block of figure 10-1, along with the schematic diagrams, is shown in Appendix B.

10.5.9 Size, Weight, and Power Requirements

10.5.9.1 Electromagnetic Actuation System Only

The momentum dumping system has the following weight, volume, and power breakdown:

Component	Weight (pound)	Volume - in.^{3}	Power (watt)
Coils	1.0	6.1	0.7
Magnetometer	2.5	97	2.0
Multipliers	0.5	15.0	0.05

Component	Weight (pound)	Volume - in^3	Power (watt)
Electronics	5.0	60.0	2.7
Total	9.0	178.1 in^3	5.45

10.5.9.2 Entire Attitude Control System

The weight, volume, and power breakdowns for the entire attitude control system are shown in table 10-2, 10-3, and 10-4, respectively. In each table, the basic system is defined in the left hand column of numbers. The last two columns add information regarding systems expanded by redundancy as discussed in paragraph 10.6.

TABLE 10-2

WEIGHT (pounds)

Component	One-scanner One electronics One roll gyro	Two-scanner One electronics Two roll gyros	Two-scanner Two electronics Two roll gyros
Wheels	9.0	9.0	9.0
Coils	1.0	1.0	1.0
Gas System	4.0	4.0	4.0
Rate Gyros	1.5	1.5	1.5
Magnetometers	2.5	2.5	2.5
Multipliers	0.5	0.5	0.5
Electronics	36.0	36.0	72.0
Roll Rate Gyro	3.5	7.0	7.0
Scanner	6.0	12.0	12.0
Totals	64.0	73.5	109.5

TABLE 10-3

VOLUME (in.^{3})

Component	One-scanner One electronics One roll gyro	Two-scanner One electronics Two roll gyros	Two-scanner Two electronics Two roll gyros
Wheels	42	42	42
Coils	8	8	8
Gas System	32	32	32
Rate Gyros	10	10	10
Magnetometers	97	97	97
Multipliers	15	15	15
Electronics	2650	2650	5300
Roll rate gyro	9	18	18
Scanner	120	240	240
Total	2983	3112	5762

TABLE 10-4

POWER (watts)

Component	22. 5
Coils	0. 7
Gas System	7. 0
Rate Gyros	7. 0
Magnetometers	2. 0
Multipliers	0. 1
Electronics	20. 0
Roll Gyro	2. 5
Scanner	6. 0
Total	67. 8

10.6 RELIABILITY ANALYSIS

10.6.1 Electromagnetic Actuation Subsystem

To·demonstrate the usefulness of the electromagnetic actuation subsystem, the reliability estimates for the torque coils and the associated components are presented below:

Component	Probability of success for 1 year
6 multipliers	0.994
3-axis magnetometer	0.990
3 torque coils	0.997
Electronics	0.930
Total system	0.912

This set of values does not include any redundancy. If redundant electronics are used throughout, the momentum dumping probability of success for 1 year becomes 0.977.

10.6.2 Total System Reliability

The reliability analyses presented are based upon the use of Minuteman components wherever applicable. A breakdown of the electronic components used in the system is shown in table 10-5. The number of components for each circuit is given, along with their failure rates. The circuit numbers refer to the block diagram of the attitude control system. This table is used to predict the reliability of the electronics portion of the system. The total failure rate for the electronics is 3.586 percent per 1000 hours, which yields a probability of success for 1 year of $P_s = e^{-0.03586 \times 8.76} = 0.73$.

The reliability of the electronics along with the other subsystems is given in table 10-6. The product of all these subsystem reliabilities will give the reliability of the entire system without redundancy.

Redundancy may be used to increase the reliability of the system. Standby redundancy is used in this system; the redundant subsystem is not turned on until the primary subsystem has failed. From table 10-6 it is obvious that the reliability of the system is heavily dependent on the reliability of the roll gyro, horizon scanner, and the electronics. Thus the reliability of the system is a function of the redundancy of these three items. This holds true

TABLE 10-5

SUMMARY OF ELECTRONIC PARTS FOR THE ENTIRE ATTITUDE CONTROL SYSTEM

Block No.	No. of Blocks/System	Signal Transistors	Power Transistors	Blocking Diodes	Zener Diodes	Tantulum Capacitors	Glass Capacitors	Resistors Wire-Wound	Resistors Metal Film	Resistors Composition	Transformers	Potentiometers	Chokes
1	3	12				6			9	3			6
2	3	9				9	3		18	15			
3	1	4	2	12	2	4			4	4	5	2	
4	3	12		12		3			6	6	3		
5	4	8		32	4				24	16			
6	2	2		6						2			
7	2	8		4	2					14			
8	5			20		5		20			5		5
9	3	3	6	12					6	6	3		6
10	3	3		3						6			
11	3	12							12	3			
12	3	9		6		9			6	24			
13	3	9		6		9	3		18	15			
14	4	4	4	12						4			
15	2	2	2							2			
16	3			12		3		12	3		3		
17	4	16		12	4	12			28	28			
18	4	8		16	4				8	20			
19	3	6		3						12			
Total No. Components		127	14	168	16	60	6	32	144	180	19	2	17
Failure Rate %/1000 hours		.127	.140	.168	.176	.090	.005	.035	.048	.027	1.900	0.02	.85

Total Number of Components = 785
Total Failure Rate = 3.586 percent/1000 hours

only for a limited range. Figure 10-5 illustrates the relationships of redundancy and reliability over this limited range.

TABLE 10-6

RELIABILITY OF SUBSYSTEMS

Subsystem	Probability of Success For
Horizon scanner	0.647
3 reaction wheels	0.999
6 multipliers	0.994
3-axis magnetometer	0.990
3 torque coils	0.997
Gas system	0.999
Roll gyro	0.557
Pitch gyro	0.999
Yaw gyro	0.999
Electronics	0.73

Figure 10-5 is somewhat optimistic since the switching scheme for switching from one unit to another has not been included in this analysis. However, the switching arrangement would be a simple, rarely actuated, ground-commanded design.

10.7 SYSTEM PERFORMANCE

The performance characteristics of the system during the three modes are listed in the following paragraphs.

10.7.1 Detumbling and Search

Assuming initial tumbling rates of 1 degree per second, the roll search rate and pitch/yaw rate nulls will be achieved in the following times:

t (roll search) = 6.9 seconds

t (pitch/yaw detumble) = 3.5 seconds

After this, the roll search rate will continue until the horizon scanner locks on. With a scanner field of view of ±67 degrees and an altitude of 6000 miles, the maximum length of time required to achieve scanner lock-on will be 360 seconds.
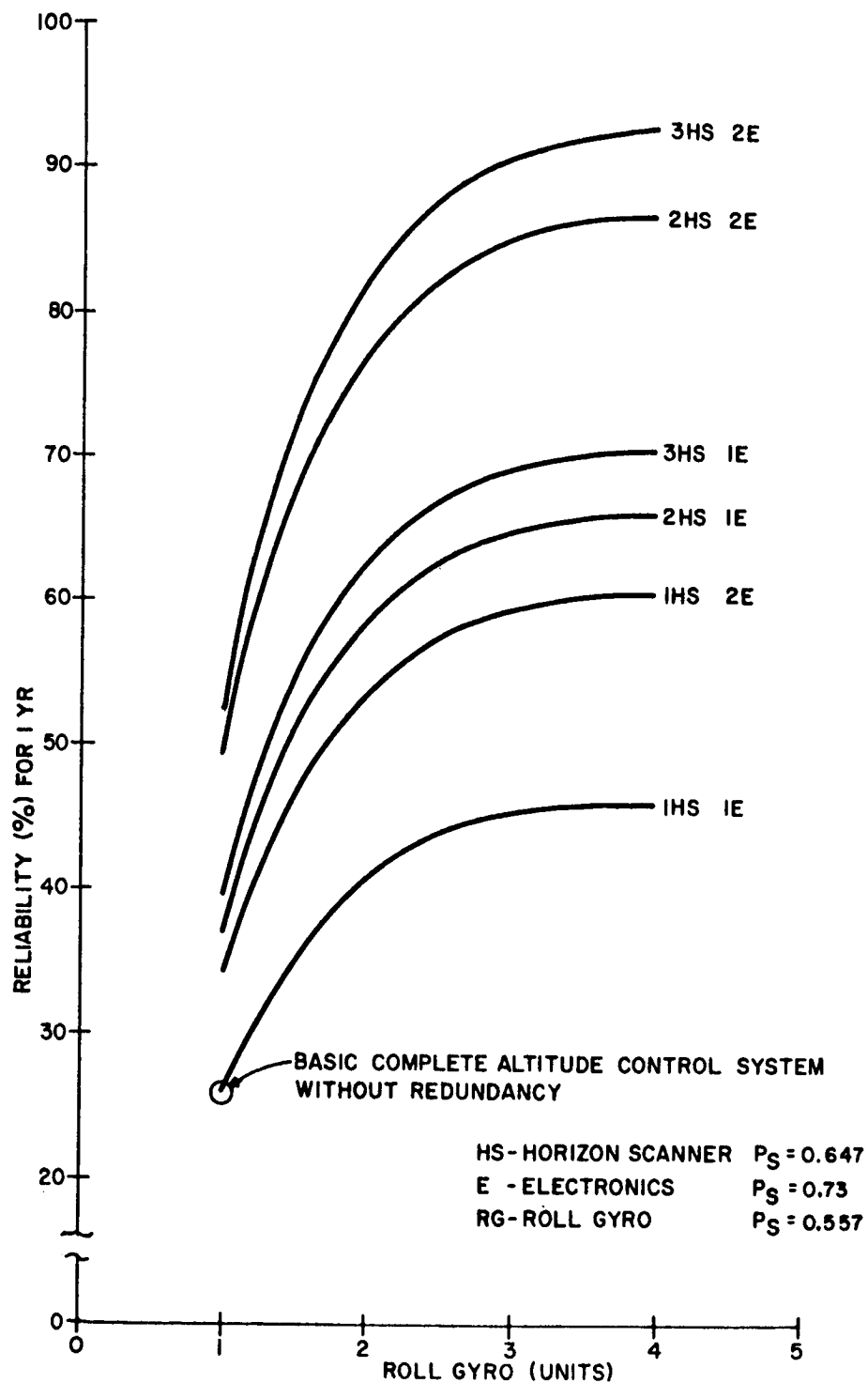
Figure 10-5. Reliability as a Function of Redundancy

10.7.2 Erect to Vertical

During the vertical erection, the position signal input is effectively limited by the maximum signal that can be transmitted through the modulator. This signal is nonlinear and shapes the switching curve on the phase plane as shown on figure 10-6. The vehicle will erect to vertical along the line of constant velocity and into the region of variable velocity command. The final limit cycle rates will be determined by the hysteresis of the switching circuits and gyro and will be approximately 0.08 degrees per second. This rate corresponds to a momentum of 0.06 lb-ft-sec in the wheels when the residual rate is absorbed by the wheels during normal pointing.
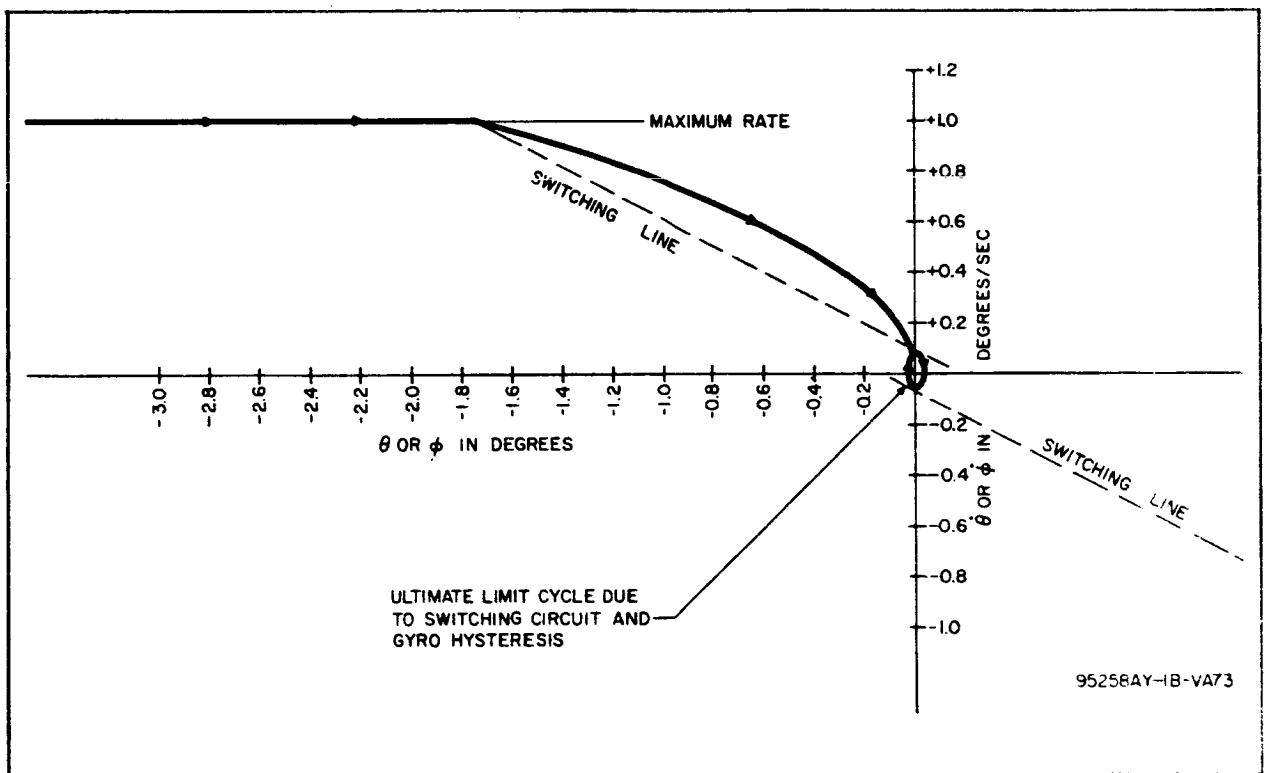

Figure 10-6.   Phase Plane Locus of Vehicle Erection Rates
vs Position Error

10.7.3 Normal Pointing

During the normal pointing mode, each of the wheel driving servo loops receives its input from the position sensing element via a lead-lag network, as shown on figure 10-7. The lead-lag network is used to provide additional
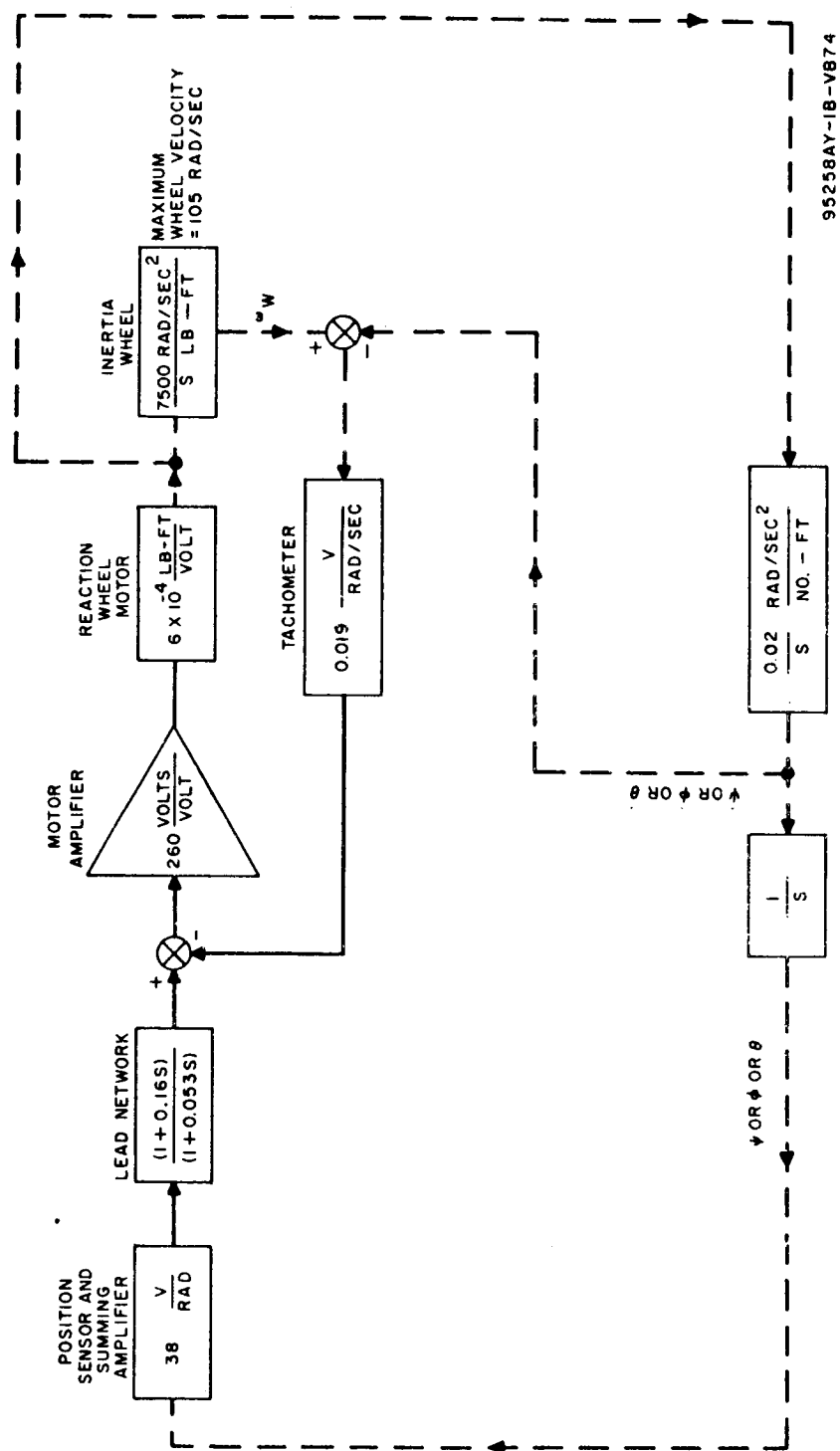
Figure 10-7. Normal Pointing Mode Operational Block Diagram

damping for stabilizing the vehicle loop. The basic motor control loop consists of high gain a-c amplifier stages driving the motor with direct tachometer feedback to the amplifier input.

The loop gain of the basic motor control servo is limited by the allowable effect of tachometer noise. This limitation imposes a maximum bandpass of 3.6 cycles per second on the motor-tachometer loop.

Since the basic control requirement imposes a maximum attitude error of 5 degrees, the minimum loop gain is set on the basis of maximum motor velocity command for this error. The loop velocity gain, which thus equals 1.54×10^{-2}/sec, permits the motor loop time constant, which rises at lower amplitude due to the effect of motor friction, to reach any level, thus assuring no limit cycle oscillation.

One of the factors upon which maximum loop gain is set is on the highest gain which will assure no limit cycle oscillation. The loop gain in this case will be set at $1/\tau_2$ where the lead-lag network is of the form $\left[1 + \tau_1 S \right] \left[1 + \tau_2 S \right]$ and the horizon sensor response is $K/1 + \tau_1 S$. The resultant gain, for $\tau_1 = 0.16$ second and $\tau_2 = 0.053$ second, will be 19 rad/sec/rad which corresponds to full motor speed command for 0.4×10^{-2} degree.

It is fairly obvious that a gain setting which would generate a limit cycle oscillation is much too high, since the horizon scanner noise would saturate the amplifier. Taking the peak horizon scanner equivalent random noise at 0.01 degree and its maximum allowable effect as 20 percent of motor amplifier saturation, the gain will be limited to full motor speed command for 3 degrees error. If most of the sensor noise is made up of 16 cps chopper frequency components, the equivalent vehicle rate will be approximately 35.5×10^{-6} sine (100 t) degrees per second. The peak vehicle rate in roll will therefore be only 0.21 percent of orbital rate (for a 6-hour orbit).

Considering that the roll rate forms the position input to the yaw axis, the equivalent yaw noise input should be limited to 0.01 degree peak at 16 cps to prevent saturation of the yaw amplifier. Consequently, the gyro must

attenuate the input roll rate by a factor of 12 at 16 cps, which predicates a gyro corner at 1.3 cycles per second. All three axes will then have the same angular excursion due to noise.

The components of pointing error are the same for the pitch and roll axes: (1) due to maximum initial momentum and disturbance torque buildup - ±3 degrees, and (2) due to horizon scanner uncertainty - ±0.3 degree. Therefore, the system should be capable of maintaining the vehicle within 5 degrees of vertical in each of two axes.

The error due to momentum buildup will be the same for yaw but the horizon scanner error factor will be replaced by the zero uncertainty of the accurate roll rate gyro. Since the non-g sensitive drift of an accurate gyro (e.g., M-H GG149) can be held to 2 degrees per hour, the resultant yaw error component will be slightly less than 2 degrees (see paragraph 10.5.3). The total accuracy in orbital plane pointing will be just under ±5 degrees maximum.

10.8 CONCLUSIONS

10.8.1 Electromagnetic Actuation Subsystem

The chief characteristics of the electromagnetic actuation subsystem for the sample vehicle in a 6-hour orbit are summarized as follows:

Reliability	91.2 percent probability of success for 1 year
Weight	9 pounds
Power	7.5 watts (approximate average)
Volume	0.1 cubic foot

These figures include the torque coils, magnetometers, multipliers, and interconnecting electronics. The three latter equipment items are essentially unaffected by orbit (or vehicle disturbance levels). While the weight, volume, and power required for the torque coils do change with disturbance level, the coils themselves are actually a small part of the above figures. These characteristics for the coils alone are:

Weight	1 pound
Power	0.5 watt (approximate average)
Volume	0.0035 cubic foot

Hence, it can be said of electromagnetic actuation for the sample system studied that it is a reliable technique (using a relative term) having reasonable and moderate weight, power, and volume characteristics. Furthermore, its weight, volume, and power are relatively insensitive to vehicle disturbance level. In addition, the weight and volume are, of course, independent of control lifetime.

The electromagnetic subsystem for removing reaction wheel momentums can be compared to a stored gas actuating subsystem used for the same purpose, first comparing for the vehicle and orbit analyzed herein.

The biased components of disturbances for the case studied (6-hour orbit) are quite low; for this reason the weight would actually be reduced by expanding the gas system used for detumbling in order to substitute it for the magnetic system. However, while the stored gas system reliability for a full year's operation is difficult to assess, that reliability is almost certainly much lower than the 91 percent probability of success for the magnetic system. The gas system involves moving parts sensitive to manufacturing tolerances and wear (six solenoid valves and a pressure regulator). In addition to the possibility of catastrophic failure, the gas system can be expected to leak to an extent that is as difficult to assess as its reliability. Furthermore, the gas system as a momentum remover must also include decision-making electronics, just as does the magnetic system. It can be stated that:

a. For the case studied, a gas system would weigh less than the magnetic system, but the weight of the latter is a moderate 9 pounds.

b. The reliability of the magnetic system is relatively high and predictable from past component experience. For example, torque coil reliability can be inferred from the history of reliability for chokes and transformers.

c. The reliability of the gas system for 1 year operation, while not well known, is probably far below 91 percent.

For orbits lower than that considered, or for vehicles affected by internal momentum disturbances, the net disturbance levels can become very much higher. As a consequence, the gas system weight would rise in a near-proportional manner, while the magnetic system weight would essentially remain at 9 pounds in the conceivable range of disturbance level. In many satellite applications the gas system would weigh more than magnetic actuation.

10.8.2 Attitude Control System

The control system evaluated performed the functions typically required in a communications satellite. A pointing accuracy of ±5 degrees was assumed as being satisfactory for such an application; therefore, obtaining adequate performance was not a doubtful or key issue in the study. The quantities of interest are reliability, weight, and power drain. While the area of the system most pertinent to the subject of this report is the electromagnetic actuation subsystem, some conclusions can be drawn regarding the entire system, which served as a background for the most pertinent area.

Reviewing the system, the principal features are:

a. Vertical control with a horizon scanner

b. Orbital plane control by means of a roll rate gyro

c. Reaction wheels

d. Momentum removal by electromagnetic actuation

e. A relatively high altitude and low momentum disturbance level

f. Short-term use of a stored gas system and pitch and yaw rate gyros for detumbling and initial erection.

The overall system has a probability of success for 1 year of 26 percent, a weight of 64 pounds, and a power drain of 66 watts. It is seen that some step must be taken to improve the reliability, where the main contributing elements are the roll rate gyro, the horizon scanner, and the electronic assembly. Using sequential redundancy with regard to these elements, and

10-32

carrying the process up to three gyros, three horizon scanners, and two sets of electronics, the characteristics become:

Ps $\cdot$ = 91 percent

Weight = 119 pounds

Power = 66 watts

A reasonable reliability is thus obtained by the sacrifice of an additional 55 pounds.

One may conclude the following with regard to the typical communications satellite attitude control system.

a. The orbit plane orientation should function only during the infrequent periods where it is required for velocity control, and then by ground command. If possible the yaw attitude corrections should result from ground interpretation of the onboard magnetometer signals, thus eliminating the unreliable roll rate gyro. As an alternative, yaw sensing might be supplied by a sun sensor.

b. Every effort should be made to eliminate the horizon scanner. This might be done by employing the gravity gradient, or by ground commands based on magnetometer signals, or by a combination of the two.

c. For further simplification, the approach of eliminating the reaction wheels by using direct magnetic actuation should be investigated from the mechanization standpoint.

APPENDIX A

VOLTAGE SCALING OF ANALOG
SIMULATIONS SIGNALS

A.1 INDIRECT ELECTROMAGNETIC ACTUATION SIMULATION

Figure A-1 is a simplified block diagram representation of the computer simulation. It will be used to show the method of voltage scaling the simulation. The method applies, with slight variation, to all simulations used.
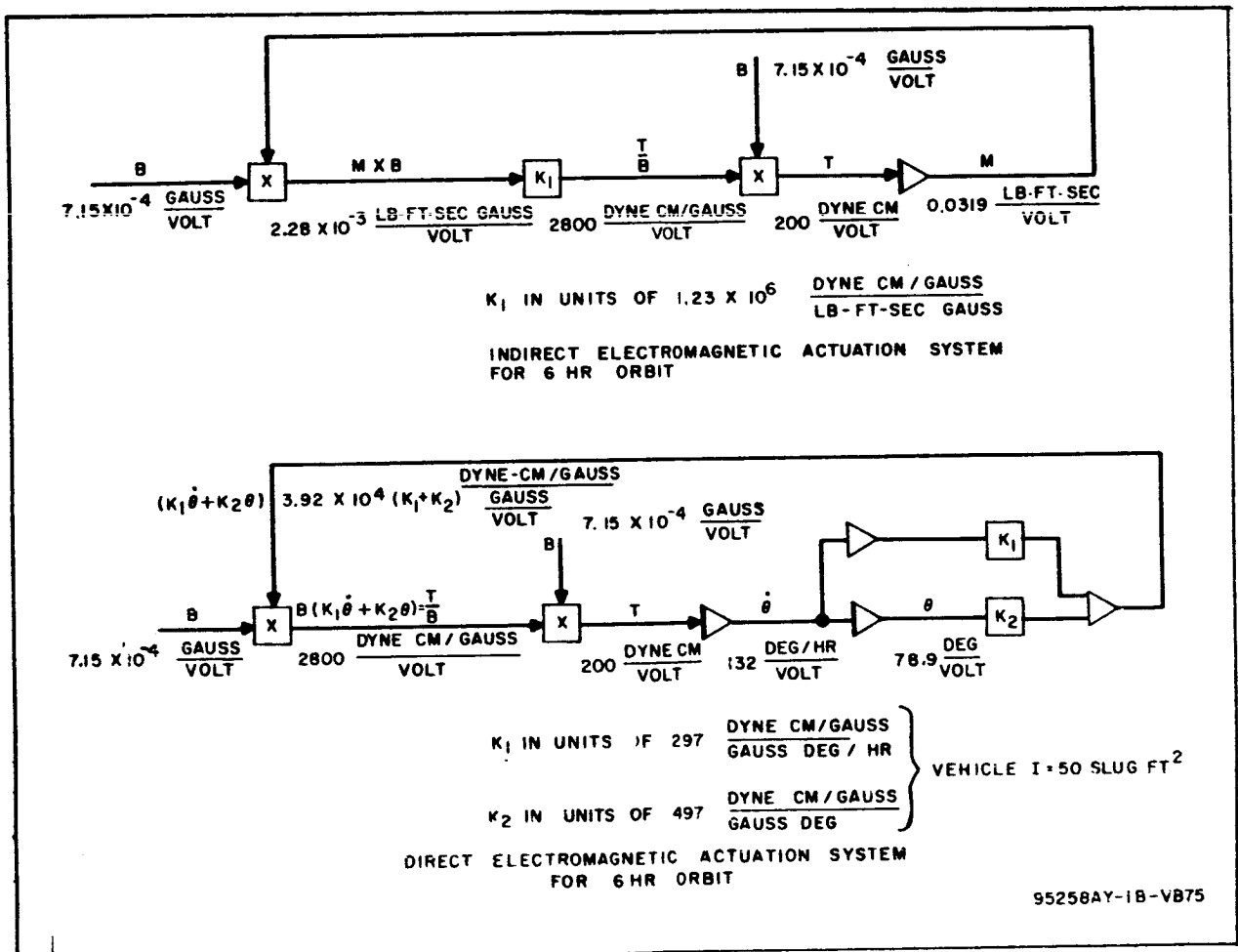

Figure A-1. Voltage Scaling for Simulations

Start by arbitrarily choosing the earth's field (B) scale and the torque (T) scale as:

B scale = 0.000715 $\frac{\text{gauss}}{\text{volt}}$

and T scale = 200 $\frac{\text{dyne-cm}}{\text{volt}}$

To calculate the momentum (M) scale, let the integrator input be 1 volt (200 dyne-cm) for 1 second machine time (2160 seconds real time). The integrator output after 1 second is 1 volt, which corresponds to

200 dyne-cm x 2160 sec

=4.32 x 10^5 dyne-cm-sec

=0.0319 lb-ft-sec

and therefore the M scale is 0.0319 $\frac{\text{lb-ft-sec}}{\text{volt}}$

The scaling of M x B is obtained by letting M be 1 volt (0.0319 lb-ft-sec) and B be 1 volt (0.000715 gauss). Then, since the multiplying servo has a gain of 0.01, its output is 0.01 volt which corresponds to:

0.0319 lb-ft-sec x 0.000715 gauss

or 2.28 x 10^{-5} lb-ft-sec-gauss,

for a scaling of 2.28 x 10^{-3} $\frac{\text{lb-ft-sec-gauss}}{\text{volt}}$

To calculate the scaling at $\frac{T}{B}$, let B be 1 volt (0.000715 gauss) and T be 0.01 volt (2 dyne-cm), then $\frac{T}{B}$ must equal 1 volt and be

$\frac{T}{B}$ x 0.000715 gauss = 2 dyne-cm

$\frac{T}{B}$ = 2800 $\frac{\text{dyne-cm}}{\text{gauss}}$

for a scaling of 2800 $\frac{\text{dyne-cm/gauss}}{\text{volt}}$

The units of coil gain (K_1) are:

$\frac{\text{output}}{\text{input}} = \frac{2800 \text{ dyne-cm/gauss}}{2.28 \times 10^{-5} \text{ lb-ft-sec-gauss}}$

$= 1.23 \times 10^6 \frac{\text{dyne-cm/gauss}}{\text{lb-ft-sec-gauss}}$

A-2

A.2 DIRECT ELECTROMAGNETIC ACTUATION SIMULATION

The voltage scaling for the direct system (figure A-1) is the same as for the indirect system, except for the addition of the position gain K_2. Assuming a vehicle I of 50 slug feet^2, the coil rate gain of

$$1.23 \times 10^6 \ K_1 \ \frac{\text{dyne-cm/gauss}}{\text{gauss-lb-ft-sec}}$$

becomes $297 \ K_1 \ \dfrac{\text{dyne-cm/gauss}}{\text{gauss-deg/hr}}$

To obtain the position gain, let the momentum be 1 volt (0.0319 lb-ft-sec) for 1 sec computer time (2160 seconds real time), the position voltage is one volt corresponding to

$$0.0319 \text{ lb-ft-sec} \times 2160 \text{ sec} \times \frac{1}{50 \text{ slug ft}^2} \text{ rad}$$

$$= 1.38 \text{ rad}$$

$$= 78.9 \text{ deg}$$

for a scaling of 78.9 deg/volt. The units of position gain then are

$$\frac{\dfrac{2800 \text{ dyne cm/gauss}}{0.000715 \text{ gauss}}}{0.01} \times 78.9 \text{ deg} = 497 \ \frac{\text{dyne-cm/gauss}}{\text{gauss-deg}}$$

SCHEMATIC DIAGRAMS

The schematic diagrams for the sample system study of section 10 are illustrated on the following pages. A short description of the function of each circuit follows.

B. 1 BLOCK 1 - MULTIPLIER EXCITATION DRIVER.

This circuit (figure B-1) is used to couple the tachometer output voltage to the multiplier displacement transducer excitation coils. It consists of a difference amplifier whose outputs are connected to two multiplier stages on series push pull.
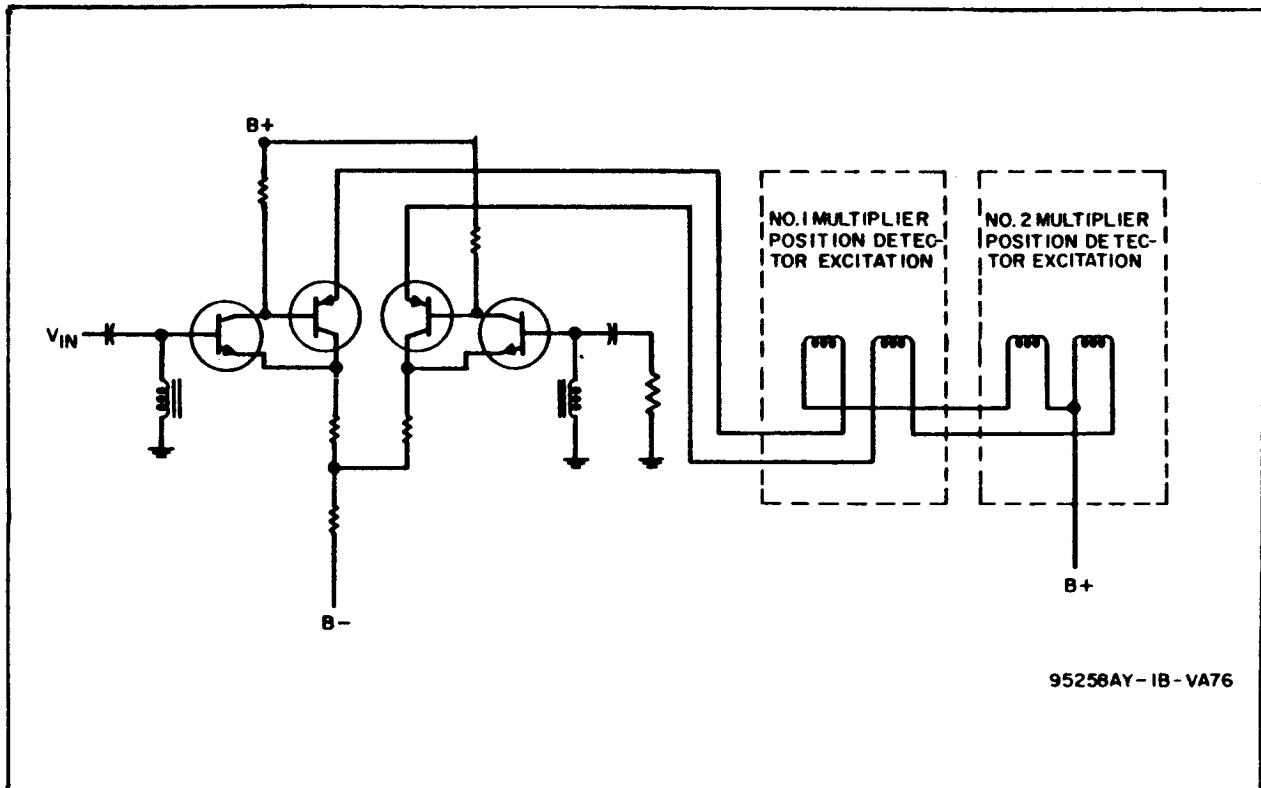

Figure B-1. Block 1 Multiplier Excitation Driver

B.2 BLOCK 2 - MULTIPLIER OUTPUT AMPLIFIERS

These are three-stage, closed loop, a-c amplifiers (figure B-2). The input and feedback resistors will be metal film for stability and reliability while performance tolerances on all other portions of the circuit are not critical.
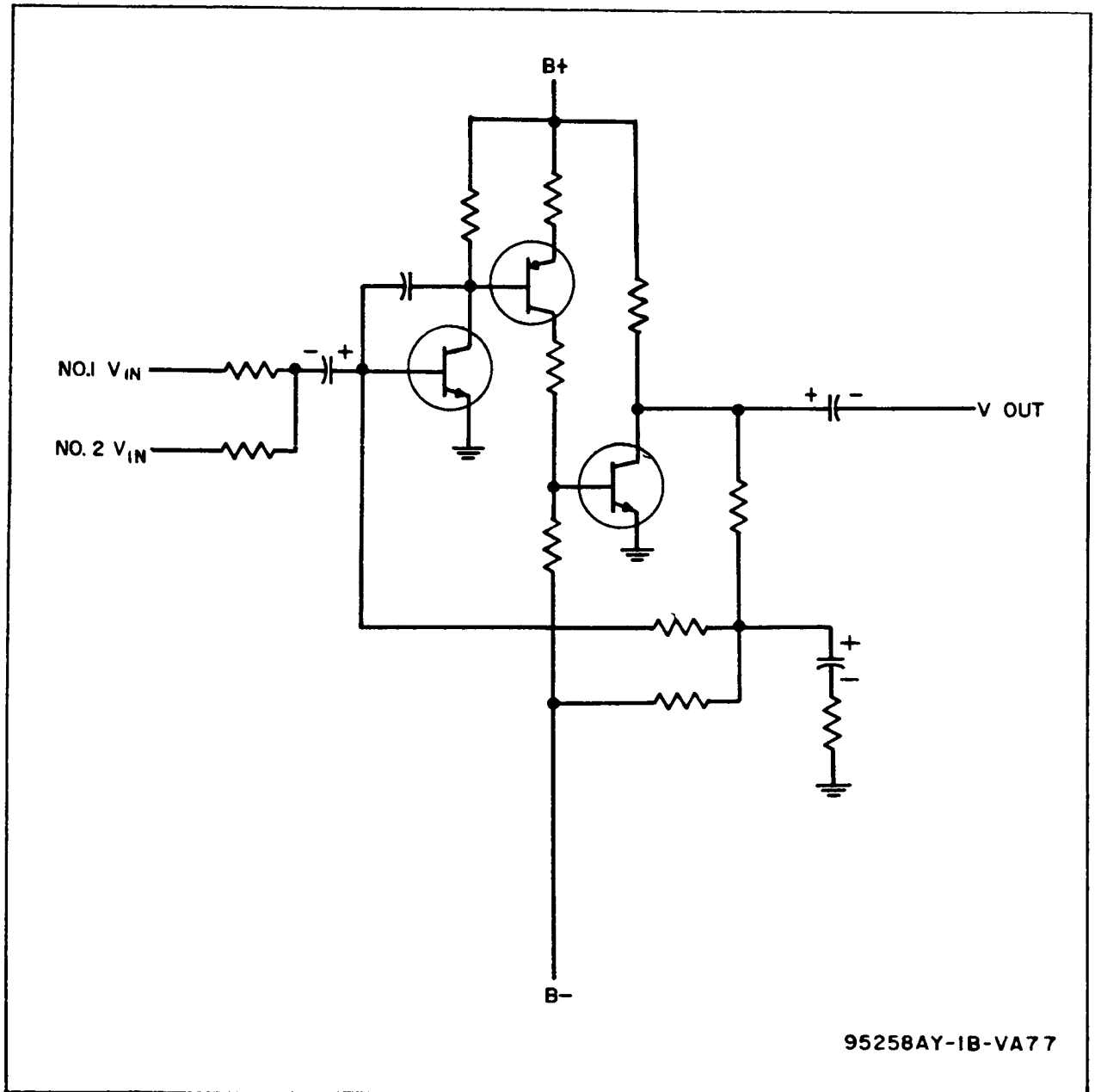

Figure B-2. Block 2 Multiplier Output Amplifier

B. 3 BLOCK 3 - POWER SUPPLY

The power supply consists of a B+ supply, a B- supply and various reference transformers (figure B-3). The B+ and B- supplies are basically the same, differing only in ground and output connections. Each of the supplies consists of emitter follower output stages, the base drive of which is controlled by a feedback circuit operating against a zener diode reference.

B. 4 BLOCK 4 - POWER DEMODULATORS

The opposed, Class B current driving stages functions as half-wave demodulators (figure B-4). The isolated emitter-follower configuration of each half permits an accurate control of current differential during the conducting half cycle.

B. 5 BLOCK 5 - DOUBLE-POLE RELAY CIRCUIT

The function of this circuit (figure B-5) is to provide the equivalent of a double-pole relay contact. The α and β signals provide the excitation, one always being the opposite polarity of the other. This results in the flip-flop transistors taking opposite states and, consequently, causing one of the two bridges to be in the conducting state while the other bridge is back-biased to cutoff. Balancing potentiometers enable accurate zero voltage setting for the conducting bridge.

B. 6 BLOCK 6 - AND GATE

This circuit (figure B-6) functions to provide an output equal to the lowest level input. When all three inputs are at the ON level, the output also is at the full ON level; otherwise, it remains close to the zero, or OFF level.

B. 7 BLOCK 7 - SWITCH DRIVER

When the input signal is at the ON level, α is near zero and β is at a B+ level (see figure B-7). When the input falls to the zero or OFF level, the α and β signals are reversed. These α and β signals are used to drive the single and double-pole relay circuits.

B. 8 BLOCK 8 - DEMODULATOR

This unit (figure B-8) is a full wave demodulator with an LC filtered output.

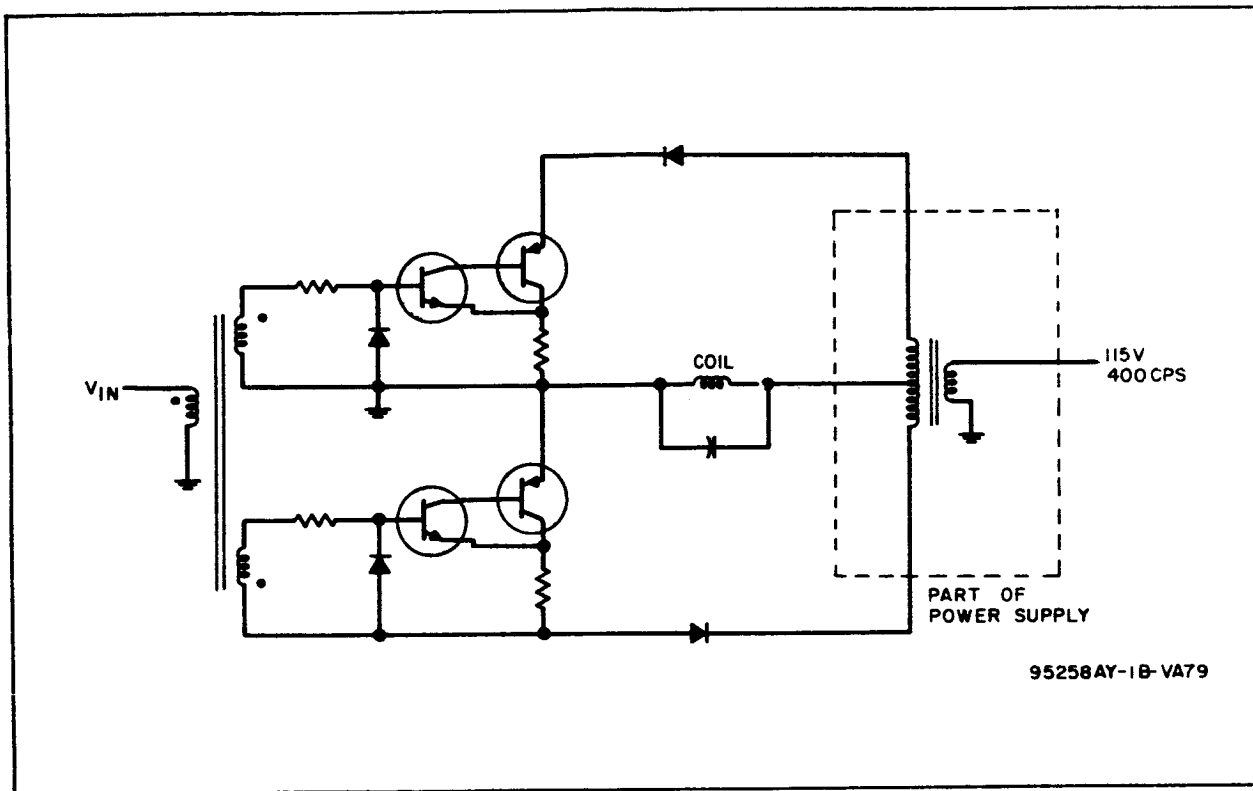Figure B-3. Block 3 Power Supply

95258AY-1B-VA79
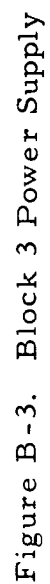
Figure B-4.   Block 4 Coil Demodulator

B.9   BLOCK 9 - MOTOR DRIVER AMPLIFIER

This circuit (figure B-9) consists of a transformer coupled push pull amplifier, and provides a linear output to the motor winding.

B.10   BLOCK 10 - PNPN SWITCH

This circuit (figure B-10) is a d-c actuated PNPN switch.

B.11   BLOCK 11 - MULTIPLIER TORQUE COIL DRIVER

This circuit (figure B-11) is a difference amplifier which drives two multiplier windings in series parallel.

B.12   BLOCK 12 - COINCIDENCE AMPLIFIERS

The three-stage, forward stages provide extremely high gain for the net a-c signal input (figure B-12).   The feedback network decouples the a-c output from the input while permitting d-c bias signals to pass.

B.13   BLOCK 13 - SUMMING AMPLIFIER

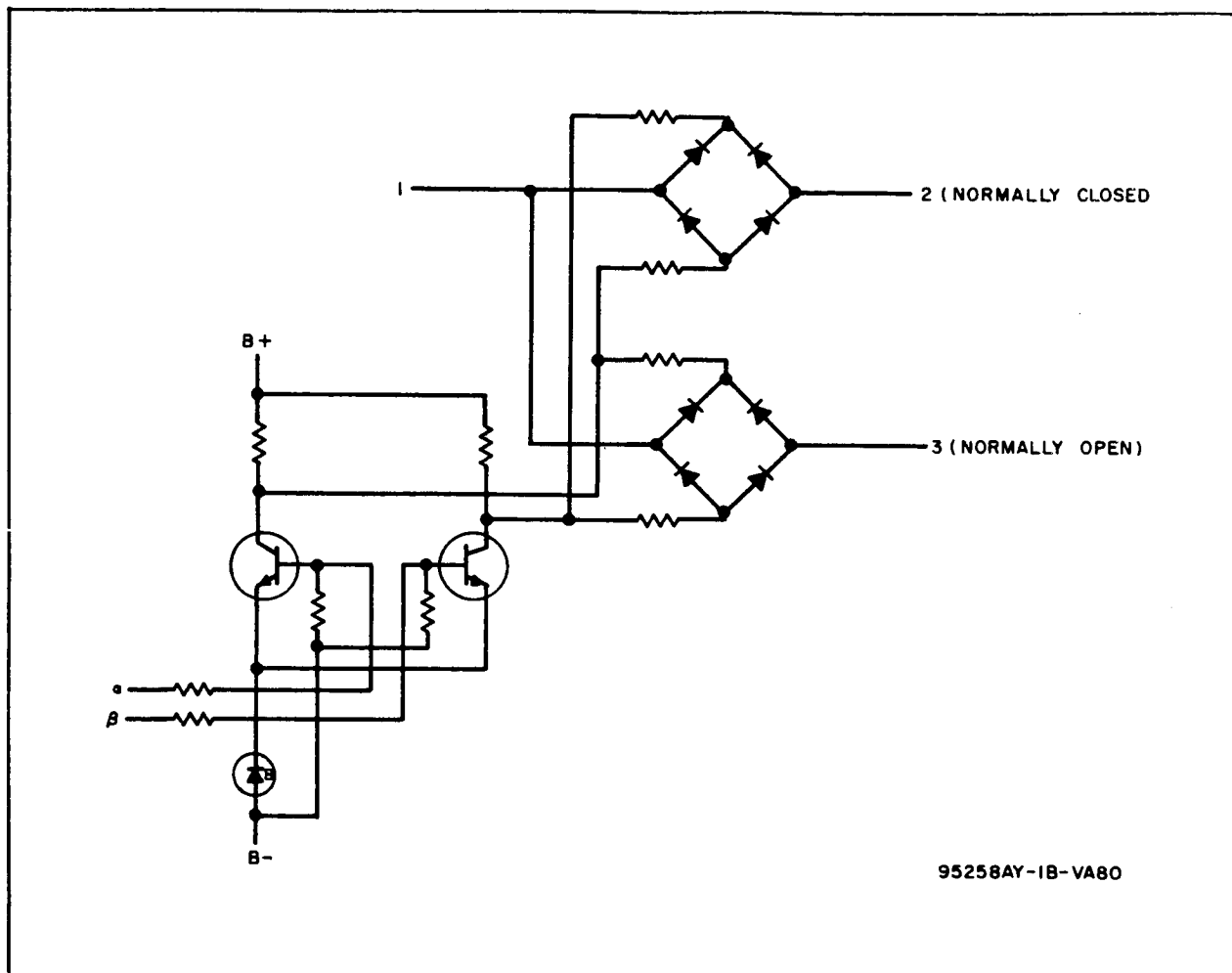This amplifier (figure B-13) is similar to block 2.

B-5

95258AY-1B-VA80

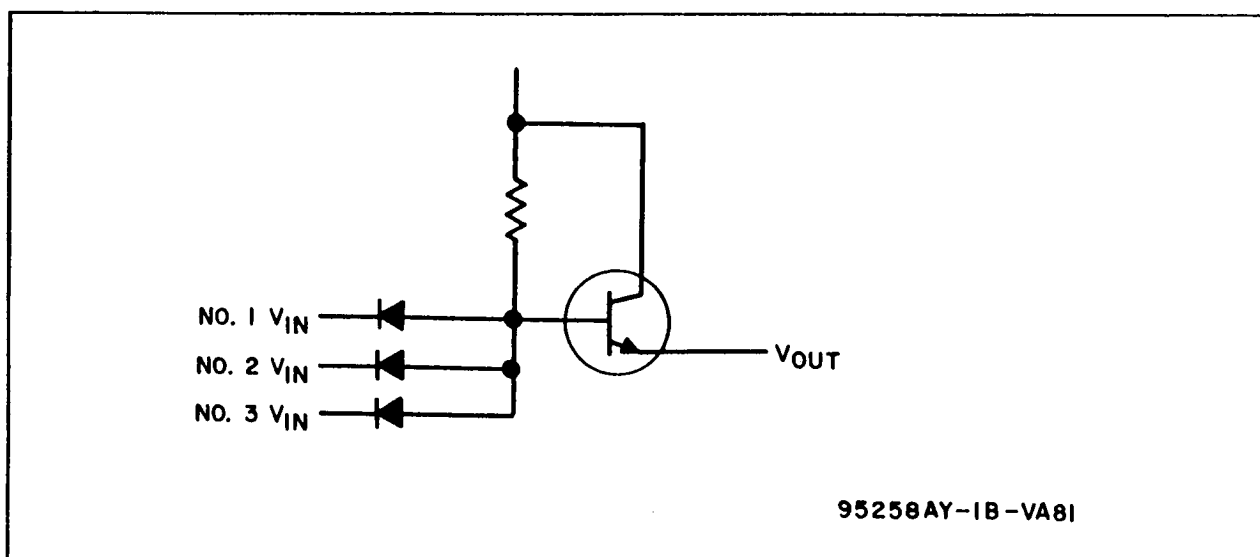Figure B-5.   Block 5 Double Throw Relay Contact Circuit

95258AY-1B-VA81

Figure B-6.   Block 6 And Gate

Figure B-7. Block 7 Switch Driver

B. 14 BLOCK 14 - OR-GATE AND EMITTER FOLLOWER

If either input is at the ON level, the output will assume the B+ (ON) level (see figure B-14), otherwise the output will be zero.

B. 15 BLOCK 15 - VALVE DRIVER

This circuit (figure B-15) consists of a two-stage emitter follower suitable for matching the very low valve impedance to the higher impedance of the switching circuit.

B. 16 BLOCK 16 - FULL WAVE MODULATOR

This circuit (figure B-16) converts a d-c signal into a 400 cps a-c square wave signal. The phase of the output is determined by the polarity of the input, and the amplitude of the output is linearly proportional to the input. During operation, the diode switching networks clamp each side of trans- former to ground on alternate half cycles, and the potentiometers provide a balance trim.

95258AY-IB-VA83

Figure B-8.   Block 8 Full Wave Demodulator

B. 17   BLOCK 17 - NULL DETECTOR

This circuit (figure B-17) provides a B+ level output for a condition where the input a-c voltage is below a predetermined level.   The high-gain a-c amplifier normally provides a bias which triggers the output flip-flop to the OFF state.   When this input signal decreases, a point will be reached where the generated bias signal will be insufficient to maintain the zero output state, and the flip-flop will revert to a B+ level.

B. 18   BLOCK 18 - SINGLE-POLE RELAY CONTACT

This circuit (figure B-18) performs the function of a single-pole, single-throw switch.   In operation, it is similar to the circuit of block 5.

B. 19   BLOCK 19 - VALVE LOGIC CIRCUIT

The valve logic circuit (figure B-19) functions to provide a B+ level for either of two outputs, depending on the level (B+ or 0) of the input.

B-8
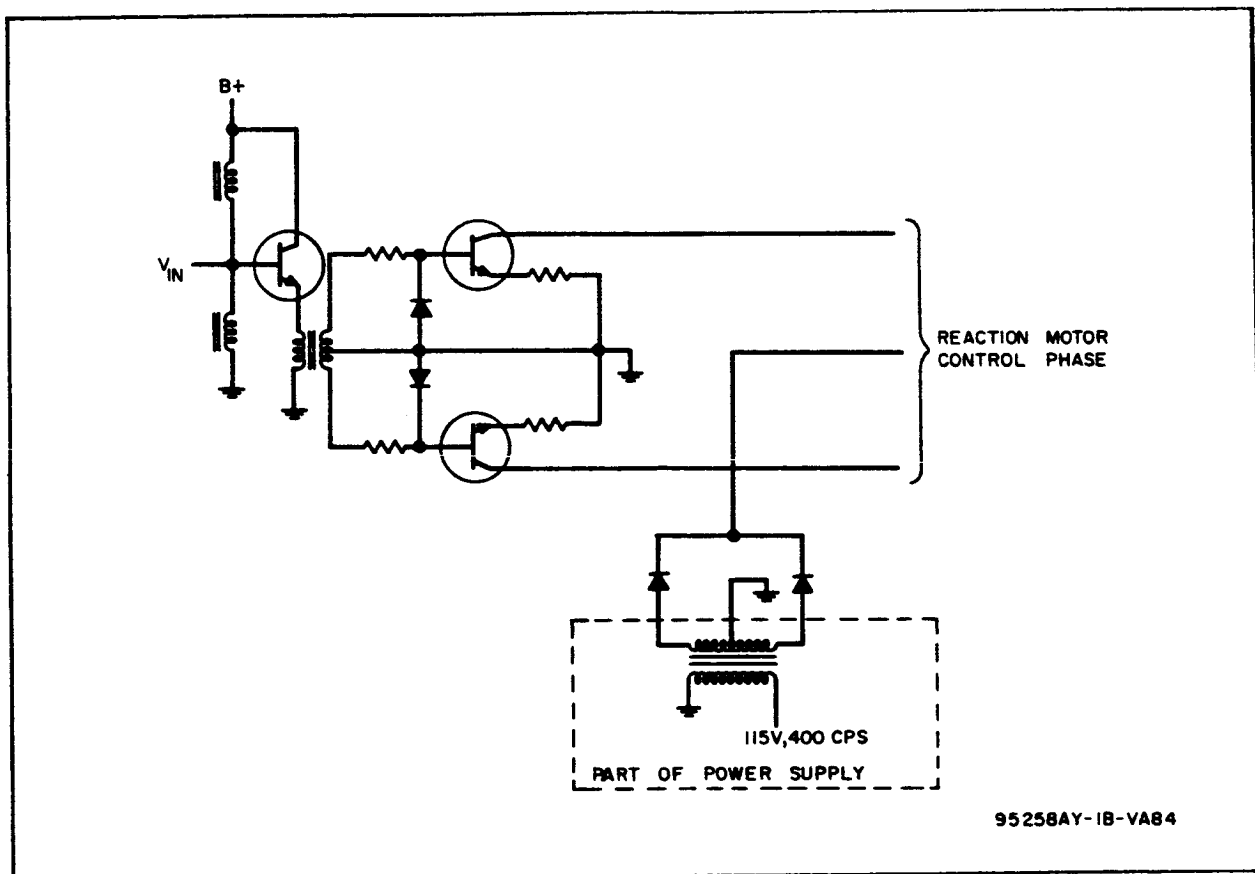
Figure B-9. Block 9 Motor Driver Amplifier
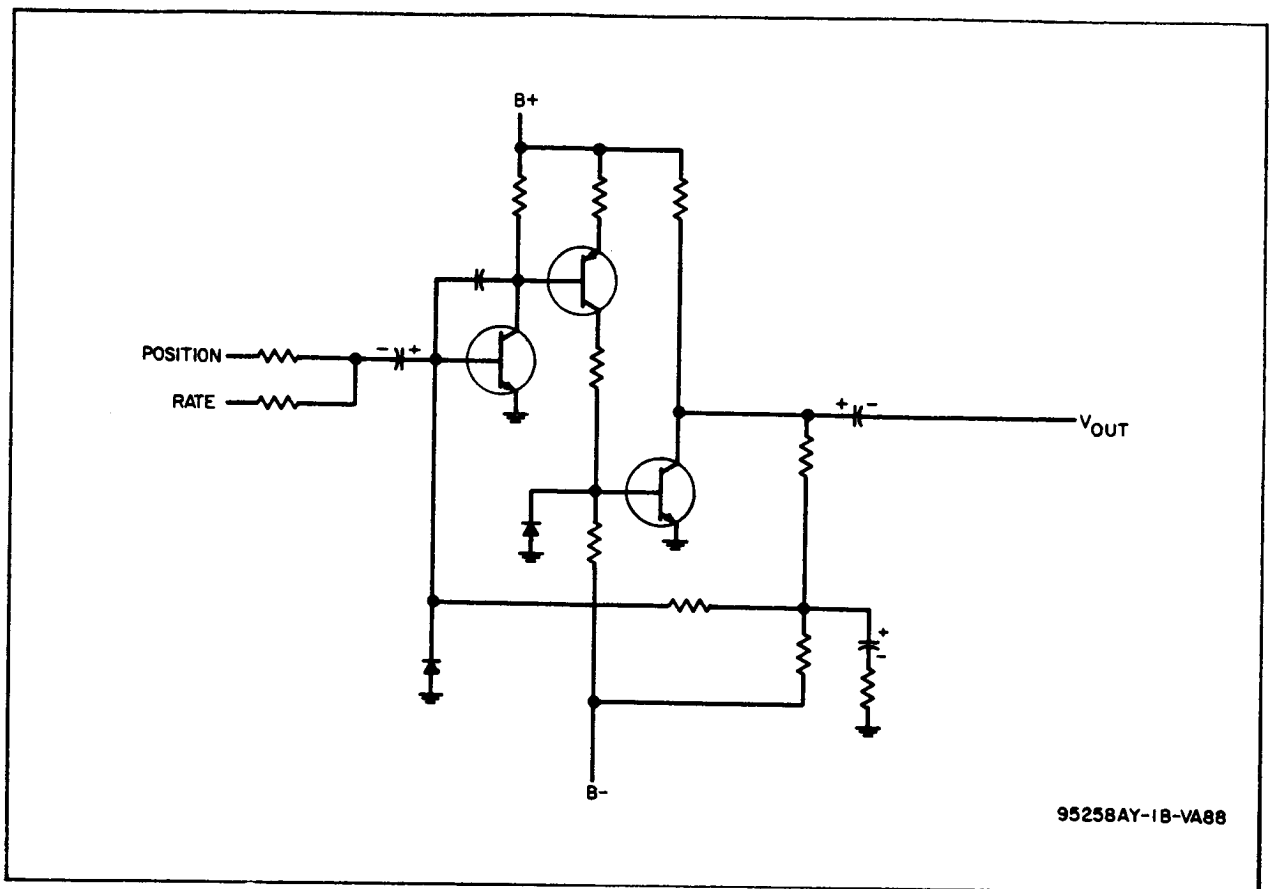
95258AY–IB–VA85

Figure B-10. Block 10 PNPN Switch Circuit

95258AY–IB–VA86

Figure B-11. Block 11 Multiplier Torque Coil Driver
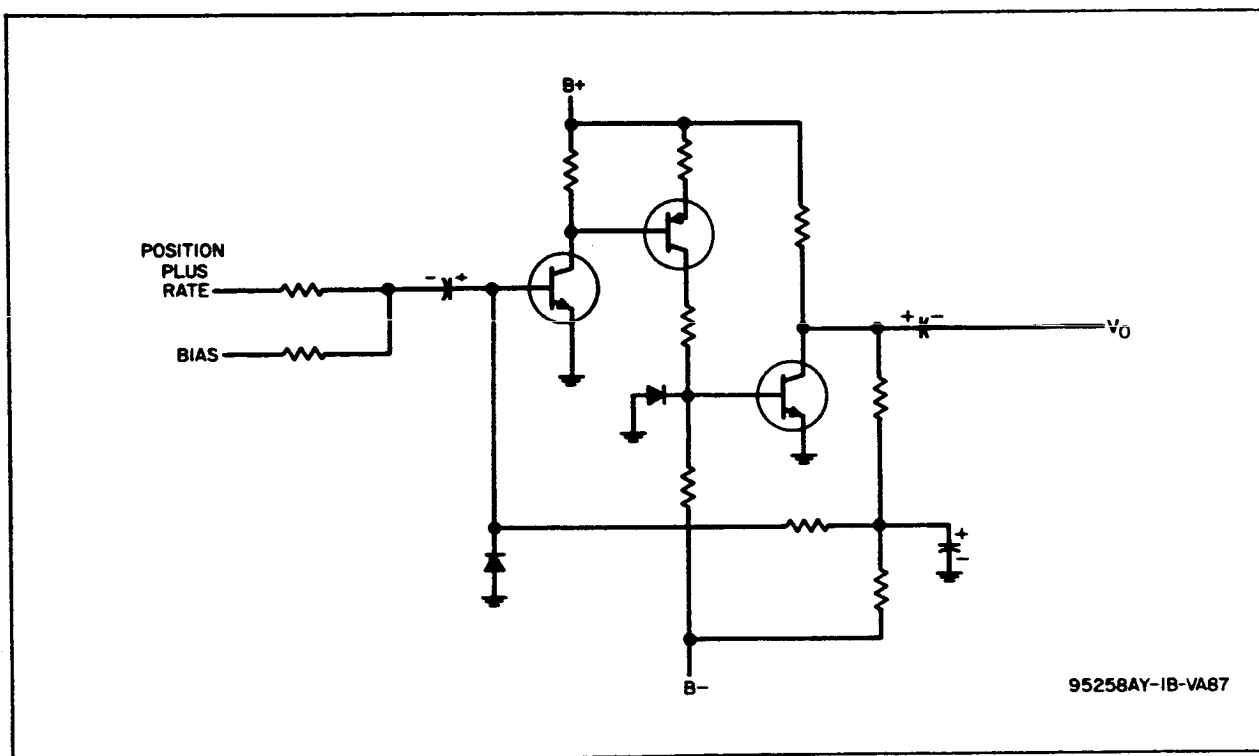
Figure B-12.   Block 12 Coincidence Amplifier
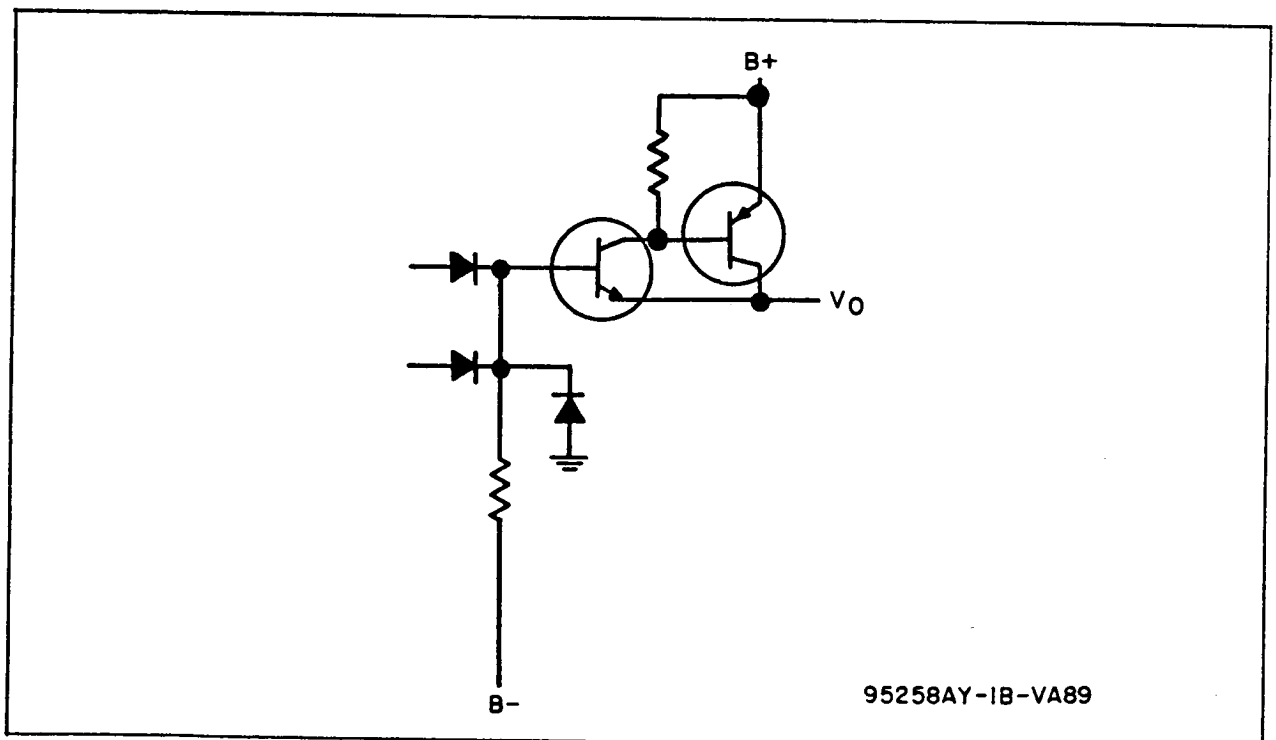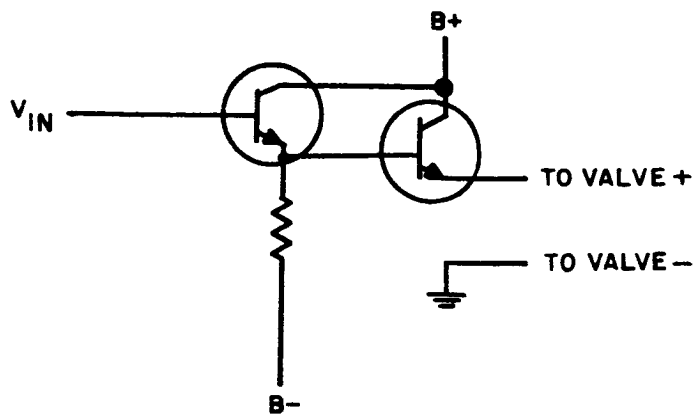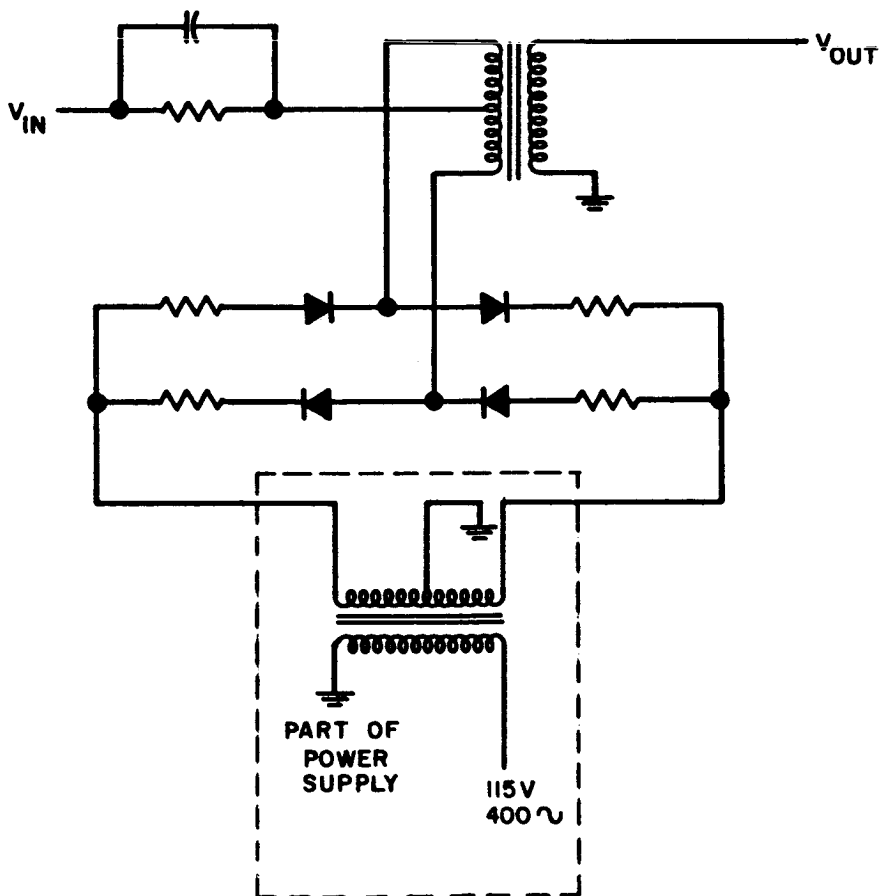
95258AY-IB-VA88

Figure B-13. Block 13 Summing Amplifier

95258AY-IB-VA89

Figure B-14. Block 14 OR Gate and Emitter Follower

Figure B-15. Block 15 Valve Driver

Figure B-16. Block 16 Full Wave Modulator and Lead Network
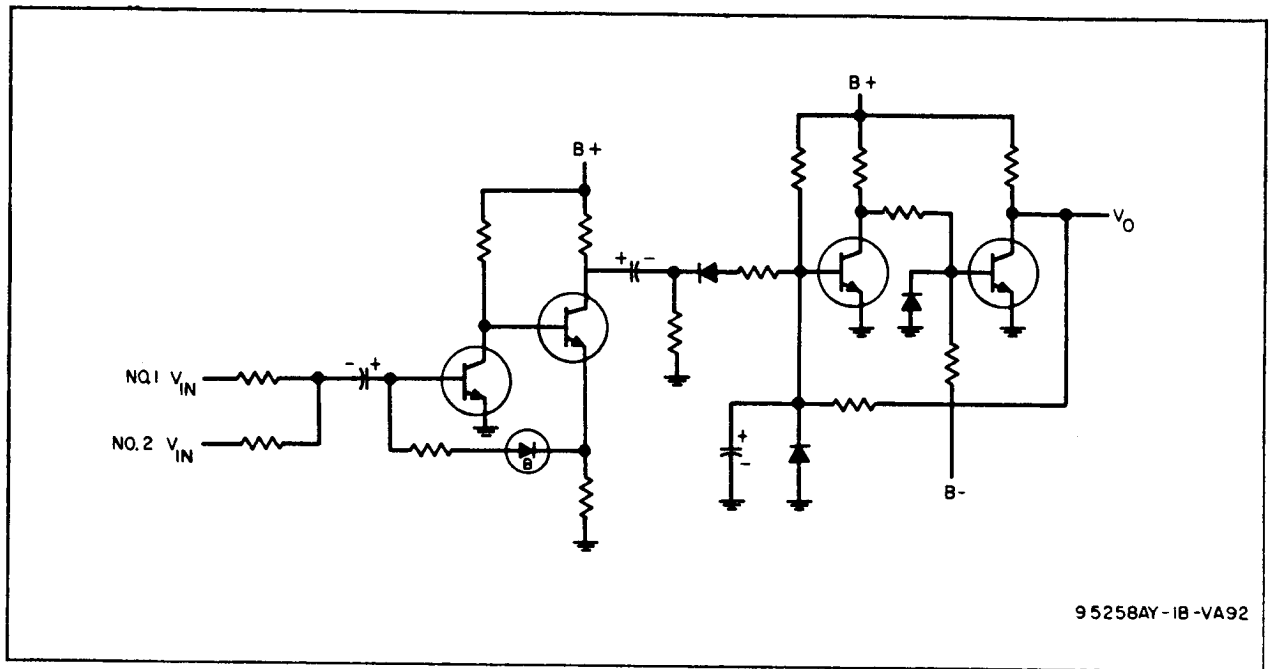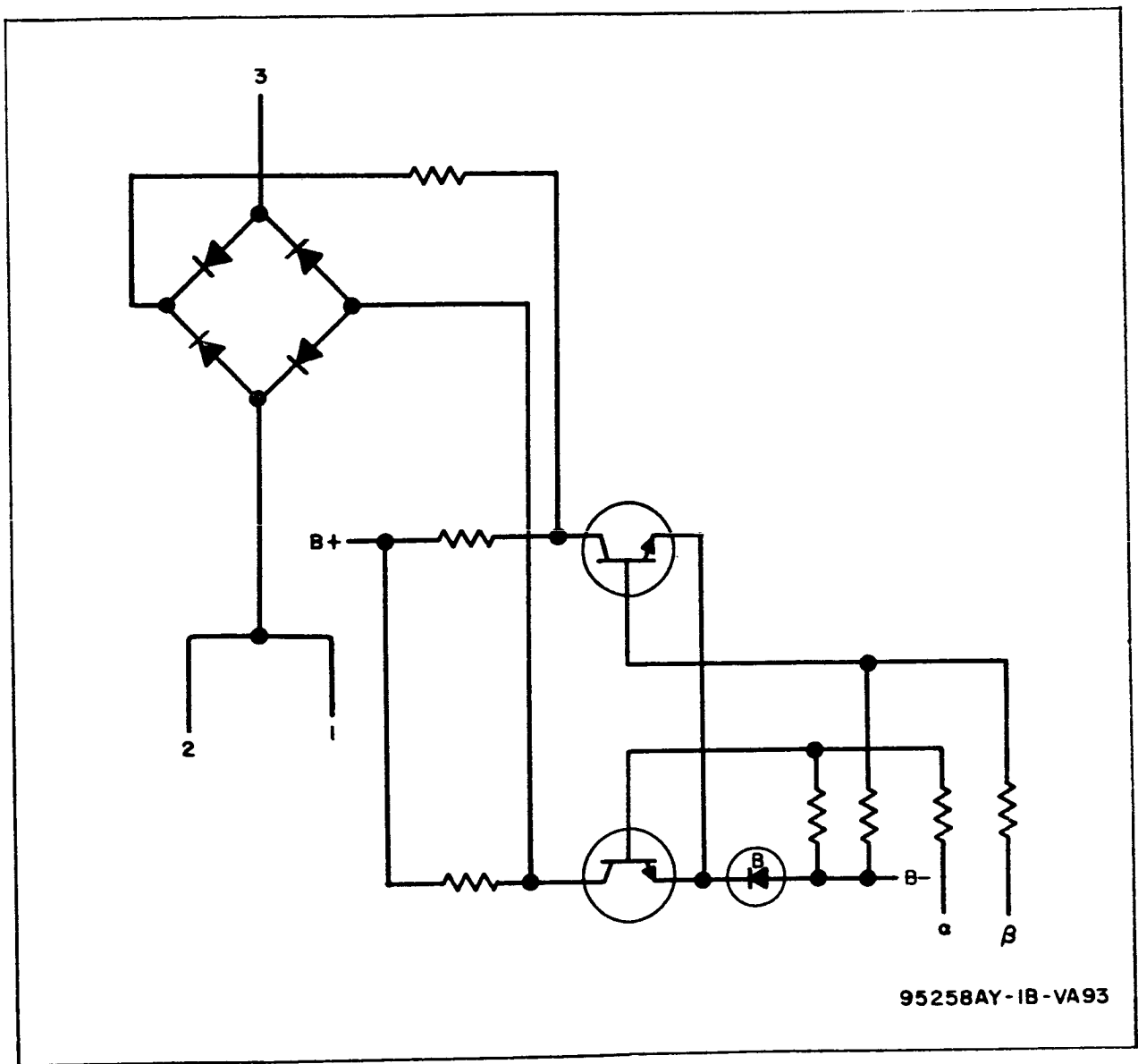
Figure B-17.   Block 17 Null Detector

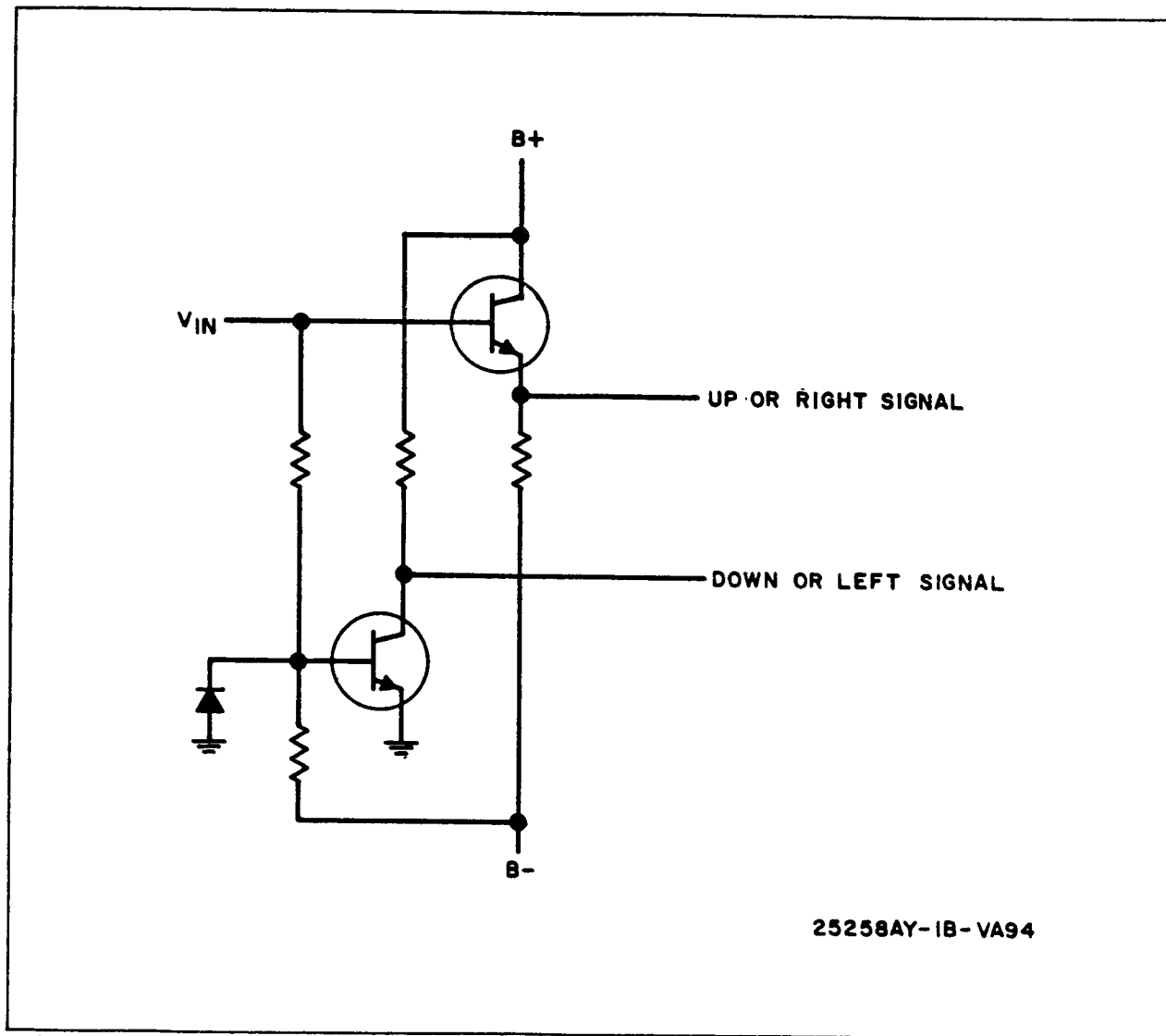Figure B-18.   Block 18 Single Throw Relay Contact Circuit

95258AY-1B-VA93

Figure B-19. Block 19 Valve Logic Circuit

25258AY-IB-VA94